

Atmospheric Corrosion of Silver Investigated by X-ray Photoelectron Spectroscopy

Dissertation

Presented in Partial Fulfillment of the Requirements for the Degree Doctor of Philosophy
in the Graduate School of The Ohio State University

By

Christine Elizabeth Lemon, B.S.

Graduate Program in Chemistry

The Ohio State University

2012

Dissertation Committee:

Heather C. Allen, Advisor

Prabir K. Dutta

Gerald S. Frankel

Samuel D. Stout

Barbara E. Wyslouzil

Copyright by
Christine E. Lemon
2012

Abstract

Atmospheric corrosion is a costly problem. Accelerated laboratory tests, such as the salt fog chamber, have been created to predict corrosion of materials without the need to expose them over long periods of time outdoors. However, these accelerated tests often do not accurately reproduce the types and rates of corrosion found in field exposures. Silver exhibits this discrepancy and has been used in recent years in an attempt to correct the shortcomings of these accelerated tests.

This study identifies Ag_2SO_3 and Ag_2SO_4 on field-exposed silver coupons. The presence of these species on field-exposed silver has been contested in the literature. Evidence suggests that Ag_2SO_3 is an intermediate step in the formation of Ag_2SO_4 . Furthermore, the presence of alkali cations, such as Na^+ , determines the final oxidation state of the sulfur species on silver. If Na^+ is present, Ag_2SO_4 is the final state, whereas Ag_2SO_3 is not found in the presence of alkali cations. The identification of sulfite and/or sulfate on field-exposed samples suggests the need for further improvement of salt fog tests which do not currently include a sulfur source.

In addition to proposing a mechanism for sulfate formation, this study also proposes a link between AgCl formation on inland samples and continental chloride sources. AgCl has been previously reported to form on silver exposed at nearly every location regardless of the proximity to marine sources. Studies have shown that ClNO_2 , which is a reservoir species for chlorine, releases Cl radical when photolyzed. High levels

of ClNO_2 have been reported at locations which are not near salt water sources. This study provides further evidence that AgCl is formed in every exposure location, with only one exception. The lack of correlation of cations, such as Na^+ , which are present in sea spray aerosols to Cl^- on silver samples, is consistent with a non-salt water source of inland chloride. The abundance of ClNO_2 and therefore Cl radical at non-marine areas may be the cause of inland AgCl formation.

Dedication

This is dedicated to the people I love.

Acknowledgments

I would like to thank my advisor Dr. Heather Allen for her encouragement that I've needed during this process. I would also like to thank Dr. Gerald Frankel, Dr. Prabir Dutta, Dr. Barbara Wyslouzil, and Dr. Samuel Stout for being on my dissertation committee and giving me advice and suggestions on my thesis work. Acknowledgement must also go to the Mandaree Enterprise Corporation and the Office of the Secretary of Defense (OSD) who has funded me during the last five years; they made all of this a reality.

Thanks also goes to the other people who have helped in various ways throughout my Ph.D., including my major collaborator, Huang Lin, who helped to teach me about corrosion; Joshua Hanna, who has helped my sanity and always answered my pestering emails; the other members of TCC (formerly the UCC); and Lisa Hommel for teaching me all about XPS. I would also like to thank Aaron Jubb, Chris Beekman, Corey Beck, Dominique Verreault, Ellen Adams, and Wei Hua, the long walks, company and great conversation throughout the years kept me from giving up long ago. I would also like to thank all of the Allen group members, past (those who laid the groundwork) and present (those who are left to continue forwards), for their camaraderie in this journey we all share.

This thesis would not have been possible had it not been for Ryan. I have not always been a pleasure to be around during the dissertation process, but he has helped to

hold me up and push me forward. The love and support I feel at home has helped more than I can ever express and it will not soon be forgotten.

Lastly and most significantly, I would like to thank my parents for always believing in me and being my cheerleaders. They always told me I could do anything I wanted to in life, and so, here I am. I literally would not be here without them.

Vita

March 23, 1985Born – Cincinnati, OH
2003.....Walnut Hills High School
2007.....B.S. Chemistry, University of Cincinnati
2007 to presentGraduate Teaching Associate, Department
of Chemistry, The Ohio State University

Publications

C. E. Lemon, N. Goldberg, E. T. Klein-Riffle, J. K. Kronberg, B. S. Ault, “Matrix Isolation and Theoretical Study of the Photochemical Reactions of C_2H_3Br and 1,2- $C_2H_2Br_2$ with CrO_2Cl_2 .” *Chemical Physics* **326** (2-3), 349-355 (2006).

Fields of Study

Major Field: Chemistry

Table of Contents

Abstract.....	ii
Dedication.....	iv
Acknowledgments.....	v
Vita.....	vii
Publications.....	vii
Fields of Study.....	vii
List of Tables.....	xii
List of Figures.....	xiii
List of Abbreviations & Symbols.....	xvi
1. Introduction.....	1
1.1 Overview.....	1
1.2 Corrosion.....	2
1.3 Atmospheric Corrosion.....	4
1.4 Atmospheric Chemistry.....	10
1.4.1 OH Radical.....	11
1.4.2 Ozone.....	12

1.4.3	Sulfur.....	13
1.4.4	Chlorine.....	16
1.5	Silver Corrosion as a Simplified Model of Metallic Corrosion	21
1.6	Problems and Goals.....	28
2.	Experimental.....	30
2.1	Sample Handling, Exposure, and Set-up.....	30
2.1.1	Field-Exposed Samples – New Hampshire.....	30
2.1.2	Field-Exposed Samples – Hawaii	33
2.1.3	Field-Exposed Samples – USA & Antarctica Single Measurements	37
2.1.4	Accelerated Laboratory Samples	43
2.1.5	Sample Storage	46
2.2	X-ray Photoelectron Spectroscopy.....	47
2.2.1	Theoretical Background.....	47
2.2.2	Instrumentation	53
2.2.3	Data Analysis	55
3.	Existence of Ag_2SO_3 and Ag_2SO_4 on Field-Exposed Silver	60
3.1	Introduction	60
3.2	Results	61
3.2.1	New Hampshire	61

3.2.2	Hawaii	67
3.2.3	U.S.A. and Antarctica Single Measurements.....	74
3.2.4	Lab-Created Samples	81
3.3	Discussion	85
3.3.1	Comparison to Literature, Confirming Identity of Species	85
3.3.2	Mechanism of Ag_2SO_3 and Ag_2SO_4 Formation – Under Vacuum	86
3.3.3	Mechanism of Ag_2SO_3 and Ag_2SO_4 Formation – Aqueous Phase	87
3.3.4	Is Ag_2SO_3 Actually An Intermediate for Ag_2SO_4 ?	95
3.3.5	Correlation with Atmospheric Measurements	101
3.3.6	Cause of Change in Ratios of $\text{Ag}_2\text{SO}_4/\text{Ag}_2\text{S}$ and $\text{Ag}_2\text{SO}_3/\text{Ag}_2\text{S}$	104
3.3.7	Why are Ag_2SO_3 and Ag_2SO_4 Not Routinely Identified in Literature?	105
3.3.8	Ag_2SO_4 Generation on Laboratory Accelerated Tests.....	106
3.3.9	Suggested Improvements for Accelerated Laboratory Tests	107
4.	The Prevalence of Atmospheric Chloride Sources in Various Environments as Detected by Silver Corrosion Analysis.....	108
4.1	Introduction	108
4.2	Results	110
4.3	Discussion	112
5.	Conclusions and Future Work	115

References.....	119
Appendix A: Tables	126
Appendix B: Pourbaix Diagrams	128
Appendix C: Attenuation Length.....	130
Appendix D: Error in XPS.....	131
Appendix E: Calculation of Film Thickness from a Reduction Curve.....	133
Appendix F: Complete XPS Spectra.....	135
Appendix G: AIRMAP Data.....	225

List of Tables

Table 1.1 Classification of environments used in previous corrosion studies.....	9
Table 1.2 Sources and sinks of atmospheric sulfur.....	16
Table 1.3 Typical sea water concentrations of selected ionic species	19
Table 1.4 Emission fluxes of atmospheric aerosol particles.....	20
Table 1.5 Sources and sinks of atmospheric hydrogen chloride.....	20
Table 1.6 Wet deposition rates of selected atmospheric species	27
Table 2.1 Exposure dates for Battelle silver coupons.....	40
Table 2.2 Relevant physico-chemical parameters of silver corrosion compounds observed in lab- and field-exposed samples.....	45
Table 2.3 Literature values of binding energies of silver and some common corrosion products of silver.....	53
Table 2.4 Energies and linewidths for the two most common XPS anode materials	53
Table 2.5 Relative sensitivity factors (RSF) and binding energies.....	59
Table 3.1 Correlation between the presence of cations and either sulfite or sulfate	97
Table 4.1 Correlation between the presence of Cl ⁻ and cations.....	114

List of Figures

Figure 1.1 Partial pressure of water vapor in air at various temperatures	9
Figure 2.1 Map of the New England region of the United States.....	31
Figure 2.2 Pictures showing the sample exposures at Appledore Island, ME.....	32
Figure 2.3 Pictures showing the sample exposures at Thompson Farm, NH.	33
Figure 2.4 Map of exposures in Hawaii.....	35
Figure 2.5 Pictures showing the sample exposures in Hawaii.....	36
Figure 2.6 (a) A map of the continental United States. (b) A map of Hawaii.	41
Figure 2.7 Photographs showing a sample exposure rack typical of those used for the nationwide single-point measurements.....	42
Figure 2.8 Map of Antarctica.....	43
Figure 2.9 Photograph of the containment box for storing silver samples	46
Figure 2.10 Diagram illustrating the physical principle of X-ray photoelectron spectroscopy.....	52
Figure 2.11 Diagram of the major components in an XPS instrument.....	55
Figure 3.1 Pictures of New Hampshire silver samples after six months of exposure	64
Figure 3.2 Sulfur 2p region scan of all samples exposed in New England	65
Figure 3.3 Reduction curves for samples exposed at Thompson Farm	66
Figure 3.4 Reduction curves for samples exposed at Appledore Island.....	66
Figure 3.5 X-ray Diffraction (XRD) spectrum of polished, clean silver	67

Figure 3.6 Pictures of silver samples exposed in Hawaii after exposure.....	69
Figure 3.7 Sulfur 2p region scan of all samples exposed in Hawaii.....	70
Figure 3.8 Sulfur 2p region of samples from Kilauea Volcano.....	71
Figure 3.9 Ratios of SO_4^{2-} to S^{2-} on each sample exposed at Kilauea Volcano.....	72
Figure 3.10 Galvanic reduction scans of samples exposed at Kaneohe MAB.....	72
Figure 3.11 Galvanic reduction scans of samples exposed at Kilauea Volcano.....	73
Figure 3.12 Galvanic reduction scans of samples exposed at Mauna Loa.....	73
Figure 3.13 Pictures of silver samples exposed across the USA and Antarctica.....	76
Figure 3.14 XPS spectra of the S 2p region for the sample exposed at Coconut Island, HI, Conroe, TX, and Daytona Beach, FL.....	77
Figure 3.15 XPS spectra of the S 2p region for the samples exposed at Long Island, NY, Lyon Arboretum, HI, and Randolph, TX.....	78
Figure 3.16 XPS spectra of the S 2p region for the sample exposed at West Jefferson, OH, Whidbey Island, WA, and Woodstock, ME.....	79
Figure 3.17 XPS spectra of the S 2p region for the sample exposed at McMurdo Station, Antarctica.....	80
Figure 3.18 Ratio of $\text{SO}_4^{2-}/\text{S}^{2-}$ or $\text{SO}_3^{2-}/\text{S}^{2-}$ on single samples exposed across the U.S.A. and Antarctica.....	80
Figure 3.19 Reduction of two lab-created samples.....	83
Figure 3.20 XPS sulfur 2p region scan of the two lab-created samples.....	83
Figure 3.21 Reduction of four lab-created samples.....	84
Figure 3.22 XPS sulfur 2p region scan of four lab created samples.....	84

Figure 3.23 Diagram of the steps needed for oxidation of SO ₂ to S(VI) in the aqueous phase.	93
Figure 3.24 pH speciation curves for sulfite and sulfate	94
Figure 3.25 Possible pathways for SO ₂ , S(IV), and S(VI) near a silver surface	94
Figure 3.26 Diagram of the possible mechanism for formation of Ag ₂ SO ₃ from Ag ₂ O + HSO ₃ ⁻	95
Figure 3.27 Drawing of the faces of silver	98
Figure 3.28 Figure of stacking of different crystal orientations for silver	98
Figure 3.29 Geometries of the (100), (110), and (111) faces of silver and silver oxide... ..	99
Figure 3.30 Diagram for the possible bond angle difference on Ag(100) and Ag(110)... ..	99
Figure 3.31 Diagram of the possible transformation of Ag ₂ SO ₃ to Ag ₂ SO ₄ on the Ag(100) surface through interaction with a cation such as Na ⁺	100
Figure 3.32 Diagram of the possible transformation of Ag ₂ SO ₃ to Ag ₂ SO ₄ on the Ag(110) surface	100
Figure 3.33 AIRMAP SO ₄ ²⁻ data from Fort Constitution & Thompson Farm	103
Figure 3.34 AIRMAP Na ⁺ data from Fort Constitution & Thompson Farm	103
Figure 4.2 AIRMAP Cl ⁻ data from Fort Constitution & Thompson Farm	113
Figure 4.3 Picture showing the heights of Mauna Loa summit, Mauna Loa observatory (MLO) and the trade wind inversion	114

List of Abbreviations & Symbols

$\%n_i$	Atomic percentage
$[S]_z$	Concentration of pollutant at height z
$[X]$	Concentration of species X
AI	Appledore Island, ME
AIRMAP	Atmospheric investigation, regional modeling, analysis and prediction
ASTM	American Society for Testing and Materials
B117	Salt fog Chamber
C	Concentration of pollutant
d	Penetration depth
dn_i/dt	Rate of reaction (mol/s)
D_w	Wet deposition rate
E_B	Binding Energy
E_F	Fermi level
E_K	Kinetic energy
E_{VAC}	Vacuum level
F	Faraday's constant (96485 C/eq)
F	Flux
FC	Fort Constitution, NH
G	Gaussian

GILDES	Gas, interface, liquid, deposition, electrodic, solid
GNP	Gross National Product
h	Planck's number
HWHM	Half width half maximum
H_X	Henry's law constant of species X
h ν	Energy of incident X-ray
I	Electrical current (A), Intensity
I_0	Intensity of source
I_{ij}	Area of peak j from element i
ISO	International Organization for Standardization
K	Instrumental constant
K_{max}	Maximum Kinetic Energy
K_{sp}	Solubility Product Constant
L	Lorentzian
$L_{ij}(\gamma)$	Angular asymmetry factor for orbital j of element i
m	Gaussian-Lorentzian mixing ratio
MAB	Marine air base
ML	Monolayer
MSE	Mercury/mercurous standard electrode
n	Number of electrons (eq/mol)
$n_i(z)$	Concentration of element i at distance z below the surface
n_i/n_k	Elemental ratio

P	Percentage of Lorentzian component
PAN	Peroxyacetyl nitrate
PM	Particulate matter
P_w	Partial pressure of water vapor
P_w^*	Saturated vapor pressure of water
P_X	Equilibrium gas phase pressure of species X
RH	Relative humidity
RSF	Relative sensitivity factor
S(IV)	$\text{SO}_2 \cdot \text{H}_2\text{O} + \text{HSO}_3^- + \text{SO}_3^{2-}$
S(VI)	$\text{HSO}_4^- + \text{SO}_4^{2-}$
T(KE)	Transmission function of analyzer
TF	Thompson Farm, NH
TRS	Total Reduced Sulfur
V_g	Deposition velocity
VOC	Volatile organic compounds
w	Half width half maximum
x0	Peak center
XPS	X-ray photoelectron spectroscopy
XRD	X-ray diffraction
ϕ	Work function of a material
ϕ_e	Energy of flooding electrons
ϕ_{sp}	Work function of spectrometer

λ	Washout coefficient, inelastic mean free path
$\lambda_{ij}(\text{KE})$	Inelastic mean free path length of peak j from element i
ν	Frequency
ν_0	Threshold frequency for a material
θ	Angle of incidence, Take off angle

1. Introduction

1.1 Overview

Accelerated laboratory tests (such as the salt fog chamber test) are not currently able to reproduce corrosion rates observed during outdoor exposures.¹⁻⁴ In order to better understand the discrepancy between field and accelerated laboratory studies, this thesis examines the corrosion of silver coupons exposed to a range of field conditions. Silver is used because it exhibits this discrepancy and the corrosion products can be readily identified. Analysis of the field samples via X-ray photoelectron spectroscopy (XPS) support the following hypotheses that provide a link between atmospheric chemistry and corrosion. (1) Corrosion products formed on silver samples are representative of local atmospheric conditions taking into account surface reactivity and meteorological transport. (2) Atmospheric sulfur species are responsible for a significant amount of corrosion on field-exposed silver. (3) The formation of Ag_2SO_4 proceeds via the intermediate Ag_2SO_3 . Together these hypotheses suggest that to improve laboratory studies, a gaseous atmosphere that more accurately reflects atmospheric conditions is necessary. In particular, SO_2 should be included in the accelerated tests.

In addition to the research presented here regarding sulfur, the XPS data also show that AgCl is formed on every silver coupon exposed outdoors. Although this is consistent with previous studies, there remain questions as to the source of AgCl corrosion products at locations not near saltwater sources.^{2,4} Inland chloride species, such

as ClNO_2 , which produce the highly reactive Cl radical, have been reported.^{5,6} Based on the ClNO_2 studies, this thesis proposes a fourth hypothesis: inland chloride sources are responsible for silver chloride formation at non-marine locations.

This dissertation is organized as follows. Chapter one provides background knowledge of corrosion and atmospheric chemistry with a focus on silver corrosion. The second chapter details the experiments performed including experimental parameters. The role of sulfate and sulfite in the atmospheric corrosion of silver is discussed in Chapter 3. The prevalence of atmospheric chloride sources in various environments, as detected by silver corrosion analysis, is presented in Chapter 4. Finally, Chapter 5 summarizes the results and suggests future directions for this study.

1.2 Corrosion

Corrosion is described as “the environmental degradation of materials”.⁷ The corrosion of metals has been studied for nearly a century due to a desire to improve the conservation of resources, safety and financial costs which are associated with the degradation of materials.⁸ A study published in 2001 found the direct cost of metallic corrosion to represent approximately 3.1% of the US Gross National Product (GNP).⁹ The direct costs include, for example, the use of alternative and more expensive materials, labor, equipment, and lost revenue. In addition to these costs, indirect factors, such as loss of productivity, nearly double the cost. This would bring the total to an estimated 6.2% GNP which would have been roughly one trillion dollars for 2011.⁹

From an electrochemical point of view, metallic corrosion is due to an irreversible redox reaction of the form:¹⁰



In order for corrosion of a metal to occur, there must be both oxidation (electron production) and reduction (electron consumption) reactions in which metal is oxidized and the oxidizing agent is reduced. This corrosion reaction involves an exchange of electrons, i.e., the generation of an electric current across the electrode-electrolyte interface. The rate of this reaction is governed by Faraday's law:¹⁰

$$I = nF \left(\frac{dn_i}{dt} \right), \quad (1.2)$$

where I is the electrical current (A), n is the number of electrons in the reaction (eq/mol), F is Faraday's constant (96,485 C/eq), and dn_i/dt is the rate of the reaction (mol/s).

The type of oxidizing agent is determined by environmental conditions (e.g. relative humidity, acidity, temperature). Under wet conditions, the oxidizing agent in basic or neutral conditions is typically dissolved oxygen (O_2), whereas solvated protons (H^+) play this role in acidic conditions. At high temperatures and dry conditions, the oxidizing agent includes gaseous compounds such as (molecular) oxygen (O_2), water vapor (H_2O), carbon dioxide (CO_2), sulfur dioxide (SO_2) or sulfate (SO_4^{2-}) containing species.

Typically, there are three types of corrosion products: dissolved ions, porous films, and compact films.¹⁰ When corrosion occurs in an acidic environment, the predominant corrosion products are dissolved ions. In neutral or basic, and often humid, conditions, corrosion will yield thick ($\approx 1\text{-}300\ \mu\text{m}$),¹¹ porous films which are not generally protective of the substrate, as in the case of iron.¹⁰ Some substrates, such as aluminum, will preferentially form compact films, such as an oxide layer, which often protects the substrate from further corrosion. The compact films will, however, be more easily penetrated under high temperatures and may become thicker and more porous. Thin films (1-3 nm), typically an oxide layer, are called passive films and they act as a small barrier to the environment.

1.3 Atmospheric Corrosion

Atmospheric corrosion is a complex form of corrosion that has been defined as: “the reaction of a metal with atmospheric oxygen [where] humidity and pollutants form an electrolyte.”¹⁰ The corrosivity of a given atmosphere has been described as depending primarily on relative humidity and the concentrations of atmospheric species like sulfur dioxide (SO_2) and chloride (Cl^-).^{8,10} SO_2 is a major pollutant in many environments since it is primarily produced through combustion of fossil fuels and volcanic emissions.¹²⁻¹⁶ Chlorides are typically found in marine aerosols¹⁷⁻¹⁹ but have also been detected over continental regions,⁵ although the sources of continental chloride are still being investigated. Relative humidity (RH) is defined as the ratio between the partial pressure

of water vapor (P_w) and the saturated vapor pressure of water (P_w^*) at a specific temperature as shown in the following equation:²⁰

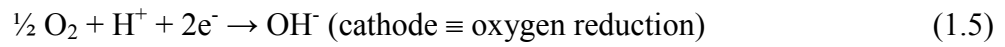
$$\text{RH} = \left(\frac{P_w}{P_w^*} \right) \times 100\%. \quad (1.3)$$

RH is highly dependent on temperature. The temperature dependence of RH is illustrated in Figure 1.1.

Atmospheric corrosion often incorporates many chemical, electrochemical and physical processes on a surface which may have several different regimes (gas, interface, liquid, deposition, electrodic, and solid).^{8,21} Models which incorporate these six regimes are termed GILDES models. Typically, corrosion of metals begins the instant bare metal is exposed to the environment and forms either an oxide or hydroxide film which is usually a few nanometers in thickness. Almost immediately following surface hydroxylation water adsorption occurs which, depending on the relative humidity, can be anywhere from a few monolayers (ML) thick up to bulk water, more than five ML, during periods of direct surface wetting.²² The variability in water adsorption can be due to many factors including, but not limited to, defects or porosity of the surface, the inherent degree of the hydrophilic nature of the substrate and the amount of aerosols in the surrounding atmosphere.⁸ It has been shown that within a fraction of a second there can be enough monolayers of water present on a metal surface to behave as a bulk system and support ion transport, especially if aerosols are present.^{8,23} Aerosols act as condensation nuclei for water and can significantly increase the amount of water on a

surface.^{24,25} Water can deposit on the surface through different processes which impacts the thickness of water on the substrate. The estimated amount of water on a metal surface covered with dew is on the order of 10 g/m², whereas the amount from rain is approximately 100 g/m².⁸

The anodic and cathodic reactions involved in atmospheric corrosion are primarily:



The sites for these reactions tend to be spatially separated on the surface and, owing to the abundance of oxygen in the atmosphere, the anodic dissolution of the metal tends to be the rate-limiting step.¹⁰ The aqueous phase acts as a medium for the dissolved metal ions as well as an electrolyte. It also allows gaseous species to dissolve, diffuse, and come into contact with the surface. Atmospheric species which are typically considered significant to the corrosion process are: carbon, nitrogen and sulfur dioxides (CO₂, NO₂, and SO₂), hydrogen chloride and sulfide (HCl and H₂S), ammonia (NH₃), molecular oxygen (O₂), ozone (O₃), and hydrogen peroxide (H₂O₂) as well as the many salt forms of these gaseous species and organic molecules.¹⁰

Metal dissolution is often a key step in atmospheric corrosion. Metal dissolution primarily occurs through the complexing of dissolved ions to the metal surface, thereby weakening the surface bonding network, and allowing the metal to dissolve into the bulk.¹⁰ This is especially the case when there are surface terminated oxides or hydroxides

which are readily replaced by dissolved ions such as bisulfate (HSO_4^-)^{10,26} which complexes with metal cations. Once a metal cation is released into the bulk, there is a newly exposed surface metal atom which may then partake in further dissolution. The dissolved metal ions can form ion pairs, and at sufficiently high concentrations, begin to form precipitates on the surface.²⁷⁻³⁰ Eventually this will lead to total surface coverage of the metal substrate and formation of a visible corrosion product layer. Further corrosion requires transport of reactive species to the substrate and/or transport of metal ions away from the substrate.

Since atmospheric corrosion is complex, attempts have been made at classifying exposure locations in order to simplify the parameters studied, see Table 1.1.^{31,32} In order to refine this classification system, several programs were launched which analyzed “coupons” (samples) exposed both within the U.S.A. and across the globe and with both long-term (months to years) and short-term (days to weeks) monitoring.^{33,34} This collection of data highlighted the need for simultaneous monitoring of key parameters such as SO_2 , Cl^- , RH, and temperature alongside corrosion data. More recently, the International Organization for Standardization (ISO) created a protocol for outdoor exposures worldwide called ISO CORRAG, which is a collaborative atmospheric exposure program.^{35,36} This program initially included copper, steel, zinc, and aluminum exposed at sites in 12 countries in Europe and North America. This study based corrosion rates on weight loss, time of wetness, and deposition rates of Cl^- and SO_2 . The goal was to create better classifications for outdoor exposure conditions and to predict long-term

corrosion rates.³⁷ Unfortunately, variability in sample exposure protocols still make comparisons from different outdoor exposures difficult.

An important goal in the study of corrosion is to reproduce and accelerate the outdoor corrosion environment in a laboratory. One technique ubiquitous amongst corrosion labs is the salt spray chamber test (ASTM B117)³⁸ where a sample is exposed to a salt fog in a closed chamber for a specified time. The fog is formed by atomizing an aqueous NaCl solution by means of a nozzle. This test is designed to model a marine environment. This accelerated laboratory test along with other ASTM standard tests are not always able to reproduce corrosion rates observed in the field.^{1-3,39} Sometimes lab tests will predict slower or faster corrosion than what is observed in the field tests. This discrepancy may be due to an oversimplification of the environment into a one or two-component system. Hence, there is a great need for new standardized testing methods or modifications to existing testing equipment.

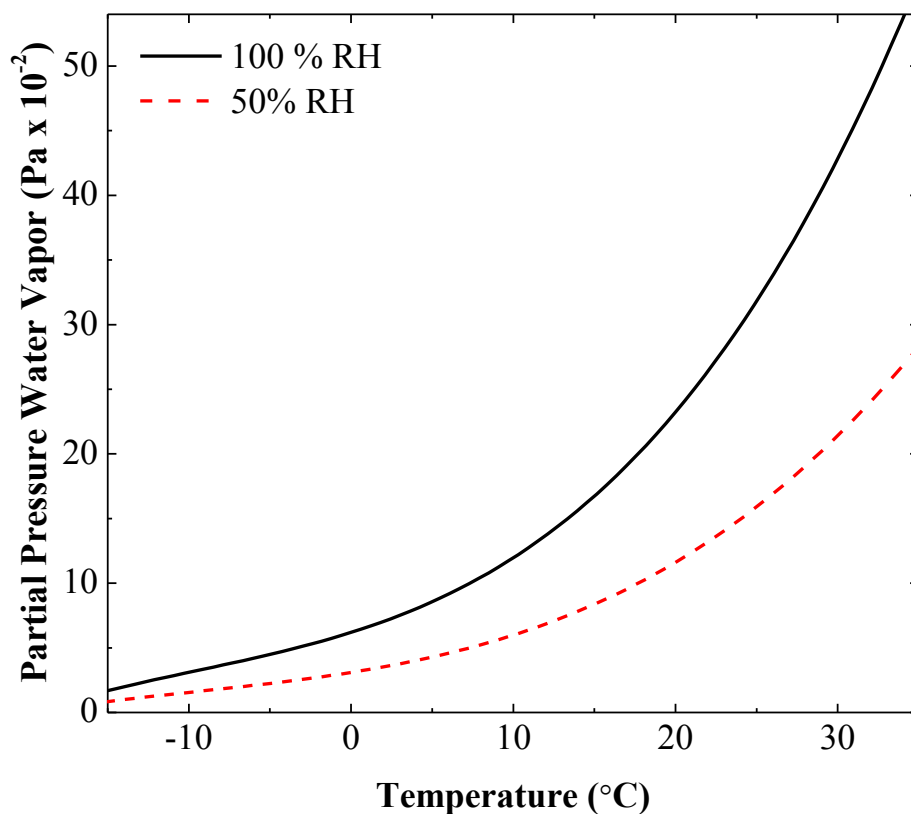


Figure 1.1 Partial pressure of water vapor in air at various temperatures and at 100% (solid black curve) and 50% (dashed red curve) relative humidity.^{40,41}

Table 1.1 Classification of environments used in previous corrosion studies.^{31,32}

	Daily SO ₂ deposition (mg/m ² •day)	Other species of interest
Rural	< 20	organic and inorganic pollutants
Urban	20-110	NO _x = NO + NO ₂
Industrial	>110	chlorides, phosphates, and nitrates
Marine		chlorides

1.4 Atmospheric Chemistry

In order to understand and accurately predict atmospheric corrosion of metals, atmospheric chemistry in the exposure location must be understood. Atmospheric chemistry is a subject involving numerous atmospheric constituents. Radicals and ions play a significant role in gas phase chemistry. Particulate matter (PM) is another key part in atmospheric chemistry since it can be both detrimental to health and air quality and can also act as a reactive site for gas phase reactions. PM refers to solid particles with a diameter of less than 10 μm suspended in air. Particulates are produced both biogenically and anthropogenically. Aerosols refer to particles and liquids suspended in a gas. These constituents evolve in time as they react with each other and themselves through competing processes. Meteorology must also be considered since it can transport atmospheric species away from the source. Therefore, pollution sources may impact the atmospheric chemistry of areas further away than would be possible without this transport.

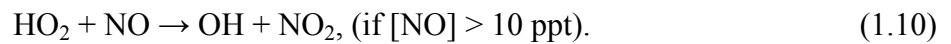
Earth's troposphere is a highly oxidizing environment for both chemical species and surfaces which are exposed to it. The most important oxidant in the troposphere is hydroxyl radical (OH), followed closely by ozone (O_3).⁴² Nitrate radical (NO_3) is the main oxidant for nighttime oxidation.^{43,44} Chlorine radical (Cl) plays a key role in oxidation in marine areas.⁴⁵⁻⁵⁰ Hydroxyl radical, ozone, sulfur, and chlorine, are discussed in the following sections with respect to a general atmospheric chemistry understanding and the possible impacts they pose to metallic surfaces, namely silver.

1.4.1 OH Radical

The OH radical is a highly reactive species (lifetime less than one second)⁵¹ with a steady-state concentration of 10^5 - 10^6 cm^{-3} .^{42,52} These two factors designate OH radical as the most important oxidant in both urban and rural environments. In rural areas, the major source of OH is the photolysis of O_3 .^{42,53}



In polluted regions, in addition to O_3 as an OH source, the presence of other species also contributes to OH production.⁴²



The OH radical then goes on to oxidize other species in the atmosphere as well as surfaces it may come in contact with. In regions with low biogenic volatile organic compounds (VOC) emissions, OH is removed by reactions involving CH_4 , CO , and O_3 .⁴²





This process leads to a photochemical destruction of tropospheric ozone in rural and remote areas.

The reaction of atomic oxygen with silver is expected to form Ag_2O easily.¹



However, the abundance of water in the outdoor environment and the reactions in (1.6) & (1.7) predicts more OH than O is present in field exposures.^{1,54} The OH radical may also lead to formation of Ag_2O .¹

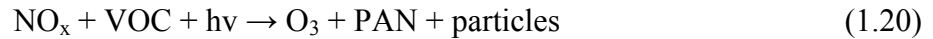
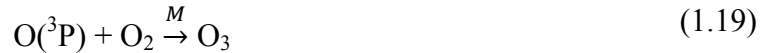
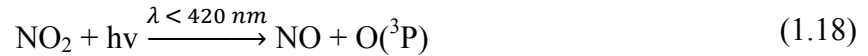


OH radical is less abundant in the troposphere due to its ability to react quickly with various species in the atmosphere and with surface adsorbed species.⁸

1.4.2 Ozone

The adverse health effects that ozone poses in the troposphere make it an important area of research.⁵⁵⁻⁵⁷ In urban areas, ozone concentrations typically range from 50-100 ppb and can exceed that significantly during high-ozone events; for comparison, rural areas are typically less than 30 ppb.^{8,58} The primary formation mechanism of O_3 in

the troposphere is through the photolysis of NO₂ which forms O(³P). Molecular oxygen then reacts with O(³P) to form ozone.⁴²



PAN = Peroxyacetyl nitrate and VOC = volatile organic compounds. Along with O(¹D) and OH, ozone can react with a metal to form an oxide such as:^{1,2}



Ozone can also contribute to oxidation of metals through its photolysis which forms O(¹D) which can lead to OH formation, Eq. (1.6). Ozone also reacts with water to form hydrogen peroxide which further generates the highly reactive OH radical.⁵⁹⁻⁶⁴

1.4.3 Sulfur

Sulfur species impact the corrosion of metals exposed in outdoor environments. Atmospheric sources and sinks of sulfur are given in Table 1.2. Total reduced sulfur (TRS) refers to hydrogen sulfide (H₂S), methyl mercaptan (CH₃SH), dimethyl sulfide ((CH₃)₂S) and dimethyl disulfide ((CH₃)₂S₂).⁶⁵⁻⁶⁸ Reduced sulfur is emitted from industrial processes such as paper milling, sewage treatment facilities, animal feeding operations, oil refineries, landfills, as well as from biota.⁶⁹ Corrosion involving reduced sulfur species tends to occur near the source since sulfur species are easily oxidized in the

atmosphere. Most corrosion involving H₂S would occur through dissolution into a surface water layer.^{8,10}



Since the atmosphere is oxidizing, sulfur species are oxidized on within days.^{42,70} Oxidized sulfur in the troposphere includes: SO₂, OCS, DMSO, H₂SO₃, H₂SO₄, and many other species. Oxidized sulfur is emitted through biogenic and anthropogenic sources. Carbonyl sulfide (OCS) is the most abundant sulfur containing species in the atmosphere.⁷¹ OCS is emitted less heavily to the atmosphere than SO₂ but is a stable intermediate in the life of sulfur compounds in the troposphere. The estimated half-life for OCS is two years with the main destructive pathways being from reaction with O(¹D) and OH radical.⁷²

Virtually all sulfur from the combustion of fossil fuels is emitted as sulfur dioxide (SO₂). Once emitted, SO₂ is oxidized in the gas phase or in aerosols. OH radical is the only substantial oxidant for SO₂ in the gas phase whose product is further oxidized by O₂ and finally reacts with water to form sulfuric acid which is highly soluble:^{73,42}



Sulfur dioxide will easily dissolve in water leading to aqueous phase oxidation: ^{73,42}



Ozone may further enhance the oxidation of sulfur in the aqueous phase: ⁴²



Surface adsorption of SO_2 may be a dominant pathway for oxidation. Metal ion catalyzed oxidation of SO_2 has been well studied in the literature. ^{42,74-77} The corrosion effect of SO_2 is discussed further in Chapter 3. Any amount of SO_2 may undergo either wet or dry deposition onto surfaces, as was given in Equations (1.23)-(1.29), forming a solvated sulfite, bisulfite, sulfate, or bisulfite ion which can then corrode the metallic surface. Slightly higher amounts of sulfate are present in non-urban areas when compared to urban locations. ²⁵

Table 1.2 Sources and sinks of atmospheric sulfur (adapted from Leygraf and Graedel, 2000).^{8,15,16}

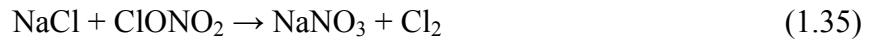
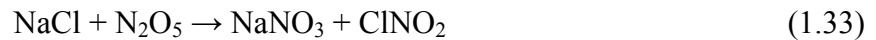
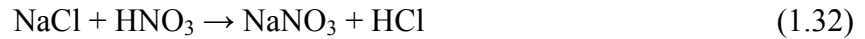
Sources & Sinks	Flux (Tg/yr)
<i>Sources (natural)</i>	
Volcanoes	9 (variable)
<i>Sources (anthropogenic)</i>	
Fossil fuel combustion	60
Industry (smelting)	5
Biomass burning	2
Total sources	76
<i>Sinks</i>	
Dry deposition	35
SO ₄ ²⁻ conversion on aerosols	30
Reaction with OH	11
Wet deposition	<1
Total sinks	76

1.4.4 Chlorine

Atmospheric chemistry and the corrosion of metals are influenced by the existence of seawater nearby, especially by sea spray aerosols.^{17,18} A list of selected species that are observed in sea water along with average concentrations is given in Table 1.3.⁴¹ Aerosol particles formed through wave action can be transported long distances.^{42,78} The emission flux for various natural and anthropogenic sources of aerosols are given in Table 1.4.^{8,42} Overall aerosol flux is governed by natural sources but anthropogenic emissions likely dominate at locations near industrial or urban areas, as seen in Tables 1.3 and 1.4. Global latitudinal mixing occurs on the time scale of one year in the troposphere and meteorology transports atmospheric components long distances.⁴²

Therefore, it is important to not only understand local sources but also sources upwind of the studied areas.

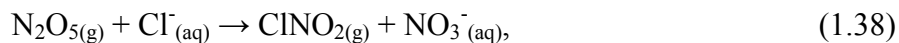
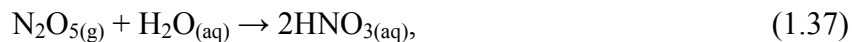
Chloride has been shown to impact metallic corrosion at marine and inland locations. Droplets of seawater produced through wave-action contain NaCl, which can react with NO_x species to produce reactive chlorine radicals.⁴²



Chloride deposition may be up to 1500 mg/m²·day in marine environments.¹⁰ Chloride concentrations have been recorded at up to 150 ppt in the marine boundary layer,⁷⁹ which is consistent with chlorine chemistry dominating in locations near saltwater sources. Studies have detected salt particles as far inland as 900 km in Alaska, indicating long-range transport.⁸⁰ With atomic chlorine measurements between 10³-10⁶ radicals/cm³ in the marine boundary layer,^{81,82} and a global annual average of approximately 10³ atoms/cm³ it is clear that chlorine chemistry is not only significant near coastal areas, but also inland.^{8,42}

There have been many studies on chlorine chemistry in the atmosphere. These studies include ammonium chloride (NH₄Cl),⁸³ hydrochloric acid (HCl),⁸⁴ the oxy-anion (OCl),⁸⁵ and many other measurements. Sources of HCl are given in Table 1.5. Since

high levels of atomic chlorine have been recorded far from any saltwater sources, there is currently discussion on continental chloride processes.^{5,6,63,79,86-91} This current work has focused on the intermediate ClNO₂ which forms at night and photolyzes during the day to produce chlorine radical.



This source for ClNO₂ and ultimately Cl is important in polluted regions, especially in those near saltwater since both NO_x and Cl⁻ are necessary.⁵ However, since the formation of ClNO₂ occurs at night, there exists the possibility for this reservoir species to transport chlorine a significant distance from the source before it is photolyzed.⁸⁸

Chlorine corrosion is of significant interest, as was discussed earlier, and progress has been made in understanding and replicating the corrosion in the lab.^{2,3} There are many possible mechanisms through which a metal chloride corrosion product can be formed. For instance, it has been shown that CH₃Cl will readily dissociate on a metal surface.⁹² Also, when O₃ is added to chloride ion containing water, Cl₂ is generated which could then react with a metal surface nearby.^{93,94}



Other forms of oxidized chlorine (ClO^- , HO_3Cl , HOCl , and ClO_4^-) could possibly react with metals.⁹⁴⁻⁹⁶ Atomic chlorine or solvated chloride ions can also form AgCl :²

These chlorine species are reactive on their own or may replace oxygen in Ag_2O to form AgCl as the final corrosion product.²

Table 1.3 Typical sea water concentrations of selected ionic species (adapted from Handbook of Chemistry and Physics).⁴⁴

Species	Concentration (mg L^{-1})
Br	65
C	28
Ca	4×10^2
Cl	1.9×10^4
F	1.3
I	6×10^{-2}
K	3.8×10^2
Mg	1.35×10^3
Na	1.05×10^4
Si	3
S	8.85×10^2

Table 1.4 Emission fluxes of atmospheric aerosol particles (adapted from Leygraf and Graedel, 2000).¹³

Sources	Flux (Tg/yr)
Natural	
<i>Direct</i>	
Soil dust	1500
Sea salt	1300
Biological debris	50
Volcanic dust	33
<i>Indirect</i>	
Sulfates from natural precursors	102
Organic matter from biogenic VOC	55
Nitrates from NO _x	22
Anthropogenic	
<i>Direct</i>	
Industrial dust	100
Soot from fossil fuels	8
Soot from biomass combustion	5
<i>Indirect</i>	
Sulfates from SO ₂	140
Biomass burning	80
Nitrates from NO _x	36

Table 1.5 Sources and sinks of atmospheric hydrogen chloride (adapted from Leygraf and Graedel, 2000).^{8,46}

Sources & Sinks	Flux (Tg/yr)
<i>Sources (natural)</i>	
Volcanoes	2.0
<i>Sources (anthropogenic)</i>	
Sea salt dechlorination	50.0
Fossil fuel combustion	4.6
Biomass burning	2.5
Incineration	2.0
Transport from stratosphere	2.0
Total sources	63.1
<i>Sinks</i>	
Surface deposition	63.1
Total sinks	63.1

1.5 Silver Corrosion as a Simplified Model of Metallic Corrosion

In order to be able to accurately predict the corrosion observed in field tests and to reproduce it in the lab, it is essential to understand the mechanisms governing outdoor corrosion processes. For this reason, there is an interest in the atmospheric corrosion of metals in different environments. Among the metals that have been studied, a considerable body of work has been devoted to silver in various environments, because silver can be used as a proxy for other materials.⁹⁷⁻¹⁰³ Silver is a metal which exhibits the aforementioned discrepancy between lab and field tests. If silver is left in a salt fog chamber it will not form any significant corrosion products even after a year or more, yet if exposed outdoors silver will form visible corrosion products within days to weeks depending on the exposure environment.^{29, 89} Also, silver corrosion products are generally more easily identifiable than other metals possessing more complex chemistries. As well as being simpler by degrees than studying alloys and/or polymer coated samples.

Another reason for the use of silver is that it also typically exhibits *uniform corrosion*, where the “loss of material [is] distributed uniformly over the entire surface exposed to the corrosive environment”¹⁰ which lends itself to analysis by standard lab techniques. Although the use of silver outdoors is not common, it has many specialized uses in electronics, solder, silverware, photography, and decorative items or jewelry, etc.^{90, 91} Silver mirror coatings are currently of interest for use in very large telescopes and other optical components where degradation of the reflecting surface is not desirable.¹⁰⁶

The physical behavior of silver has been studied for decades, yet a fundamental understanding of the corrosion processes involved in its degradation is still lacking.^{38, 85,}
⁹³ In order to have a more complete picture of how corrosion occurs on a silver surface, a knowledge of the atmospheric chemistry governing the degradation is necessary. Before a link can be made between the atmospheric chemistry of a region and the corrosion observed on a silver coupon, accurate identification of corrosion products and their formation mechanisms are necessary.

The atmospheric corrosion of silver has been discussed in the literature and a brief summary is given here.¹⁰⁰ As stated in section 1.3, corrosion is often initiated only after adsorption of water has occurred. Surface layers of water facilitate ion transport and silver dissolution, thus promoting the corrosion process. The adsorption of water in air onto a silver surface has been demonstrated to follow the equation:¹⁰⁰

$$\ln(ML) = 2.73 \left(\frac{p_w}{p_w^*} \right) - 0.366, \quad (1.41)$$

where ML is the number of monolayers of water adsorbed on the surface and p_w/p_w^* is the partial pressure of water at 25°C. With a temperature of about 25°C, there are at least a few monolayers of water on the surface even at low RH.¹⁰⁰ As is the case with most metals, water plays a key role in the corrosion process of silver as it allows absorption of gases and promotes dissolution. The anodic oxidation of silver is written as:



In acidic solution, this reaction is balanced by oxygen reduction and hydrogen evolution.



Whereas in neutral solution those reactions are instead:



In order to understand the dynamics of species adsorbed in water, both Henry's law and solubility product constants must be known. The solubility of a gas is governed by Henry's law:¹⁰⁸

$$H_X = [\text{X}]_{aq}/P_X, \quad (1.47)$$

where H_X is the Henry's law constant of species X, $[\text{X}]_{aq}$ is the concentration of species X in the aqueous phase, and P_X is the equilibrium gas phase pressure of species X. The Henry constants of some selected atmospheric species are given in Appendix A. The solubility product constant (K_{sp}) describes the solubility of a solid chemical in water and is equal to the concentration of products over reactants where each concentration is raised to its stoichiometric coefficient (P or R , respectively).

$$K_{sp} = \frac{[products]^P}{[reactants]^R} \quad (1.48)$$

The solubility trend of several common silver corrosion products is as follows.



The K_{sp} values of these compounds are also given in Appendix A.⁴¹

Atmospheric corrosion involves both atmospheric particles and gases which are deposited onto surfaces and/or dissolved in surface adsorbed water. These particles and gases are removed from the air through both wet and dry deposition. These terms refer to the state of the pollutant, not to that of the surface on which they deposit. Wet deposition, D_W , can be described by:⁴²

$$D_W = \lambda C, \quad (1.49)$$

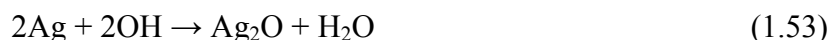
where λ is the washout coefficient (fraction removed in unit time by rain below cloud base) and C is the concentration of pollutant.^{33,94,95} Besides meteorology, other factors may affect wet deposition, such as solubility, type of solvent, pH, temperature, etc. Dry deposition, is typically defined as deposition velocity, V_g , by the following equation.⁴²

$$V_g = -F/[S]_z, \quad (1.50)$$

where F is the flux of a species to the surface (amount of species deposited per unit area per sec) and $[S]_z$ is the concentration of pollutant at a height z .

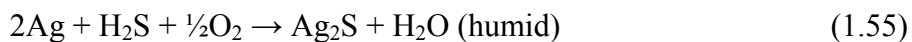
Wet deposition rates for some atmospheric constituents have been reported in the literature and are listed in Table 1.6.¹¹¹ The values are a product of the indoor concentrations of these species and the empirical deposition velocities over a range of humidity. Ionic species may also be deposited onto the surface; these include Cl^- , SO_4^{2-} , NO_3^- and to a lesser extent S_2^- , CO_3^{2-} , and organics. The presence of adsorbed salts will increase the surface wetting due to their hygroscopic nature and should therefore increase the ability of atmospheric species to adsorb onto the surface.^{24,112} The wet deposition rates of chloride, sulfate and nitrate are also given in Table 1.6.¹¹³ The deposition rate of these ions is calculated by adding the products of the concentrations and deposition velocities for both fine and coarse particulates.

Silver, a noble metal, is different from many metals in that it is only predicted to form a surface oxide layer under wet conditions, at $\text{pH} \geq 12$, and in the presence of strong oxidizers.^{85,99} In these conditions, Ag_2O is only stable in a limited high pH range and can be formed on silver following several reactions (see the Pourbaix diagrams in Appendix B).



Even when there is a native oxide layer present, it may be readily replaced by other ionic species which have a higher binding preference, such as chloride or sulfide.^{2,100}

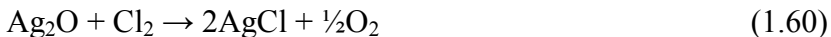
A typical corrosion product on silver surfaces exposed to the environment is Ag₂S which may be formed through the reaction of silver with H₂S, OCS or other reduced forms of sulfur:^{100,115-117}



The presence of oxidizing species such as O₃ and NO₂ has been shown to increase the formation rate of Ag₂S.¹⁰⁷ It has been demonstrated that there is no “ready route” to oxidize Ag₂S into Ag₂SO₄ due to an unfavorable energy barrier.^{100,117} Silver sulfate has been formed from the reaction of silver with either SO₂ or sulfate/sulfite ions in laboratory studies.^{118,119} However, it is stated in literature that “the corrosion of silver to form silver sulfate has had little evidence as a process or product”.¹⁰⁰

Although historically, Ag₂S was thought to be the dominant corrosion product for silver, many studies have also shown high levels of AgCl, often exceeding the amounts of Ag₂S.^{1,4} In the past, AgCl was thought to form on silver surfaces predominantly through the adsorption/reaction of either HCl or molecular chlorine, Cl₂. It has been demonstrated more recently in lab studies that AgCl formation may occur in the presence of HCl, Cl₂,

or NaCl, not directly as a combination with Ag, but rather through an Ag₂O intermediate.²



or in solution, by the following reaction.



Since accelerated lab tests were previously unable to create AgCl, modifications have been proposed.³ These include introduction of O₃ and UV light to the salt fog tests. This modification of the B117 chamber can be used to reliably generate AgCl and resulted in calculated acceleration factors of up to 20 times that of marine environments.³

Table 1.6 Wet deposition rates of selected atmospheric species (adapted from Graedel, 1992).¹⁰⁰

Species	Deposition Rate (ng/cm ² ·s)	Species	Deposition Rate (ng/cm ² ·s)
O ₃	1.3 × 10 ⁻³	Cl ⁻	1.0 × 10 ⁻⁶
H ₂ O ₂	5.0 × 10 ⁻⁴	SO ₄ ²⁻	8.6 × 10 ⁻⁶
H ₂ S	1.3 × 10 ⁻⁵	NO ₃ ⁻	3.8 × 10 ⁻⁶
OCS	1.5 × 10 ⁻⁵		
SO ₂	4.0 × 10 ⁻³		
HCl	2.4 × 10 ⁻⁵		
NH ₃	3.5 × 10 ⁻⁴		
NO ₂	4.6 × 10 ⁻⁵		
HNO ₃	5.5 × 10 ⁻⁴		
HCHO	6.3 × 10 ⁻⁵		
HCOOH	2.3 × 10 ⁻⁴		
CH ₃ COOH	2.5 × 10 ⁻⁴		

1.6 Problems and Goals

There has been much work on the atmospheric corrosion of silver over the years and one major improvement has been suggested for improving the accuracy of lab tests.¹⁻

⁴ However, there remains a missing connection between outdoor corrosion and accelerated lab tests. The accelerated lab tests are still not able to accurately reproduce the corrosion seen in the field. If one desires a true accelerated test, the mechanism for corrosion needs to be the same in the lab as it is for the field.

Therefore, the focus of this thesis is to understand the surface of the silver and the corrosion products formed on it in order to determine which atmospheric components play a major role in the corrosion process of silver. The hypotheses which will be discussed in this thesis are:

- 1) Corrosion products formed on silver samples are representative of local atmospheric conditions taking into account meteorological transport.
- 2) Atmospheric sulfur species are responsible for a significant amount of corrosion on field-exposed silver.
- 3) The formation of Ag_2SO_4 proceeds via the intermediate Ag_2SO_3 , and is dependent on the presence of cations.
- 4) AgCl formation at non-marine locations supports recent measurements of inland ClNO_2 and Cl radical discussed in the literature.

This dissertation is organized as follows. Background of corrosion and atmospheric chemistry is given in Chapter 1. The experiments performed including experimental parameters are given in Chapter 2. Chapter 3 discusses the role of sulfate

and sulfite in the atmospheric corrosion of silver. Chapter 4 discusses a possible link between recent inland chloride measurements and the ubiquitous detection of silver chloride in outdoor corrosion measurements. Finally, Chapter 5 summarizes the results and suggests future directions for silver corrosion studies.

2. Experimental

2.1 Sample Handling, Exposure, and Set-up

2.1.1 *Field-Exposed Samples – New Hampshire*

Samples which were 99.99% pure silver (Lucas-Milhaupt) measuring 3.0” (long) x 0.50” (wide) x 0.011” (thick), polished to 1200 grit on metallographic paper (Buehler) and cleaned in warm isopropanol (Fisher, 99.9%) were exposed at two locations, Figure 2.1, Appledore Island, ME and Thompson Farm, NH. Half of the samples were exposed vertically with a cover (Figure 2.2 and Figure 2.3) in order to minimize contamination from the surroundings, such as animals, humans, or direct rain wash-off and half were left unsheltered. (Also pictured are polymer coated steel samples which were analyzed by another researcher.) The samples were all exposed at the same time beginning in October 2010 and were returned in 1, 2, 3, 4, and 6 month intervals. Samples were sent via airmail in sealed and clean glass vials. At all times, sample handling was done by wearing nitrile gloves. Standards were also sent together with the samples for exposure. The standards remained in sealed glass vials during the length of exposure but were sent together with the samples which were exposed outdoors. These two locations were chosen since there is a long history of atmospheric chemistry data collected at these sites from the University of New Hampshire. The atmospheric chemistry is significantly different between the Farm and Island. Thompson Farm is a mixed forest area (not an active farm site) at an elevation of approximately 130 ft, (43.1078N, 70.9517W).

Appledore Island is a 95 acre island located 6.5 miles off the coast of New Hampshire, in the Isles of Shoals. The island is at sea level, and the balcony on which the samples were mounted was around 200 m from the shoreline (42.97N, 70.62W).

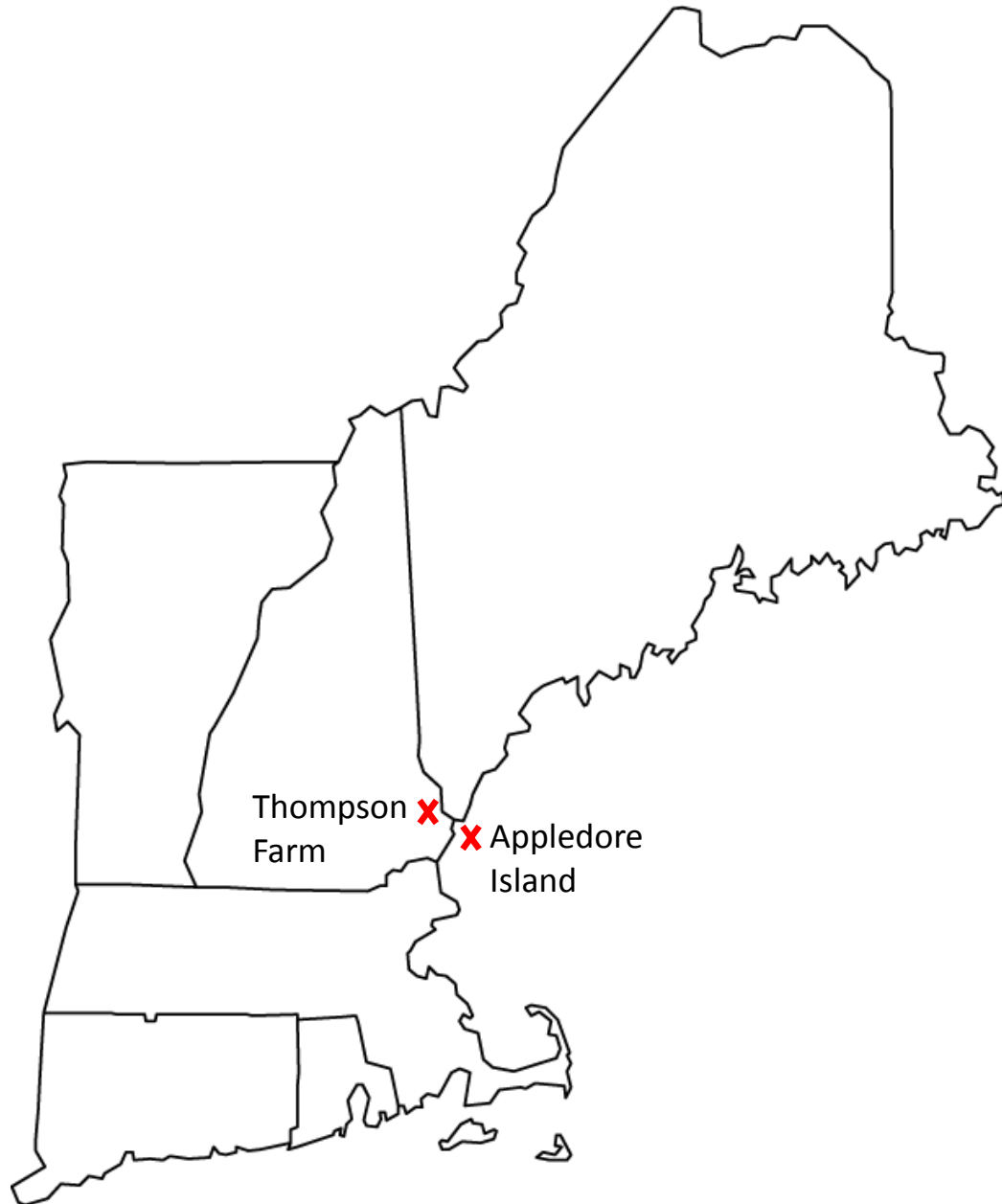


Figure 2.1 Map of the New England region of the United States showing the location of the two exposure sites from the work done with the University of New Hampshire: Thompson Farm (NH) and Appledore Island (ME).



Figure 2.2 Pictures showing the sample exposures at Appledore Island, ME. Top is unsheltered and bottom has a slight overhang to minimize contamination and wash-off.



Figure 2.3 Pictures showing the sample exposures at Thompson Farm, NH. Top is unsheltered and bottom has a slight overhang to minimize contamination and wash-off.

2.1.2 *Field-Exposed Samples – Hawaii*

Samples which were 99.99% pure silver (Lucas-Milhaupt) measuring 3.0” (long) x 0.50” (wide) x 0.011” (thick), polished to 1200 grit on metallographic paper (Buehler) and cleaned in warm isopropanol (Fisher, 99.9%) were exposed at three locations: Kaneohe marine air base on Oahu (marine), Kilauea volcano on the big island (volcanic),

and Mauna Loa observatory on the big island (alpine, no vegetation). A map of these locations is given in Figure 2.4. Kaneohe MAB is located within 100 ft of breaking waves and the sample test racks faced the shoreline. Kilauea volcano erupted days after the samples were deployed on the test racks.^{120,121} Mauna Loa observatory is located at an elevation of approximately 3.4 km. This elevation keeps the samples above the temperature inversion layer (trade inversion) at 2 km about 75% of the year.^{122,123} Therefore, most of the atmospheric species at this elevation are isolated from the ground-level.¹²⁴

The samples were exposed vertically, half without a cover and half with a cover (Figure 2.5) in order to minimize contamination from the surroundings, such as animals, humans, or direct rain wash-off. The samples were all exposed beginning in March 2011 and were returned at 1, 3, and 6 month intervals. Samples were sent via airmail in sealed and clean glass vials. At all times, sample handling was done by wearing nitrile gloves. Standards were also sent together with the samples for exposure. The standards remained in sealed glass vials during the length of exposure but were sent together with the samples which were exposed outdoors. These three sites were chosen since the climate and terrains are diverse. Differences in these environments were proposed to yield differing types of corrosion. Also, an existing collaboration with the University of Hawaii allowed deployment of samples to existing test racks.

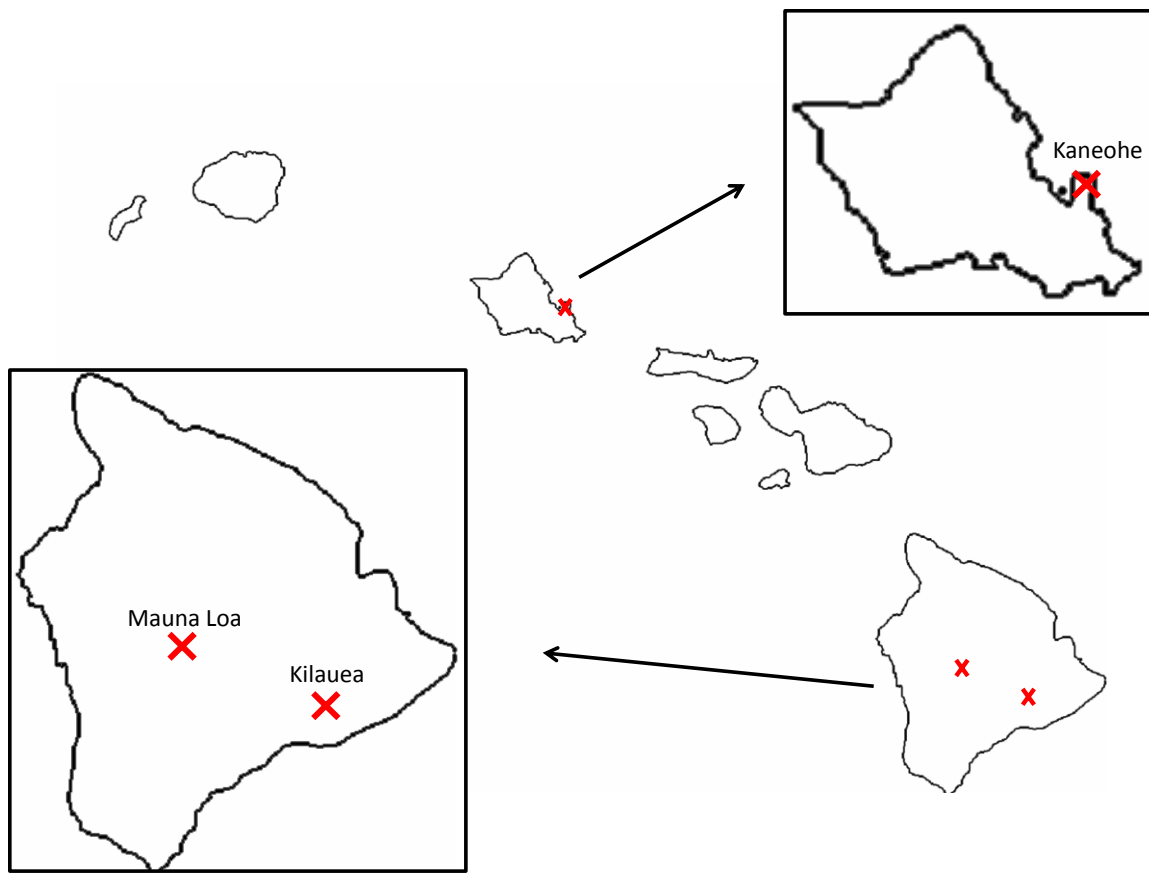


Figure 2.4 Map of exposures in Hawaii. Kaneohe marine air base was on the eastern coast of Oahu. Mauna Loa observatory and Kilauea volcano are both on the big island.

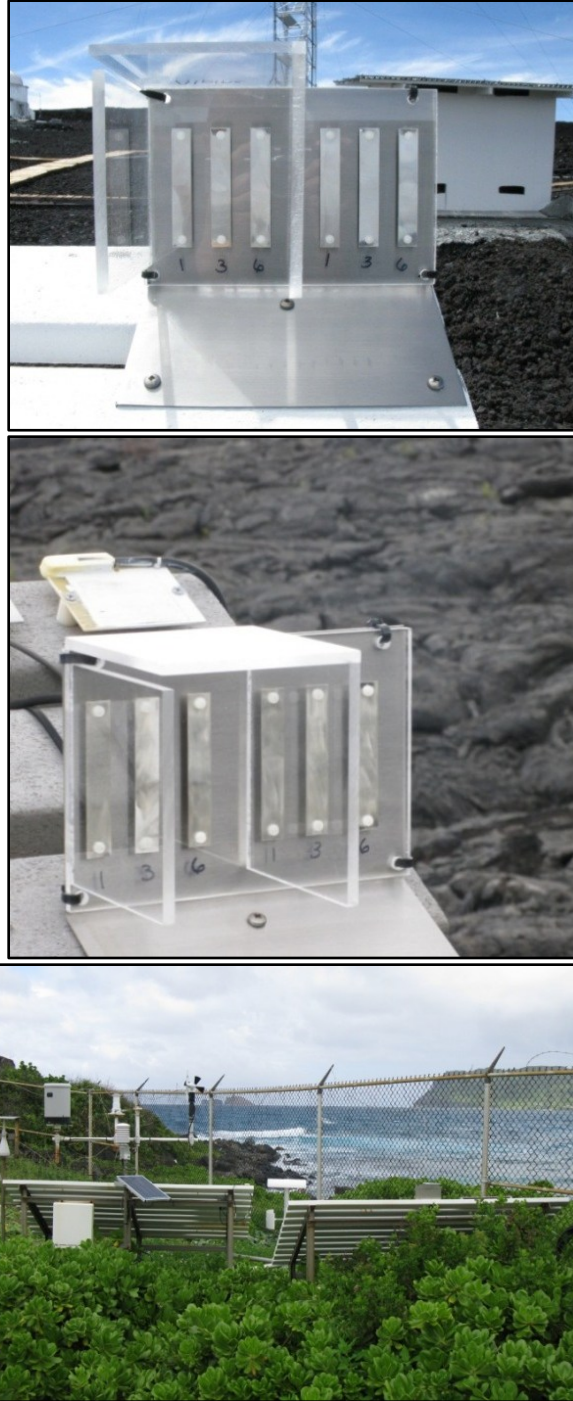


Figure 2.5 Pictures showing the sample exposures at Mauna Loa observatory (top), Kilauea volcano (middle), Kaneohe marine air base (bottom) in Hawaii. Half the samples were covered by a slight overhang to minimize wash-off and contamination and the other half were unsheltered. Identical racks were used at all 3 locations and were mounted onto existing exposure racks which were at 45°.

2.1.3 *Field-Exposed Samples – USA & Antarctica Single Measurements*

Field-exposed samples were received from W. Abbott at Battelle Memorial Institute (Columbus, Ohio). The samples were 99.99% pure silver (Handy & Harmon) measuring 3.5” (long) x 0.50” (wide) x 0.030” (thick), polished to 600 grit on metallographic paper (Buehler) and cleaned in warm isopropanol (Fisher, 99.9%). Samples were exposed outdoors for three months at multiple locations, Table 2.1. Exposure sites, indicated in Figure 2.6, include: Whidbey Island Naval Air Station, WA; Oahu (Lyon Arboretum and Coconut Island), HI; Randolph Air Force Base, TX; Montgomery Army Airfield, Conroe, TX; Battelle Memorial Institute, West Jefferson, OH; Daytona Beach, FL; Gabreski Airfield, Long Island, NY; and Woodstock, ME. The samples were exposed vertically with a cover (Figure 2.7) in order to minimize contamination from the surroundings, or direct rain wash-off.

The samples were polished no more than one month before being shipped to the exposure location. The samples were mounted onto plastic cards immediately after polishing and were stored in poly, zip lock bags. Samples were typically shipped no more than a few days before deployment date. They were shipped via air mail, pre-mounted on the plastic cards, in the poly bags and placed inside plastic VHS cases. The samples were returned to Battelle within 1-2 days after being removed from exposure in the same manner as originally shipped. The samples were then removed from the plastic cards and stored in glass vials until they were given to me. They were analyzed via XPS within one week of receiving them. The samples were always handled with gloves, and if they were cut it was with cleaned tin snips or scissors.

- Coconut Island is a 28 acre island in Kane'ohē Bay off the northeast coast of Oahu, HI, and is a coral reef. It is a marine research facility of the University of Hawai'i.¹²⁵
- Conroe, TX is about 40 miles north of Houston. Montgomery Army Airfield is the exact location that the sample was exposed.
- Daytona Beach, FL is located on the Atlantic Ocean and has a humid sub-tropical climate; average rainfall for the year is about 50 inches.
- Long Island, NY is an island extending into the Atlantic Ocean just east of New York City and is loosely described as a humid sub-tropical climate. Gabreski Airport is on Long Island and is approximately 80 miles east of New York City.
- Lyon Arboretum on Oahu, HI is a 200 acre arboretum and botanical garden, most of which is an artificial lowland tropical rainforest.
- Randolph air force base in Texas is located about 15 miles east-northeast of San Antonio.
- West Jefferson, OH is approximately 20 miles west of Columbus, the sample used here was exposed at a branch of Battelle Memorial Institute which is surrounded by farmland and bordered by the Big Darby Creek.
- Whidbey Island, WA is about 30 miles north of Seattle. The northern end of the island is the location of N.A.S. Whidbey, here the average rainfall is 26 inches and the soil is composed mostly of rock, this is home to a lightly used airfield. Central Whidbey Island is a rural agricultural area.
- Woodstock, ME is located approximately 25 miles east of the New Hampshire border.

These locations were chosen as an ongoing campaign of silver corrosion data by William Abbott at Battelle Memorial Institute and were requested to give a wide range of single point measurements for comparison.

Most samples were analyzed by XPS at two locations on the surface. Spot A was a darker area whereas Spot B was slightly lighter, to the eye. In addition, the samples were rinsed with deionized water and dried with nitrogen gas. This rinsing process was repeated three times. The sample was then rescanned on approximately the same spot as Spot A, a dark section of the sample. Only Randolph and West Jefferson were not scanned in a second location before rinsing.

A sample was also received from W. Abbott at Battelle Memorial Institute (Columbus, Ohio) which was exposed outdoors near an airfield at McMurdo Station, Antarctica (Figure 2.8) for two years and was received for analysis in March of 2009. The sample was prepared in the same way as those mentioned above. It was 99.99% pure silver (Handy & Harmon) measuring 3.5" (long) x 0.50" (wide) x 0.030" (thick), polished to 600 grit on metallographic paper (Buehler) and cleaned in warm isopropanol (Fisher, 99.9%). The sample was exposed vertically with a cover (similar to that in Figure 2.7) in order to minimize contamination from the surroundings, such as animals, humans, or direct rain wash-off.

Time A and B refer to the amount of time elapsed between receipt of the sample and when it was run on the XPS. Time A was run within one week of receiving the sample, while Time B was run nearly two years later. The rinsing technique is the same as for the single measurements across the USA. In addition, the samples were rinsed with

deionized water and dried with nitrogen gas. This rinsing process was repeated three times.

McMurdo Station is a United States operated station on the Ross Ice Shelf on West Antarctica. There are around 1000 residents during the summer and about 200 in the winter months.¹²⁶ Temperatures range from -50 to 11°C with an average of -18°C. There is little precipitation and the average wind speed is 11 mph gusting up to 116 mph. There has been much research on climate change at this station and some work on corrosion has been done here as well.^{83-85,126-130}

Table 2.1 Exposure dates for Battelle silver coupons.

Location	Dates of Exposure	Film Thickness by Reduction, A	
		AgCl	Ag ₂ S
Whidbey, WA	8/13/08-11/17/08	3766	163
Woodstock, ME	6/29/04-9/30/04	211	
Long Island, NY	5/22/08-8/26/08	1650	54
Daytona Beach, FL	10/6/10-1/6/10	4825	54
West Jefferson, OH	12/6/08-3/6/09	550	
Lyon Arboretum, HI	11/22/08-2/25/09	634	
Coconut Island, HI	11/24/08-2/25/09	6052	
Randolph, TX	10/12/08-1/12/09	2073	136
Conroe, TX	10/5/08- 1/5/09	1735	240
West Jefferson, OH	5/27/10-6/27/10	555	30
Daytona Beach, FL	6/7/10-7/7/10	730	102
McMurdo, ANT	1/07-1/09	899	

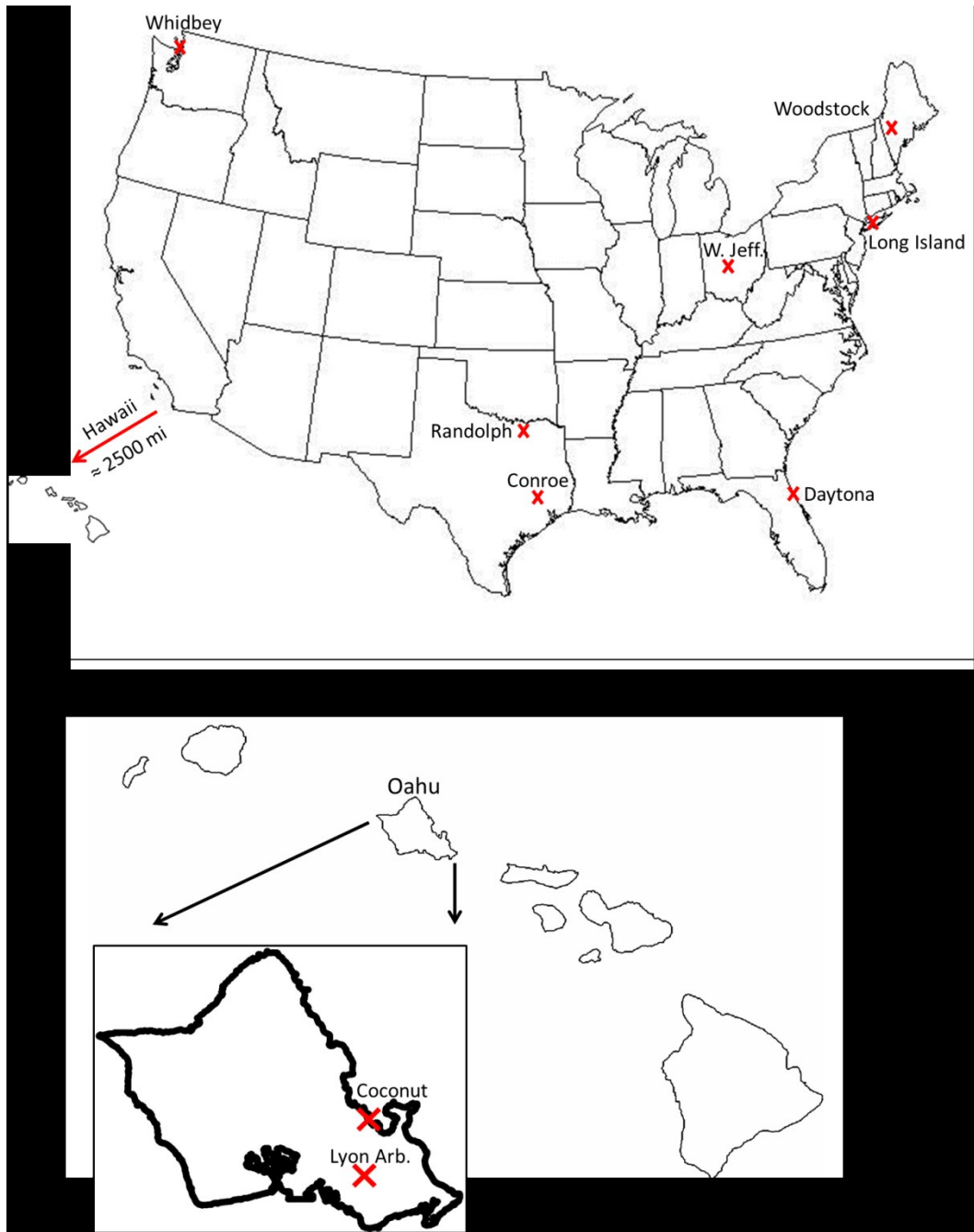


Figure 2.6 (a) A map of the continental United States showing the locations of the exposure sites: Whidbey Island Naval Air Station, WA; Randolph Air Force Base, TX; Montgomery Army Airfield, Conroe, TX; West Jefferson, OH; Daytona Beach, FL; Gabreski Airfield, L Long Island, NY; and Woodstock, ME. The prevailing winds are to the east in direction on average across the contiguous 48. (b) A map of Hawaii with an inset showing the two locations on Oahu: Lyon Arboretum and Coconut Island. The prevailing winds are on average to the west across Hawaii.



Figure 2.7 Photographs showing a sample exposure rack typical of those used for the nationwide single-point measurements. The set-up has a slight overhang to minimize contamination and wash-off.

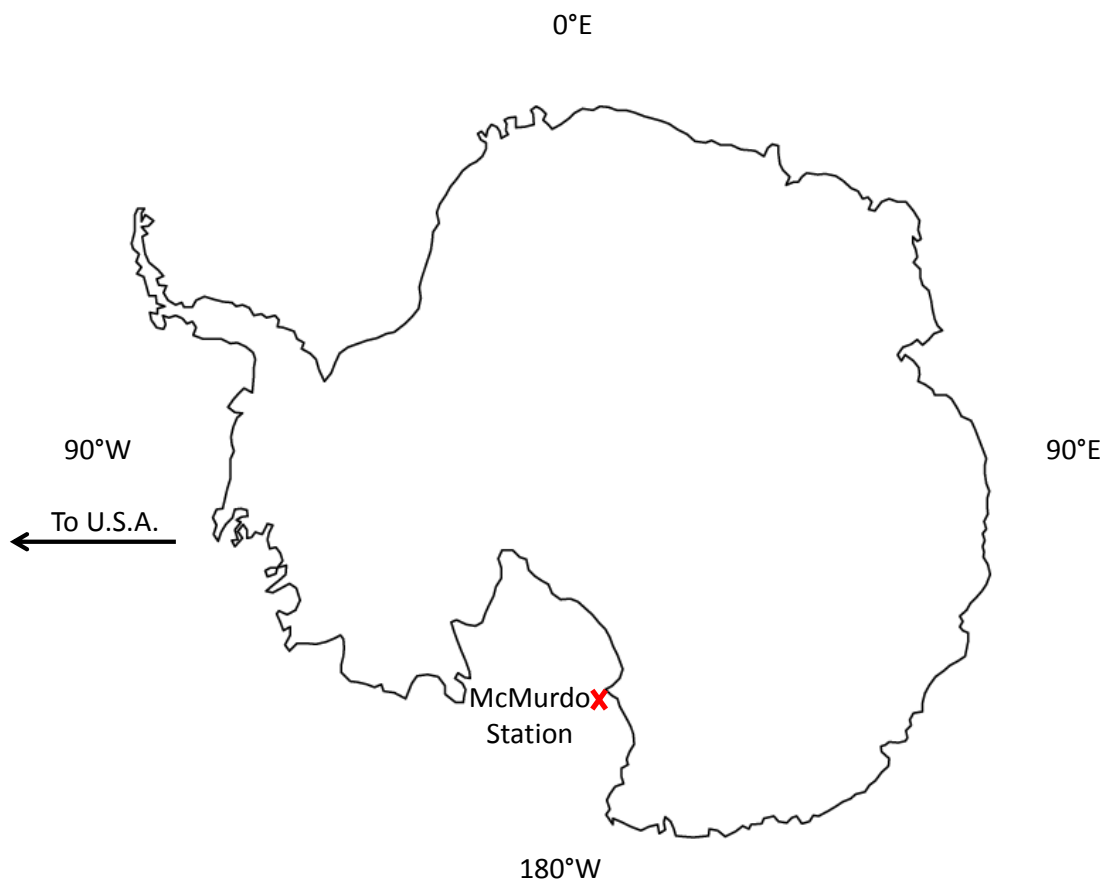


Figure 2.8 Map of Antarctica showing the location of the sample exposed at McMurdo Station for two years.

2.1.4 Accelerated Laboratory Samples

The silver samples used in accelerated laboratory tests were prepared by Huang Lin at Ohio State University.¹³¹ The samples were 99.99% pure silver (Lucas-Milhaupt) approximately 17 mm x 17 mm x 2 mm and were wet polished to 1200 grit on silicon carbide (SiC) paper (Buehler) then ultrasonically cleaned in ethanol (Fisher, 99.9%) for 5 min. The samples were then dried in a desiccator for 24 hr before exposure.

The experimental apparatus (glass chamber) used in the laboratory exposures has been shown previously.⁵⁴ Briefly, oxygen gas is passed through an ozone generator creating between 50 ppb to 50 ppm O₃. This is then combined with a mixture of dry and water-saturated N₂ gas in order to produce the desired % RH. A 254 nm UV lamp with an intensity of approximately 4 mW/cm² was used as the exciting light source.

In order to reproducibly crystallize NaCl on the silver surface, fast evaporation of a NaCl/ethanol solution was used on polished silver samples. The solution was prepared in two steps. First, NaCl was dissolved in deionized (DI) water to make a 1.67 wt% NaCl solution and then it was diluted with pure ethanol to reach a concentration of 990 µg/ml NaCl. Before exposure, 146 µl NaCl/ethanol solution was transferred onto the sample surface with a pipette, which generated 50 µg/cm² loading of NaCl on the samples, and then coupons were immediately placed in a vacuum pumped desiccator. The solution completely dried within 6 min, but the samples were kept in the evacuated desiccator for 30 min to make sure no ethanol remained on surface.

Following the lab preparation, all samples were analyzed with XPS and galvanostatic reduction. For the XPS analysis, a survey scan was taken of each sample with pass energy of 80 eV and region scans with pass energy of 20 eV were obtained for any region with appreciable signal. Galvanostatic reduction was used to quantify the types and amounts of corrosion products after analysis with XPS.^{1-4,54,133} A Gamry Reference 600 potentiostat with a mercury/mercurous standard electrode (MSE) was used for all reductions in this study. With this technique, a constant current is applied to the sample surface to reduce the corrosion products electrochemically. An area of 1 cm² in

the center of the sample was reduced at a cathodic current density of 0.1 mA/cm² in deaerated 0.1 M Na₂SO₄ solution at pH 10. The solution was deaerated using an N₂ gas purge for more than one hour prior to reduction.

Reduction potentials of various compounds observed in this thesis are given in Table 2.2. Since the thickness of the corrosion layer scales linearly with the charge generated, the reduction charge is used to calculate corrosion film thickness. A reduction charge of 1 C/cm² is approximately equal to a 2.68 μm-thick film (if the film is assumed to be made entirely of AgCl). The necessary calculations leading to this value are given in Appendix E. Reduction potential typically scales with free energy, a stable corrosion product will have a more negative free energy and a more negative reduction potential. The exception is Ag₂SO₄ which does not follow this trend.

Table 2.2 Relevant physico-chemical parameters of silver corrosion compounds observed in lab- and field-exposed samples. *No reduction potential is available for Ag₂SO₃, Ag₂CO₃ or AgNO₃ in the literature.^{4,41,131,133}

Compound	Density (g/cm ³)	Molecular Weight (g/mol)	ΔG (kJ/mol)	Reduction Potential (V _{MSE})
Ag ₂ O	7.14	231.7	-11.22	-0.12 to -0.18
AgNO ₃	4.35	169.9	-33.49	*
Ag ₂ S	7.23	247.8	-40.70	-1.2
AgCl	5.56	143.3	-109.88	-0.25 to -0.4
Ag ₂ SO ₃	5.52	295.8	-411.56	*
Ag ₂ CO ₃	6.08	275.8	-436.81	*
Ag ₂ SO ₄	5.45	311.8	-618.89	-0.08 to -0.1

2.1.5 *Sample Storage*

A picture of the box for storage of the silver samples after XPS analysis is shown in Figure 2.9. It is a two-level clear acrylic box with ½ inch holes drilled in the separating shelves, which was built by American Plastic Distributing (Columbus, OH). There is a two inch space at the bottom which can be used for desiccant. The relative humidity was controlled by flowing dry air into the sealed box via the top swage-lock ports. The samples were placed in glass vials upon receipt by airmail and then stored in departmentalized plastic containers which are also shown in Figure 2.9. The blue labels were used as sample identifiers.



Figure 2.9 Photograph of the containment box for storing silver samples before/after XPS analysis.

2.2 X-ray Photoelectron Spectroscopy

2.2.1 Theoretical Background

The basic XPS experiment involves a sample placed under ultrahigh vacuum that is irradiated with X-rays, inducing emission of electrons (photoelectrons).¹³⁵ A simplified diagram of the physical principle of XPS is shown in Figure 2.10. The emission of photoelectrons is due to a transfer of energy from the incoming photon to the core-level electrons. The emitted electrons are then separated based on their kinetic energy and counted. The energy of the ejected electrons is based on the local environment of the electrons and the number emitted is proportional to the abundance of the element in the sample.¹³⁵ The emission of electrons upon irradiation is described by the photoelectric effect:¹³⁵

$$K_{max} = h\nu - \phi, \quad (2.1)$$

where K_{max} is the maximum kinetic energy of the ejected electron, h is Planck's constant, ν is the frequency of the incoming light, and ϕ is the work function of the material which is the minimum energy needed to remove an electron from the surface. The work function is defined by:

$$\phi = hv_0, \quad (2.2)$$

where ν_0 is the threshold frequency for the material.¹³⁵

The consequences of the photoelectric effect are four-fold in that electrons will only be ejected when $\nu \geq \nu_0$. Then once sufficient energy to stimulate emission is exceeded the emission of electrons is proportional to the amount of incident photons. The kinetic energy of the ejected electrons is proportional to the frequency of incident photons. Lastly, the entire process from excitation to emission is on the order of 10^{-16} s.

Binding energy refers to the strength of the bond between an electron and an atom. The binding energy will increase with oxidation state and with the addition of electron withdrawing groups. Binding energy increases with a decrease in the distance between the electron and nucleus as well as a decrease in the number of electrons around the nucleus.¹³⁵ The binding energy of the electrons to their respective atom is given by the Einstein equation:

$$E_B = h\nu - E_K, \quad (2.3)$$

where $h\nu$ is the energy of the incident X-ray, and E_K is the kinetic energy of the ejected photoelectrons which is measured in the experiment.¹³⁵ Binding energy is typically reported in electron-volts (eV), which is equivalent to 1.6×10^{-19} J. In a typical XPS experiment, the energy of the X-ray beam is about 8.3 keV, which is more than adequate to remove core-level electrons (< 1400 eV).¹³⁵ Table 2.3 gives the literature values of binding energies for silver and common silver corrosion compounds.

Atoms bound to the host atom and the strength of their bonds will also impact the binding energy of electrons. Typically only ionic and covalent bonds contribute to

observable shifts in the binding energy.¹³⁵ When considering the added amount of energy needed to overcome the bonds to the surface, Eq. (2.3) becomes:

$$E_B^F = h\nu - E_K - \phi_{sp}, \quad (2.4)$$

where the binding energy is now referenced to the Fermi level.¹³⁵ Here, ϕ_{sp} is the work function of the spectrometer which is equal to the work function of the sample (ϕ), when the two are in electrical contact, and is related to the Fermi level (E_F) and the vacuum level (E_{vac}) by:¹³⁵

$$\phi_{sp} = E_F - E_{vac}. \quad (2.5)$$

The Fermi level is the energy level separating the valence and conducting bands of a material at 0 K and the vacuum level is the energy level at which the electrons are no longer affected by any material.

The two most common sources for the production of X-rays in XPS are Mg $K\alpha$ and Al $K\alpha$, information about these sources is presented in Table 2.4. Since X-rays have a very long penetration depth, the emitted electrons can undergo one of three possible fates:¹³⁵ (i) if the escaping electrons are near the surface, they will not be subjected to collisional losses and are directly emitted and contribute to the photoemission peak; (ii) if the escaping electrons are only slightly buried in the bulk and have collisions before being emitted, they will contribute to the background of the spectrum; (iii) finally, any electrons which are too far into the bulk and incur enough collisions to lose their kinetic energy will not be emitted at all. Typically, 1 keV electrons will only be able to penetrate

approximately 10 nm.¹³⁵ The depth of penetration can be estimated using an attenuation length plot which has been both experimentally and theoretically determined (see Appendix C).¹³⁵

An explanation of penetration depth for XPS is found using Beer's law:

$$I = I_0 e^{(-d/\lambda \cos\theta)}, \quad (2.6)$$

where I is intensity, λ is the inelastic mean free path or the thickness through which 63% of the electrons will lose their energy, d is the penetration depth, and θ is the angle of incidence.¹³⁵ The bulk sample may be considered to be the source (I_0) here since the range of the substrate which emits electrons is significantly larger than the depth from which they may escape. For a surface layer which has different composition than the bulk, the intensity is given by a modified Beer's law:

$$I = I_0 [1 - e^{(-d/\lambda \cos\theta)}]. \quad (2.7)$$

The sampling depth is defined as 3λ ,¹³⁵ based on the maximum depth from which 95% of electrons are detected. For most XPS experiments, λ is likely between 1-4 nm, such that the sampling depth would be in the range 3-12 nm.¹³⁵ Therefore any surface films which are thicker than ≈ 12 nm will not allow probing of the substrate. As to the detection limits of XPS, the technique is able to detect all elements, except H and He, which are present at concentrations greater than 0.1 atomic percent (at. %).¹³⁵

Some materials, including those in this study with thick corrosion layers, do not have sufficient electrical conductivity to compensate for the build-up of a positive charge created by constant ejection of electrons. In this case, the sample is completely isolated

and a charge neutralizer is used which floods the surface with low energy electrons to stabilize the surface. The electrons are transported to the surface via a magnetic immersion lens. In the case of charge neutralization, Eq. (2.4) then becomes:

$$E_B^{vac} = E_B^F + \phi_s = h\nu - E_K + \phi_e, \quad (2.8)$$

where ϕ_e is the energy of the flooding electrons.¹³⁵ Since the binding energy of insulating materials is now dependent on both the vacuum energy and the energy of the flooding electrons, it is more difficult to determine its absolute value. To circumvent this problem, an internal standard is used. The carbon (C) 1s or silver (Ag) 3d bands are both suitable standards as the positions of these peaks are well known literature values. Since the silver samples used in this study are typically conducting, it is only necessary to use the charge neutralization when a thick corrosion product layer is present (≥ 10 nm).

The background of XPS spectra decreases gradually with increasing binding energy (decreasing kinetic energy) due to inelastic scattering effects.¹³⁵ There is a drop in the background signal after an electron emission event due to a loss of scattering electrons at that binding energy. If the region being studied involves electron pairs (p, d, or f orbitals) two energetically equivalent final states are possible. Based on whether the electron has spin up or down, there is a coupling between the spin and the orbital angular momentum of the electron that may lead to splitting of the degenerate state into two components (or formation of a doublet).¹³⁵ The total angular momentum (j) of an electron is found by summing the individual electron angular (l) and spin (s) momenta, $j = l + s$. For example, this spin-orbit coupling can be observed in the XPS spectra of chlorine,

silver, and sulfur. For the Ag 3d orbital, the principal quantum number (n) equals 3. The electron spin momentum quantum number can be $s = -1/2$ or $+1/2$, depending on whether the spins of the two electrons are parallel or antiparallel. Hence, $l = n - 1 = 2$ such that $j^- = 2 - 1/2 = 3/2$ and $j^+ = 2 + 1/2 = 5/2$. In this way, the Ag 3d orbital splits into two different energy states, $3d^{3/2}$ and $3d^{5/2}$, respectively.

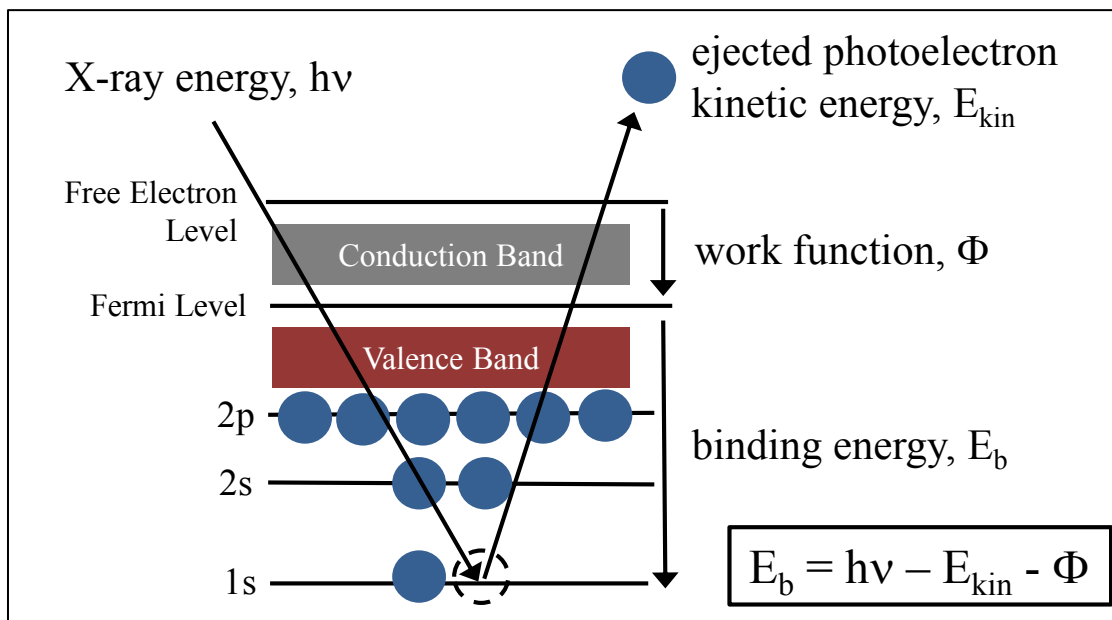


Figure 2.10 Diagram illustrating the physical principle of X-ray photoelectron spectroscopy.

Table 2.3 Literature values of binding energies of silver and some common corrosion products of silver.¹³⁶⁻¹³⁸

Compound	Binding energy (eV)					
	Ag 3d	Cl 2p	C 1s	N 1s	O 1s	S 2p
Ag	368.3					
AgCl	368.3	198.6				
Ag ₂ CO ₃	368.0		288.7		531.0	
AgNO ₃	368.4			406.8	532.5	
Ag ₂ O	367.9				529.5	
Ag ₂ S	368.2					161.0
Ag ₂ SO ₄	368.0				531.7	168.6
Ag ₂ SO ₃	368.1				531.7	167.5

Table 2.4 Energies and linewidths for the two most common XPS anode materials.¹³⁵

Anode Material	Emission Line	Energy (eV)	Width (eV)
Mg	K α	1253.6	0.7
Al	K α	1486.6	0.85

2.2.2 Instrumentation

The surface chemical composition of silver samples exposed at various outdoor locations was determined using an X-ray photoelectron spectrometer (Kratos Axis Ultra, Kratos Analytical) equipped with a semi-hemispherical analyzer and channeltron detectors. A simple schematic of the XPS instrument is shown in Figure 2.11. The spectrometer is calibrated against three standards (copper, silver, and gold) and the

linearity of the BE scale is calibrated by adjusting the energy difference between the peaks of these known sample positions. X-rays from the monochromatic Al-K α line (1486.6 eV) were used for all XPS measurements in conjunction with the hybrid lens mode and a 300 \times 700 μ m spot size aperture. The power on the anode was 120 W (10 mA, 12 kV) and the vacuum in the analysis chamber was maintained at approximately 10⁻⁹ Torr.

The adventitious C 1s peak (binding energy (BE) = 284.9 eV) was used as a standard to correct for charging effects and was compared to the shift experienced by the Ag 3d band (BE = 368.3 eV). Survey scans were taken using a pass energy of 80 eV and the high-resolution region scans were taken using a pass energy of 20 eV. The pass energy is determined from the electrostatic fields in the hemispherical analyzer which only allow electrons of a specific energy range to pass to the detector.¹³⁸ The smaller the pass energy the higher the resolution will be, since the hemispherical analyzer is more selective to electron energies passing through to the detector; this effectively narrows the peaks in the spectrum. For survey scans only one scan was recorded, but for the high-resolution region scans four different runs were averaged to determine the binding and kinetic energies with an accuracy of \pm 0.2 eV. If charging effects were observed to cause a shift in the position of the adventitious C 1s peak a charge neutralizer (tungsten filament) was used. The charge neutralizer was run with a filament current of 2.1 A, a charge balance of 2.4 V, and a filament bias of 1.3 V.

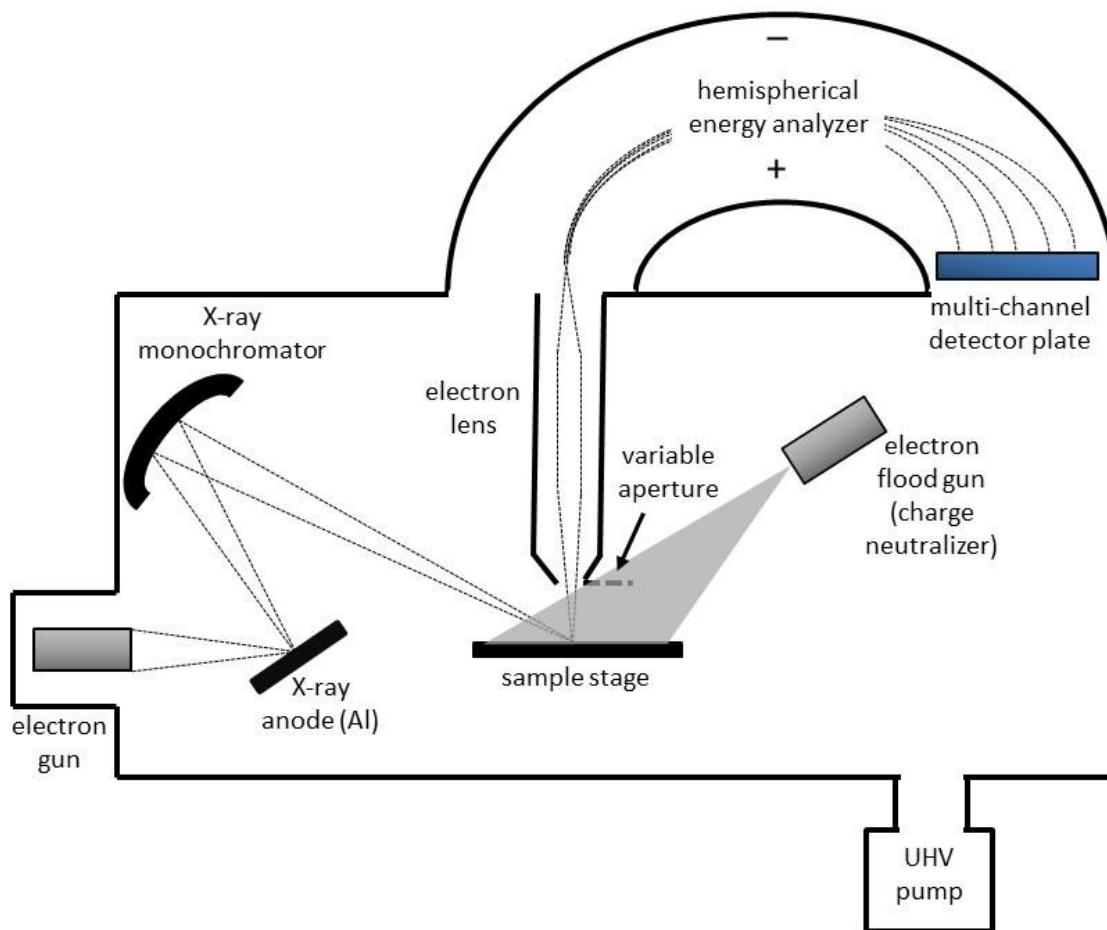


Figure 2.11 Diagram of the major components in an XPS instrument (adapted from Vickerman and Gilmore, 2009).¹³⁵

2.2.3 Data Analysis

Prior to fitting the experimental XPS spectrum, the background was subtracted using a Shirley function.¹³⁹⁻¹⁴¹ Each peak was fit using the instrument software (CasaXPS 2.3.14) by a Voigt function which can be defined as:¹⁴²

$$GL(x; w, x_0, m) = \exp\left(-4 \ln 2(1 - m) \frac{(x-x_0)^2}{w^2}\right) / \left(1 + 4m \frac{(x-x_0)^2}{w^2}\right), \quad (2.9)$$

where G stands for Gaussian, L for Lorentzian, x_0 is the peak center, w is the half-width at half maximum (HWHM), and m is the Gaussian-to-Lorentzian mixing ratio which is determined by:

$$m = P/100, \quad (2.10)$$

where P is the percentage of Lorentzian component, such that $GL(0)$ and $GL(100)$ represent pure Gaussian and Lorentzian functions, respectively. In the present study, $GL(60)$ was used for nearly all fitted peaks, with the exception of Ag fitted peaks which were usually fit using $GL(90)$.

The work function in Eq. (2.4) is that of the spectrometer since the sample was placed in electrical contact with the spectrometer.¹³⁵ ϕ_{sp} is calibrated using gold, and silver standards and adjusted until the known BE values are obtained. Once the peaks have been fit, the relative compositions of the standards were estimated by calculating the peak area under each component peak using the instrument software package. The intensity of the XPS signal is found using:¹³⁵

$$I_{ij} = KT(KE)L_{ij}(\gamma)\sigma_{ij} \int_0^d n_i(z) e^{-z/\lambda(KE)\cos\theta} dz, \quad (2.11)$$

where I_{ij} is the area of the peak j from element i , K is an instrumental constant, $T(KE)$ is the transmission function of the analyzer, $L_{ij}(\gamma)$ is the angular asymmetry factor for

orbital j of element i , σ_{ij} is the photoionization cross-section of peak j from element i , $n_i(z)$ is the concentration of element i at a distance z below the surface, $\lambda_{ij}(KE)$ is the inelastic mean free path length of peak j from element i , and θ is the take-off angle of the photoelectrons measured with respect to the surface normal, which is zero in this study.¹³⁵

If it can be assumed that the elemental concentrations are homogeneous within the sampling depth (from 0 to d) (the concentration is independent of the distance z), then Eq. (2.11) can be integrated to give:

$$I_{ij} = KT(KE)L_{ij}(\gamma)\sigma_{ij}n_i\lambda(KE)\cos\theta\left(1 - \exp\left(-\frac{d}{\lambda(KE)\cos\theta}\right)\right). \quad (2.12)$$

Further assuming a sampling depth much greater than the electron mean free path (typically, $d \geq 3\lambda$), then the exponential factor in Eq. (2.12) can be neglected. The area of a peak then becomes:

$$I_{ij} = KT(KE)L_{ij}(\gamma)\sigma_{ij}n_i\lambda(KE)\cos\theta. \quad (2.13)$$

Areas are divided by the relative sensitivity factor (RSF) of the atom, which is found during calibration of the instrument. This method ensures that the counts detected from one part of the spectral range may be compared against other areas of the spectral range and further may be compared across different instruments. Binding energies and RSF values for the regions scanned in this study are found in Table 2.5. The scaled area

under the curve for each section of this work is found in the respective sections. Typically, elemental ratios (n_i/n_k) or atomic percentages ($\%n_i$) are given due to the inexactness of the peak analysis. This ratio has the advantage that many of the constants and instrumental factors found in Eq. (2.5) can be cancelled out. The atomic percent of element i ($\%n_i$) is found by:

$$\%n_i = 100(n_i/\sum n_i). \quad (2.14)$$

The units for the y -axis in XPS spectra are generally given as counts per second (CPS) which is a measure of intensity.¹³⁵ CPS has not been normalized or adjusted by RSFs and is the intensity measured by a counting detector.

A clean, polished silver sample was used to calculate an error associated with the XPS technique. The sample was etched with argon ions while in the vacuum chamber until the carbon (C 1s) peak was sufficiently reduced to be indistinguishable from the noise. This sample was scanned multiple times each day for several days in one month. The area under the curve was calculated as described above. The error within one day was around 1% and the error of all measurements for the month was around 4%. This shows that although it is better to take measurements in one day, the error associated with scanning the samples over different days is relatively insignificant. The calculation and values used are given in Appendix D. This means that even though exact intensity on samples cannot be directly compared, approximate intensities may. CPS is not considered an arbitrary unit in this thesis due to a lack of an internal standard.

Table 2.5 Relative sensitivity factors (RSF) and binding energies for the regions of interest investigated in the present work. These values were found during instrument calibration.

Element	RSF	Scanned region (eV)
Ag 3d	5.721	380 – 360
C 1s	0.278	290 – 275
N 1s	0.477	415 – 385
O 1s	0.780	540 – 525
Na 1s	1.685	1080 – 1060
Mg 1s	0.157	1313 – 1293
S 2p	0.668	180 – 150
Cl 2p	0.851	210 – 190
K 2p	1.409	310 – 290
Ca 2p	1.767	356 – 340

3. Existence of Ag_2SO_3 and Ag_2SO_4 on Field-Exposed Silver

This chapter focuses on the detection of silver sulfate (Ag_2SO_4) and silver sulfite (Ag_2SO_3) on field-exposed silver samples with X-ray photoelectron spectroscopy (XPS). In contrast, existing literature does not consider Ag_2SO_4 and Ag_2SO_3 to be major corrosion products.¹⁰⁰ The mechanism for the formation of Ag_2SO_4 in the field is not yet known, but this study presents evidence which suggests Ag_2SO_3 is the intermediate that is then further oxidized to form Ag_2SO_4 .

3.1 Introduction

Chapter 1 described the various species and parameters which have an impact on the corrosion of metals, specifically in regards to silver corrosion. Since outdoor corrosion is such a complex system, it is necessary to perform lab tests which employ only parameters that can be controlled. The ensuing corrosion rates may then be compared against the corrosion rates of other materials or environments. However, as was mentioned earlier, many of these lab tests are oversimplified in the parameters which are chosen to represent the outdoor environment. This oversimplification leads to results which do not wholly represent the real environment but are still used as a means to screen materials before they undergo more realistic, lengthy, and costly analysis. Lab tests also allow mechanistic studies of individual or coupled parameters which are important to outdoor exposures. Silver exhibits a discrepancy when comparing lab to field-exposed

samples. Therefore, silver is a good material to test which parameters are different between the lab and field.

All experimental parameters are detailed in Chapter 2.

3.2 Results

3.2.1 *New Hampshire*

Silver samples exposed in New Hampshire were analyzed by XPS upon receipt; pictures of the samples are shown in Figure 3.1. The sulfur 2p region scans are shown in Figure 3.2. The colors of all spectra shown are: black, red, green, blue, and purple which correspond to 1, 2, 3, 4, and 6 months respectively. Spectra taken on the unsheltered and sheltered samples exposed at Thompson Farm are on the top left and right, respectively. Spectra from the unsheltered and sheltered samples exposed at Appledore Island are on the bottom left and right, respectively.

There are four peaks (two doublets) present in all of the graphs. The energy of the doublet at lower binding energy is the same energy for all spectra. Literature XPS values for common silver corrosion products are given in Table 2.3. The primary peak is observed at 161.0 eV with a doublet at 162.2 eV, this is consistent with literature values of Ag_2S . The energy of the doublet at higher binding energy is different for the farm and island exposed samples. The doublet for the samples exposed at the farm is observed at 167.3 and 168.5 eV. For the island-exposed samples this doublet is shifted to 168.6 and 169.8 eV. These peaks at 167.3 and 168.6 eV are consistent with expected binding energies of Ag_2SO_3 and Ag_2SO_4 , respectively. The sulfur region scan reveals the

existence of Ag_2S , Ag_2SO_4 and Ag_2SO_3 . However, the silver and oxygen region scans shown in Appendix F are below spectral resolution and thus cannot be used to confirm the presence of these species.

Although it is not valid to compare peak intensities from different samples, it is possible to compare the intensity of the doublet associated with Ag_2S to that of Ag_2SO_4 or Ag_2SO_3 within the same spectrum; these are shown as insets on Figure 3.2. It is clear that the ratios of sulfate/ sulfide and sulfite/sulfide vary over time. The change in the ratio of these species is consistent with a changing corrosion film. Contrary to intuition which might assume a linear growth in the abundance of more oxidized species on the surface over time, this is not observed here. Instead, on the Farm exposed samples, the ratio between SO_3^{2-} and S^{2-} decreases initially, then dramatically increases during the third month and then decreases again. On the Island exposed samples, the second month shows a dramatic increase in the ratio between SO_4^{2-} and S^{2-} again decreasing over time. XPS analysis reveals the composition at the surface and comparing ratios gives information about the relative amounts of species in the top 10 nm of the surface film.

Recall from Chapter 2 that intensities for spectra collected on the same day are comparable within 1%. Therefore, all of the spectra from the same month are comparable since they were analyzed on the same day. By comparing the spectra from the 3 month exposed samples (green trace), differences between the farm and island as well as between sheltered and unsheltered samples are observed. Based on intensities and ratios in Figure 3.2, the sheltered farm samples have more sulfite than the unsheltered farm samples. The amount of sulfate from the island is greater on the unsheltered than

sheltered samples. Also the amount of sulfate on the island samples is greater than the amount of sulfite on the farm samples.

A typical method for analyzing corrosion products is galvanic reduction. This technique was described in Chapter 2. Figure 3.3 and Figure 3.4 show the reduction curves for the samples exposed in New Hampshire, as collected by Huang Lin.¹³¹ The potential at which a plateau occurs indicates the identity of the species. A list of these potentials is given in Table 2.2. The samples all have a plateau which can be attributed to AgCl (between -0.25 and -0.4 V_{MSE}) and most samples also have the plateau for Ag₂S (-1.2 V_{MSE}). Only the sheltered samples from Thompson Farm have plateaus at a higher potential than AgCl. This is at -0.04 for the 4 month sample and at -0.09 for the 6 month sample. The identity of this species is not known in the literature, so this technique cannot confirm whether or not Ag₂SO₃ or Ag₂SO₄ are present on these samples.

X-ray diffraction (XRD) was performed on a clean piece of silver. This sample was polished and handled in the same manner as those which were exposed in New Hampshire. The spectrum is shown in Figure 3.5, the black trace is the spectrum from the silver sample and the red lines are reference values.¹⁴³ The numbers on top of the peaks indicate the crystal orientation and those below are the peak positions. Using TOPAS Academic V4.1 for fitting, a slight preferred orientation for the (220) orientation is calculated. Literature values for (200) and (220) gives a ratio for (220)/(200) of ≈ 0.617 .¹⁴⁴ Whereas the fitting program yields a ratio for (220)/(200) of ≈ 0.878 . However, these values are close, so if there is a preferred surface orientation, it is only slight. The

(100) and (110) faces are not observed since they are forbidden by diffraction rules; for n, k, l , all must be even or odd.¹⁴⁵

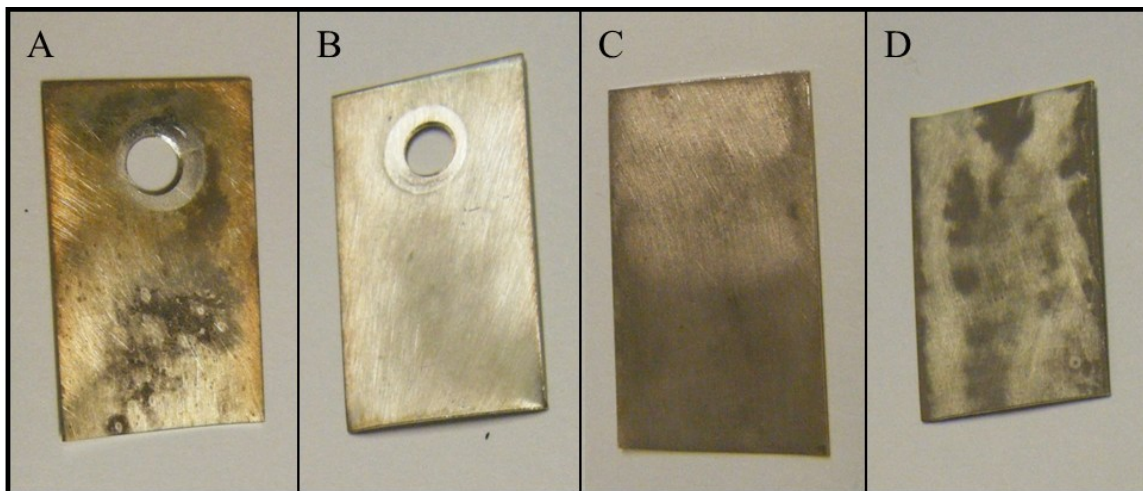


Figure 3.1 Pictures of New Hampshire silver samples after six months of exposure beginning in October 2010. (A) Thompson Farm sheltered, (B) Thompson Farm unsheltered, (C) Appledore Island sheltered, (D) Appledore Island unsheltered.

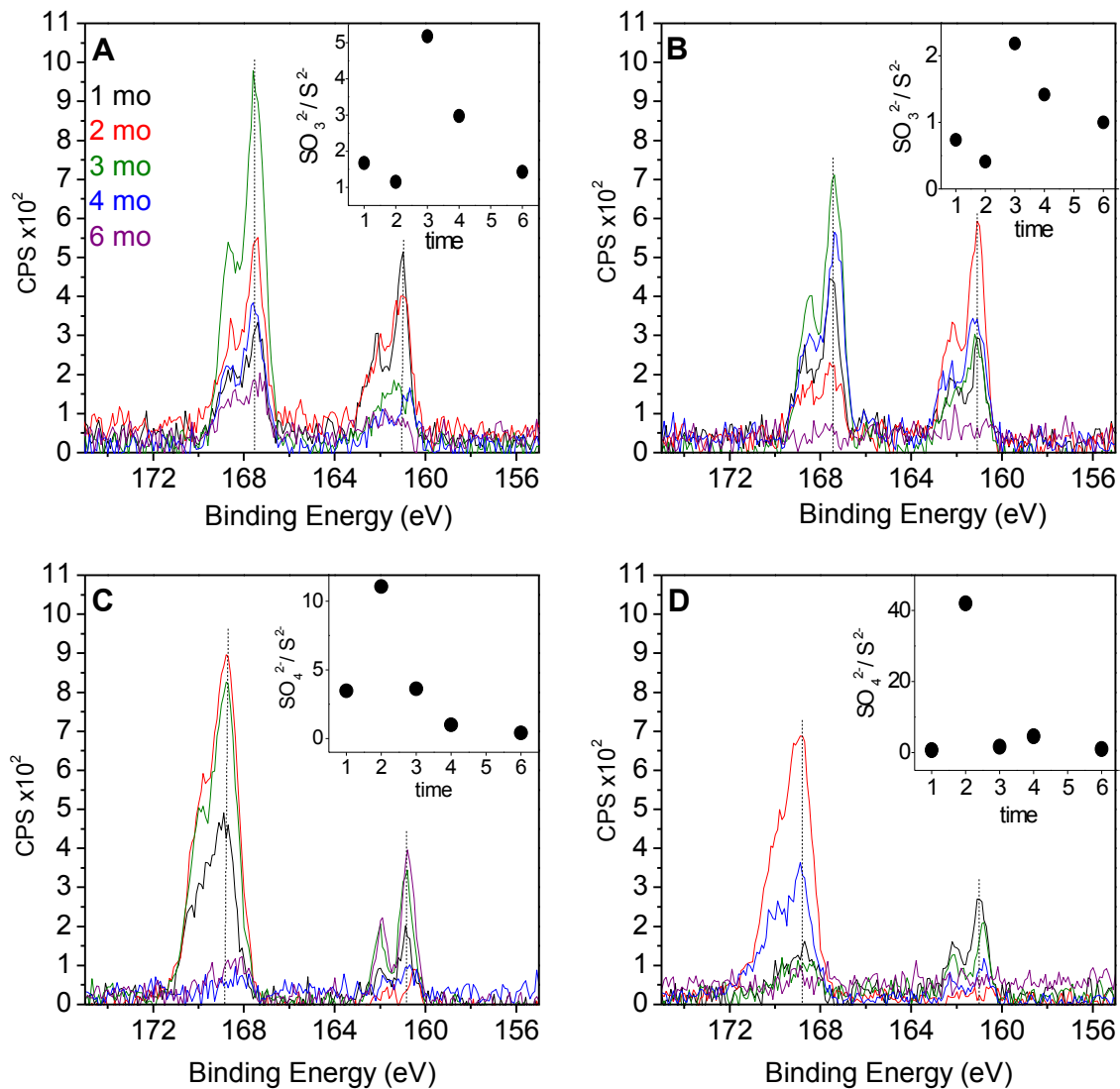


Figure 3.2 Sulfur 2p region scan of all samples exposed at Thompson Farm, NH (A & B) and Appledore Island, ME (C & D). Samples were exposed to both sheltered (A & C) and unsheltered (B & D) conditions. Black, red, green, blue, and purple spectra correspond to 1, 2, 3, 4, and 6 month exposures, respectively. Insets compare the ratios of SO_4^{2-} to S^{2-} on each sample.

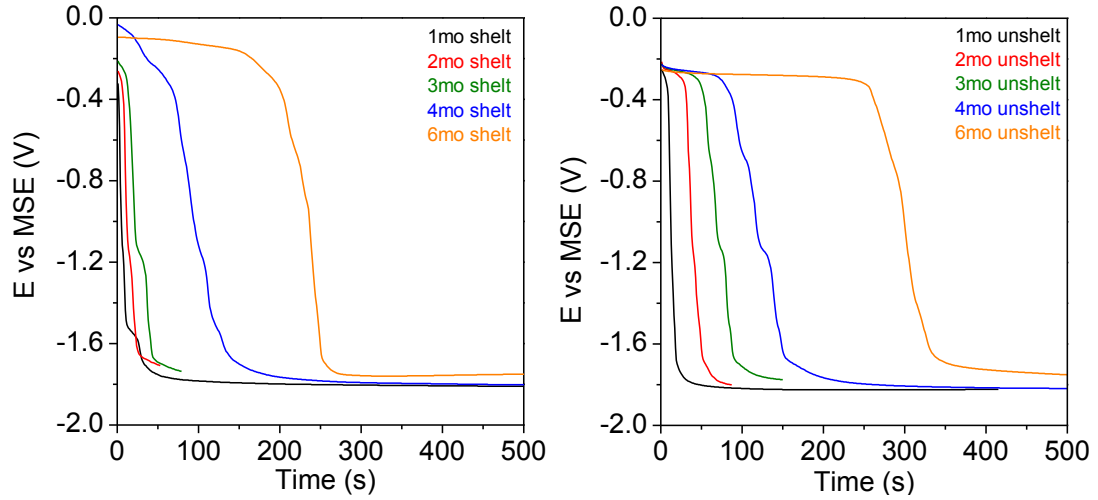


Figure 3.3 Reduction curves for samples exposed at Thompson Farm, sheltered (left) and unsheltered (right). Data courtesy of Huang Lin.¹³¹

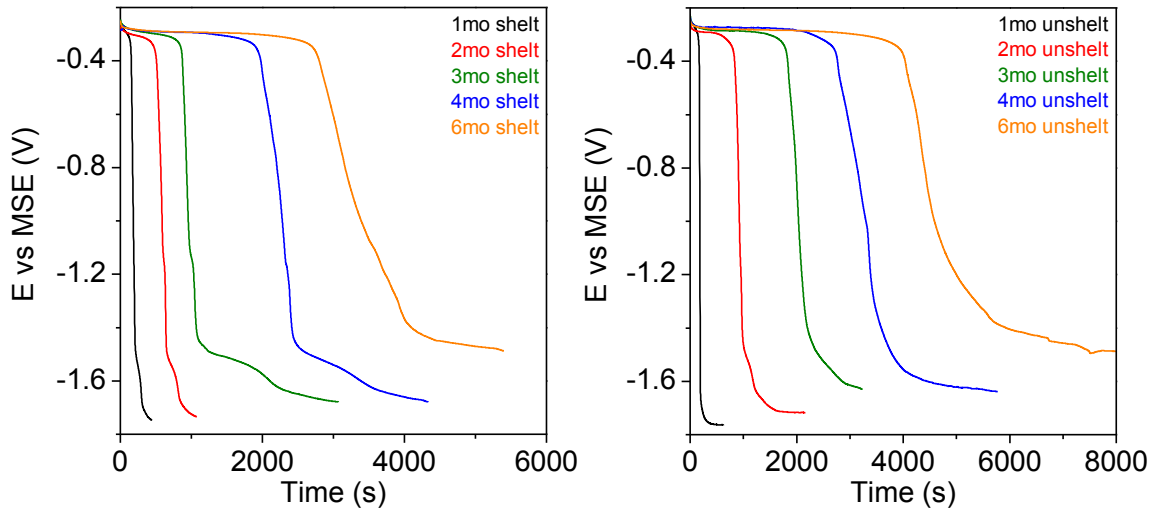


Figure 3.4 Reduction curves for samples exposed at Appledore Island, sheltered (left) and unsheltered (right). Data courtesy of Huang Lin.¹³¹

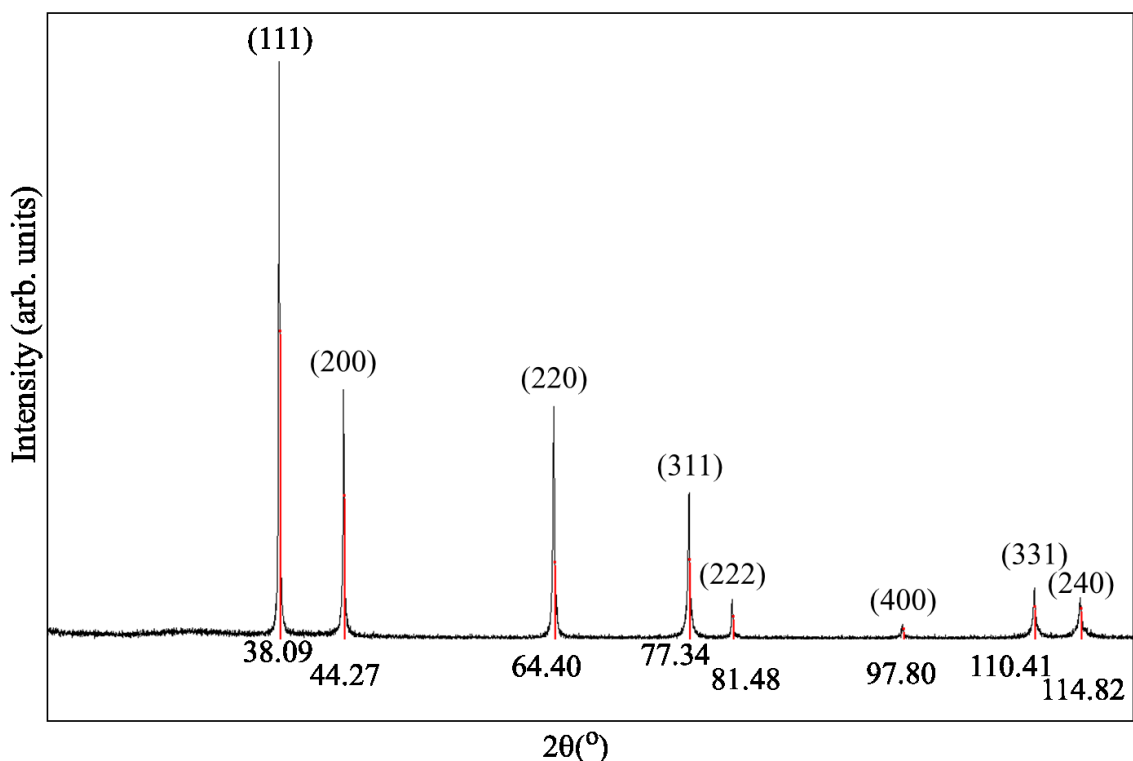


Figure 3.5 X-ray Diffraction (XRD) spectrum of polished, clean silver sample identical to those used in New Hampshire exposures. Black trace is the collected spectrum, red lines are database values,¹⁴³ numbers on the top indicate the crystal face, numbers on bottom are the peak positions.

3.2.2 Hawaii

Samples which were received from Hawaii are shown in Figure 3.3. The samples were analyzed by XPS upon receipt, the sulfur 2p spectra are given in Figure 3.4. The black, red, and green traces are the 1 month, 3 month, and 6 month samples. The sheltered and unsheltered samples exposed at Kaneohe marine air base (MAB) are on the top left and right, respectively. Sheltered and unsheltered samples from Kilauea Volcano sheltered and unsheltered are in the middle on the left and right, respectively. Lastly, the

sheltered and unsheltered samples from Mauna Loa are on the bottom on the left and right, respectively.

The peaks from these Hawaiian samples in Figure 3.4 are similar to those in Figure 3.2 from New Hampshire. The doublets are at 168.6 and 169.8 eV and at 161.0 and 162.2 eV. These doublets are assigned to Ag_2SO_4 and Ag_2S , respectively. The one month volcanic unsheltered sample appears to show evidence of Ag_2SO_3 with a peak around 167.5 eV, but is hard to resolve due to the poor signal to noise resolution. In order to look at the trends on different samples, the ratios of Ag_2SO_4 to Ag_2S are plotted as insets on Figure 3.4. The only obvious amount of Ag_2S was observed on the volcanic unsheltered sample.

The 3 and 6 mo volcanic samples had a vertical striping pattern with very dark in the center, white on both sides of that and dark again near the edges, as seen in Figure 3.3. Thus, scans were run on these sections in order to identify the species in each stripe, Figure 3.5 shows the spectra which were taken in these different regions. The one month sample was homogeneous to the eye, so only one scan was taken. On the three month sample, a scan was taken on the dark center (black trace) and on the white stripe (red trace). The six month sample, scans were taken on the dark center, white stripe, and dark edge; black, red, and green traces, respectively.

The cause of this striping phenomenon is still unknown. It should be noted that there was volcanic activity at this site three days after the samples were placed on the test rack. The Kamoamoa Fissure Eruption began on March 6, 2011.^{120,121} The sputter from the eruption reached 100 feet into the air and nearby vegetation including trees were

ignited resulting in biomass burning. This eruption and emission of atmospheric gases and particulates may have caused the striping on the samples. By allowing more water adsorption on the surface this may have led to product transport vertically down the surface, but this is purely a conjecture.

Galvanostatic reduction was performed on the samples exposed at these locations by Huang Lin.¹³¹ The results are given in Figure 3.10, Figure 3.11, and Figure 3.12. Kaneohe and Kilauea have plateaus which are consistent with AgCl, -0.25 to $-0.4 V_{MSE}$. Kaneohe has Ag₂S on the 6 month samples, at $-1.2 V_{MSE}$. The sample from Mauna Loa does not have a plateau associated with AgCl, instead the plateau is consistent with the Ag₂O potential in the literature, -0.12 to $-0.18 V_{MSE}$.¹ This is the first report of Ag₂O on field-exposed silver by reduction analysis.

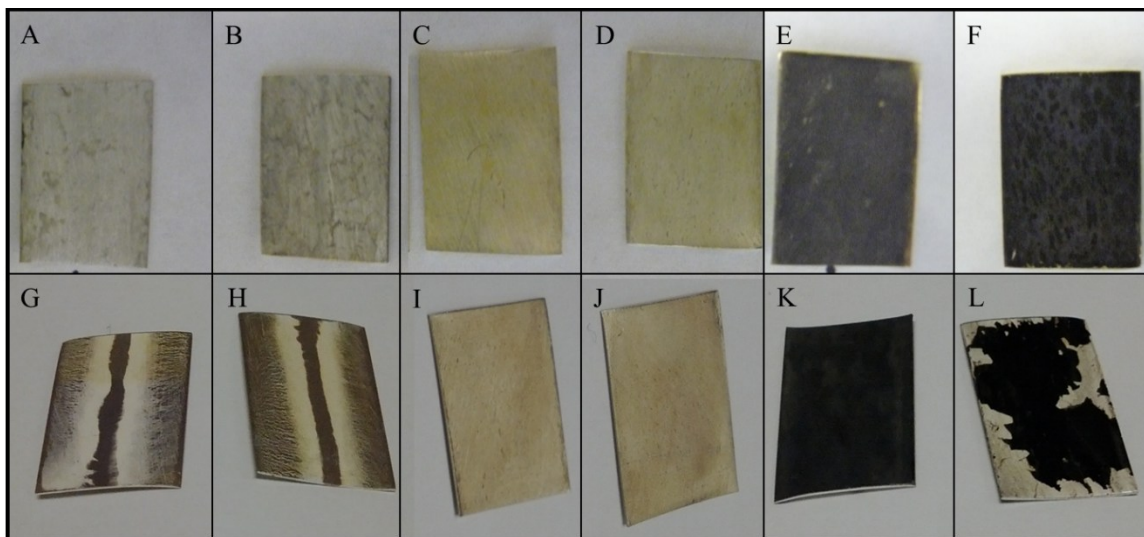


Figure 3.6 Pictures of silver samples exposed in Hawaii beginning in March 2011 after exposure, 1 month (A-F) and 6 months (G-L) are shown. Kilauea Volcano sheltered (A & G), unsheltered (B & H), Kaneohe MAB sheltered (C & I), unsheltered (D & J), Mauna Loa sheltered (E & K), unsheltered (F & L).

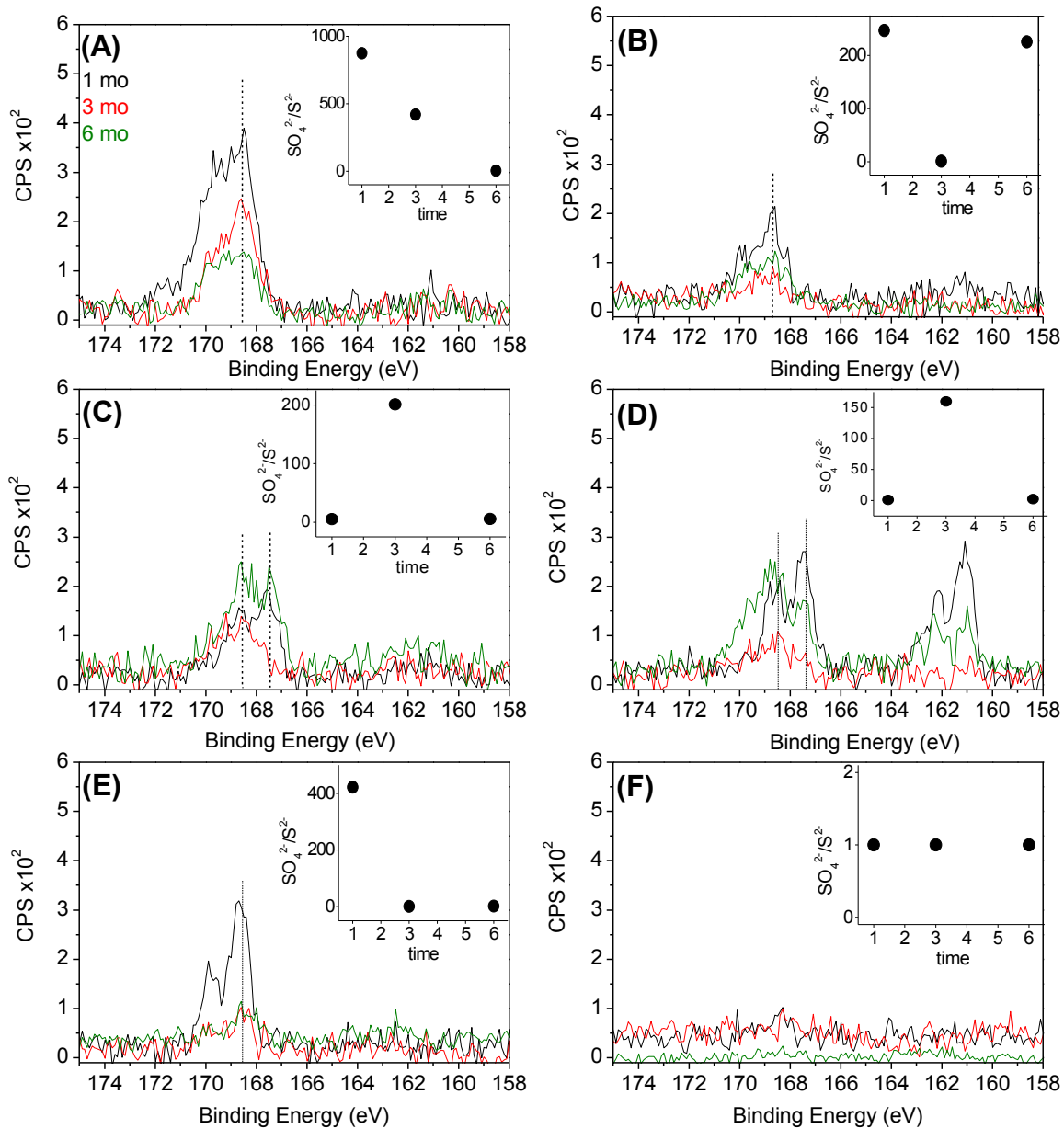


Figure 3.7 Sulfur 2p region scan of all samples exposed at Kaneohe MAB (A & B), Kilauea Volcano (C & D), and Mauna Loa Observatory (E & F) in Hawaii. Samples were exposed under both sheltered (A, C, & E) and unsheltered (B, D, and F) conditions. Black, red, and green spectra correspond to 1, 3, and 6 month exposures, respectively. Insets compare the ratios of SO_4^{2-} to S^{2-} on each sample.

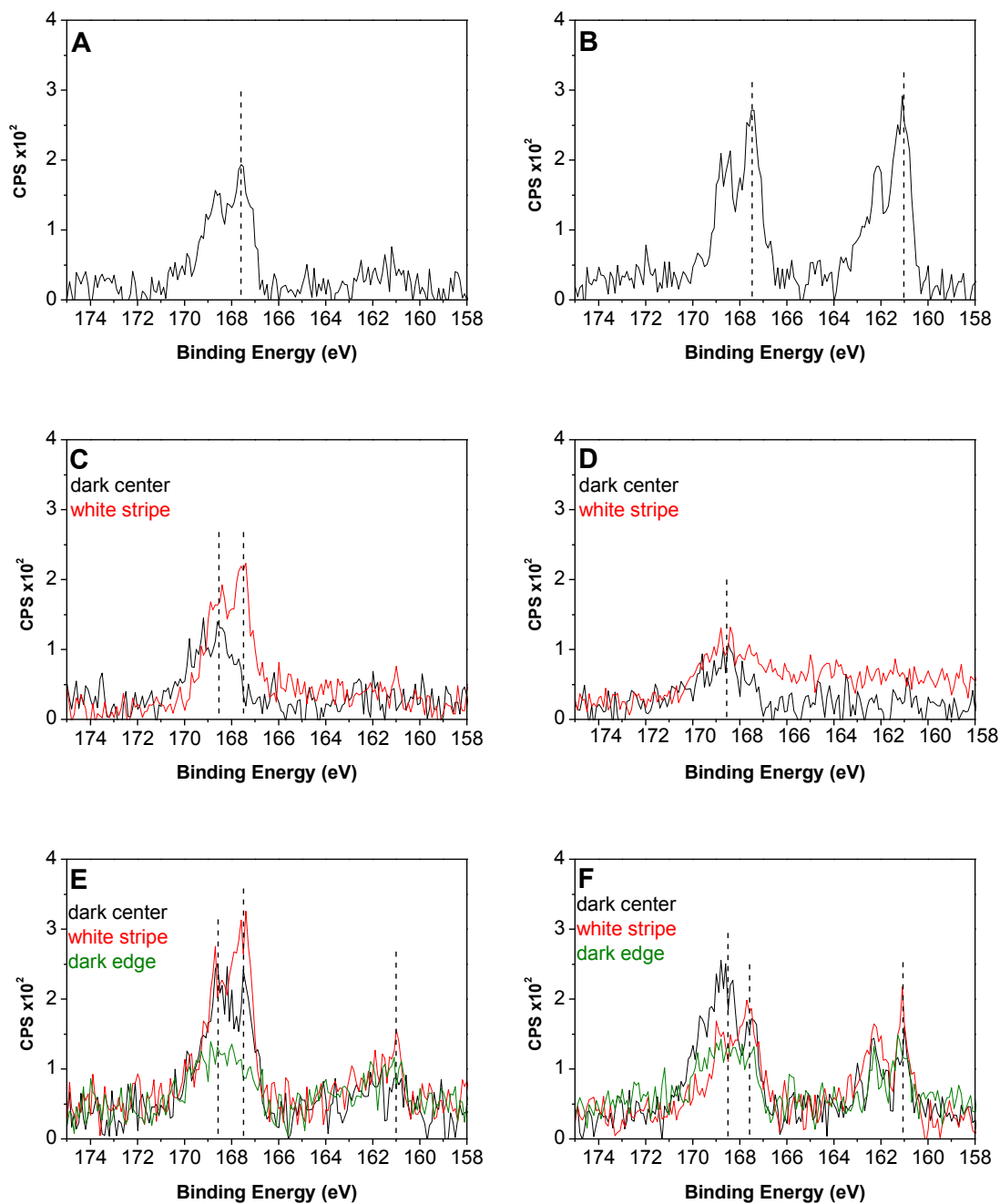


Figure 3.8 Sulfur 2p region of samples from Kilauea Volcano, 1 month (A & B), 3 months (C & D), and 6 months (E & F). A, C, & E are sheltered while B, D, & F are unsheltered.

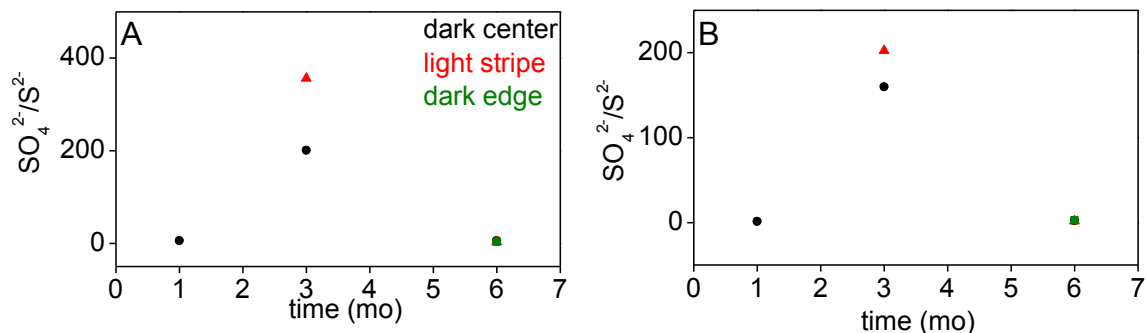


Figure 3.9 Ratios of SO_4^{2-} to S^{2-} on each sample exposed at Kilauea Volcano. Samples were exposed to both sheltered (A) and unsheltered (B) conditions.

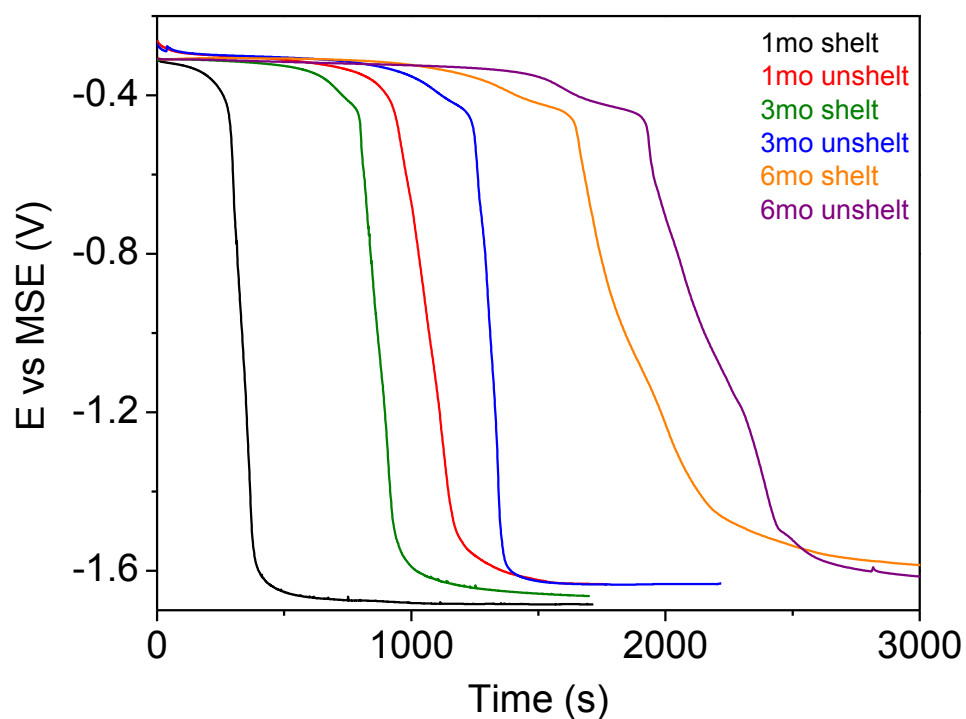


Figure 3.10 Galvanic reduction scans of samples exposed at Kaneohe MAB, sheltered and unsheltered. Data courtesy of Huang Lin.¹³¹

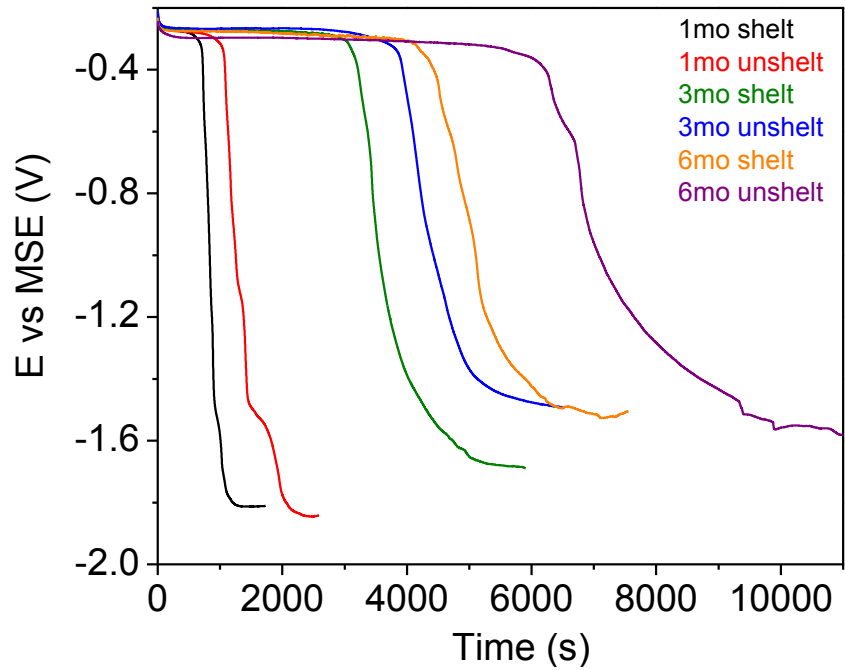


Figure 3.11 Galvanic reduction scans of samples exposed at Kilauea Volcano, sheltered and unsheltered. Data courtesy of Huang Lin.¹³¹

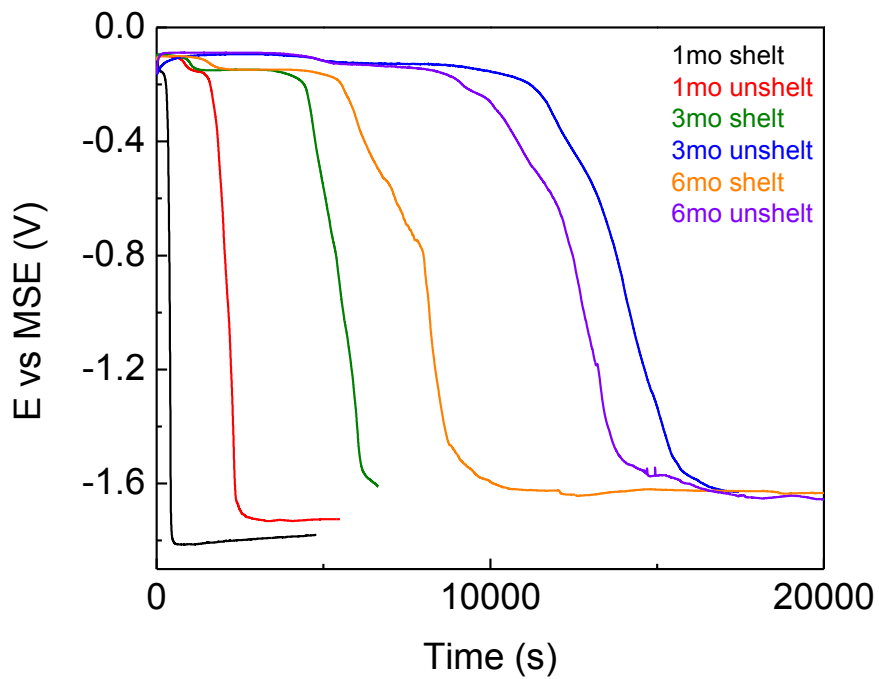


Figure 3.12 Galvanic reduction scans of samples exposed at Mauna Loa, sheltered and unsheltered. Data courtesy of Huang Lin.¹³¹

3.2.3 *U.S.A. and Antarctica Single Measurements*

Samples were exposed for 3 months at nine locations across the United States, and one in Antarctica for 2 years, Figure 3.13 shows pictures of the samples after exposure. These samples were not duplicated and are therefore referred to as “single measurements.” Sulfur (S 2p) spectra are shown in Figures 3.14-3.17. Most samples were scanned at two locations on the surface. Spot A was a darker area whereas Spot B was slightly lighter, to the eye. In addition, the samples were rinsed with deionized water and dried with nitrogen gas. This rinsing process was repeated three times. The sample was then rescanned on approximately the same spot as Spot A, a dark section of the sample. Only Randolph and West Jefferson were not scanned in a second location before rinsing. The black spectrum in these figures is spot A, unrinsed. The red spectrum is spot A, rinsed. The green spectrum is spot B, unrinsed.

The sample from Antarctica was scanned upon initial receipt and again 2 years later. Time A unrinsed and Time B unrinsed were taken on approximately the same spot. Time A was upon receiving the sample and Time B was taken two years later. The sample was kept in a sealed glass vial in the containment box shown in Chapter 2. The rinsed and unrinsed sample scans were on a different piece of the sample, but which looked similar to the eye. The sulfate decreases with rinsing and increases slightly with time in the vial. The sulfide appears to remain consistently low across all three spectra.

The peaks from these exposures correlate well with the other samples discussed earlier. Coconut Island and Lyon Arboretum have a doublet at 161.0 and 162.2 eV which corresponds to Ag_2S . Coconut Island, Conroe, Daytona, West Jefferson, Whidbey, and

McMurdo have a doublet at 168.6 and 169.8 eV which is consistent with Ag_2SO_4 . Randolph & Woodstock have a doublet at 167.3 and 168.5 eV which is assigned to Ag_2SO_3 . The sample from Lyon Arboretum had no evidence of Ag_2S , Ag_2SO_3 , or Ag_2SO_4 .

The ratios of either Ag_2SO_4 or Ag_2SO_3 are shown in Figure 3.18, except for Coconut Island and Lyon Arboretum which had no appreciable amount of Ag_2S . As opposed to the New Hampshire samples which had more sulfate than sulfite, these samples show that sulfite can be greater than sulfate. If nothing else, this finding demonstrates that the ratios of $\text{SO}_3^{2-}/\text{S}^{2-}$ and $\text{SO}_4^{2-}/\text{S}^{2-}$ are highly dependent on the location of exposure.

These single point measurements were not reduced by Huang Lin, as the samples from New Hampshire and Hawaii were. However, these samples were reduced by William Abbott at Battelle and these values are given in Table 2.1. Only AgCl and Ag_2S were reported for these samples. The absence of sulfite or sulfate is consistent with the measurements of the samples from New Hampshire and Hawaii.

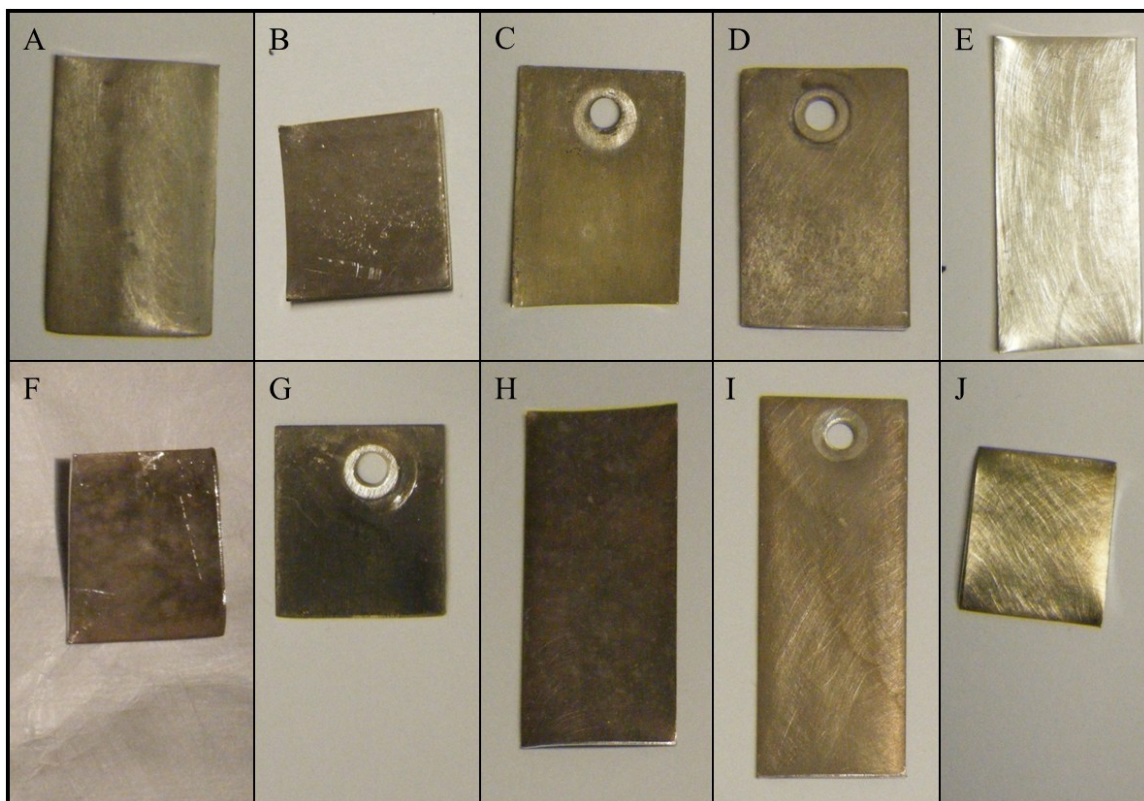


Figure 3.13 Pictures of silver samples exposed across the USA and Antarctica. All samples were exposed for 3 months, except Antarctica which was exposed for 2 years. (A) Coconut Island, HI, (B) Conroe, TX, (C) Daytona Beach, FL, (D) Long Island, NY, (E) Lyon Arboretum, HI, (F) McMurdo Station, ANT, (G) Randolph AFB, TX, (H) West Jefferson, OH, (I) Whidbey Island, WA, (J) Woodstock, ME.

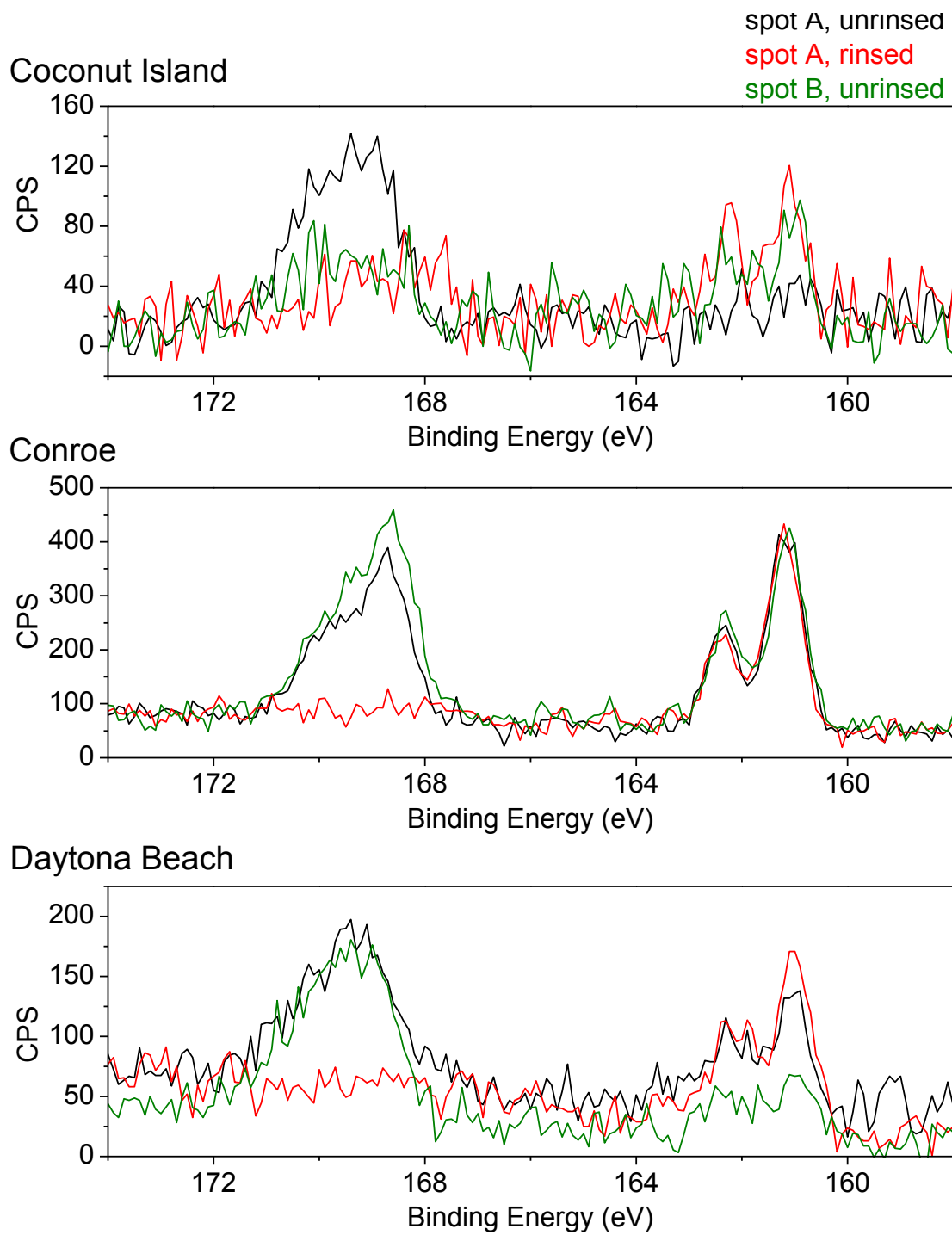


Figure 3.14 XPS spectra of the S 2p region for the sample exposed at Coconut Island, HI (top), Conroe, TX (middle), and Daytona Beach, FL (bottom). Spot A, unrinsed (black) and Spot A, rinsed (red) were taken on a portion of the sample which was slightly darker than Spot B, unrinsed (green).

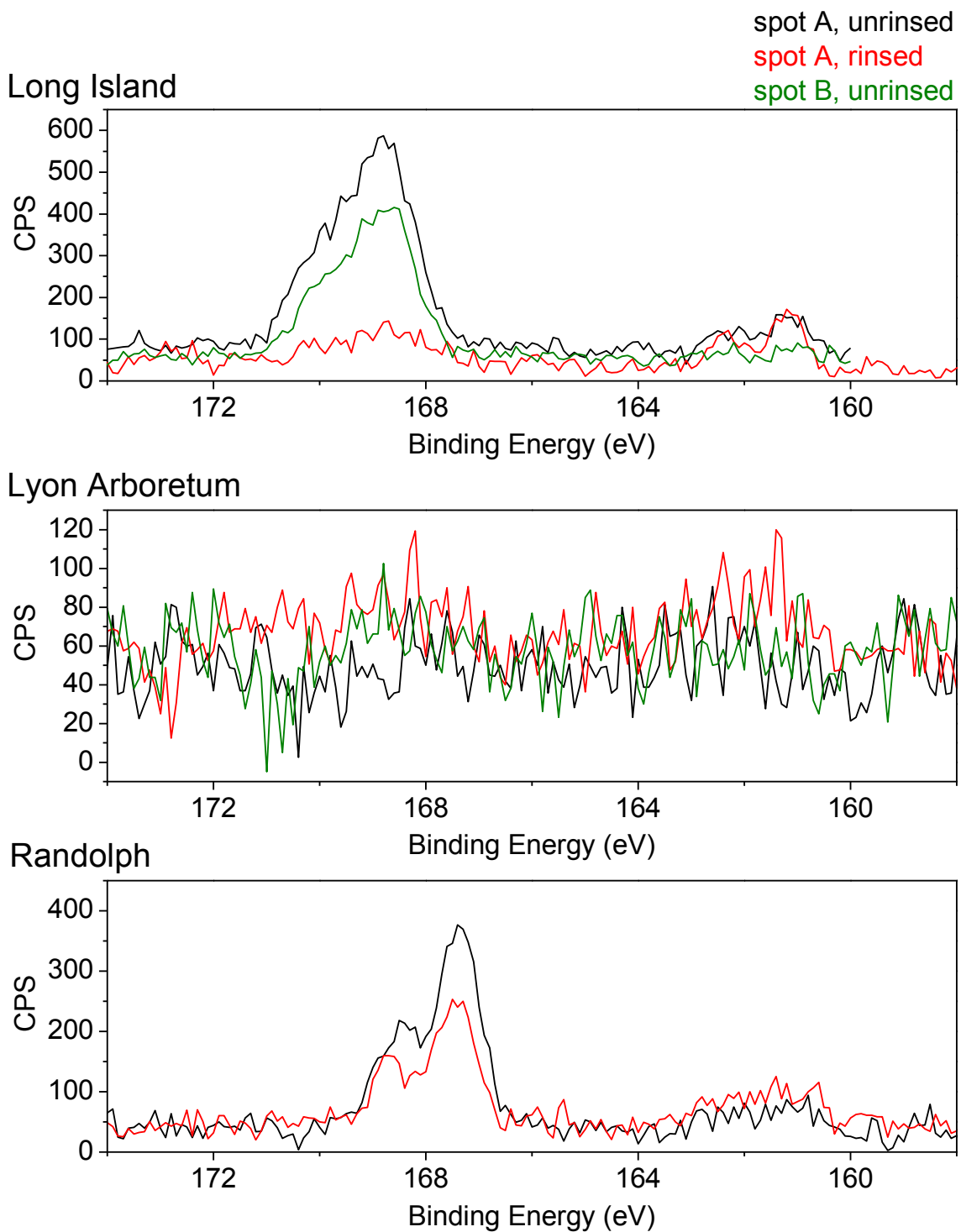


Figure 3.15 XPS spectra of the S 2p region for the samples exposed at Long Island, NY (top), Lyon Arboretum, HI (middle), and Randolph, TX (bottom). Spot A, unrinsed (black) and Spot A, rinsed (red) were taken on a portion of the sample which was slightly darker than Spot B, unrinsed (green).

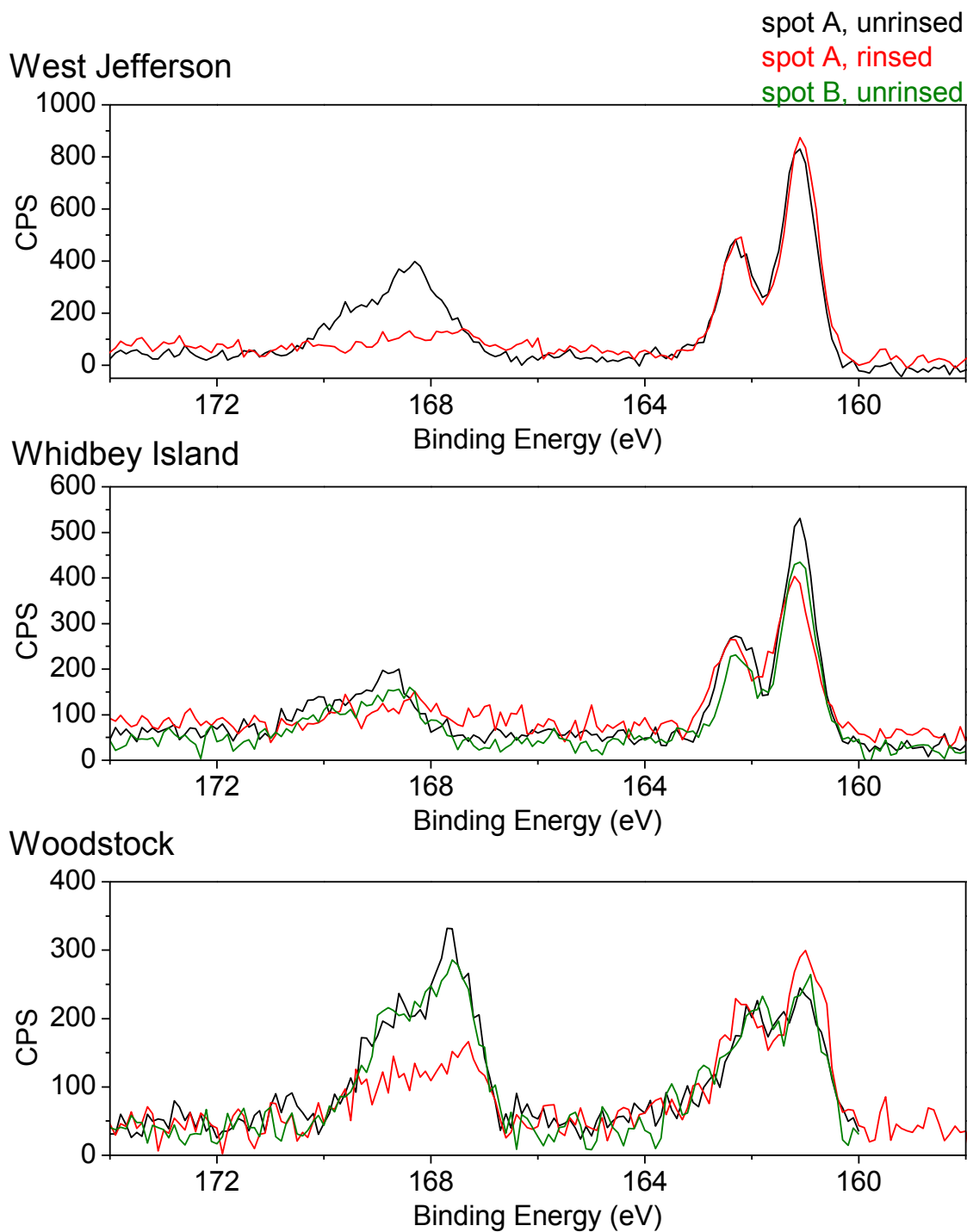


Figure 3.16 XPS spectra of the S 2p region for the sample exposed at West Jefferson, OH (top), Whidbey Island, WA (middle), and Woodstock, ME (bottom). Spot A, unrinsed (black) and Spot A, rinsed (red) were taken on a portion of the sample which was slightly darker than Spot B, unrinsed (green).

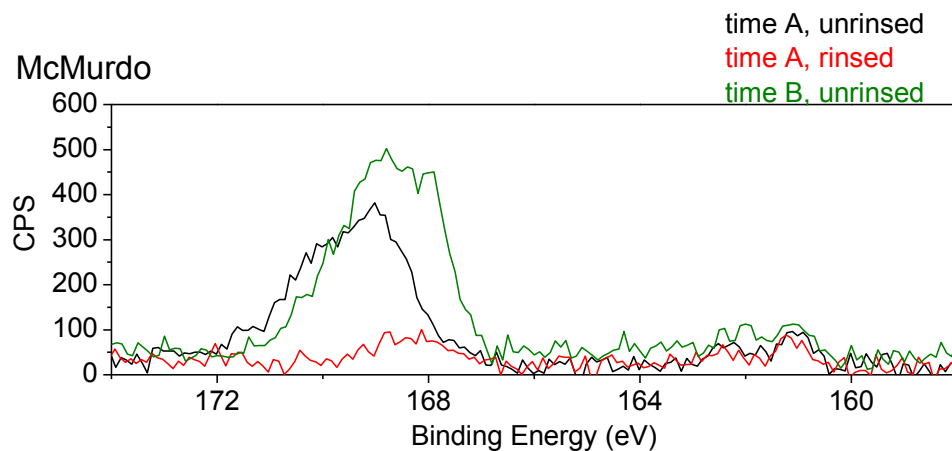


Figure 3.17 XPS spectra of the S 2p region for the sample exposed at McMurdo Station, Antarctica. Time A, unrinsed (black), time A, rinsed (red), and time B, unrinsed (green) are shown. Time B was almost 2 years after Time A.

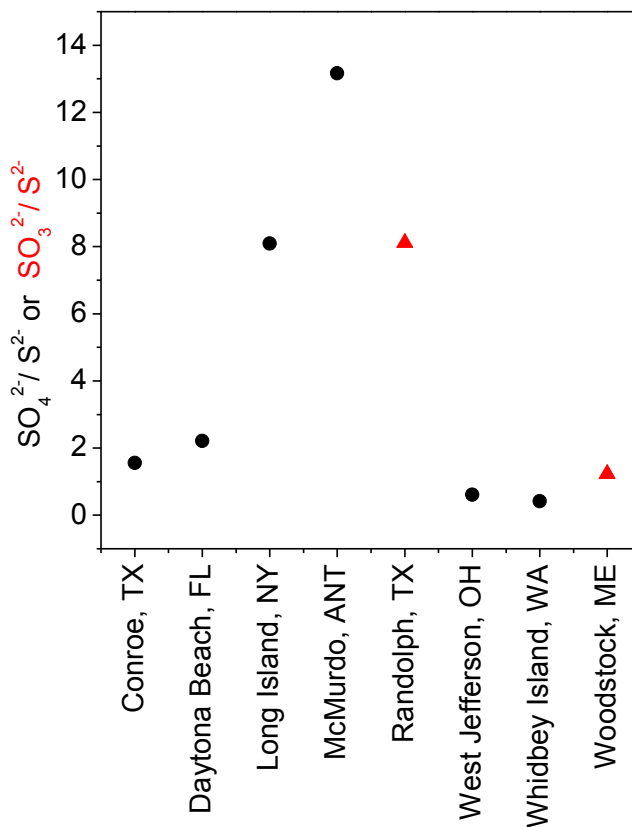


Figure 3.18 Ratio of $\text{SO}_4^{2-}/\text{S}^{2-}$ (black circles) or $\text{SO}_3^{2-}/\text{S}^{2-}$ (red triangles) on single samples exposed across the U.S.A. and Antarctica. These values were taken from Spot A, unrinsed spectra shown in Figures 3.14-3.17. Note: Coconut Island, HI and Lyon Arboretum, HI are not shown because there was no sulfide detected in these scans.

3.2.4 Lab-Created Samples

This chapter focuses on the detection of Ag_2SO_4 on field-exposed samples which were analyzed with XPS. In order to better understand how Ag_2SO_4 may be formed, an attempt was made to generate Ag_2SO_4 by exposure of Ag to H_2SO_4 in the lab. One sample was polarized at $+0.7 V_{\text{MSE}}$ for 15 s in 0.1 M H_2SO_4 and the formation charge was 280 mC/cm^2 . Formation charge refers here to the total charge on the Ag sample during formation of Ag_2SO_4 . Another sample was galvanostatically oxidized at $+0.025 \text{ mA/cm}^2$ for 600 s in 0.1 M H_2SO_4 with a formation charge of 15 mC/cm^2 .

The galvanic reduction (performed by Huang Lin¹³¹) and XPS spectra are shown in Figure 3.19 and Figure 3.20, respectively. The black trace is a sample which was polarized at $+0.7 V_{\text{MSE}}$ for 15 seconds in 0.05 M H_2SO_4 . The red trace is a sample which was galvanostatically oxidized at $+0.025 \text{ mA/cm}^2$ for 600 sec in 0.1 M H_2SO_4 . According to the XPS results, both methods were able to form Ag_2SO_4 , but reduction was not able to detect Ag_2SO_4 on either sample.

Ag_2S is another compound typically found on field-exposed silver samples. Seemingly the simplest way to form Ag_2SO_4 or Ag_2SO_3 would be to simply oxidize Ag_2S . To this end, a clean, polished silver sample was polarized in 0.1 M Na_2S for 1 s at $-0.13 V_{\text{MSE}}$. The sample was then exposed in dry conditions with 254 nm UV light (3.68 mW/cm^2), and 0.63 ppm O_3 for 38 hrs. Another sample was prepared in the same manner but was exposed for 22 hrs in 90% RH. Since it is likely that Ag_2O will also form under these conditions, two other samples were prepared to test the effect of Ag_2S on the formation of Ag_2O . One of these samples was polarized in 0.1 M Na_2S for 15 s at -0.13

V_{MSE} , while the other was not exposed to Na_2S at all. Both samples were then exposed to 5.5 ppm O_3 and 254 nm UV light (3.68 mW/cm^2) at 90% RH for 68 hrs.

The galvanic reduction (by Huang Lin¹³¹) and XPS spectra are given in Figure 3.21 and Figure 3.22, respectively. The black trace is a silver sample which was polarized in 0.1 M Na_2S for 1 s at $-0.13 V_{MSE}$, then exposed to 0% RH, 0.63 ppm O_3 and UV light for 38 hours. The red trace is a silver sample which was polarized in 0.1 M Na_2S for 1 s at $-0.13 V_{MSE}$, then exposed to 90% RH, 0.63 ppm O_3 and UV light for 22 hours. The blue trace is a silver sample which was polarized in 0.1 M Na_2S for 15 s at $-0.13 V_{MSE}$, then exposed to 90% RH, 5.5 ppm O_3 and UV light for 68 hours. The green trace is a silver sample which was not polarized in Na_2S ; it was exposed to 90% RH, 5.5 ppm O_3 and UV light for 68 hours. All samples were exposed to UV light at 254 nm with an intensity of 4 mW/cm^2 . XPS reveals Ag_2SO_3 formation on the black and blue samples and possibly Ag_2SO_4 on the red sample. There was no Ag_2S , Ag_2SO_3 or Ag_2SO_4 on the green sample. Reduction detected only Ag_2S on the red and black samples. The plateau for the green sample at a higher potential is associated with Ag_2O . The blue sample shares this plateau as well as another at higher potential which may be associated with sulfite or sulfate. However, the potential of Ag_2SO_3 and Ag_2SO_4 are not widely reported in the literature.

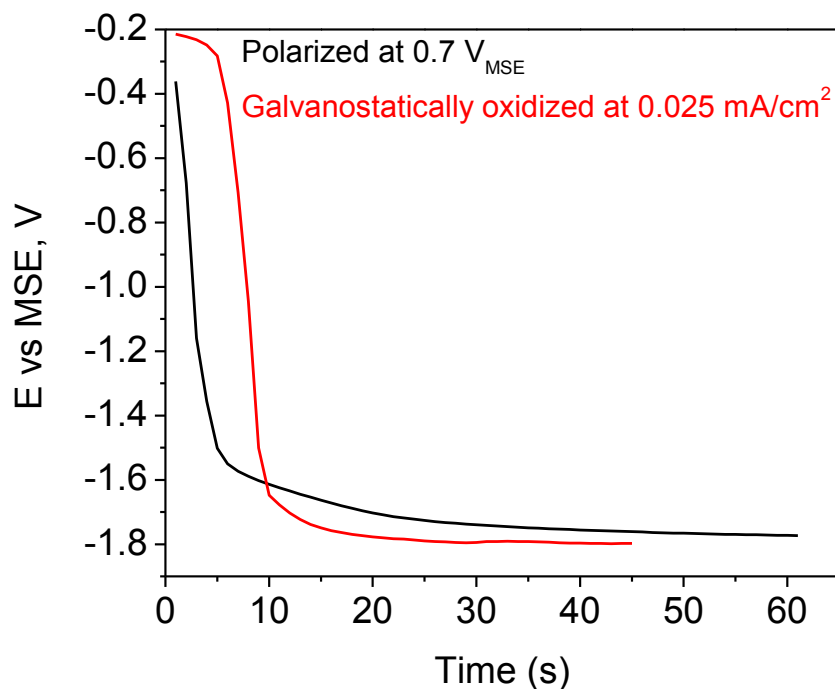


Figure 3.19 Reduction of two lab-created samples. The black trace was polarized in H_2SO_4 at $0.7 V_{\text{MSE}}$, the red trace was galvanostatically oxidized in H_2SO_4 at 0.025 mA/cm^2 . Data courtesy of Huang Lin.¹³¹

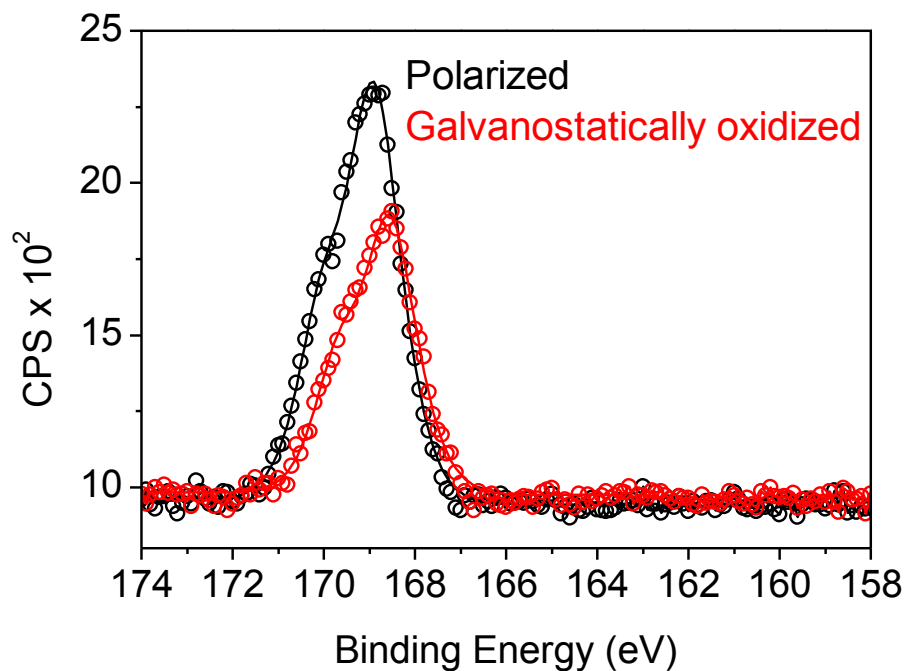


Figure 3.20 XPS sulfur 2p region scan of the two lab-created samples shown in Figure 3.19.

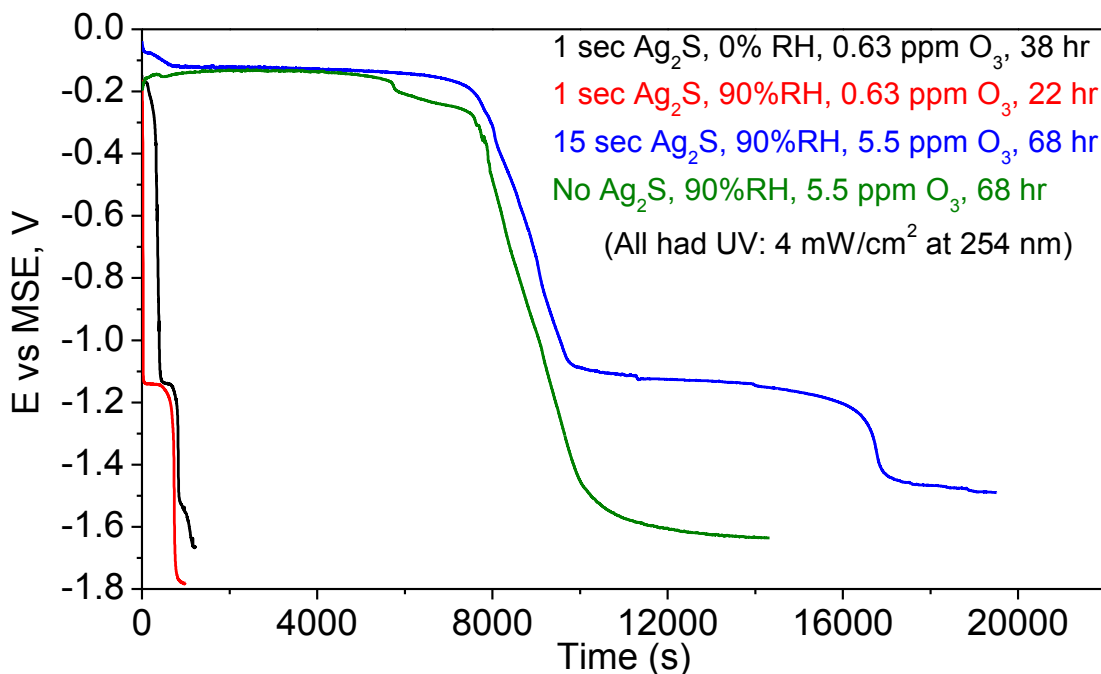


Figure 3.21 Reduction of four lab-created samples. Data courtesy of Huang Lin.¹³¹

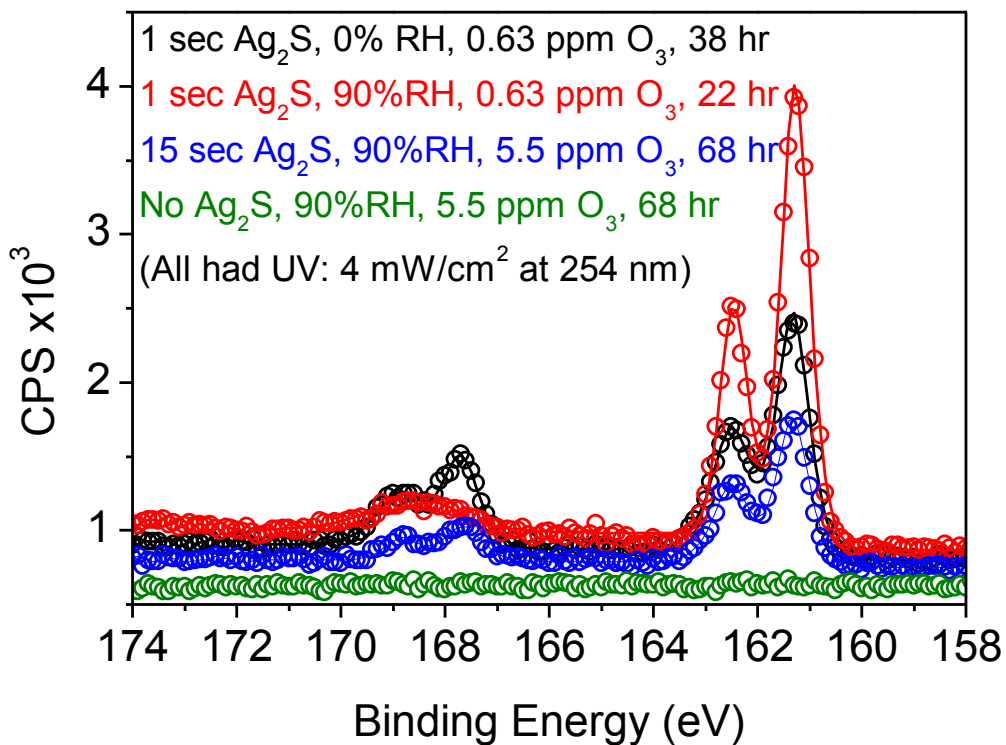


Figure 3.22 XPS sulfur 2p region scan of four lab created samples shown in Figure 3.21.

3.3 Discussion

3.3.1 *Comparison to Literature, Confirming Identity of Species*

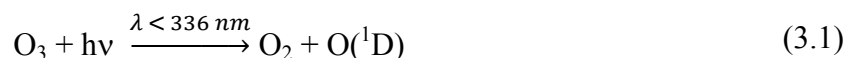
The XPS results presented in the previous section show that either Ag_2SO_3 or Ag_2SO_4 were routinely detected on field-exposed silver samples. Although the literature is scarce on Ag_2SO_4 formation with exposure of silver, there is less in regards to Ag_2SO_3 .¹⁴⁶ Since these species are not widely reported in the literature, their identity and formation mechanism are of significance. The first step in understanding the role of sulfur in the corrosion of silver is to confirm the identity of the species detected on the field-exposed silver coupons.

Although Ag_2SO_4 has not been widely accepted as a corrosion product in outdoor exposure of silver, there is some mention of it in the literature in regards to XPS assignments.^{136,137} These literature values are consistent with the peak position seen on many samples in this study, 168.6 eV. The other doublet pair seen in the sulfur region is observed around 167.3 eV and is tentatively assigned to Ag_2SO_3 . The shift that would be expected for the binding energy separation of sulfate and sulfite, based on the shift of $\text{Na}_2\text{SO}_4 \rightarrow \text{Na}_2\text{SO}_3$, is approximately 1.5 eV.¹⁴⁷ If Ag and Na are similar, this binding energy shift would yield an expected Ag_2SO_3 value of approximately 167.1 eV. The few literature values found for Ag_2SO_3 give a value of 167.5 eV.¹³⁷ These values are close to the binding energy observed in this study, so the doublet at 167.3 eV is assigned to Ag_2SO_3 .

3.3.2 Mechanism of Ag_2SO_3 and Ag_2SO_4 Formation – Under Vacuum

Since it is unlikely that pure silver would react directly with sulfate to form Ag_2SO_4 , due to the unfavorable thermodynamics which were described earlier,^{8,100,117} other mechanisms must exist. One possibility is that Ag_2SO_4 could be formed through a conversion of silver oxide into silver sulfate similar to the formation of $AgCl$.^{2,3} This process could be Ag_2O reacting with SO_2 or a more oxidized form of sulfur and forming Ag_2SO_4 immediately or it could proceed via an intermediate phase of Ag_2SO_3 .^{118,119}

Since Ag_2SO_4 and Ag_2SO_3 have not been identified as corrosion products on field-exposed silver, there has been very little reported in the literature as to how it may be formed. However, there has been work done on monocrystalline silver in order to understand its catalytic properties.^{148–151} These studies have shown that SO_2 will not adsorb onto Ag unless there is a surface oxide layer (Ag_2O). Ag_2O can be formed under dry conditions according to:^{1,2}



Once there is oxide at the surface, Ag_2SO_3 will form on $Ag(110)$ and $Ag(100)$.^{148–151} Ag_2SO_4 will also form on $Ag(110)$ when an oxide layer is present.^{148–150} The fact that the silver must have a surface oxide layer present in order to form Ag_2SO_3 or Ag_2SO_4 is not unlike the formation mechanism for $AgCl$ given in the literature.^{1,2}

Of interest is the finding that on the $Ag(100)$ surface Ag_2SO_4 will only form in the presence of an alkali.¹⁵¹ This is consistent with a cation removing electron density from

an oxygen of the Ag_2SO_3 making the sulfur electropositive and promoting binding of the sulfur to a neighboring surface oxide, thereby forming Ag_2SO_4 . This phenomenon and how it may impact corrosion in the field is discussed later. Although these studies give insight into the mechanism of sulfate and sulfite formation, they are not identical to the corrosion tests performed in this study. They were done on monocrystalline samples under ultra-high vacuum, whereas the samples in this study are polycrystalline and are under atmospheric pressure.

3.3.3 Mechanism of Ag_2SO_3 and Ag_2SO_4 Formation – Aqueous Phase

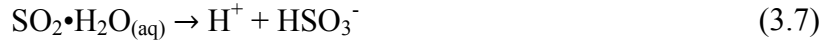
SO_2 is very reactive with water and surfaces in the real world have water adsorbed. If there is a source of SO_2 near the corrosion test site and SO_2 can make it to the sample before hydrolyzing, the SO_2 will find water on the surface. Therefore it is unlikely that SO_2 is able to react with a dry surface oxide layer. However, there are several other possibilities for the formation of Ag_2SO_4 and Ag_2SO_3 .

First consider the fate of SO_2 in the atmosphere which undergoes gas phase oxidation. The major source of oxidation of SO_2 in the gas phase is by OH radical; at an OH radical concentration of 1×10^6 radicals/cm³ the lifetime of SO_2 is approximately 13 days for Eqn (3.3).⁴² The lifetimes of Eqn (3.4) and (3.5) are extremely fast ($<1\mu\text{s}$) in comparison.^{152,153}





SO_2 can also undergo oxidation in aqueous solution, whether in aerosol form or with co-adsorbed water once adsorbed onto a silver surface.^{42,70}



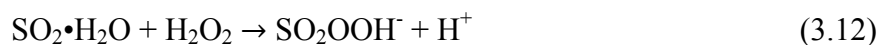
The combination of these species, $\text{SO}_2 \cdot \text{H}_2\text{O}$ (hydrated SO_2), HSO_3^- (bisulfite), SO_3^{2-} (sulfite), is abbreviated as S(IV). Likewise, S(VI) is the combination of both SO_4^{2-} (sulfate) and H_2SO_4 (sulfuric acid). In order for SO_2 to be oxidized into S(VI) several steps are needed: transport of SO_2 to the interface ($\sim 10^{-10} - 10^{-4}$ s), across the interface ($< 10^{-8} - 10^{-1}$ s), S(IV) equilibration (≤ 1 ms), transport to bulk ($\sim 10^{-6} - 1$ s), oxidation of S(IV) into S(VI) (rate limiting step), these are depicted in Figure 3.23.^{42,70,154} These times were calculated assuming an aerosol radius of $10^{-5} - 10^{-2}$ and a pH range of 2-6; gaseous and aqueous diffusion constants are $0.126 \text{ cm}^2/\text{s}$ and $1.8 \times 10^{-5} \text{ cm}^2/\text{s}$, respectively.^{42,70,154}

Oxidation of S(IV) can be accomplished by many species dissolved in aqueous solution, these include O_3 , H_2O_2 , CH_3COOH , O radical, NO_y , and OH radical (among other species). By ozone:^{155,156}

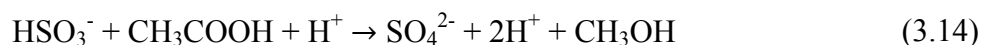


By hydrogen peroxide:¹⁵⁷





By acetic acid:¹⁵⁵



By oxygen in the presence of a catalyst:^{42,155,158}

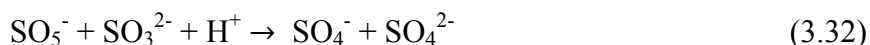
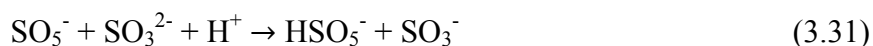


By NO_y :^{42,70}

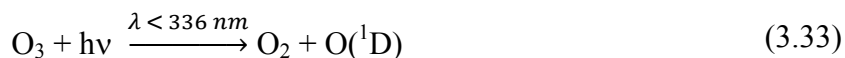


By hydroxyl radical:^{42,70}





The formation of Ag_2SO_3 or Ag_2SO_4 from pure Ag would require a change in oxidation state of silver from 0 to +1. However, if the reaction started with Ag_2O , the silver is already oxidized to a +1 state. Since Ag_2O can be formed under wet conditions according to:^{1,2}



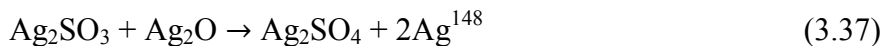
It follows that the various forms of oxidized sulfur could react with Ag_2O to yield Ag_2SO_3 or Ag_2SO_4 . (It should also be mentioned that literature reports no evidence of silver hydroxide formation when silver oxide is subjected to water.)¹⁵⁹ The possible species involved could be: SO_2 , H_2SO_3 , HSO_3^- , SO_3^{2-} , H_2SO_4 , HSO_4^- , or SO_4^{2-} . However, as stated previously, it is unlikely that SO_2 would be involved since it is readily oxidized

in the aqueous phase. Also, according to the speciation curves for the pH dependence of sulfates and sulfites (Figure 3.24), and since it is unlikely that the pH on the surface or in aerosols would be less than 2, we can also rule out H_2SO_3 , H_2SO_4 , and HSO_4^- . This leaves HSO_3^- , SO_3^{2-} and SO_4^{2-} to interact with the Ag_2O ; Figure 3.25.

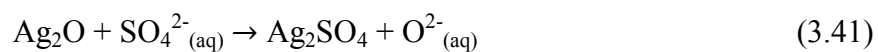
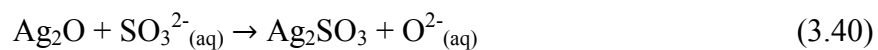
The reactions of Ag or Ag_2O with SO_3^{2-} and SO_4^{2-} have not been discussed in detail in the literature. However, reaction of silver oxide with bisulfite could lead to formation of silver sulfite.¹⁴⁶



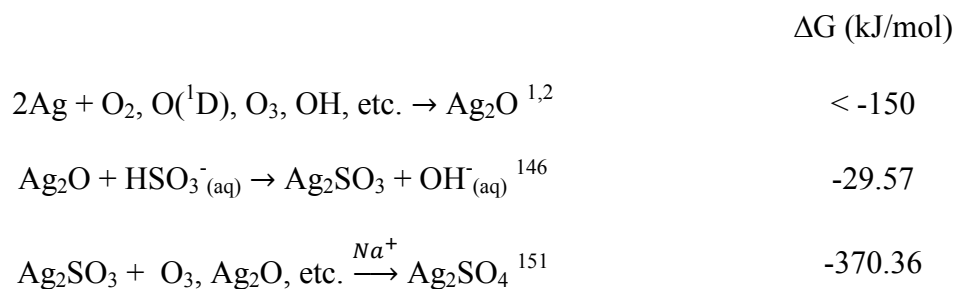
This reaction produces Ag_2SO_3 which was detected on samples that were free of alkali cations. A diagram of the reaction of HSO_3^- with Ag_2O to form Ag_2SO_3 is presented in Figure 3.26. In the presence of cations, such as Na^+ , or Ca^+ , Ag_2SO_3 was not detected, but Ag_2SO_4 was detected. This phenomenon was noted in the literature for $\text{Ag}(100)$ ¹⁵¹ and is discussed in greater detail in the next subsection. Briefly, a cation can withdraw electron density from an oxygen atom thus leaving the sulfur electropositive. The positive charge on the sulfur can then attract another oxygen atom. This oxygen could come from a number of places: a neighboring silver oxide, dissolved O_3 , or possibly $\text{O}(^3\text{P})$ or another oxygen donating species which is dissolved in solution.^{148,160,161}



Consideration was also given to the reaction of silver oxide with SO_3^{2-} and SO_4^{2-} , however, these reactions yield O^{2-} , which is an unlikely product.



In summary, the reactions to form Ag_2SO_3 and Ag_2SO_4 on the field-exposed silver proposed here are:



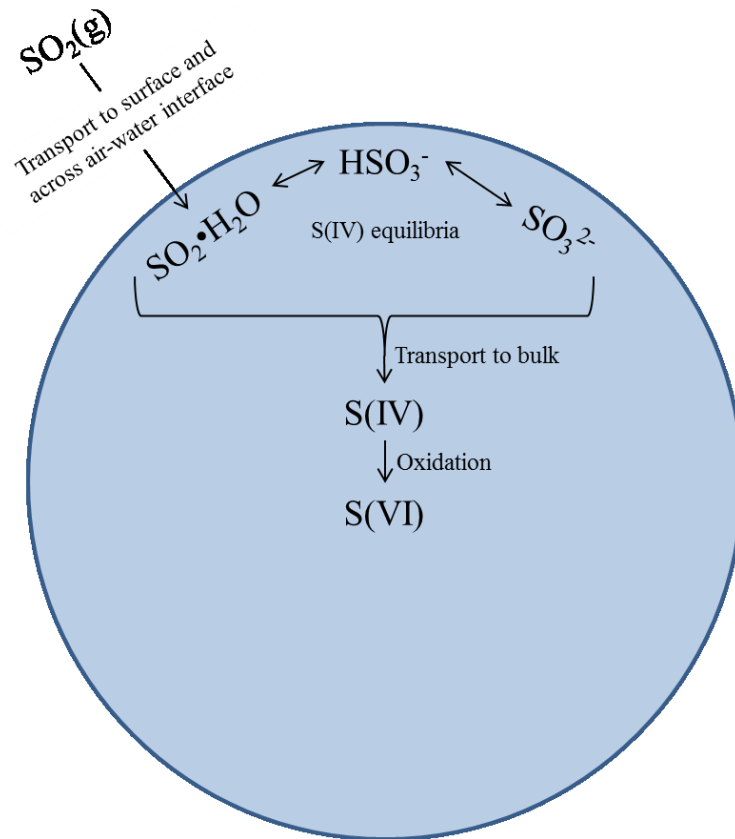


Figure 3.23 Diagram of the steps needed for oxidation of SO_2 to S(VI) in the aqueous phase.^{42,70}

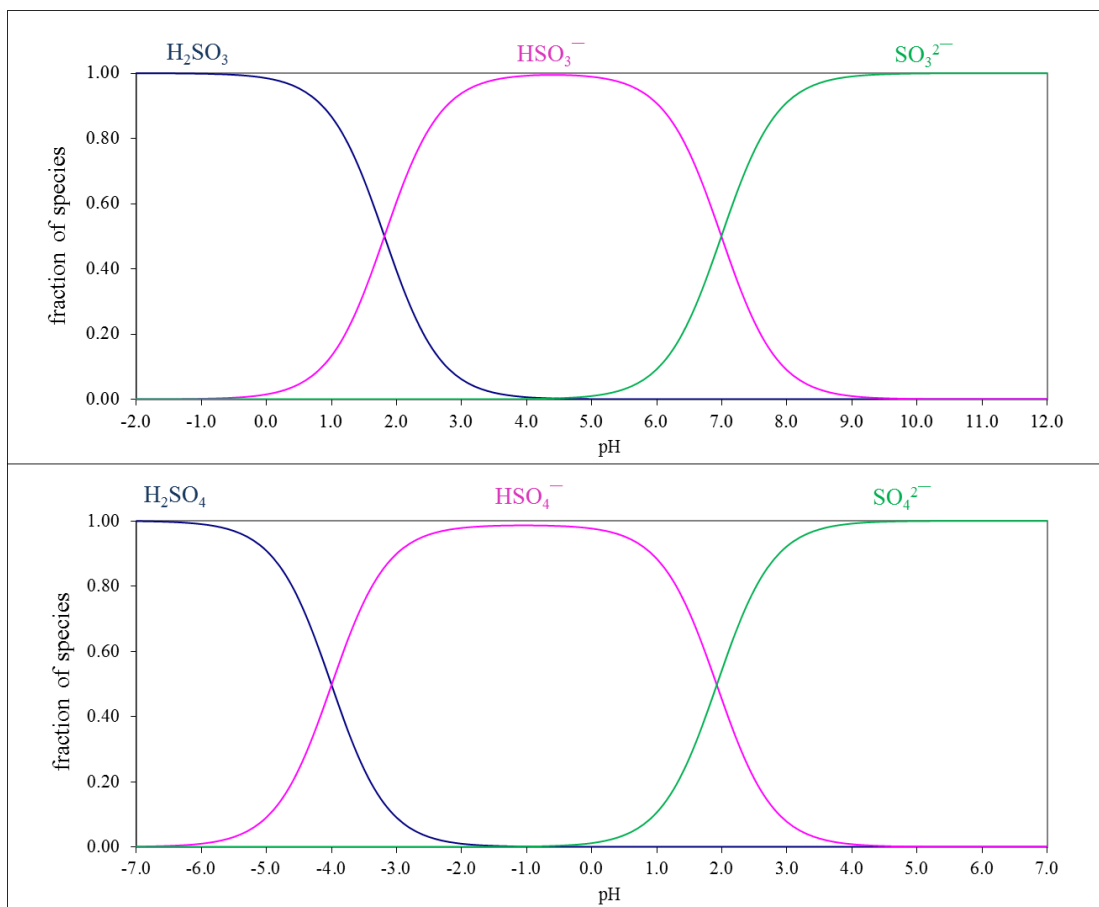


Figure 3.24 pH speciation curves for sulfite (top) and sulfate (bottom).⁴¹

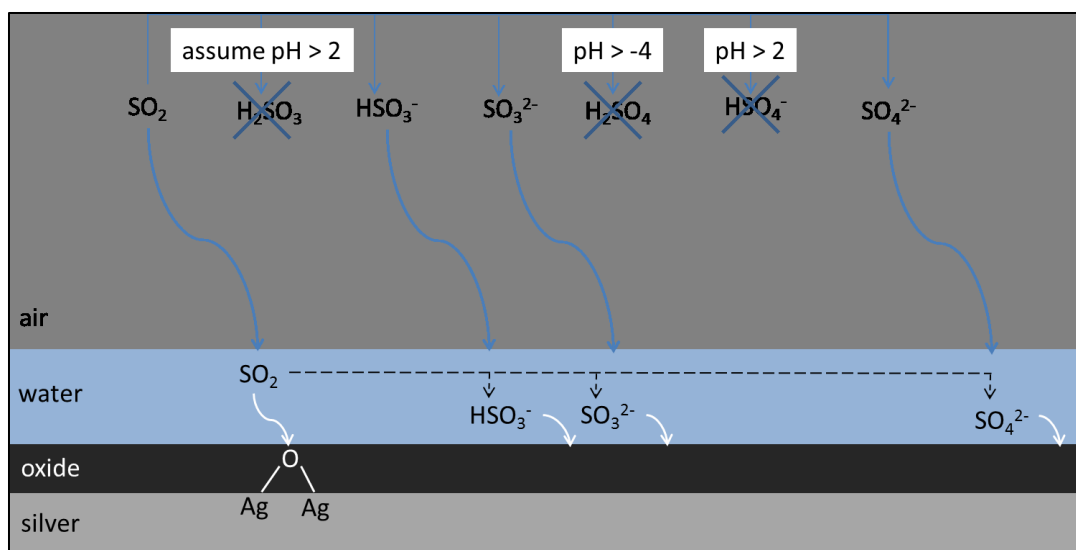


Figure 3.25 Possible pathways for the fate of SO₂, S(IV), and S(VI) near a silver surface. Some species are ignored since they are only present at a very low pH.

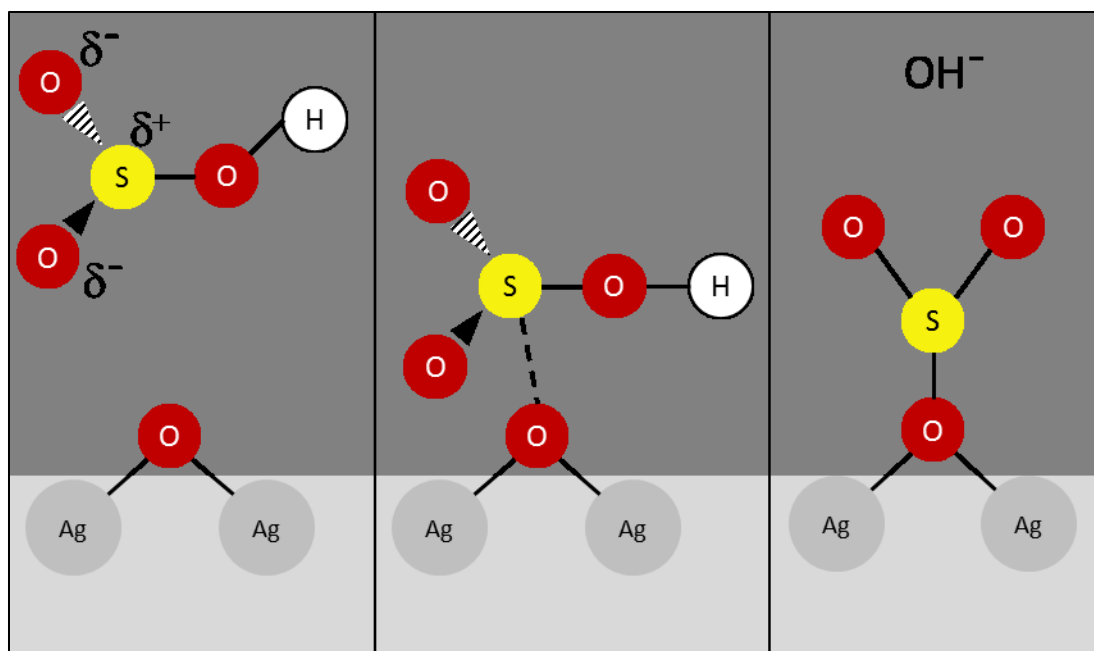


Figure 3.26 Diagram of the possible mechanism for formation of Ag_2SO_3 from $\text{Ag}_2\text{O} + \text{HSO}_3^-$. First, the HSO_3^- approaches the surface, then the sulfur attaches to the oxygen from the Ag_2O , then Ag_2SO_3 is formed as OH^- leaves the surface.

3.3.4 *Is Ag_2SO_3 Actually An Intermediate for Ag_2SO_4 ?*

If Ag_2SO_3 is an intermediate step in the formation of Ag_2SO_4 , then why do some samples stop at this intermediate phase while others go on to form the fully oxidized product? The answer may lie in the presence (or lack thereof) of alkalis on the sample. It was briefly discussed earlier that in literature, $\text{Ag}(100)$ did not form Ag_2SO_4 unless in the presence of alkalis.¹⁵¹ This is due to an alkali cation, such as Na^+ , pulling electron density from the oxygen of sulfite which leaves the sulfur electropositive and promotes binding of the sulfur to another neighboring oxide. Indeed, the samples which had evidence of Ag_2SO_3 did not have alkalis present, but those that had Ag_2SO_4 did. The correlation between alkali cations and the presence of either Ag_2SO_3 or Ag_2SO_4 is shown in Table

3.1. Na^+ is used in the correlation table since sodium was present if any other alkali cations were as well. The XPS results for elements detected (other than sulfur) are given in Appendix F. The consistency between the results of this study and those reported for Ag(100) indicate that the presence of alkalis dictates whether sulfate or sulfite is formed on field-exposed samples.

The dependence of the formation of Ag_2SO_4 on an alkali cation is only found in the literature for the Ag(100) orientation.¹⁵¹ Silver has a face centered cubic crystal structure (fm3m). Diagrams of the (100), (110), and (111) faces are presented in Figure 3.27 – Figure 3.29. Literature has shown that the oxygen atoms of silver oxide on a Ag(110) face are located at the positions indicated by red circles in Figure 3.29.^{149,162} The literature reports that for other crystal faces, such as (110) both sulfite and sulfate will form.^{148–150} The observation that Ag_2SO_4 formation is only dependent on the presence of alkali cations for the (100) face and not for the (110) face shown in the literature may be an effect of the spacing of oxygen atoms on the silver surface and the angles formed as a result of this spacing, Figure 3.30. However, this has not been discussed in the literature. There is also the difference in reactivity between the different faces. For a fcc crystal structure: $110 > 100 > 111$.^{163,164} This predicts that the Ag(110) plane is more reactive than the (100).

Table 3.1 Correlation between the presence of alkali cations and either sulfite or sulfate. Na⁺ is used as an indicator of the presence of alkali cations since Na⁺ was always present if other cations were also observed with XPS. Other cations found with XPS include: Ca²⁺, K⁺, and Mg²⁺. The numbers shown in the table correlate with the locations indicated on the right. For locations 1-5, an “s” indicates the sample was sheltered, “u” means unsheltered, and the number at the end specifies the number of months the sample was exposed. There are more of numbers 1-6 because there were multiple samples at these sites. The single measurements are numbers 7-15.

SO ₃ ²⁻						1s1 1s2 1s3	1s4 1s6	1u1 1u2	1u3 1u4	11 15	
SO ₄ ²⁻	2s1 2s2 2s3 2s6 2u1	2u2 2u3 2u4	3s6 3u1 3u6 4s1 4s3	4s6 4u1 4u6 6 7	8 9 12 13 14			5s1			
Neither SO ₃ ²⁻ nor SO ₄ ²⁻		2s4 2u6	3u3	4u3		1u6	5s3 5s6	5u1 5u3	5u6	10	
		Na ⁺				No Na ⁺					

- 1 Thompson Farm, NH
- 2 Appledore Island, E
- 3 Kaneohe MAB, HI
- 4 Kilauea volcano, HI
- 5 Mauna Loa, HI
- 6 Coconut Island, HI
- 7 Conroe, TX
- 8 Daytona Beach, FL
- 9 Long Island, NY
- 10 Lyon Arboretum, HI
- 11 Randolph, TX
- 12 McMurdo, ANT
- 13 W. Jefferson, OH
- 14 Whidbey Island, WA
- 15 Woodstock, ME

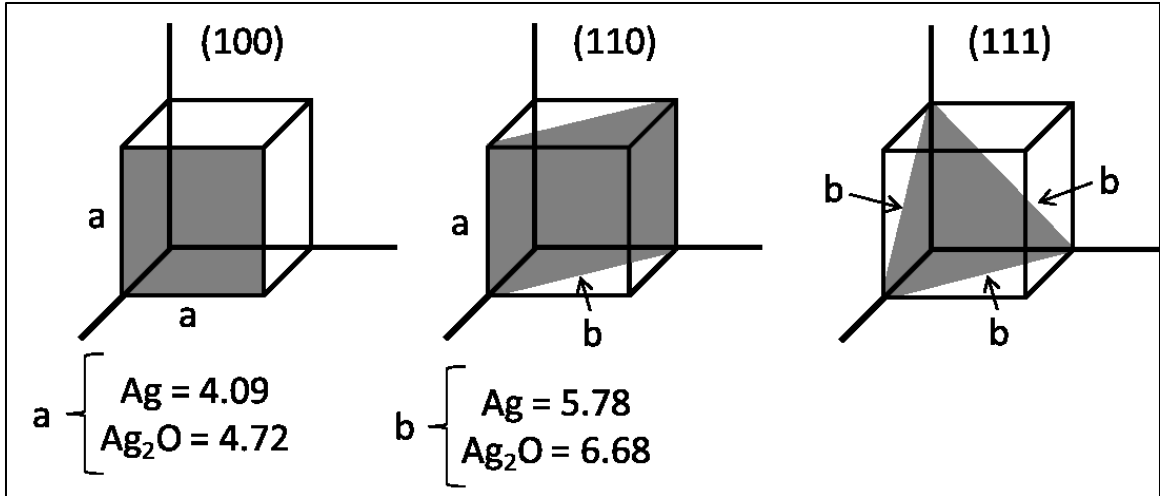


Figure 3.27 Drawing of the faces of silver. a and b values are given for both silver and silver oxide.^{165,166} b values were calculated using the law of cosines: $c^2 = a^2 + b^2 - 2ab * \cos c$.

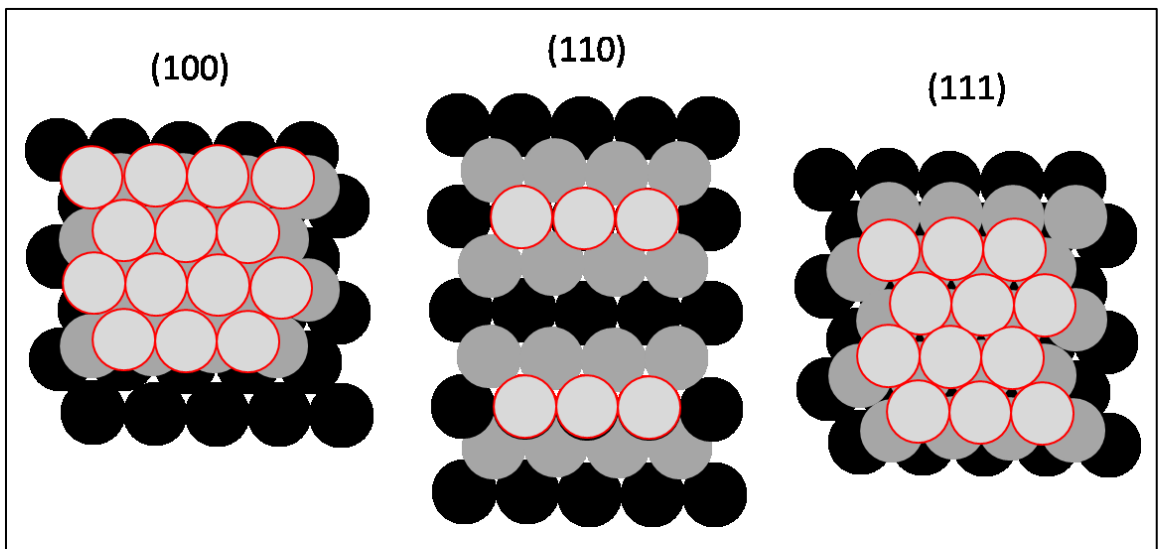


Figure 3.28 Figure of stacking of different crystal orientations for silver, top-down view. Light gray circles with a red outline are the top layer, regular gray circles are the second layer and black circles represent the third/bottom layer.

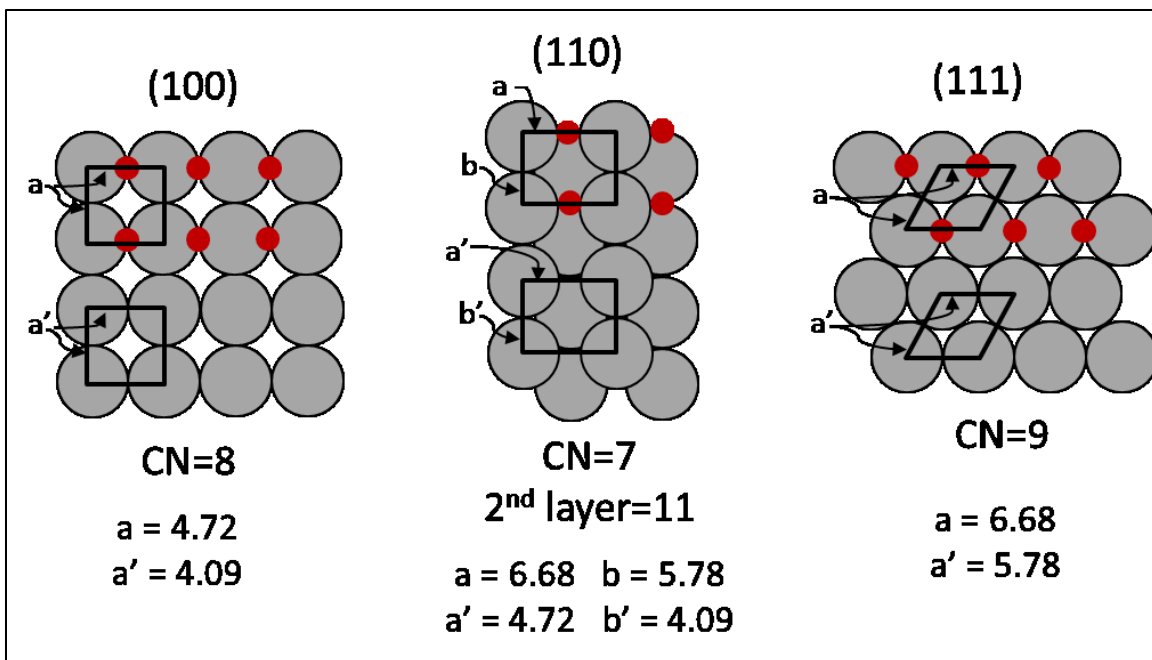


Figure 3.29 Geometries of the (100), (110), and (111) faces of silver and silver oxide. Coordination numbers (CN) are given for each face as well as the distances between silver atoms, numbers are given in Angstroms. Values were calculated using Figure 3.27.

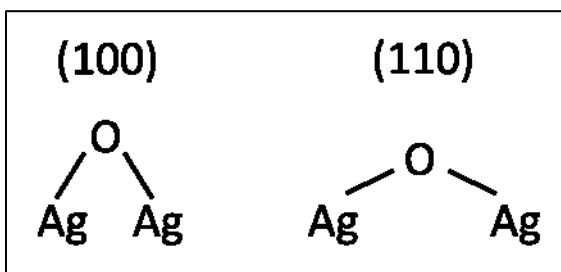


Figure 3.30 Diagram for the possible bond angle difference on Ag(100) and Ag(110) that may result in the need for alkali cations to produce Ag_2SO_4 on the (100) face.

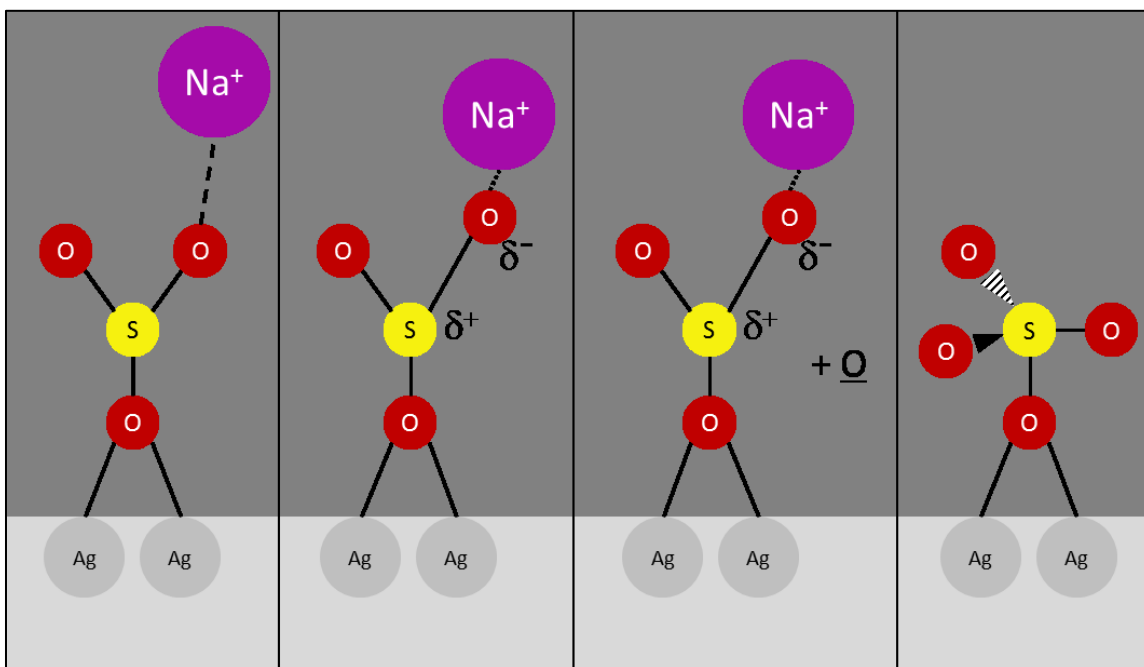


Figure 3.31 Diagram of the possible transformation of Ag_2SO_3 to Ag_2SO_4 on the $\text{Ag}(100)$ surface through interaction with a cation such as Na^+ . The sodium pulls electron density from the oxygen, which in turn leaves the sulfur atom electropositive. The sulfur will then bind to an oxygen atom ($\underline{\text{O}}$), where $\underline{\text{O}}$ could be from: a neighboring Ag_2O , dissolved O_3 , or other oxygen donating species.

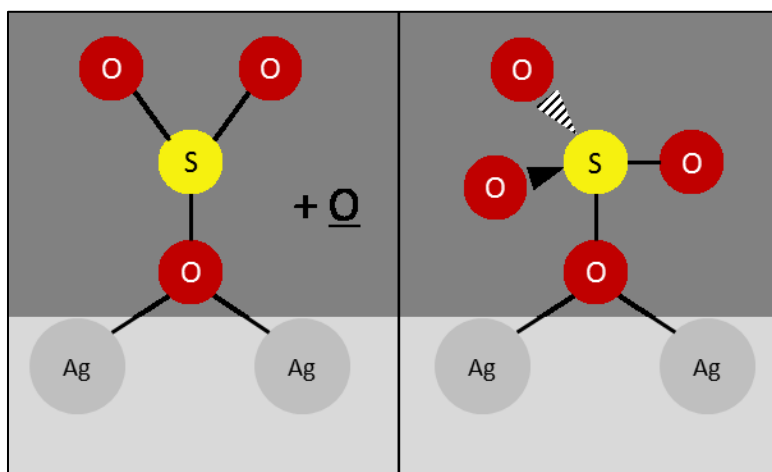


Figure 3.32 Diagram of the possible transformation of Ag_2SO_3 to Ag_2SO_4 on the $\text{Ag}(110)$ surface. The sulfur will bind to an oxygen atom ($\underline{\text{O}}$), where $\underline{\text{O}}$ could be from: a neighboring Ag_2O , dissolved O_3 , or other oxygen donating species.

3.3.5 *Correlation with Atmospheric Measurements*

The results already discussed show evidence that atmospheric chemistry plays a significant role in the corrosion products formed on silver samples. An extensive amount of atmospheric chemistry data has been published from the University of New Hampshire's Atmospheric Investigation, Regional Modeling, Analysis and Prediction (AIRMAP) program.¹⁶⁷⁻¹⁷³ This work has focused on Appledore Island and Thompson Farm among other sites in New England. The monitoring in this area was the motivation for the placement of samples at these sites. Among the research published, they have noted anthropogenic and photochemically aged aerosols dominated by SO_4^{2-} and NH_4^+ with $[\text{SO}_4^{2-}]$ reaching a maximum of 23.7 nmol/m^3 in the summer.¹⁷⁰ The impact of local sources was found to be much more substantial as compared to sources which were further away.¹⁶⁸

Unfortunately by the time the silver samples were exposed, much of the monitoring in New Hampshire at these sites had come to an end. However, there is a long history of monitoring in this area and if it is assumed that overall trends have not changed too drastically, the data may be useful in validating the XPS results. Although monitoring of SO_2 or SO_4^{2-} will not shed light on why Thompson Farm had sulfite and Appledore Island had sulfate present, information about the abundance of cations may. The amounts of common cations in aerosols were detected at Thompson Farm and at Fort Constitution. Since no cation information was available from Appledore Island, Fort Constitution is used here. Fort Constitution is a site which is inland from Appledore Island but the

proximity to the ocean allows Fort Constitution to be used as a proxy for Appledore Island.

Bulk aerosol sampling was used at Thompson Farm (TF) and Fort Constitution (FC) to monitor common inorganic ions. Samples were collected on 90 mm Teflon filters for 24 hour time intervals.^{170,174} After collection, the filters were extracted into a water/methanol solution, preserved in chloroform, and analyzed by ion chromatography (IC).¹⁷⁵ The amount of sulfate at TF and FC is shown in Figure 3.34. Figure 3.35 shows the amount of sodium ions collected on filters from January 2001 – December 2003. Other cations are shown in Appendix G. Although there is variation over short time periods, overall, the amount of sulfate at TF and FC is similar during the 4 year sampling period. However, the amounts of the cations sampled at FC were much greater than at TF. Therefore, the observation of fewer cations on the TF silver samples is consistent with aerosol sampling measurements. The similarity in oxidized sulfur and the difference in cation concentrations support the theory that alkali species are responsible for the type of oxidized sulfur on the silver coupons.

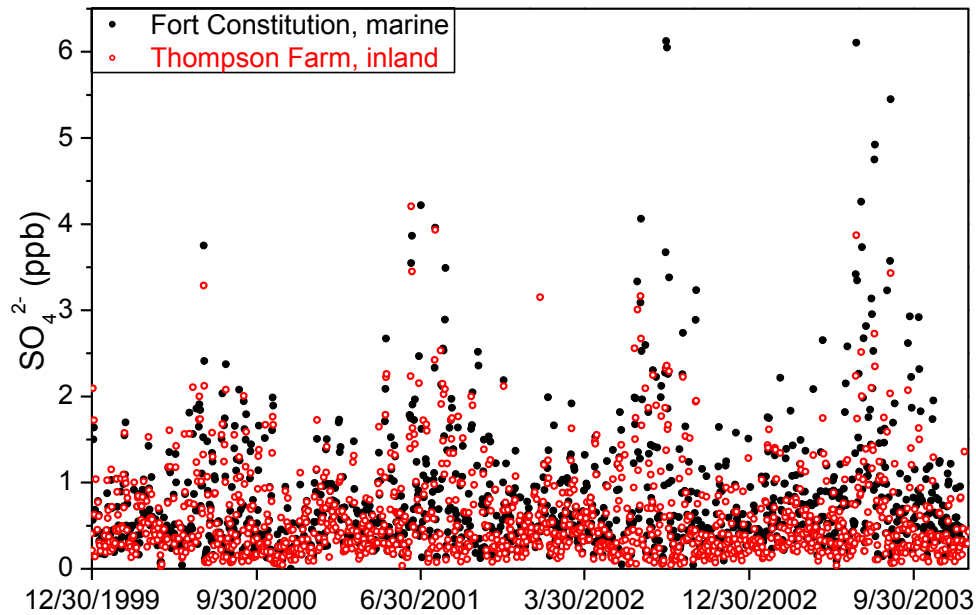


Figure 3.33 AIRMAP SO_4^{2-} data from Fort Constitution & Thompson Farm.^{170,174} The solid black circles are data from Fort Constitution and the open red circles are the data from Thompson Farm. Samples were taken every 24 hours.

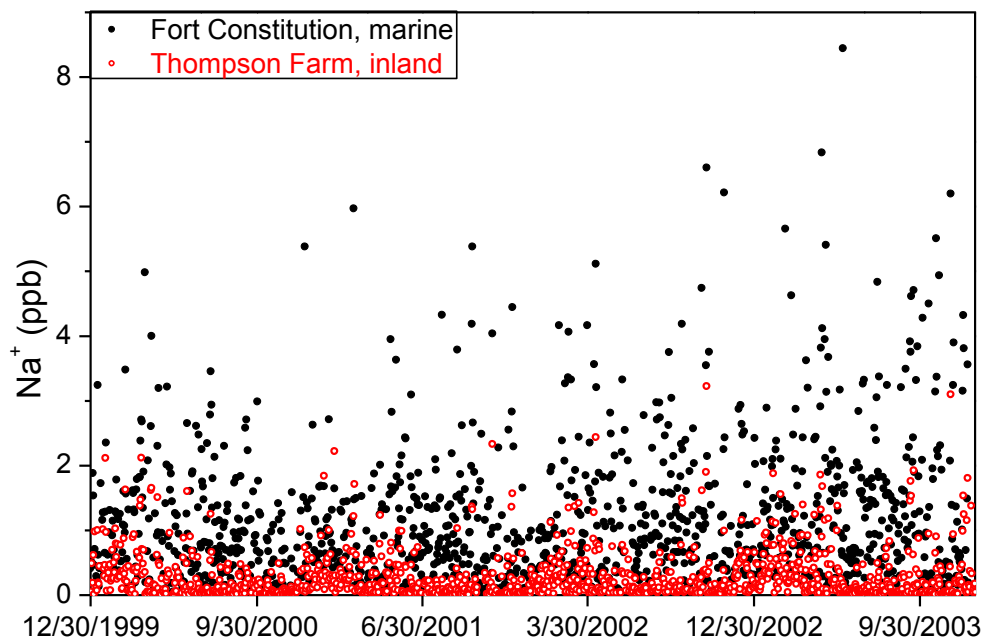


Figure 3.34 AIRMAP Na^+ data from Fort Constitution & Thompson Farm.^{170,174} The solid black circles are data from Fort Constitution and the open red circles are the data from Thompson Farm. Samples were taken every 24 hours.

3.3.6 *Cause of Change in Ratios of Ag_2SO_4/Ag_2S and Ag_2SO_3/Ag_2S*

The variability in the ratios of the sulfur 2p peaks over time for both the New Hampshire and Hawaii samples may be attributed to several factors. These include: continuation of new deposition leading to a change in film thickness and composition; surface rinsing especially in the case of the unsheltered samples which leads to solvation of highly soluble species such as Ag_2SO_4 ; evolution of products once adsorbed onto the surface either in solid phase or aqueous phase.

Continuous deposition of new species would change the composition of the product layer. Take the Appledore Island, New Hampshire samples as an example. Since XPS can only measure a small depth (~10 nm) if the sulfate was only deposited at the beginning of exposure, assume only during the first 2 months, then as new species were deposited which did not include SO_4^{2-} the amount of SO_4^{2-} would decrease as the film thickness increased. Although there is some variability in aerosol composition over time (Figure 3.34), this may not be the complete explanation.

Surface rinsing could also explain why the amounts of sulfate and sulfite change over time. In regards to marine samples (Appledore Island, NH and Kaneohe MAB, HI), the amount of sulfate is much greater on the sheltered samples when compared to the unsheltered samples. This is consistent with the higher solubility of sulfate and sulfite relative to sulfide as described earlier. Higher humidity and surface wetting at locations very close to waterlines with wave-action may result in more surface rinsing. This impact of surface rinsing is consistent with the rinsing of the single measurements shown in Figures 3.8-3.11. The impact of surface wetting supports the idea that sheltering may

inhibit sample wash-off to some degree. The solubility of sulfate is not conducive to remaining on a sample which is experiencing wash off. This could be very significant since many outdoor exposures are done at 45° with no sheltering. If the solubility of Ag_2SO_4 leads to transport of silver off of the surface, there could be significant corrosion which is being neglected.

Finally, it is also possible that the species on the surface could be evolving over time and resulting in more Ag_2S . This would mean that the oxidized sulfur species are being reduced from sulfite or sulfate into sulfide. However, since it is unlikely that a silver surface would be a reducing environment for oxidized sulfur species, the results from this study do not support this argument.

3.3.7 *Why are Ag_2SO_3 and Ag_2SO_4 Not Routinely Identified in Literature?*

Ag_2SO_3 and Ag_2SO_4 are not detected on any of the samples which were analyzed with reduction. This is consistent with literature that does not report Ag_2SO_4 or Ag_2SO_3 on corroded silver coupons.^{4,100} A possible explanation for the lack of sulfate or sulfite detection in the literature is that these species are soluble. Galvanic reduction involves submerging the corroded sample in solution, often either NaCl or Na_2SO_4 . Both of these solutions increase the solubility of the sulfate or sulfite adsorbed on the surface. It is also possible that while in solution, a more soluble product could be replaced by a less soluble product. Na_2SO_4 is currently used by the Frankel and Kelly labs since it was shown that any Ag_2O present from corrosion would be converted to AgCl in the presence of NaCl .² Perhaps the Ag_2SO_3 or Ag_2SO_4 is being replaced with dissolved Cl once it has been

placed in the reduction solution to form AgCl. Overall, it is likely that the solubility of silver sulfite and sulfate plays a key role in the discrepancy between XPS and galvanostatic reduction.

3.3.8 *Ag₂SO₄ Generation on Laboratory Accelerated Tests*

A few attempts to create Ag₂SO₄ in the lab were made. These are shown in Figure 3.19 – Figure 3.22. The small plateau in Figure 3.19 for the sample which was galvanostatically oxidized in H₂SO₄ is at the potential for AgCl, not Ag₂SO₄. There was a small amount of both Na⁺ and Cl⁻ observed in the XPS results (shown in Appendix F). Even though reduction found no evidence of Ag₂SO₄, it was detected with XPS (Figure 3.20). Ag₂SO₃ is not ruled out since there was a shoulder on the lower binding energy side which may have been caused by sulfite. This highlights the need to use XPS when detecting sulfite and sulfate since reduction cannot detect them.

The second set of lab tests examined the impact of oxidation on a silver sulfide surface, Figure 3.21 and Figure 3.22. The sample which had no Ag₂S, also had no Ag₂SO₃ or Ag₂SO₄ formed (Figure 3.22). However, the other three samples had a small amount of sulfite or sulfate. XPS detects oxidized sulfur on these samples, although it is much less than AgS. One of the samples (blue spectrum) even has a small reduction plateau (Figure 3.21) at -0.072 V_{MSE} which is associated with Ag₂SO₄. This suggests that although Ag₂SO₃ and Ag₂SO₄ are not easily formed from the oxidation of Ag₂S, it may be possible.

Further accelerated tests need to be done to reproduce the corrosion products found on field-exposed samples. Bare silver and oxidized silver should be exposed in the presence of SO₂ (with and without RH, O₃, UV light, and NaCl). In the presence of water vapor, SO₂ should readily become HSO₃⁻ which should form Ag₂SO₃. If NaCl is also present, then Ag₂SO₄ should be formed instead of or in conjunction with Ag₂SO₃. If these parameters do not yield sulfite and sulfate, then a bisulfite salt solution could be used instead.

3.3.9 *Suggested Improvements for Accelerated Laboratory Tests*

If the suggested laboratory tests in the previous section provide further evidence for the formation of Ag₂SO₃ and Ag₂SO₄, then the modifications that currently exist for the salt spray chamber should be further improved. By adding a source of either SO₂ or HSO₃⁻ solution, Ag₂SO₃ and Ag₂SO₄ should be able to form in the currently modified test chamber. Since other materials are also susceptible to corrosion by SO₂, it would make sense that it should be included in the test chamber. With this final modification, oxides, chlorides, sulfides and sulfates can be generated in laboratory tests. In order to have an accurate accelerated test, the key parameters must be included. Having multiple adjustable parameters would allow refinement of the exposure conditions to reproduce different environments. Even though this may not lead to a large acceleration factor, it would allow one test chamber to be used to model very different atmospheric conditions.

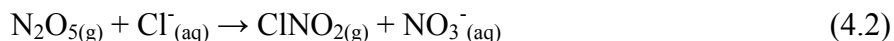
4. The Prevalence of Atmospheric Chloride Sources in Various Environments as Detected by Silver Corrosion Analysis

This chapter provides data which shows that AgCl is formed on field-exposed silver with little dependence on proximity to a saltwater source. The cause of widespread AgCl formation regardless of environment has been called to attention in recent literature.²⁻⁴ This chapter suggests a link between silver corrosion and recent atmospheric studies which show high levels of ClNO₂ and Cl radical across the United States.

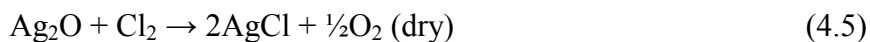
4.1 Introduction

Reactive halogen species, especially the chlorine radical, may contribute to the local oxidative capacity of an environment.^{5,17,45,81,176-179} Considering that the rate constant of the chlorine radical reaction with atmospheric trace species has been shown to be up to 100 times that of OH radical,^{79,180,181} chlorine radicals and their precursors may exert a considerable impact on the local environment.^{42,79,86,182} Active chlorine compounds which serve as precursors for the chlorine radical (Cl) include: chlorine molecules (Cl₂), nitryl chloride (ClNO₂), chlorine nitrate (ClONO₂), dichlorine peroxide (Cl₂O₂) and nitrosyl chloride (ClNO) along with many other species.^{63,86-90,127,183} Although chlorine radicals have been observed in relatively high concentrations in both the marine boundary layer as well as in coastal urban locations, it has long been suggested that there is an unrecognized source of Cl₂.⁶⁴

Recently, it was shown that significant concentrations of the chlorine radical precursor ClNO_2 were observed far from any coastline.⁵ The study proposed that a sizeable amount of chlorine radicals found in the troposphere arises from anthropogenic sources. This finding indicates that there are sources generating reactive chlorine far from salt-water sources. Mechanisms for the formation of ClNO_2 and Cl are:^{5,63,86-90}



Previous literature on silver corrosion states that Ag_2S is the dominant corrosion species in most environments.¹⁰⁰ However, recent silver exposures have shown that AgCl is often the dominant corrosion product.^{2,4} Additionally, AgCl has been detected at inland sites.⁴ It is not surprising that high levels of chloride are observed on samples from marine environments where there is an abundance of saltwater aerosols, but it is interesting that inland samples also exhibit high levels of chloride deposition. The mechanism for AgCl formation has been shown to proceed through an Ag_2O intermediate in dry or wet conditions.^{2,3}



Since AgCl has been reported at areas which are not near saltwater sources, silver corrosion may reflect these non-marine sources of chloride.

4.2 Results

Samples which were exposed at various locations across the United States and Antarctica were described in detail in Chapter 2. Nearly every sample which was exposed had AgCl as a corrosion product. A sample of the XPS chlorine 2p region scan data is shown in **Error! Reference source not found.**, complete spectra from every sample is given in Appendix F. There is a doublet at 198.6 and 200.2 eV in these spectra which agrees well with literature values of AgCl.¹³⁶ Although some samples appear to have more or less AgCl on the surface, nearly every site has some measureable amount. The one exception is Mauna Loa, HI. Only the one month samples had a detectable amount of AgCl, the three and six month samples did not. Galvanostatic reduction confirms the presence of AgCl on these samples, the results are shown in Chapter 3, Figures 3.3, 3.4, 3.10, 3.11, 3.12, and Table 2.1.

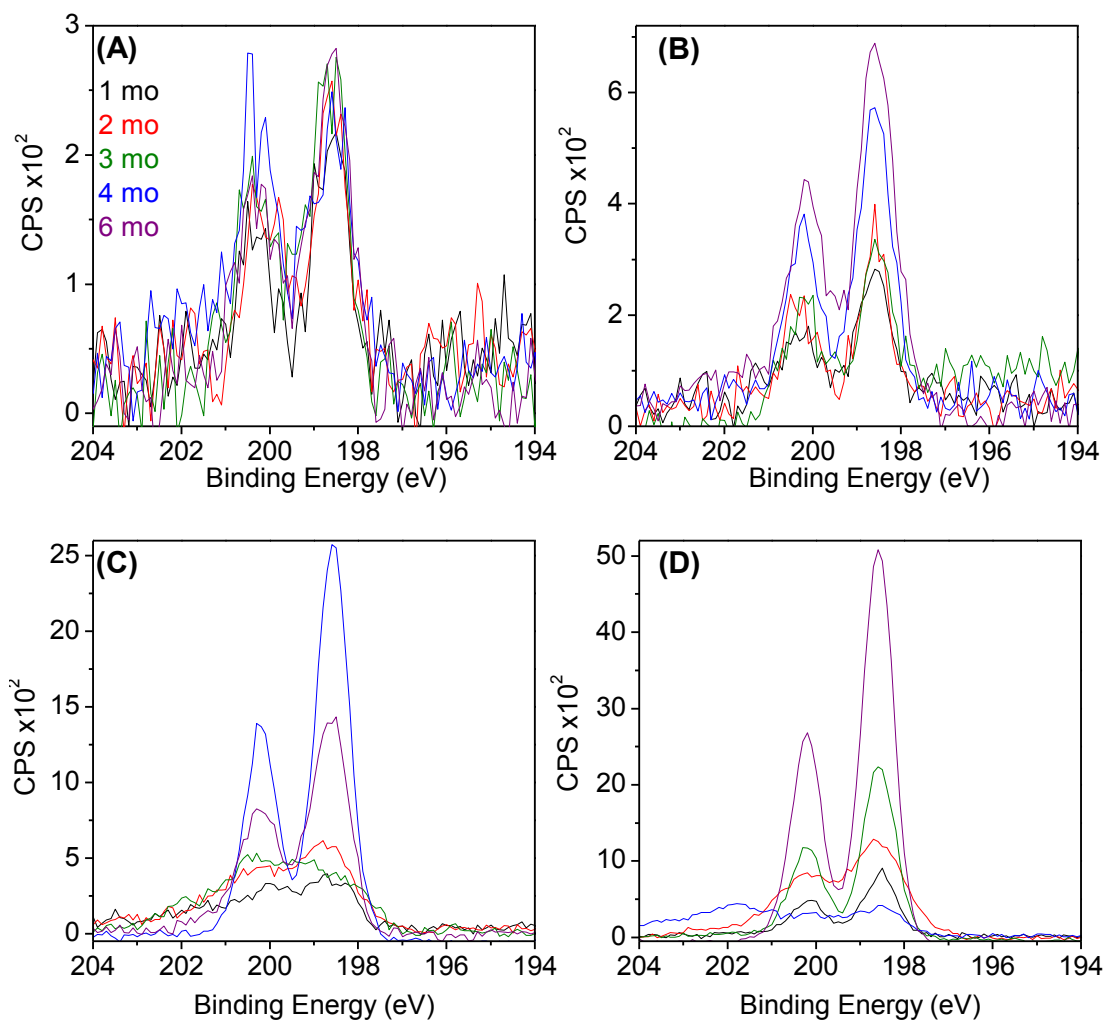


Figure F.48 XPS Cl 2p region scans of all samples exposed at Thompson Farm, NH (A) sheltered (B), unsheltered and Appledore Island, ME (C) sheltered, (D) unsheltered. Black, red, green, blue, and purple spectra correspond to 1, 2, 3, 4, and 6 month exposures, respectively.

4.3 Discussion

Wave action is a significant source for particles in coastal areas.^{45,184} Chloride ions may make up a significant portion of aerosols in coastal areas.^{17,42} This is consistent with literature and the sample exposures in this study which observed AgCl on samples near saltwater sources.^{1,2,4} A sample was exposed at Kilauea volcano and although not typically thought of as a chloride source, volcanoes can emit hydrochloric acid (HCl)¹⁸⁵ and are known to be very corrosive.⁹⁷ However, there are several samples which were neither near saltwater nor a volcano and still had AgCl formation. Mauna Loa, HI was the only location which did not reproducibly form AgCl on the surface, and this may be attributed to the height and insularity of the location (above the marine temperature inversion layer) which inhibits transport of local ground-level species to the sampling sight.¹²²⁻¹²⁴ Mauna Loa's summit is 4.17 km above sea level, with the observatory at 3.4 km. The samples were exposed near the observatory which is above the trade wind inversion located approximately 2 km above sea level. These values are shown in Figure 4.3.

As was discussed in Chapter 3, the University of New Hampshire has a long (10+ years) history of atmospheric chemistry data. Some ion collection data were shown in Chapter 2, which included Na⁺. Figure 4.2 shows that chloride (Cl⁻) is detected both at marine and inland monitoring locations. This is consistent with the AgCl that was formed at two monitoring locations in New England, Thompson Farm (inland) and Appledore Island (marine). Furthermore, Table 4.1 is a correlation table for Cl⁻ and Na⁺. Cl⁻ was

detected on every sample exposed in this study, with the exception of Mauna Loa. This table shows that there is little correlation between the detection of AgCl and Na⁺.

Only sodium is presented in Table 4.1 since if other cations were present (K⁺, Ca²⁺, or Mg²⁺), sodium was also present. The lack of a correlation between alkali cations and Cl⁻ supports the hypothesis that inland AgCl formation is not caused by long-range transport of sea salt particles, but is instead caused by an inland source that is not associated with sodium or other salts. This is consistent with continental chloride measurements of ClNO₂ and Cl radical.

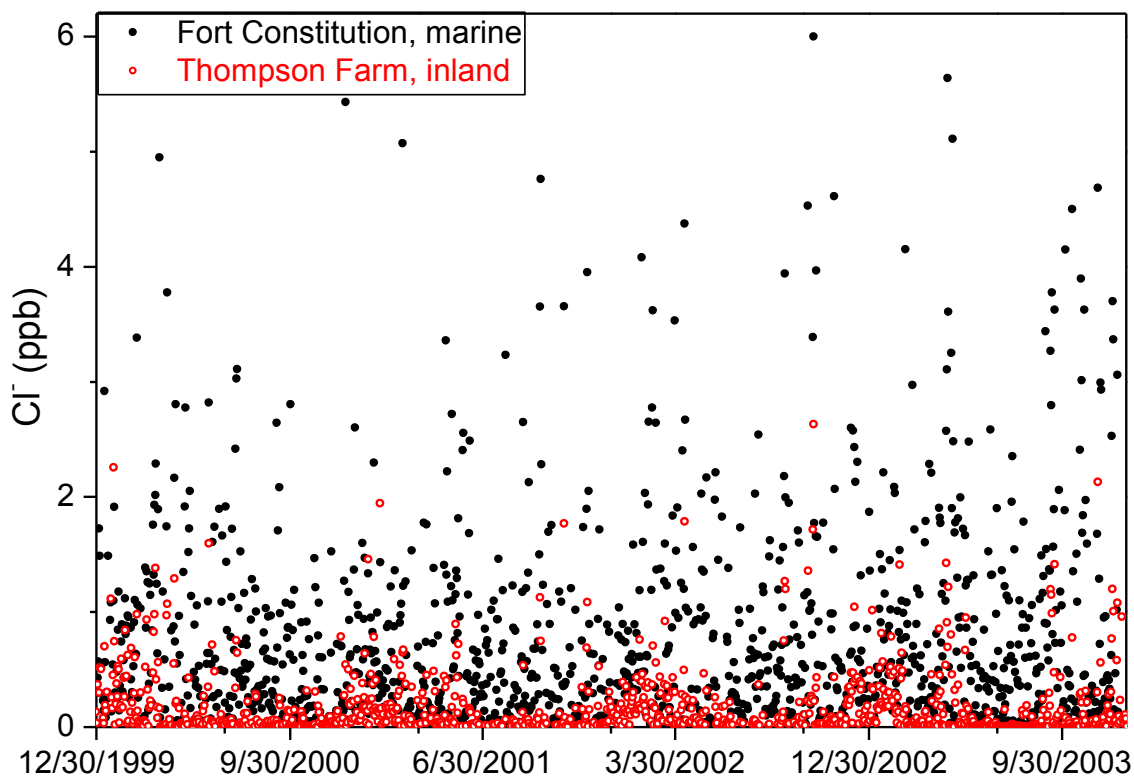


Figure 4.1 AIRMAP Cl⁻ data from Fort Constitution & Thompson Farm.^{170,174} The solid black circles are data from Fort Constitution and the open red circles are the data from Thompson Farm. Samples were taken every 24 hours. One data point from FC at 8.8 ppb is not shown.

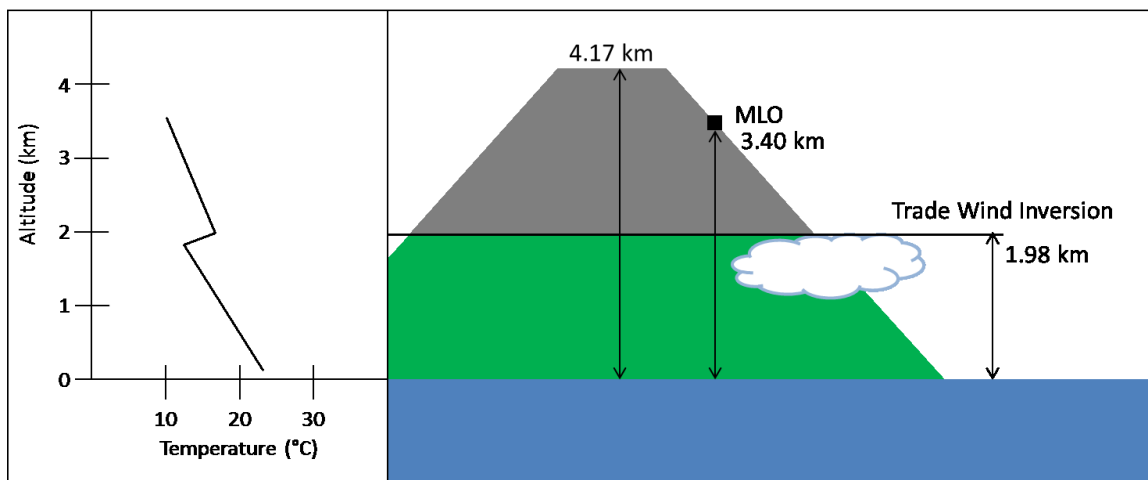


Figure 4.2 Picture showing the heights of Mauna Loa summit, Mauna Loa observatory (MLO) and the trade wind inversion. The graph on the left is adapted from Mendonca and Iwaoka.¹²⁴

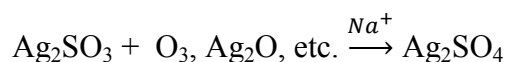
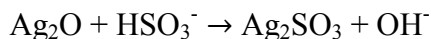
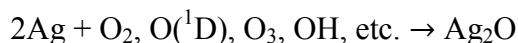
Table 4.1 Correlation between the presence of Cl^- and alkali cations. Na^+ is used as an indicator of the presence of cations since Na^+ was always present if other cations were also observed with XPS. Other cations found with XPS include: Ca^{2+} , K^+ , and Mg^{2+} . The numbers shown in the table correlate with the locations indicated on the right. For locations 1-5, an “s” indicates the sample was sheltered, “u” means unsheltered, and the number at the end specifies the number of months the sample was exposed.

Cl^-	2s1	2u1	3s1	3u6	4u3	9	1s1	1u1	5s1	1 Thompson Farm, NH
	2s2	2u2	3s3	4s1	4u6	12	1s2	1u2	5u1	2 Appledore Island, E
	2s3	2u3	3s6	4s3	6	13	1s3	1u3	10	3 Kaneohe MAB, HI
	2s4	2u4	3u1	4s6	7	14	1s4	1u4	11	4 Kilauea volcano, HI
	2s6	2u6	3u3	4u1	8	14	1s6	1u6	15	5 Mauna Loa, HI
No Cl^-							5s3	5u3		7 Conroe, TX
							5s6	5u6		8 Daytona Beach, FL
										9 Long Island, NY
										10 Lyon Arboretum, HI
										11 Randolph, TX
										12 McMurdo, ANT
										13 W. Jefferson, OH
										14 Whidbey Island, WA
										15 Woodstock, ME
			Na^+							
										No Na^+

5. Conclusions and Future Work

This dissertation shows evidence that sulfite and sulfate are critical in the corrosion process on silver. This is the first report of detection of these species on field-exposed silver. This study shows evidence of Ag_2SO_3 or Ag_2SO_4 detected on 37 out of 48 samples exposed in different atmospheric environments in locations from New Hampshire to Hawaii and in Antarctica.

The proposed reaction mechanism for the formation of Ag_2SO_3 and Ag_2SO_4 on field-exposed silver is:



The bisulfite ion is proposed to be the primary source of the sulfite and sulfate present on the silver coupons. In the presence of alkali cations, such as Na^+ , Ag_2SO_4 is formed from the intermediate Ag_2SO_3 ; whereas, in the absence of these cations, Ag_2SO_3 is the final product. The difference in alkali cation concentration on inland vs. marine samples is consistent with previous aerosol measurements.^{170,174}

The ratio of oxidized to reduced sulfur species varies over time on field-exposed samples. The variability in this ratio is consistent with the higher solubility of Ag_2SO_3

and Ag_2SO_4 when compared with Ag_2S .⁴¹ Evidence of this solubility was also observed upon systematic rinsing of the single measurement samples after exposure was completed. The higher solubility of Ag_2SO_3 and Ag_2SO_4 explains why these species are not readily identified with galvanostatic reduction which immerses the sample in solution.

Attempts were made to form Ag_2SO_4 on silver coupons in the lab.¹³¹ The formation employed either polarization in H_2SO_4 , galvanostatic oxidation in H_2SO_4 , or oxidation of Ag_2S . Analysis of XPS results found Ag_2SO_3 or Ag_2SO_4 on all of the samples as opposed to reduction which only found Ag_2SO_4 on one of the samples which oxidized Ag_2S . These studies prove that although reduction may not detect sulfate or sulfite, XPS often does. Also, the evidence of Ag_2S oxidation to Ag_2SO_3 or Ag_2SO_4 is in contrast with literature which states that this pathway is unavailable due to the change in sulfur's oxidation state from -2 to +4 or +6.¹⁰⁰ The detection of Ag_2SO_3 and Ag_2SO_4 on field-exposed silver warrants some further investigations, but has shown that surface-sensitive techniques, e.g. XPS or ToF-SIMS (time of flight secondary ion mass spectroscopy) are needed in order to accurately understand corrosion.

The detection of AgCl on silver coupons at every location of outdoor exposure in recent studies has raised questions as to the source of the chloride.²⁻⁴ The two possibilities are either long-range transport of marine aerosols to inland sites, or an unknown local chloride source. Evidence of AgCl formation was presented in this study which is consistent with past measurements, showing AgCl formation at nearly every site regardless of the proximity to saltwater sources.⁴ Aerosol measurements show higher

levels of both Na^+ and Cl^- near marine areas when compared to inland sites.^{170,174} The source of continental chloride has been attributed to ClNO_2 which yields Cl radical when photolyzed.^{5,63,86-90} The data from this study supports ClNO_2 as the source of AgCl on inland samples since there is no correlation between Na^+ and Cl^- on the field-exposed samples.

As was mentioned previously, extensive research has been carried out on the corrosion mechanisms needed to form AgCl ,^{1,2} including modifications to the ASTM-B117 salt spray test.³ With the addition of O_3 and UV light in the chamber, Ag_2O and AgCl are able to be formed and give a significant acceleration to field studies. However, as Ag_2SO_4 and Ag_2SO_3 have been found at numerous sites in this study, it is further recommended that a source for these species be added as well. If the mechanism proposed in this study for Ag_2SO_4 formation is correct, addition of SO_2 to the parameters already used in the modified salt fog test may lead to even better replication of field conditions. Since in the presence of high relative humidity, SO_2 will produce HSO_3^- . Therefore, using the typical B117 chamber (NaCl and RH), with the modification of UV light and O_3 , and further adding SO_2 may reproducibly form Ag_2SO_3 and Ag_2SO_4 in the lab. This certainly warrants testing based on the results found in this study.

Further work should also be done to test the variability of the composition of corrosion products on field-exposed samples. In order to test reproducibility, more than one sample should be exposed for testing, preferably three samples for each exposure. Also the effects of surface rinsing should be tested. For instance, studying the severity of corrosion with freshwater, freshwater with identified contaminants, and saltwater should

be tested and compared to samples which are not rinsed. In addition, different frequencies of rinsing should be compared.

Often, there is a desire to understand the atmospheric conditions in locations with harsh conditions but this is not always easy (Antarctica and Kilauea volcano for instance). Since silver corrosion provides information about the species in an environment, it could be very useful in places where conditions are too harsh for sensitive equipment or humans. Although analysis of silver corrosion may not offer such great details as on-site monitoring techniques such as ion chromatography or aerosol mass spectroscopy, it may still ensure a preliminary evaluation about the oxidative capacity of the local environment. Corrosion product monitoring can establish long-term changes in corrosivity and can be used as a proxy for the changes in atmospheric chemistry at a location of interest.

Silver coupons are a reactive substrate for atmospheric deposition; this lends Ag to being a good monitor for chloride, sulfide, oxidized sulfur, and even oxidized organics. However, there are a few weaknesses in using silver. First, silver is not inexpensive, nor is surface-sensitive analysis using XPS or ToF-SIMS if one is not readily available for use. Second, some silver corrosion products are soluble. This study showed evidence that sheltering can often reduce the impact of surface rinsing, but it cannot be completely mitigated. Therefore, certain very soluble species such as nitrates are not able to be monitored with this technique. However, even with these drawbacks, silver remains a relatively easy and efficient way to get a general sense of an environment's corrosivity.

References

- (1) Chen, Z. Y.; Liang, D.; Ma, G.; Frankel, G. S.; Allen, H. C.; Kelly, R. G. *Corr. Eng. Sci. Tech.* **2010**, *45*, 169–180.
- (2) Liang, D.; Allen, H. C.; Frankel, G. S.; Chen, Z. Y.; Kelly, R. G.; Wu, Y.; Wyslouzil, B. E. *J. Electrochem. Soc.* **2010**, *157*, C146–C156.
- (3) Wan, Y.; Macha, E. N.; Kelly, R. G. *Corrosion* **2012**, *68*, 0360011–03600110.
- (4) Abbott, W. H. *A Decade of Corrosion Monitoring in the World's Military Operating Environments*; Columbus, OH: Battelle Columbus Operations, 2008.
- (5) Thornton, J. A.; Kercher, J. P.; Riedel, T. P.; Wagner, N. L.; Cozic, J.; Holloway, J. S.; Dube, W. P.; Wolfe, G. M.; Quinn, P. K.; Middlebrook, A. M.; Alexander, B.; Brown, S. S. *Nature* **2010**, *464*, 271–274.
- (6) Simon, H.; Kimura, Y.; McGaughey, G.; Allen, D. T.; Brown, S. S.; Coffman, D.; Dibb, J.; Osthoff, H. D.; Quinn, P.; Roberts, J. M.; Yarwood, G.; Kemball-Cook, S.; Byun, D.; Lee, D. *Atmos. Environ.* **2010**, *44*, 5476–5488.
- (7) Latanision, R. M. *Mater. Performance* **1987**, *26*, 9–16.
- (8) Leygraf, C.; Graedel, T. E. *Atmospheric Corrosion*; John Wiley & Sons: New York, New York, 2000.
- (9) Koch, G. H.; Brongers, M. P. H.; Thompson, N. G.; Virmani, Y. P.; Payer, J. H. *Corrosion Costs and Preventative Strategies in the United States*; CC Technologies Laboratories, Inc.: Dublin, OH, 2001.
- (10) Landolt, D. *Corrosion and Surface Chemistry of Metals*; CRC Press: Boca Raton, FL, 2007.
- (11) Yano, S.; Wang, M.; Ichikawa, T. U.S. Patent 7,153,566 **2006**.
- (12) Bertine, K. K.; Goldberg, E. D. *Science* **1971**, *173*, 233–235.
- (13) Reddy, M. S.; Venkataraman, C. *Atmos. Environ.* **2002**, *36*, 677–697.
- (14) Penkett, S. A.; Jones, B. M. R.; Brice, K. A.; Eggleton, A. E. *J. Atmos. Environ.* **1979**, *13*, 123–137.
- (15) Bates, T. S.; Lamb, B. K.; Guenther, A.; Dignon, J.; Stoiber, R. E. *J. Atmos. Chem.* **1992**, *14*, 315–337.
- (16) Graedel, T.; Benkovitz, C.; Keene, W.; Lee, D.; Marland, G. *Water Air Soil Pollut.* **1995**, *85*, 25–36.
- (17) Vogt, R.; Crutzen, P. J.; Sander, R. *Nature* **1996**, *383*, 327–330.
- (18) Fitzgerald, J. W. *Atmos. Environ. A* **1991**, *25*, 533–545.
- (19) ODowd, C.; Smith, M.; Consterdine, I.; Lowe, J. *Atmos. Environ.* **1997**, *31*, 73–80.
- (20) Perry, R. H.; Green, D. W. *Perry's Chemical Engineers' Handbook*; 7th ed.; McGraw-Hill.
- (21) Graedel, T. *Corrosion Sci.* **1996**, *38*, 2153–2180.
- (22) Yan, B. D.; Meilink, S.; Warren, G.; Wynblatt, P. *Components, Hybrids, and Manufacturing Technology, IEEE Transactions on* **1987**, *10*, 247–251.
- (23) Schutz, L.; Kramer, M. *J. Atmos. Chem.* **1987**, *5*, 173–184.

- (24) Novakov, T.; Penner, J. *Nature* **1993**, 365, 823–826.
- (25) Heintzenberg, J. *Tellus Ser. B-Chem. Phys. Meteorol.* **1989**, 41, 149–160.
- (26) Virtanen, S.; Schmuki, P.; Davenport, A.; Vitus, C. *J. Electrochem. Soc.* **1997**, 144, 198–204.
- (27) Fuoss, R. M. *J. Am. Chem. Soc.* **1958**, 80, 5059–5061.
- (28) Rudolph, W. W.; Irmer, G.; Hefter, G. T. *Phys. Chem. Chem. Phys.* **2003**, 5, 5253–5261.
- (29) Eigen, M.; Tamm, K. *Zeitschrift Fur Elektrochemie* **1962**, 66, 93–107.
- (30) Eigen, M.; Tamm, K. *Zeitschrift Fur Elektrochemie* **1962**, 66, 107–121.
- (31) Kucera, V.; Mattsson, E. In *Corrosion Mechanisms*; Mansfield, F., Ed.; Marcel Dekker: New York, 1987; pp. 211–284.
- (32) Revie, R. W. *Uhlig's Corrosion Handbook*; John Wiley & Sons, 2011.
- (33) Uller, L.; Morcillo, M. *Proceedings of the 11th International Corrosion Congress* **1990**, 2, 2.35–2.45.
- (34) Kucera, V.; Coote, A. T.; Henriksen, J. F.; et al. *Proceedings of the 11th International Corrosion Congress* **1990**, 2, 2.433–2.442.
- (35) Dean, S. W. In *Degradation of Metals in the Atmosphere, ASTM STP 965*; American Society for Testing and Materials: Philadelphia, 1988; pp. 385–431.
- (36) ISO/TC 9223:1992: Corrosion of metals and alloys - Corrosivity of atmospheres - Classification.
- (37) Norm ISO N. 9223 **1989**.
- (38) ASTM Standard B117, 2011, “Standard Practice for Operating Salt Spray (Fog) Apparatus,” ASTM International, 2011, DOI: 10.1520/B0117-11, www.astm.org.
- (39) Deflorian, F.; Rossi, S.; Fedrizzi, L.; Zanella, C. *Prog. Org. Coat.* **2007**, 59, 244–250.
- (40) Lenntech.com Calculator for Relative Humidity.
- (41) *CRC Handbook of Chemistry and Physics*; 84th ed.; CRC: Boca Raton, FL, 2003.
- (42) Finlayson-Pitts, B. J.; Pitts, J. N. *Chemistry of the Upper and Lower Troposphere*; Academic Press, 2000.
- (43) Wayne, R. P.; Barnes, I.; Biggs, P.; Burrows, J. P.; Canosamas, C. E.; Hjorth, J.; Lebras, G.; Moortgat, G. K.; Perner, D.; Poulet, G.; Restelli, G.; Sidebottom, H. *Atmos. Environ. A* **1991**, 25, 1–203.
- (44) Atkinson, R. *J. Phys. Chem. Ref. Data* **1991**, 20, 459–507.
- (45) Finlayson-Pitts, B. J. *Res. Chem. Intermediat.* **1993**, 19, 235–249.
- (46) Graedel, T. E.; Keene, W. . *Glob. Biogeochem. Cycle* **1995**, 9, 47–77.
- (47) Andreae, M. O.; Crutzen, P. J. *Science* **1997**, 276, 1052–1058.
- (48) Finlayson-Pitts, B. J.; Pitts Jr., J. N. *Science* **1997**, 276, 1045–1052.
- (49) De Haan, D.; Brauers, T.; Oum, K.; Stutz, J.; Nordmeyer, T.; Finlayson-Pitts, B. *Int. Rev. Phys. Chem.* **1999**, 18, 343–385.
- (50) Hemminger, J. *Int. Rev. Phys. Chem.* **1999**, 18, 387–417.
- (51) Isaksen, I. S. A.; Dalsoren, S. B. *Science* **2011**, 331, 38–39.
- (52) Dorn, H.; Brandenburger, U.; Brauers, T.; Hausmann, M.; Ehhalt, D. *Geophys. Res. Lett.* **1996**, 23, 2537–2540.
- (53) DeMore, W. B.; Sander, S. P.; Golden, D. M.; Hampson, R. F.; Kurylo, M. J.; Howard, C. J.; Ravishankara, A. R.; Kolb, C. E.; Molina, M. J. *JPL Publication* **1997**, 4.

- (54) Liang, D. Environmental and Alloying Effects on Corrosion of Metals and Alloys. Ph.D. Thesis, The Ohio State University: USA, 2009.
- (55) Lippmann, M. *JAPCA J. Air Waste Ma.* **1989**, *39*, 672–695.
- (56) Lippmann, M. *J. Expo. Anal. Environ. Epidemiol.* **1993**, *3*, 103–129.
- (57) Weschler, C. J. *Environ. Health Perspect.* **2006**, *114*, 1489–1496.
- (58) Singh, H. B.; Ludwig, F. L.; Johnson, W. . *Atmos. Environ.* **1978**, *12*, 2185–2196.
- (59) Gurol, M. D.; Akata, A. *AICHE J.* **1996**, *42*, 3283–3292.
- (60) Peyton, G.; Glaze, W. *Environ. Sci. Technol.* **1988**, *22*, 761–767.
- (61) Taube, H. *Trans. Farad. Soc.* **1957**, *53*, 656–665.
- (62) Wagner, I.; Karthausser, J.; Strehlow, H. *Berich. Bunsen. Gesell.* **1986**, *90*, 861–867.
- (63) Knipping, E. M.; Lakin, M. J.; Foster, K. L.; Jungwirth, P.; Tobias, D. J.; Gerber, R. B.; Dabdub, D.; Finlayson-Pitts, B. J. *Science* **2000**, *288*, 301–306.
- (64) Oum, K. W.; Lakin, M. J.; DeHaan, D. O.; Brauers, T.; Finlayson-Pitts, B. J. *Science* **1998**, *279*, 74.
- (65) U.S. EPA Method 16A - Determination of Total Reduced Sulfur Emissions from Stationary Sources (Impinger Technique).
- (66) Schwartz, S. E. *Nature* **1988**, *336*, 441–445.
- (67) Charlson, R. J.; Lovelock, J. E.; Andreae, M. O.; Warren, S. G. *Nature* **1987**, *326*, 655–661.
- (68) Charlson, R. J.; Schwartz, S. E.; Hales, J. M.; Cess, R. D.; Coakley, J.; Hansen, J. E.; Hofmann, D. J. *Science* **1992**, *255*, 423–430.
- (69) U.S. EPA Method 16B - Determination of Total Reduced Sulfur Emissions from Stationary Sources.
- (70) Seinfeld, J. H.; Pandis, S. N. *Atmospheric Chemistry and Physics: From Air Pollution to Climate Change*; Second ed.; John Wiley & Sons, Inc.: Hoboken, New Jersey, 2006.
- (71) Hazardous Substances Data Bank **1994**.
- (72) Chemical Summary for Carbonyl Sulfide **1994**.
- (73) Svensson, J. E.; Johansson, L. G. *J. Electrochem. Soc.* **1993**, *140*, 2210–2216.
- (74) Freiberg, J. *Environ. Sci. Technol.* **1974**, *8*, 731–734.
- (75) Freiberg, J. *Atmos. Environ.* **1975**, *9*, 661–672.
- (76) Freiberg, J. *Atmos. Environ.* **1976**, *10*, 121–130.
- (77) Ibusuki, T.; Ohsawa, M.; Takeuchi, K. *Atmos. Environ. A* **1990**, *24*, 1325–1330.
- (78) Covert, D.; Kapustin, V.; Bates, T.; Quinn, P. *J. Geophys. Res. Atmos.* **1996**, *101*, 6919–6930.
- (79) Spicer, C. W.; Chapman, E. G.; Finlayson-Pitts, B. J.; Plastringe, R. A.; Hubbe, J. M.; Fast, J. D.; Berkowitz, C. M. *Nature* **1998**, *394*, 353–356.
- (80) Shaw, G. E. *J. Geophys. Res. Atmos.* **1991**, *96*, 22369–22372.
- (81) Pszenny, A. A. P.; Keene, W. C.; Jacob, D. J.; Fan, S.; Maben, J. R.; Zetwo, M. P.; Springeryoung, M.; Galloway, J. N. *Geophys. Res. Lett.* **1993**, *20*, 699–702.
- (82) Singh, H.; Gregory, G.; Anderson, B.; Browell, E.; Sachse, G.; Davis, D.; Crawford, J.; Bradshaw, J.; Talbot, R.; Blake, D.; Thornton, D.; Newell, R.; Merrill, J. *J. Geophys. Res. Atmos.* **1996**, *101*, 1907–1917.
- (83) Mazzera, D. M.; Lowenthal, D. H.; Chow, J. C.; Watson, J. G.; Grubisic, V. *Atmos. Environ.* **2001**, *35*, 1891–1902.

- (84) Pueschel, R. F.; Snetsinger, K. G.; Goodman, J. K.; Toon, O. B.; Ferry, G. V.; Oberbeck, V. R.; Livingston, J. M.; Verma, S.; Fong, W.; Starr, W. L.; Chan, K. *R. J. Geophys. Res. Atmos.* **1989**, *94*, 11271–11284.
- (85) Solomon, S.; Sanders, R. W.; Miller, H. L. *J. Geophys. Res. Atmos.* **1990**, *95*, 13807–13817.
- (86) Finlayson-Pitts, B. J.; Ezell, M. J.; Pitts Jr., J. N. *Nature* **1989**, *337*, 241–244.
- (87) Ravishankara, A. R. *Proc. Natl. Acad. Sci.* **2009**, *106*, 13639–13640.
- (88) von Glasow, R. *Nature* **2010**, *464*, 168–169.
- (89) Finlayson-Pitts, B. J.; Hemminger, J. C. *J. Phys. Chem. A* **2000**, *104*, 11463–11477.
- (90) Raff, J. D.; Njegic, B.; Chang, W. L.; Gordon, M. S.; Dabdub, D.; Gerber, R. B.; Finlayson-Pitts, B. J. *Proc. Natl. Acad. Sci.* **2009**, *106*, 13647–13654.
- (91) George, C.; Behnke, W.; Zetzsch, C. *ChemPhysChem* **2010**, *11*, 3059–3062.
- (92) Ali, A. K. M.; Saleh, J. M.; Hikmat, N. A. *J. Chem. Soc. Farad. Trans.* **1987**, *83*, 2391–2406.
- (93) von Gunten, U. *Water Res.* **2003**, *37*, 1443–1467.
- (94) Yeatts, L.; Taube, H. *J. Am. Chem. Soc.* **1949**, *71*, 4100–4105.
- (95) Levanov, A. V.; Kuskov, I. V.; Koiaidarova, K. B.; Zosimov, A. V.; Antipenko, E. E.; Lunin, V. V. *Kinet. Catal.* **2005**, *46*, 138–143.
- (96) Knipping, E. M.; Dabdub, D. *J. Geophys. Res. Atmos.* **2002**, *107*.
- (97) Watanabe, M.; Hokazono, A.; Handa, T.; Ichino, T.; Kuwaki, N. *Corr. Sci.* **2006**, *48*, 3759–3766.
- (98) Watanabe, M.; Shinozaki, S.; Toyoda, E.; Asakura, K.; Ichino, T.; Kuwaki, N.; Higashi, Y.; Tanaka, T. *Corrosion* **2006**, *62*, 243–250.
- (99) Johansson, E.; Leygraf, C. *Brit. Corros. J.* **1999**, *34*, 27–33.
- (100) Graedel, T. *J. Electrochem. Soc.* **1992**, *139*, 1963–1970.
- (101) Abbott, W. H. *Mater. Perf.* **1985**, *24*, 46–50.
- (102) Abbott, W. H. *Mater. Perf.* **1991**, *30*, 55–58.
- (103) Tullmin, M.; Roberge, P. R. *IEEE T. Reliab.* **1995**, *44*, 271–278.
- (104) Brusic, V.; Angelopoulos, M.; Graham, T. *J. Electrochem. Soc.* **1997**, *144*, 436–442.
- (105) Rice, D. W.; Peterson, P.; Rigby, E. B.; Phipps, P. B. P.; Cappell, R. J.; Tremoureux, R. *J. Electrochem. Soc.* **1981**, *128*, 275–284.
- (106) McCord, K. M.; Klinglesmith, D. A.; Jurgenson, C. A.; et al. *Proc. of the SPIE* **2009**, *7425*.
- (107) Abbott, W. H. *IEEE T. Reliab.* **1974**, *PHP-10*, 24–27.
- (108) Engel, T.; Reid, P. *Thermodynamics, Statistical Thermodynamics, & Kinetics*; Second.; Pearson Prentice Hall: New Jersey, 2010.
- (109) Shaw, R. W. In *Meteorological Aspects of Acid Rain*; Bhumralker, C. M., Ed.; Acid Precipitation; Butterworth: Stoneham, MA, 1984; Vol. 1, pp. 33–55.
- (110) Martin, A. *Atmos. Environ.* **1984**, *18*, 1955–1961.
- (111) Nazaroff, W. W.; Cass, G. R. *Environ. Sci. Technol.* **1986**, *20*, 924–934.
- (112) Tang, I. N.; Munkelwitz, H. R. *Atmos. Environ. A* **1993**, *27*, 467–473.
- (113) Sinclair, J. D.; Psotakelty, L. A.; Weschler, C. J. *Atmos. Environ.* **1988**, *22*, 461–469.
- (114) Czanderna, A. W. *J. Phys. Chem.* **1964**, *68*, 2765–2771.

- (115) Wagner, C. *J. Chem. Phys.* **1953**, *21*, 1819–1827.
- (116) Bouquet, S.; Bodin, C.; Fiaud, C. *CR Acad Sci II* **1993**, *316*, 459–464.
- (117) Kim, H.; Payer, J. H. *J. Corr. Sci. Engin.* **1999**, *1*, 14.1–14.10.
- (118) Laskin, A.; Gaspar, D. J.; Wang, W. H.; Hunt, S. W.; Cowin, J. P.; Colson, S. D.; Finlayson-Pitts, B. J. *Science* **2003**, *301*, 340–344.
- (119) Shamay, E. S.; Johnson, K. E.; Richmond, G. L. *J. Phys. Chem. C* **2011**, *115*, 25304–25314.
- (120) Latest Kilauea Eruption Gets a Name. *Star Advertiser* **2011**.
- (121) New Eruption Spews 2.5 Million Cubic Meters of Lava per Day. *Star Advertiser* **2011**.
- (122) Price, S.; Pales, J. C. *Monthly Weather Review* **1963**, *91*, 665–680.
- (123) Hahn, C.; Merrill, J.; Mendonca, B. J. *Geophys. Res.-Atmos.* **1992**, *97*, 10291–10309.
- (124) Mendonca, B. G.; Iwaoka, W. T. *Journal of Applied Meteorology* **1969**, *8*, 213–219.
- (125) University of Hawaii Hawai'i Institute of Marine Biology
<http://www.hawaii.edu/HIMB/info.html> (accessed Aug 24, 2012).
- (126) The United States in Antarctica. Report of the U.S. Antarctic Program External Panel **1997**.
- (127) Solomon, S.; Garcia, R. R.; Rowland, F. S.; Wuebbles, D. J. *Nature* **1986**, *321*, 755–758.
- (128) Kerminen, V.-M.; Teinilä, K.; Hillamo, R. *Atmos. Environ.* **2000**, *34*, 2817–2825.
- (129) Morcillo, M.; Chico, B.; de la Fuente, D.; Almeida, E.; Joseph, G.; Rivero, S.; Rosales, B. *Cold Reg. Sci. Technol.* **2004**, *40*, 165–178.
- (130) Otieno-Alego, V.; King, G.; Hughes, J.; Gillett, R. *Corrosion & Prevention* **2000**, Paper 010 Page 1–8.
- (131) Lin, H.; Frankel, G. S. Unpublished Research.
- (132) Nishio, G.; Kitani, S.; Takahash.k *Ind. Eng. Chem. Process Design and Development* **1974**, *13*, 408–415.
- (133) ASTM Standards for Corrosion Testing of Metals, in ASTM Standards, ASTM Standard B117, 2011, “Standard Practice for Operating Salt Spray (Fog) Apparatus,” ASTM International, 2011, DOI: 10.1520/B0117-11, www.astm.org. **2007**.
- (134) Larsson, L. O. *Acta Chem. Scand.* **1969**, *23*, 2261–2269.
- (135) *Surface Analysis - The Principal Techniques*; John C. Vickerman; Ian S. Gilmore, Eds.; Second.; John Wiley & Sons, Ltd: West Sussex, UK, 2009.
- (136) Kaushik, V. K. *J. Electron Spectrosc.* **1991**, *56*, 273–277.
- (137) Fukuda, Y.; Fukushima, T.; Sulaiman, A.; Musalam, I.; Yap, L.; Chotimongkol, L.; Judabong, S.; Potjanart, A.; Keowkangwal, O.; Yoshihara, K.; Tosa, M. *J. Electrochem. Soc.* **1991**, *138*, 1238–1243.
- (138) Casa Software Ltd. CasaXPS Help Manual.
- (139) Shirley, D. A. *Phys. Rev. B* **1972**, *5*, 4709–4714.
- (140) Castle, J. .; Chapman-Kpodo, H.; Proctor, A.; Salvi, A. . *J. Electron Spectrosc.* **2000**, *106*, 65–80.
- (141) Végh, J. *J. Electron Spectrosc.* **2006**, *151*, 159–164.
- (142) Evans, S. *Surf Interface anal* **1991**, *17*, 85–93.

- (143) International Centre for Diffraction Data *Powder Diffraction File 4-783*; Newton Square, PA.
- (144) Suh, I.; Ohta, H.; Waseda, Y. *J. Mater. Sci.* **1988**, *23*, 757–760.
- (145) Rohrer, G. S. *Structure and Bonding in Crystalline Materials*; Cambridge University Press, 2001.
- (146) Schnoeller, J.; Wiesinger, R.; Kleber, C.; Hilfrich, U.; Schreiner, M.; Hutter, H. *Anal. Bioanal. Chem.* **2008**, *390*, 1543–1549.
- (147) Turner, N. H.; Murday, J. S.; Ramaker, D. E. *Anal. Chem.* **1980**, *52*, 84–92.
- (148) Outka, D.; Madix, R.; Fisher, G.; Dimaggio, C. *J. Phys. Chem.* **1986**, *90*, 4051–4057.
- (149) Outka, D.; Madix, R. *Surf. Sci.* **1984**, *137*, 242–260.
- (150) Alemozafar, A. R.; Guo, X. C.; Madix, R. J.; Hartmann, N.; Wang, J. *Surf. Sci.* **2002**, *504*, 223–234.
- (151) Santra, A. K.; Bird, D. P. C.; Sykes, E. C. H.; Williams, F. J.; Goldoni, A.; Baraldi, A.; Lambert, R. M. *J. Phys. Chem. B* **2001**, *105*, 10062–10068.
- (152) Li, W. K.; McKee, M. L. *J. Phys. Chem. A* **1997**, *101*, 9778–9782.
- (153) Morokuma, K.; Muguruma, C. *J. Am. Chem. Soc.* **1994**, *116*, 10316–10317.
- (154) Schwartz, S. E.; Freiberg, J. E. *Atmos. Environ.* **1981**, *15*, 1129–1144.
- (155) Hoffmann, M. R.; Calvert, J. G. *Chemical Transformation Modules for Eulerian Acid Deposition Models*; U.S. Environmental Protection Agency: Research Triangle Park, NC, 1985; Vol. 2, The Aqueous-Phase Chemistry.
- (156) Hoffmann, M. *Atmos. Environ.* **1986**, *20*, 1145–1154.
- (157) Mcardle, J.; Hoffmann, M. *J. Phys. Chem.* **1983**, *87*, 5425–5429.
- (158) Martin, L.R. *SO₂, NO, and NO₂ Oxidation Mechanisms: Atmospheric Considerations*; Calvert, J.G., Ed.; Butterworth: Stoneham, MA, 1984.
- (159) Wang, C. B.; Deo, G.; Wachs, I. E. *J. Phys. Chem. B* **1999**, *103*, 5645–5656.
- (160) Ermakov, A. N.; Purmall, A. P. *Kinet. Catal.* **2001**, *42*, 479–489.
- (161) Yermakov, A. N.; Larin, I. K.; Ugarov, A. A.; Purmal', A. P. *Kinet. Catal.* **2003**, *44*, 476–489.
- (162) Sun, Q.; Shen, B. R.; Fan, K. N.; Deng, J. *Chem. Phys. Lett.* **2000**, *322*, 1–8.
- (163) Mackenzie, J. K.; Nicholas, J. F. *J. Phys. Chem. Solids* **1962**, *23*, 197–205.
- (164) Wise, H.; Oudar, J. *Material Concepts in Surface Reactivity and Catalysis*; Courier Dover Publications, 2002.
- (165) Wyckoff, R. *Am. J. Sci.* **1922**, *3*, 184–188.
- (166) Swanson, H. E.; Tatge, E. *Standard X-ray Diffraction Powder Patterns*; Natl. Bur. Std. Circular 539: Washington, D.C., 1953; Vol. 1.
- (167) Talbot, R.; Mao, H.; Sive, B. *J. Geophys. Res.* **2005**, *110*, 1–16.
- (168) Chen, M.; Talbot, R.; Mao, H.; Sive, B.; Chen, J.; Griffin, R. J. *J. Geophys. Res. Atmos.* **2007**, *112*, 1–13.
- (169) Mao, H. T.; Talbot, R. *J. Geophys. Res. Atmos.* **2004**, *109*, 1–17.
- (170) Ziemba, L. D.; Fischer, E.; Griffin, R. J.; Talbot, R. W. *J. Geophys. Res. Atmos.* **2007**, *112*, 1–13.
- (171) Keene, W. C.; Stutz, J.; Pszenny, A. A. P.; Maben, J. R.; Fischer, E. V.; Smith, A. M.; von Glasow, R.; Pechtl, S.; Sive, B. C.; Varner, R. K. *J. Geophys. Res. Atmos.* **2007**, *112*, 1–15.

- (172) Keene, W. C.; Pszenny, A. A. P.; Maben, J. R.; Stevenson, E.; Wall, A. J. *Geophys. Res. Atmos.* **2004**, *109*, 1–16.
- (173) Fischer, E.; Pszenny, A.; Keene, W.; Maben, J.; Smith, A.; Stohl, A.; Talbot, R. J. *Geophys. Res. Atmos.* **2006**, *111*, 1–14.
- (174) AIRMAP: Atmospheric Investigation, Regional Modeling, Analysis and Prediction <http://airmap.unh.edu/> (accessed May 15, 2012).
- (175) DeBell, L. J.; Vozzella, M.; Talbot, R. W.; Dibb, J. E. *J. Geophys. Res.* **2004**, *109*, 1–16.
- (176) Behnke, W.; Scheer, V.; Zetzsch, C. *Production of a Photolytic Precursor of Atomic Cl from Aerosols and Cl⁻ in the Presence of O₃*; Grimvall, A.; deLeer, E. W. B., Eds.; Naturally-Produced Organohalogen; Kluwer Academic Publ: Dordrecht, 1995.
- (177) Singh, H. B.; Kasting, J. F. *J. Atmos. Chem.* **1988**, *7*, 261–285.
- (178) Keene, W. C.; Pszenny, A. A. P.; Jacob, D. I.; Duce, R. A.; Galloway, J. N.; Schultz-Tokos, J. J.; Sievering, H.; Boatman, J. F. *Global Biogeochem. Cy.* **1990**, *4*, 407–430.
- (179) Maben, J. R.; Keene, W. C.; Pszenny, A. A. P.; Galloway, J. N. *Geophys. Res. Lett.* **1995**, *22*, 3513–3516.
- (180) Molina, M. J.; Rowland, F. S. *Nature* **1974**, *249*, 810–812.
- (181) Atkinson, R. *J. Phys. Chem. Ref. Data* **1997**, *26*, 215–290.
- (182) Thompson, A. M. *Science* **1992**, *256*, 1157–1165.
- (183) Roberts, J. M.; Osthoff, H. D.; Brown, S. S.; Ravishankara, A. R. *Science* **2008**, *321*, 1059–1060.
- (184) Vignati, E.; de Leeuw, G.; Berkowicz, R. *J. Geophys. Res. Atmos.* **2001**, *106*, 20225–20238.
- (185) Mankin, W. G.; Coffey, M. T.; Goldman, A. *Geophys. Res. Lett.* **1992**, *19*, 179–182.
- (186) Pourbaix, M. *Atlas of Electrochemical Equilibria in Aqueous Solutions*; 2nd ed.; Natl Assn of Corrosion, 1974.

Appendix A: Tables

Table A.1 Thermodynamic parameters (K_{sp} , ΔH , ΔS , and ΔG) used in this study.⁴¹

Formula	K_{sp}	Enthalpy, ΔH (kJ/mol)	Entropy, ΔS (J/mol·K)	Free Energy, ΔG (kJ/mol)
Ag	0	0	42.55	0
Ag ⁺				+105.58
Ag ₂ O	3.6×10^{-11}	-31.05	121.34	-11.22
Ag ₂ S	8×10^{-51}	-29.41	150.62	-40.70
Ag ₂ SO ₄	1.2×10^{-5}	-715.88	200.41	-618.89
AgCl	1.77×10^{-10}	-127.07	96.23	-109.88
AgNO ₃	51.6	-124.39	140.92	-33.47
Ag ₂ CO ₃	8.46×10^{-12}	-505.85	167.36	-436.81
Ag ₂ SO ₃	1.5×10^{-14}	-490.78	158.16	-411.56
AgNO ₂	6×10^{-4}	-45.06	128.20	19.08
AgClO ₂	2.0×10^{-4}	8.79	134.56	75.73
Cl radical		121.29	165.06	105.31
Cl ⁻		-167.15	56.48	-131.25
Cl ₂		0	222.97	0
CO ₂		-393.51	213.68	-394.38
H ₂		0	130.58	0
H ₂ O(g)		-241.82	188.72	-228.59
H ₂ O(l)		-285.83	69.91	-237.18
H ₂ O ₂ (g)		-136.11	232.88	-105.48
H ₂ O ₂ (l)		-187.78	109.62	-120.42
H ₂ S		-20.17	205.77	-33.05
HSO ₃ ⁻		-626.22	139.75	-527.8
H ₂ SO ₄		-813.99	156.9	-690.07
O radical		249.17	160.95	231.75
O ₂		0	205.03	0
O ₃		142.67	238.82	163.18
OH radical		38.95	183.64	34.23
OH ⁻		-229.99	-10.75	-157.27
SO ₂		-296.83	248.11	-300.19
SO ₃ ²⁻		-635.55	-29.29	-486.60
SO ₄ ²⁻				-909.3
S ²⁻				+33.05
S ₂ O ₃ ²⁻				-648.5

Table A.2 Some Henry's constant (H) values which were used in this study.⁴¹

Formula	H (M/atm)
O ₂	1.3×10^{-3}
H ₂	7.8×10^{-4}
CO ₂	3.4×10^{-2}
N ₂	6.1×10^{-4}
CO	9.5×10^{-4}
NO ₂	1×10^{-2}
O ₃	$\sim 1 \times 10^{-2}$
SO ₂	1.2
H ₂ S	0.087
OCS	0.022
CS ₂	0.055
NH ₃	62
OH	30
HCl	1.1

Appendix B: Pourbaix Diagrams

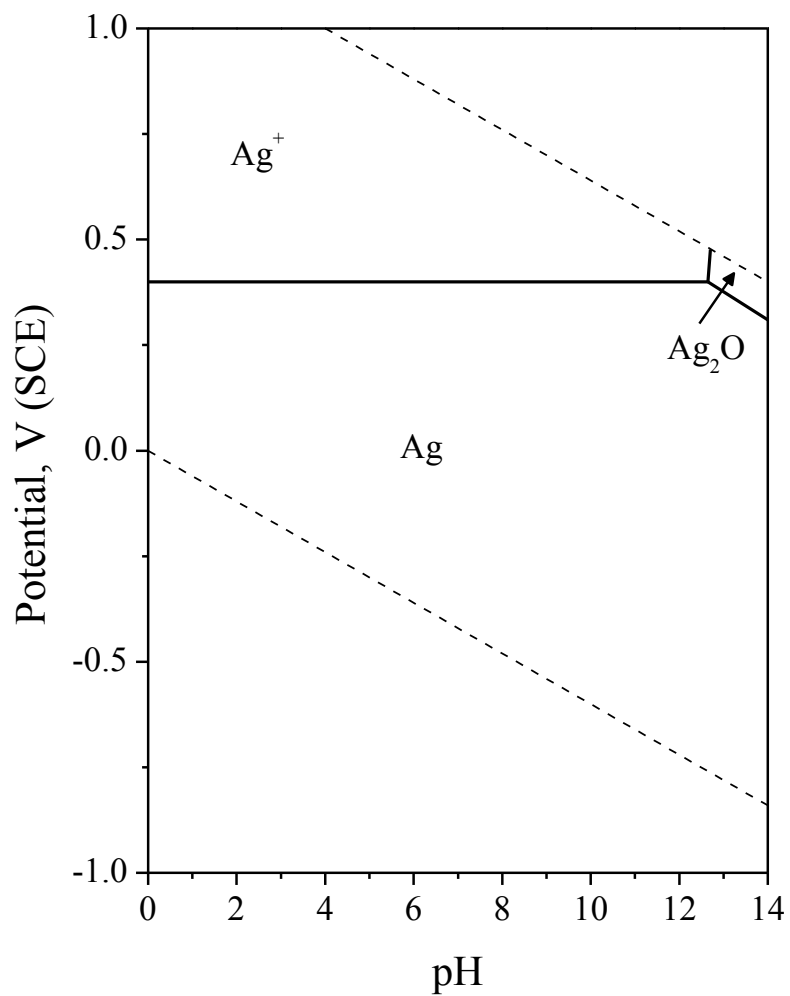


Figure B.1 Potential-pH diagram for Ag-H₂O at 25°C, for [dissolved Ag] = 1 μM. The region of water stability is bounded by the dashed lines (adapted from Pourbaix, 1974).¹⁸⁶

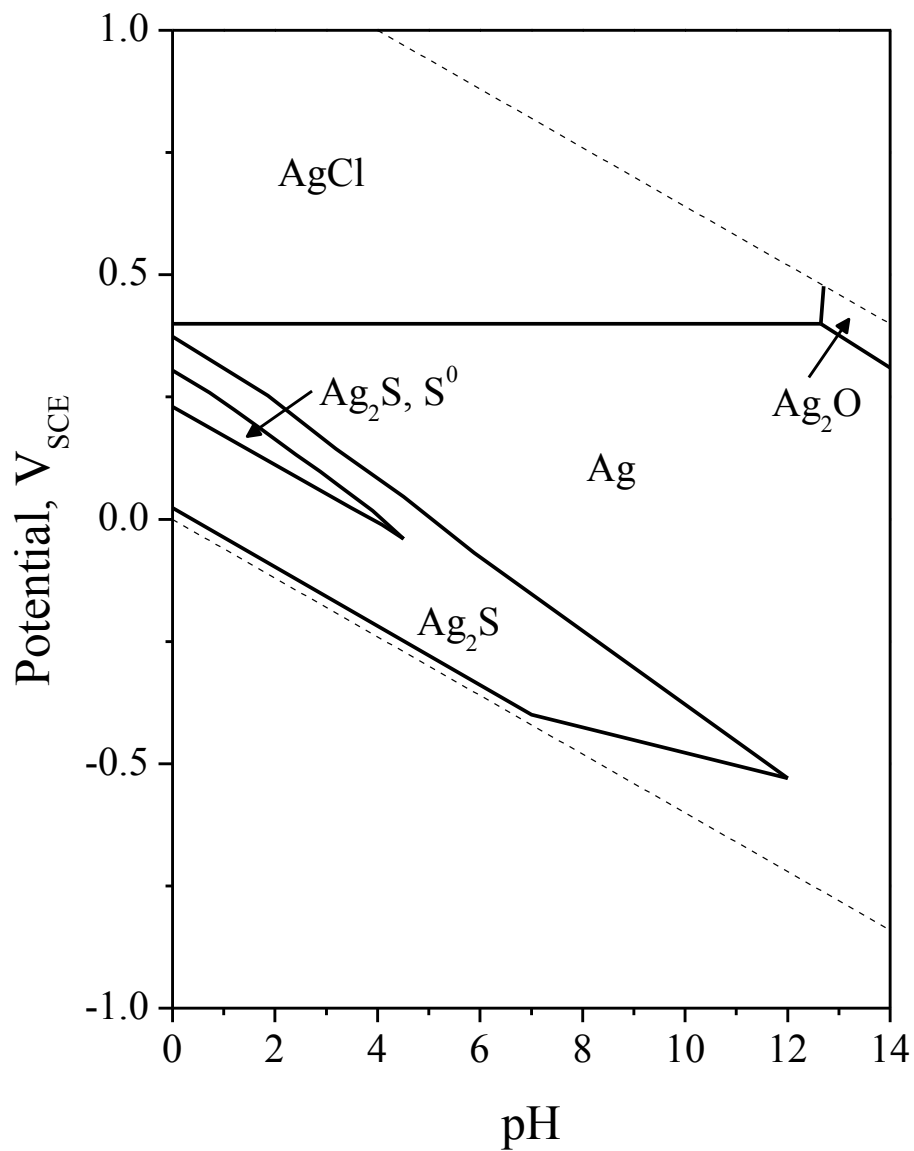


Figure B.2 Potential-pH diagram for Ag-S-Cl-CO₂-H₂O system at 25°C, for an activity of sulfur of 0.1 M, activity of chlorine of 0.05 M, total carbon concentration of 0.01 M, and for [dissolved Ag] = 1 μM. Similar to silver in a freshwater environment. The region of water stability is bounded by the dashed lines (adapted from Pourbaix, 1974).¹⁸⁶

Appendix C: Attenuation Length

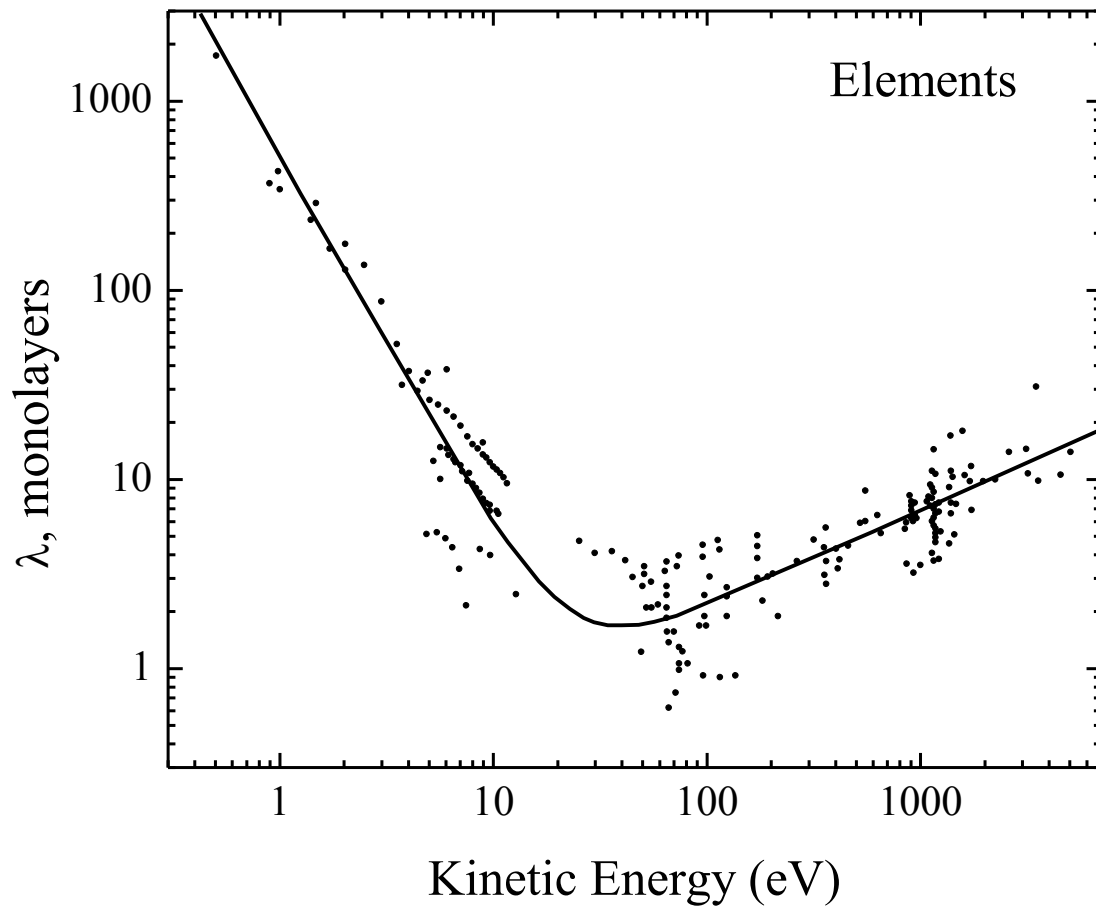


Figure C.1 Attenuation length plot indicating the kinetic energy of exiting electrons for a given number of monolayers. The dots are different elements and the line is a fit to the data (adapted from Vickerman and Gilmore, 2009).¹³⁵

Appendix D: Error in XPS

Date	Area under the curve	Average	Stdev
6/2/2012	140562.6	141820.7	1233.449
	141204.7		
	142107.2		
	143408.1		
6/15/2012	138638.8	139620.5	920.0871
	139256.5		
	139774.7		
	140812		
7/2/2012	136731.7	137299.1	543.6178
	137134.1		
	137189.4		
	137237.1		
	138203		
7/3/2012	134680.3	135911.5	919.0821
	135960.1		
	136104.9		
	136900.7		
7/4/2012	139024.3	142909.4	4465.731
	139265		
	141053.6		
	146203.5		
	149000.4		
7/5/2012	135440.5	139338.8	4778.431
	135866		
	137083.2		
	138362.6		
	141129.2		
	148151.5		
7/6/2012	128032.5	128517	693.9948
	128032.5		
	128119.9		
	128772		
	129628		
7/8/2012	126766.4	128986.7	2173.564
	129083.4		
	131110.3		
Average	137112	136800.4	45883.84
Stdev	5609.079	1965.995	1714.196

The same clean silver sample was analyzed via XPS over multiple days. Before each scan, the sample was etched with the argon ion beam until the carbon 1s signal was not detectable above the noise. To see the error within a day, take the standard deviation (stdev) divided by the average. This value (error) ranges from 3.4-0.4% across the different days. The average error for one day is about 1.4% (1965.995/136800.4). By taking the average and stdev of all days, the error can be found for the total to be about 4.1% (5609.079/137112).

Appendix E: Calculation of Film Thickness from a Reduction Curve

Assuming that all oxidized silver is in the form of Ag^+ , the most abundant oxidation state of silver, the reduction reaction is (see Eq. (1.42)):



Now, according to Faraday's law (see Eq. (1.2)):

$$1 \text{ mole of electrons} = 96454.56 \text{ C} = \text{charge of 1 mole of } \text{Ag}^+.$$

Since the ordinate axis in the reduction curves is time (for example, a reduction plateau spanning $t = 1000 \text{ s}$) and since a constant surface current of $I_s = 0.1 \text{ mA/cm}^2$ is applied, then by multiplying both these quantities, the surface charge over the reduction plateau may be calculated as:

$$Q_s = I_s t = 1000 \text{ s} \times 0.1 \frac{\text{mA}}{\text{cm}^2} = 100 \text{ mC/cm}^2. \quad (\text{E.2})$$

If one further assumed that the corrosion film is completely comprised of AgCl , the number of moles of Ag^+ per unit area can be calculated by:

$$N_s = \frac{Q_s}{F} = \left(\frac{100 \text{ mC/cm}^2}{96454.56 \text{ C/mol}} \right) \times \frac{0.001 \text{ C}}{\text{mC}} \approx 1.03 \times 10^{-6} \text{ mol/cm}^2. \quad (\text{E.3})$$

In the case of Ag^{2+} , the number of moles would be equal to the total charge divided by $2F$.

Finally, by multiplying Eq. (E.3) by the atomic weight and dividing by the density of AgCl, the thickness of the corrosion film is calculated:

$$d = \frac{N_s M_{\text{AgCl}}}{\rho_{\text{AgCl}}} = \left(\frac{1.03 \times 10^{-6} \text{ mol/cm}^2 \times 143.32 \text{ g/mol}}{5.56 \text{ g/cm}^3} \right) \times \frac{10^7 \text{ nm}}{\text{cm}} \approx 270 \text{ nm}. \quad (\text{E.4})$$

If there is more than one plateau, then the total charge is read at the end of the last plateau (excluding hydrogen evolution).

Appendix F: Complete XPS Spectra

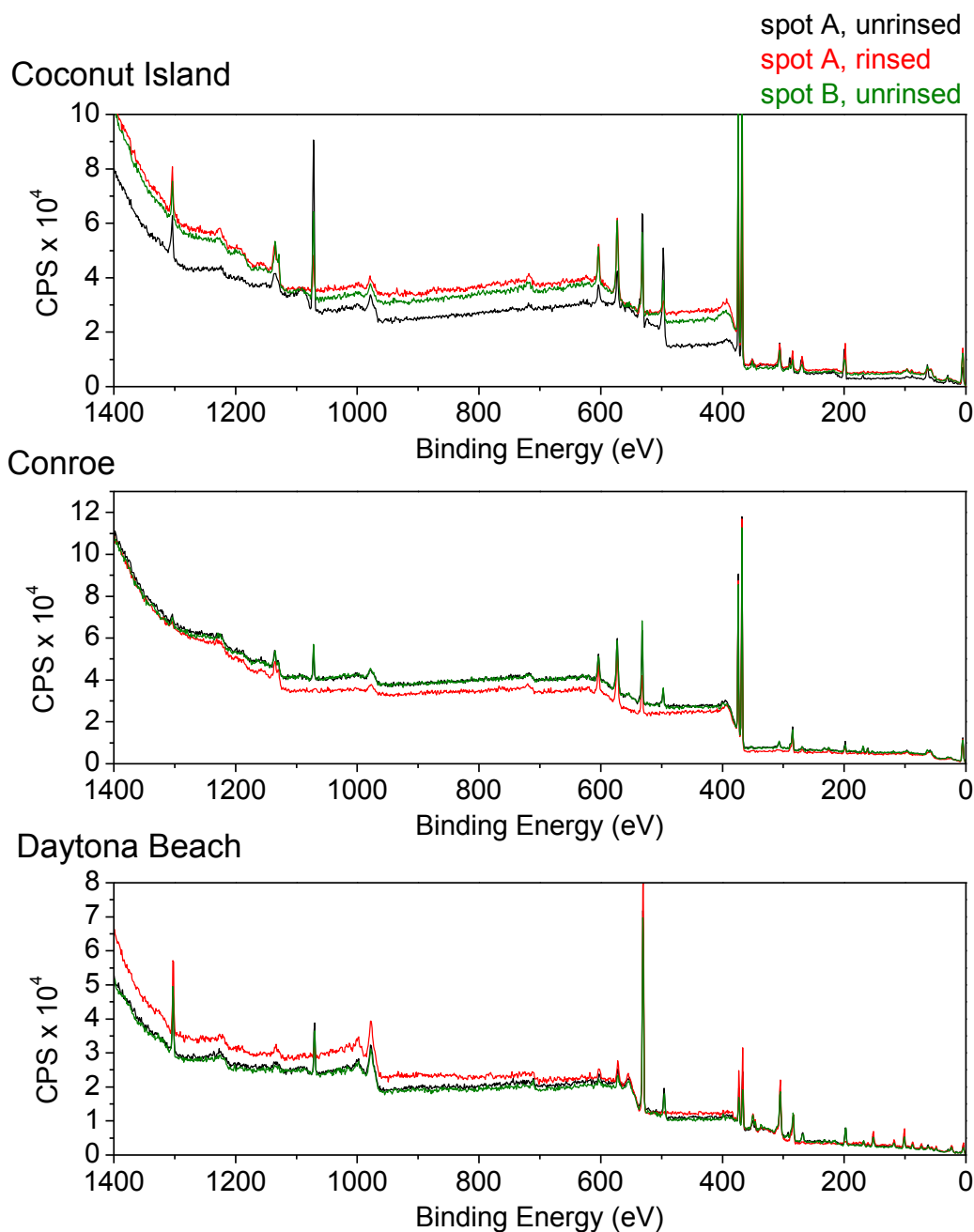


Figure F.1 XPS survey spectra for the samples exposed at Coconut Island, HI (top), Conroe, TX (middle), and Daytona Beach, FL (bottom). The black, red, and green spectra are on spot A unrinsed (dark area), spot A rinsed, and spot B unrinsed (light area), respectively.

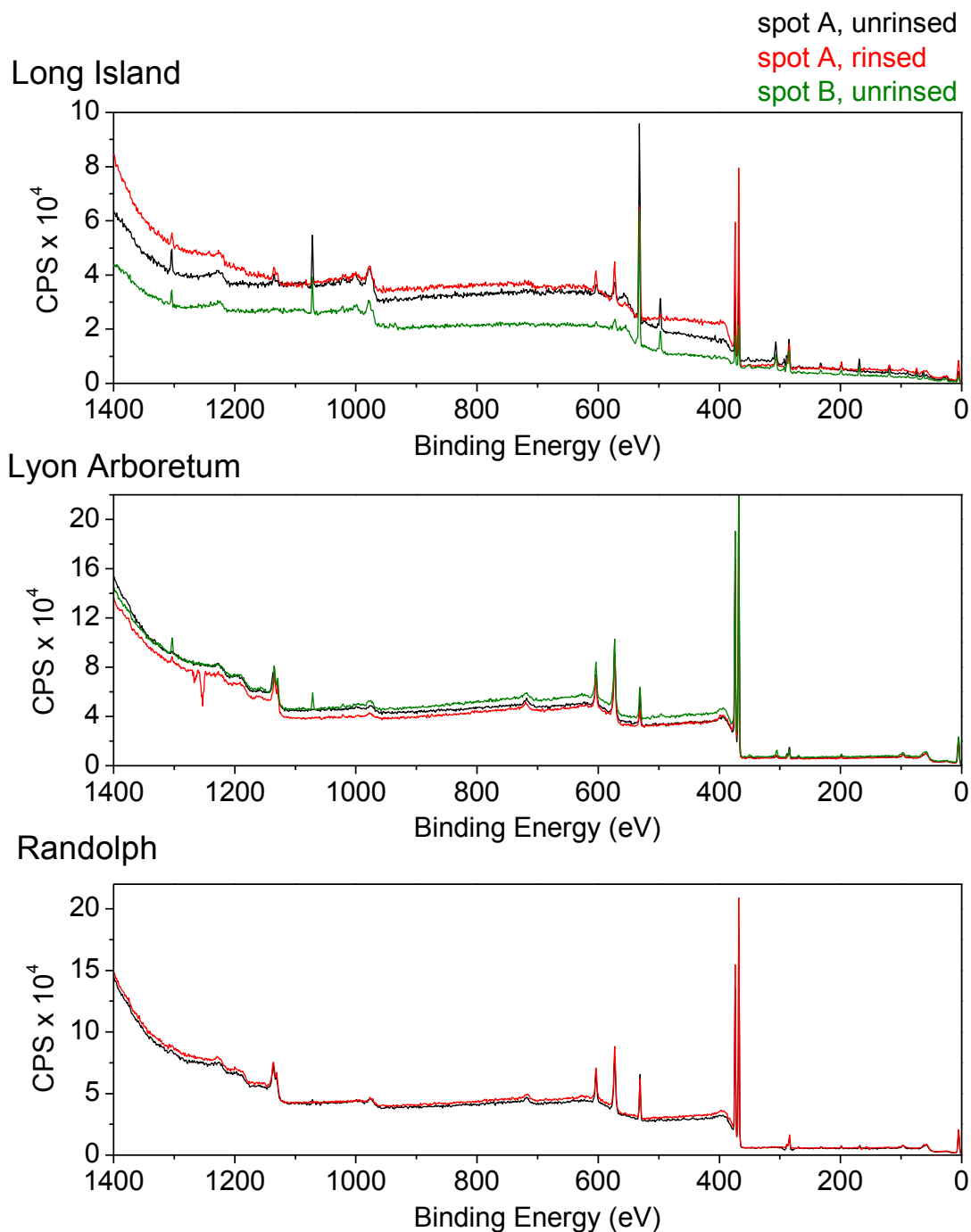


Figure F.2 XPS survey spectra for the samples exposed at Long Island, NY (top), Lyon Arboretum, HI (middle), and Randolph, TX (bottom). The black, red, and green spectra are on spot A unrinsed (dark area), spot A rinsed, and spot B unrinsed (light area), respectively.

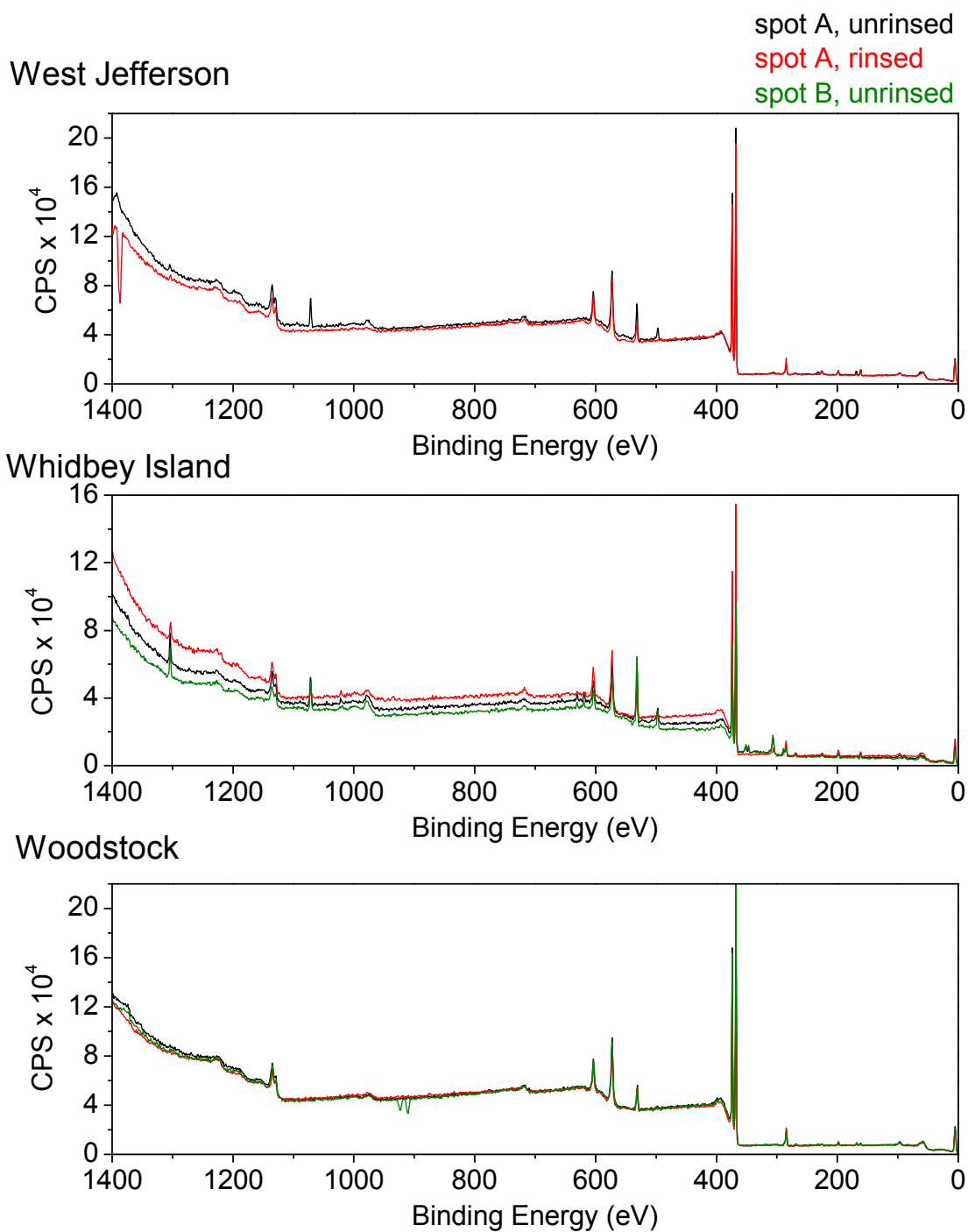


Figure F.3 XPS survey spectra for the samples exposed at West Jefferson, OH (top), Whidbey Island, WA (middle), and Woodstock, ME (bottom). The black, red, and green spectra are on spot A unrinsed (dark area), spot A rinsed, and spot B unrinsed (light area), respectively.

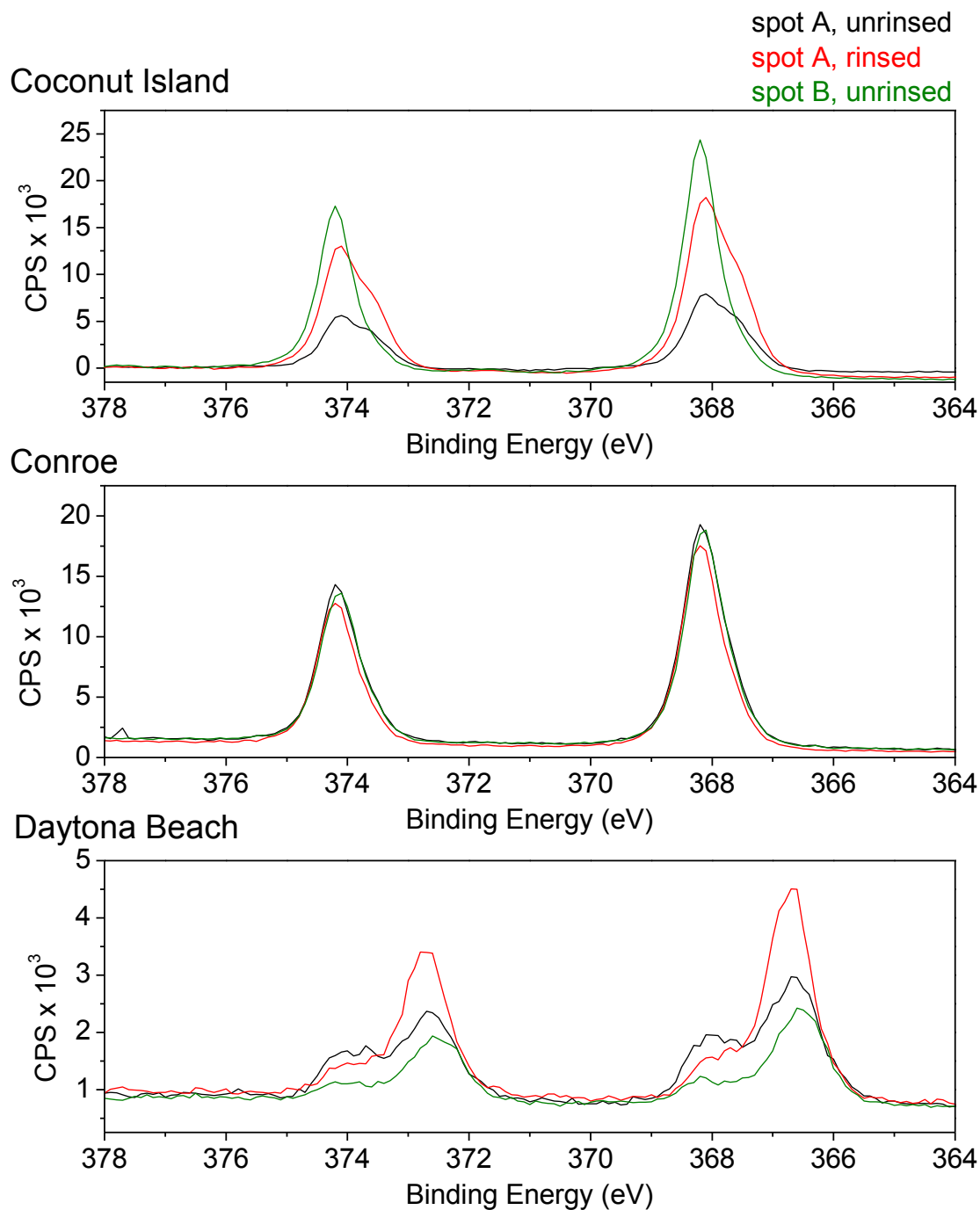


Figure F.4 XPS Ag 3d spectra for the samples exposed at Coconut Island, HI (top), Conroe, TX (middle), and Daytona Beach, FL (bottom). The black, red, and green spectra are on spot A unrinsed (dark area), spot A rinsed, and spot B unrinsed (light area), respectively.

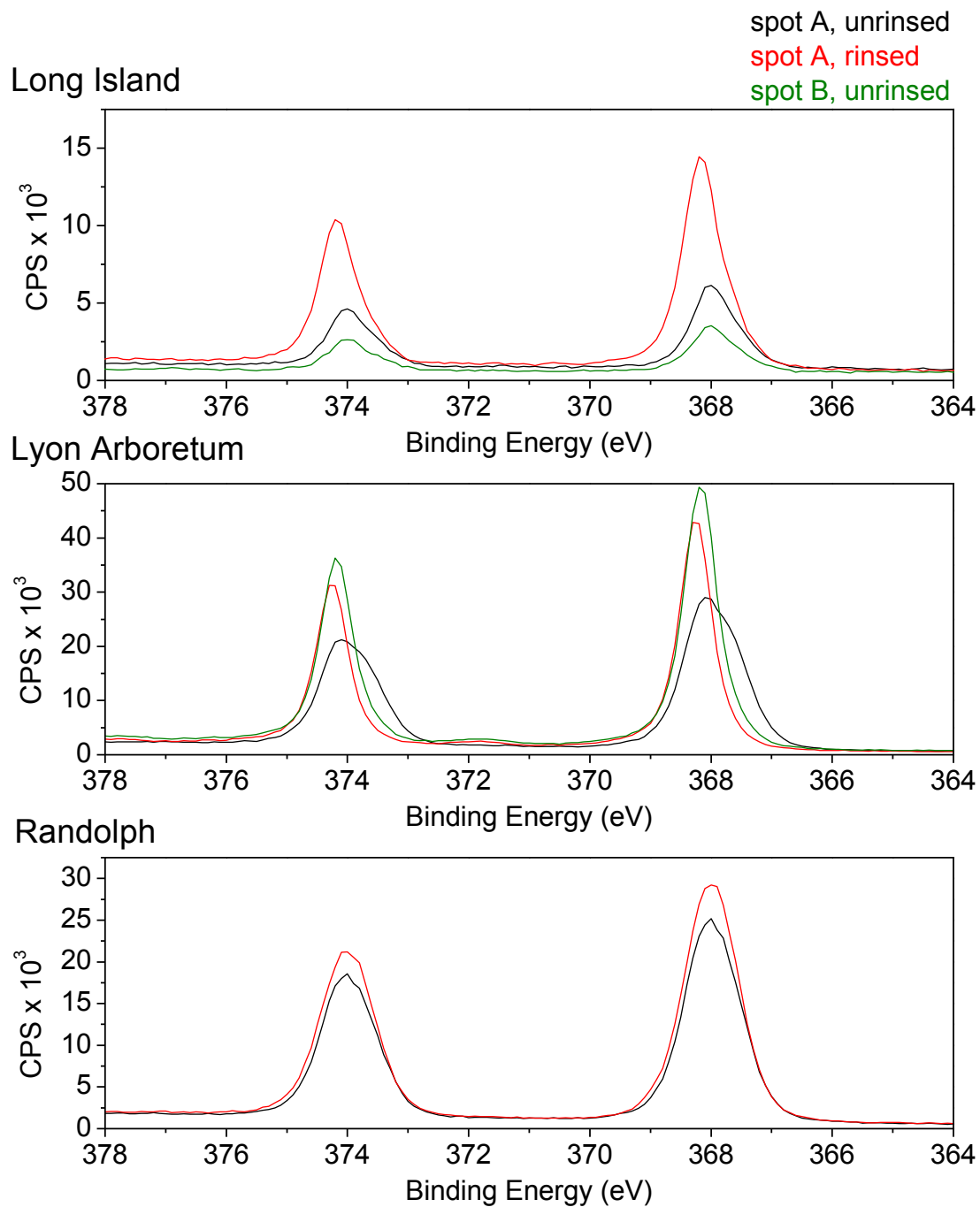


Figure F.5 XPS Ag 3d spectra for the samples exposed at Long Island, NY (top), Lyon Arboretum, HI (middle), and Randolph, TX (bottom). The black, red, and green spectra are on spot A unrinsed (dark area), spot A rinsed, and spot B unrinsed (light area), respectively.

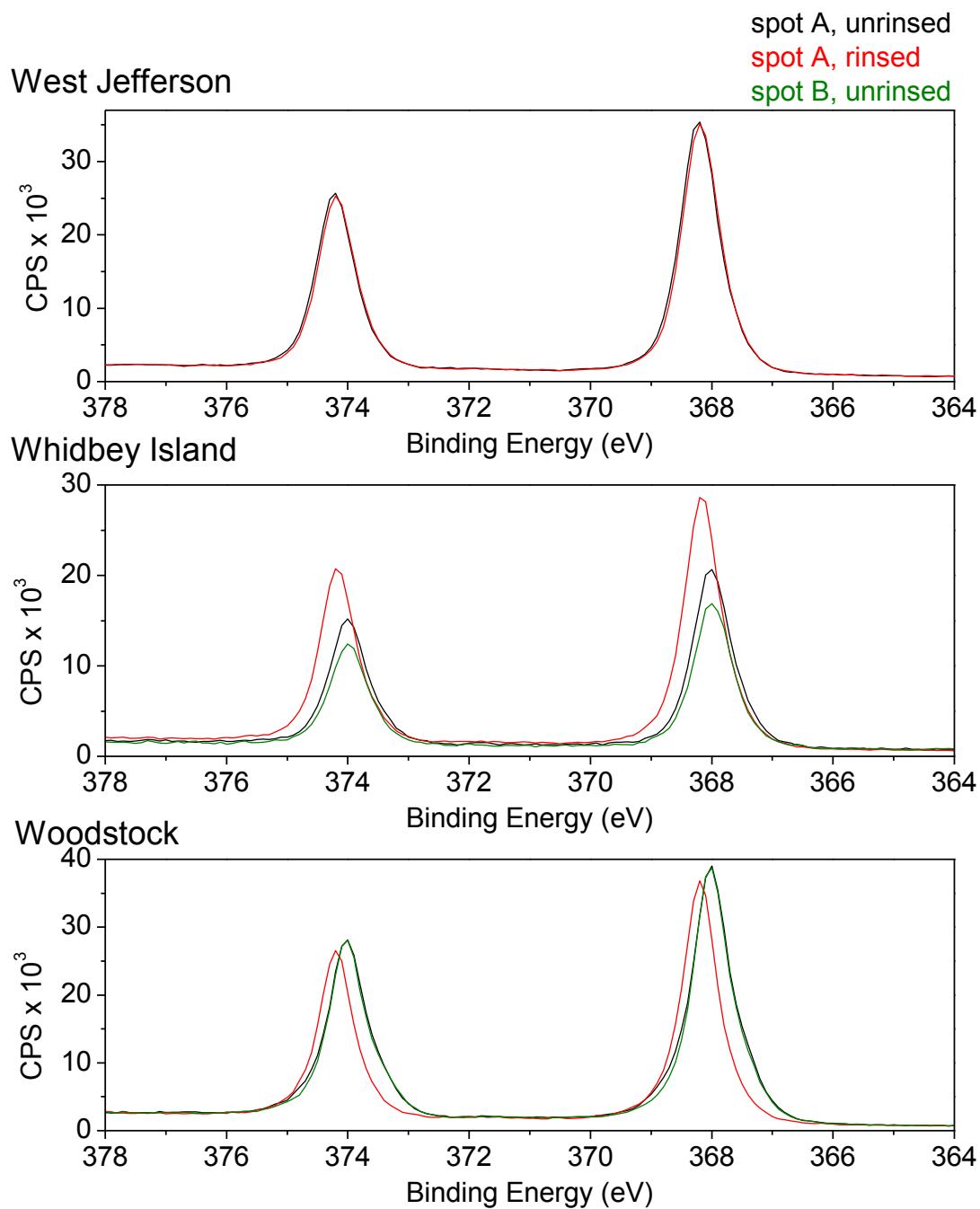


Figure F.6 XPS Ag 3d spectra for the samples exposed at West Jefferson, OH (top), Whidbey Island, WA (middle), and Woodstock, ME (bottom). The black, red, and green spectra are on spot A unrinsed (dark area), spot A rinsed, and spot B unrinsed (light area), respectively.

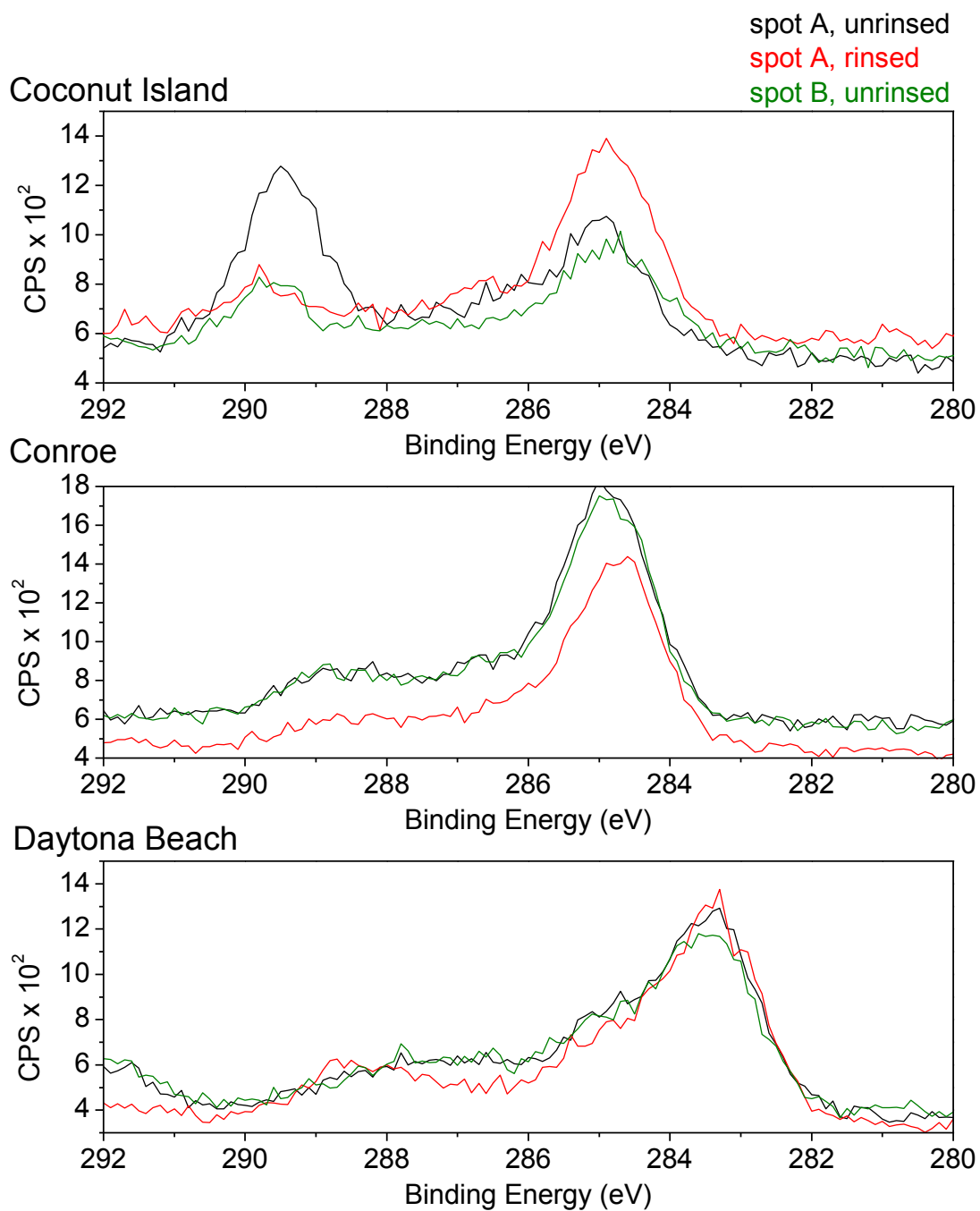


Figure F.7 XPS C 1s spectra for the samples exposed at Coconut Island, HI (top), Conroe, TX (middle), and Daytona Beach, FL (bottom). The black, red, and green spectra are on spot A unrinsed (dark area), spot A rinsed, and spot B unrinsed (light area), respectively.

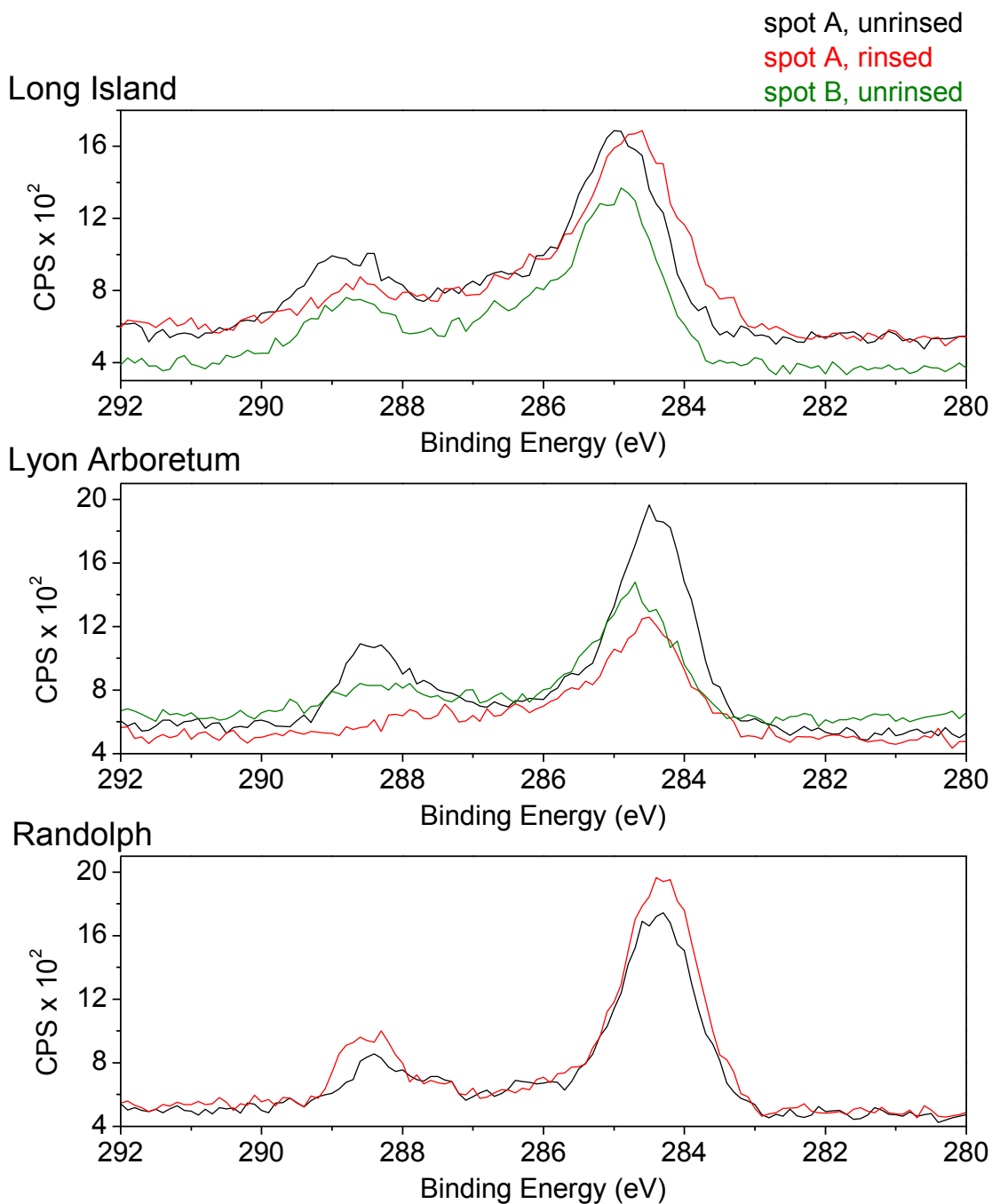


Figure F.8 XPS C 1s spectra for the samples exposed at Long Island, NY (top), Lyon Arboretum, HI (middle), and Randolph, TX (bottom). The black, red, and green spectra are on spot A unrinsed (dark area), spot A rinsed, and spot B unrinsed (light area), respectively.

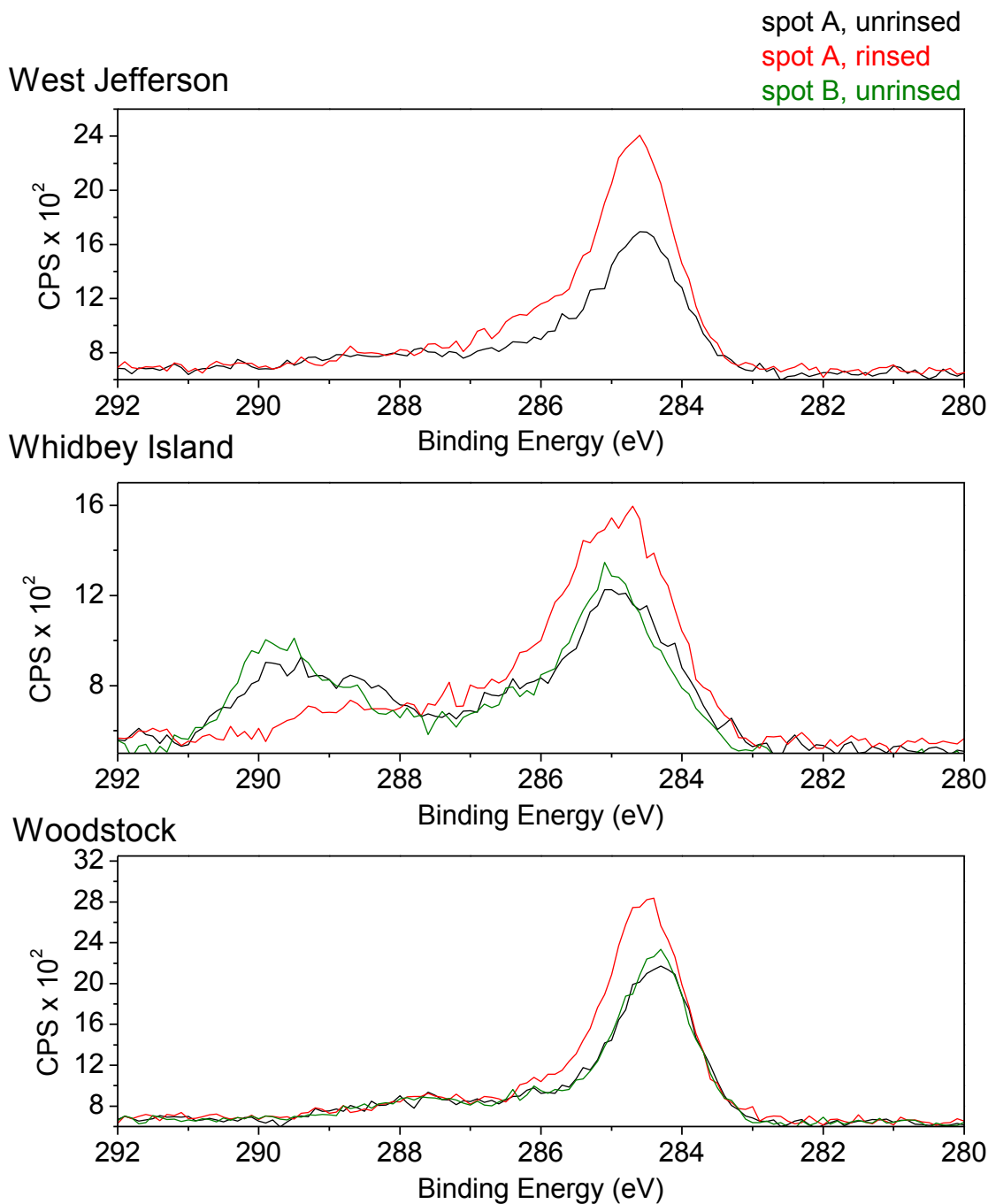


Figure F.9 XPS C 1s spectra for the samples exposed at West Jefferson, OH (top), Whidbey Island, WA (middle), and Woodstock, ME (bottom). The black, red, and green spectra are on spot A unrinsed (dark area), spot A rinsed, and spot B unrinsed (light area), respectively.

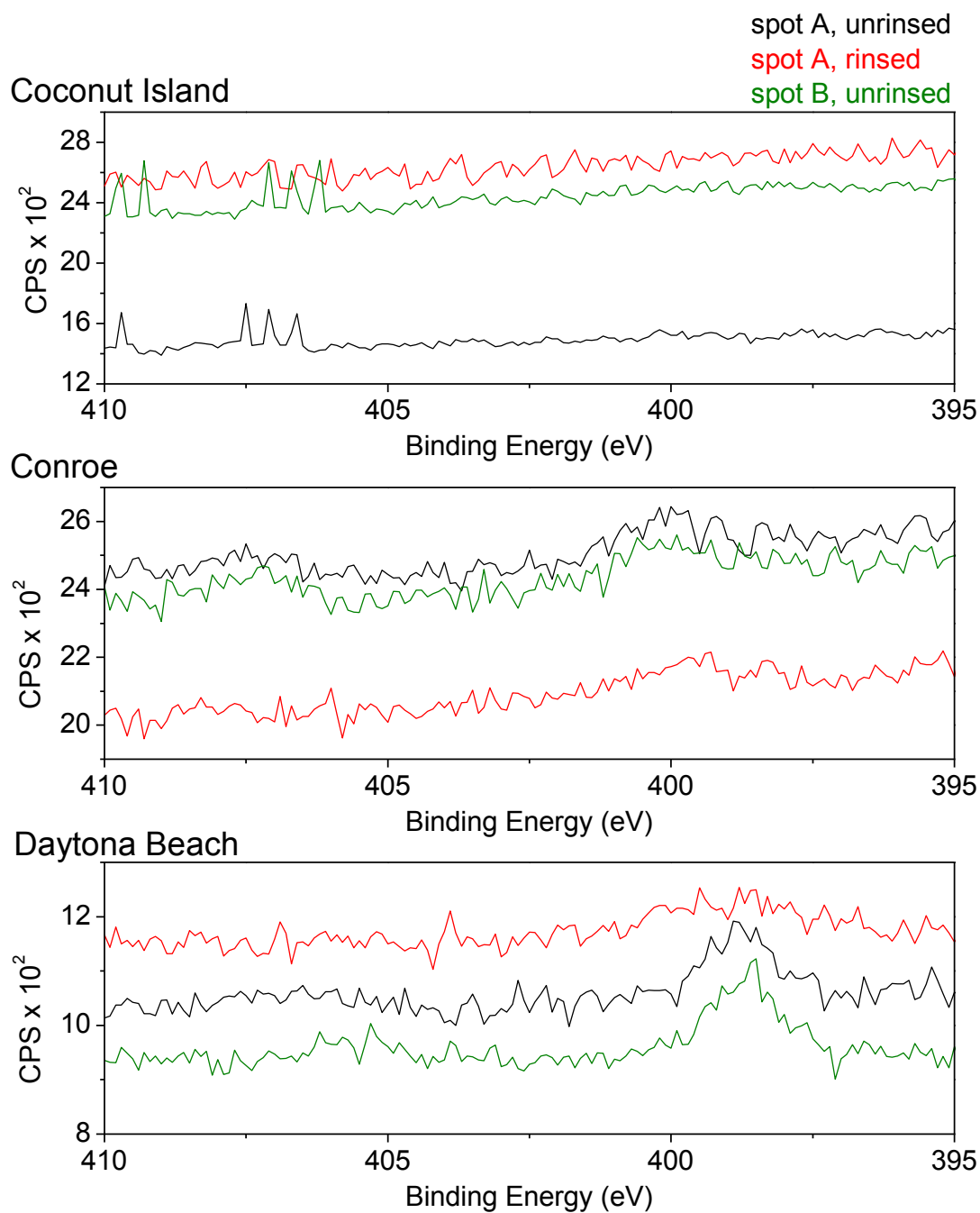


Figure F.10 XPS N 1s spectra for the samples exposed at Coconut Island, HI (top), Conroe, TX (middle), and Daytona Beach, FL (bottom). The black, red, and green spectra are on spot A unrinsed (dark area), spot A rinsed, and spot B unrinsed (light area), respectively.

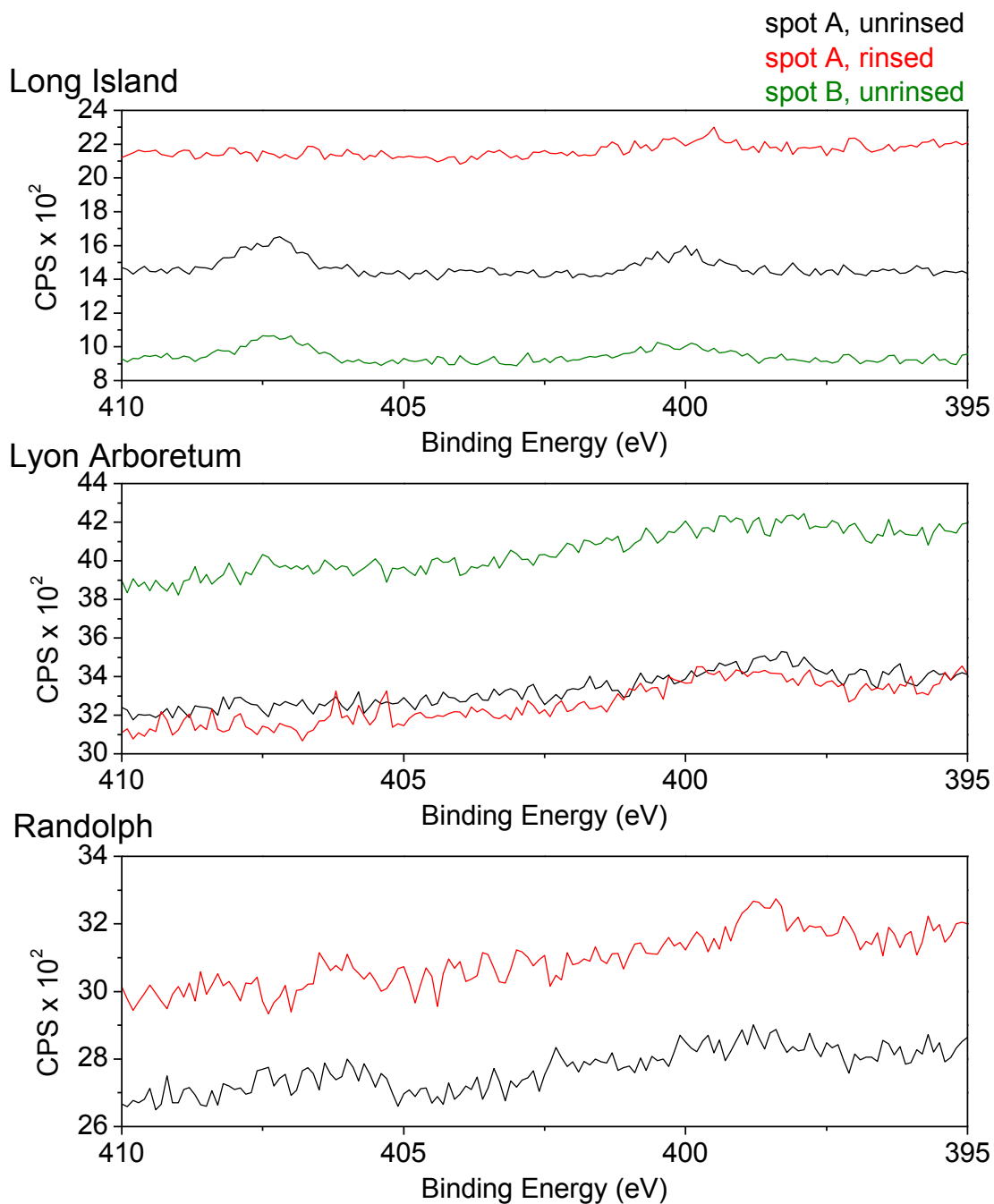


Figure F.11 XPS N 1s spectra for the samples exposed at Long Island, NY (top), Lyon Arboretum, HI (middle), and Randolph, TX (bottom). The black, red, and green spectra are on spot A unrinsed (dark area), spot A rinsed, and spot B unrinsed (light area), respectively.

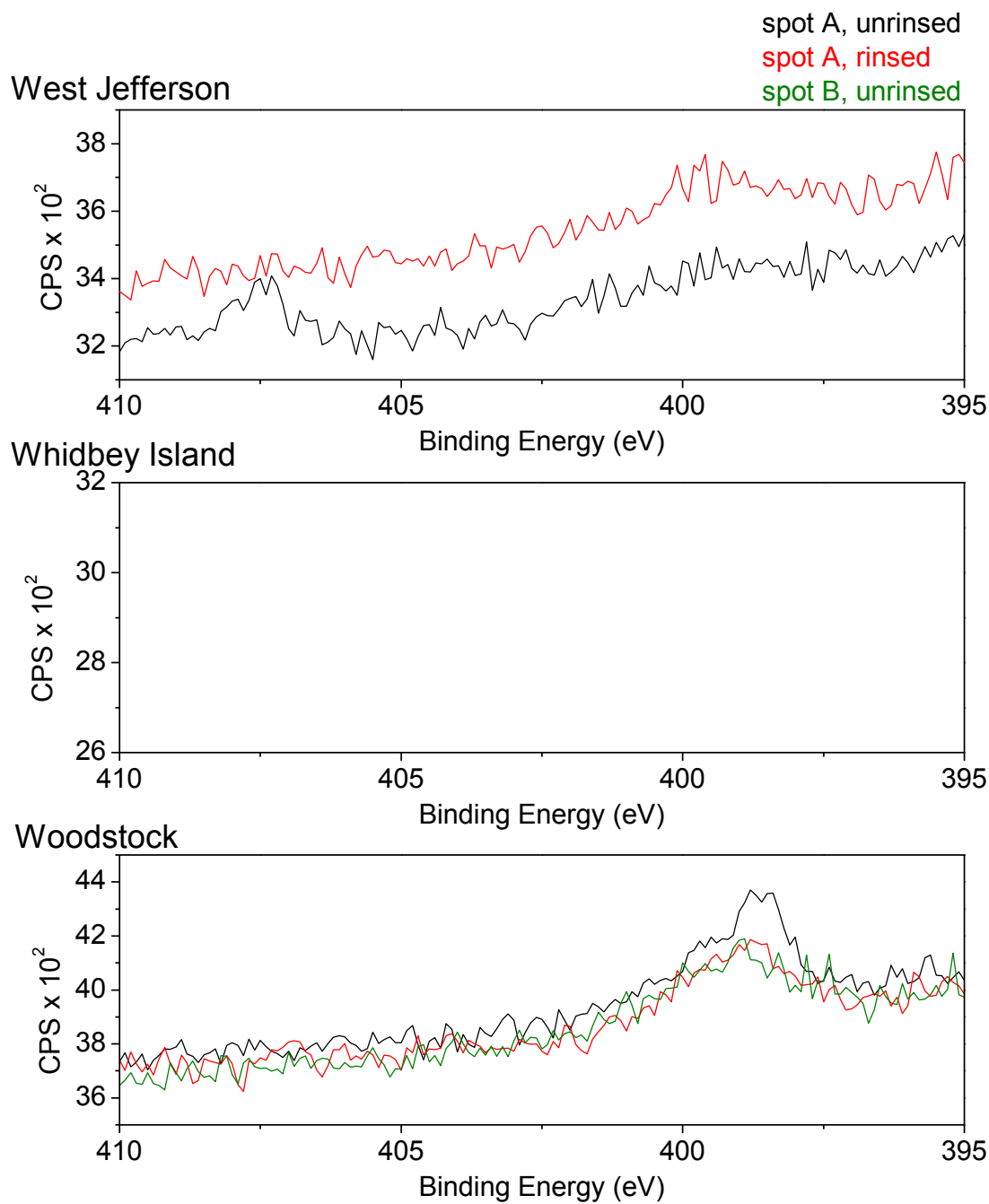


Figure F.12 XPS N 1s spectra for the samples exposed at West Jefferson, OH (top), Whidbey Island, WA (middle), and Woodstock, ME (bottom). The black, red, and green spectra are on spot A unrinsed (dark area), spot A rinsed, and spot B unrinsed (light area), respectively.

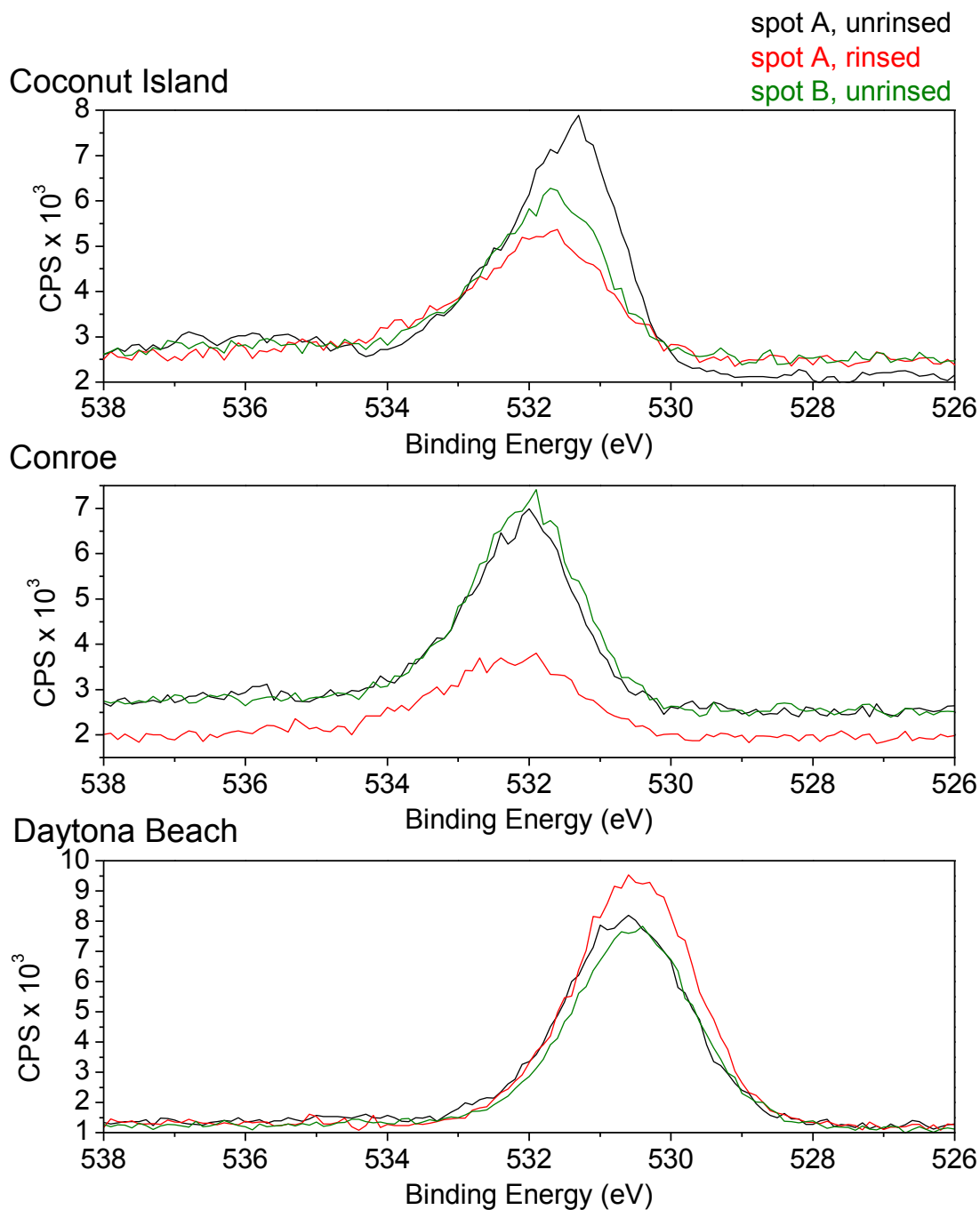


Figure F.13 XPS O 1s spectra for the samples exposed at Coconut Island, HI (top), Conroe, TX (middle), and Daytona Beach, FL (bottom). The black, red, and green spectra are on spot A unrinsed (dark area), spot A rinsed, and spot B unrinsed (light area), respectively.

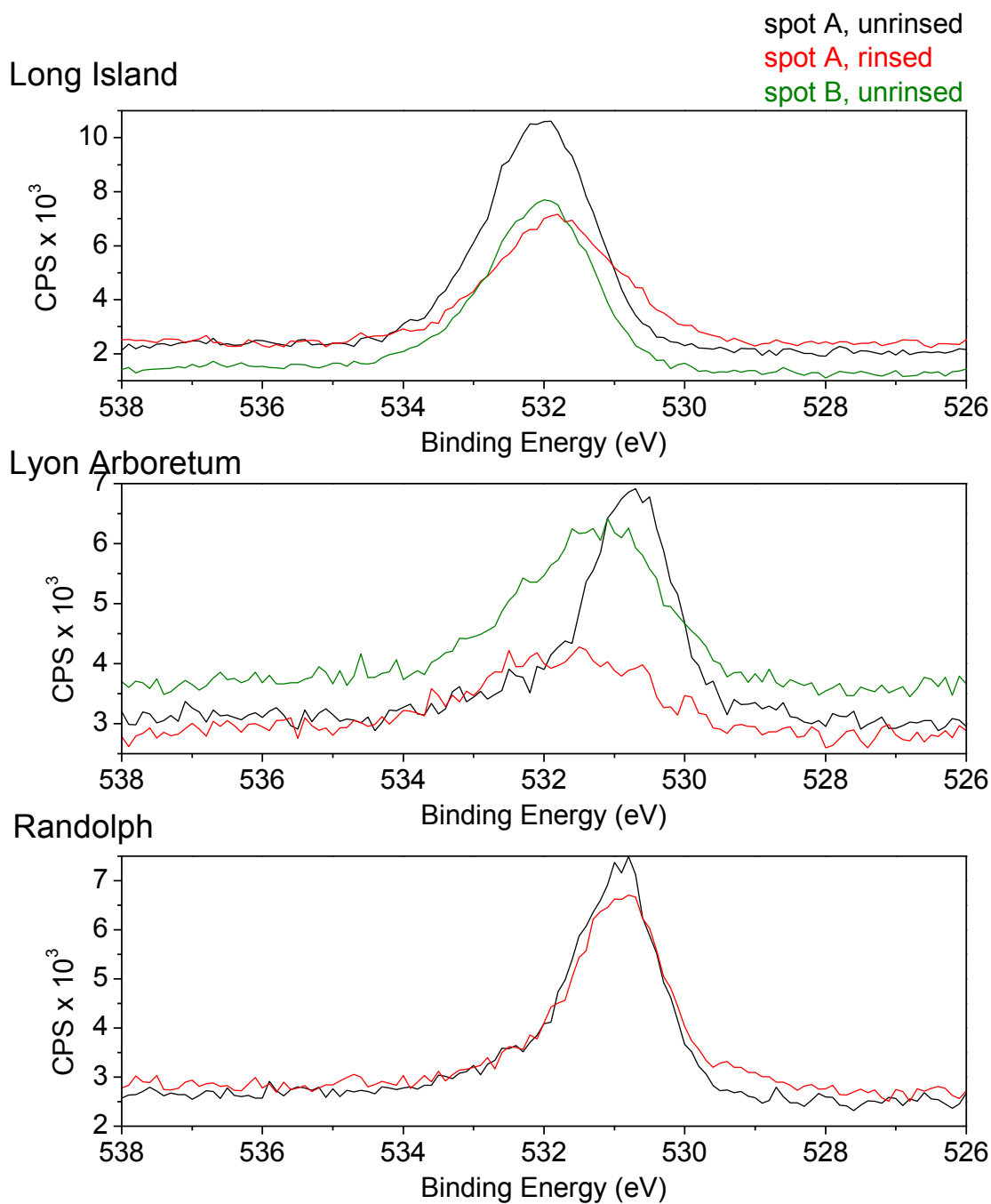


Figure F.14 XPS O 1s spectra for the samples exposed at Long Island, NY (top), Lyon Arboretum, HI (middle), and Randolph, TX (bottom). The black, red, and green spectra are on spot A unrinsed (dark area), spot A rinsed, and spot B unrinsed (light area), respectively.

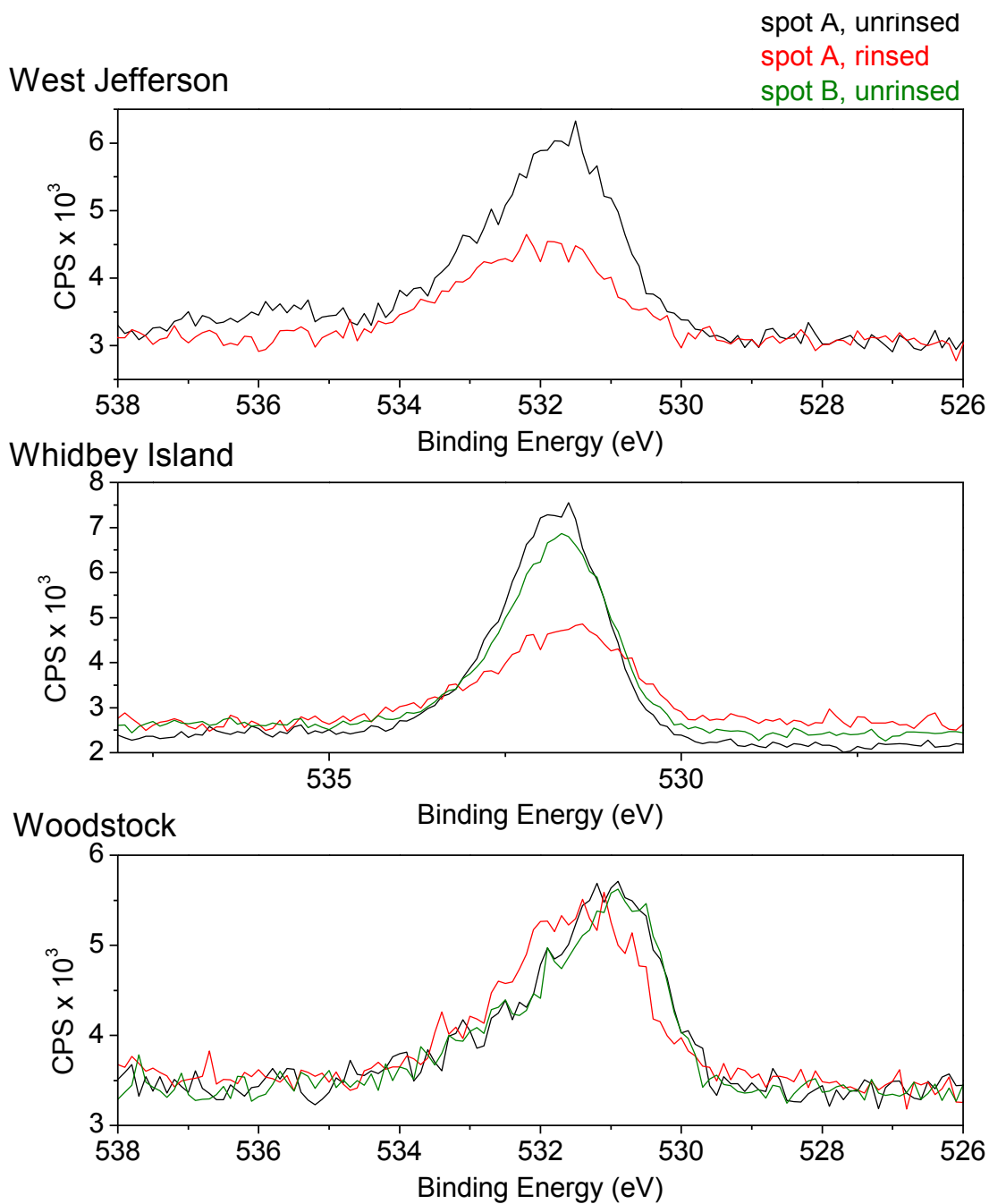


Figure F.15 XPS O 1s spectra for the samples exposed at West Jefferson, OH (top), Whidbey Island, WA (middle), and Woodstock, ME (bottom). The black, red, and green spectra are on spot A unrinsed (dark area), spot A rinsed, and spot B unrinsed (light area), respectively.

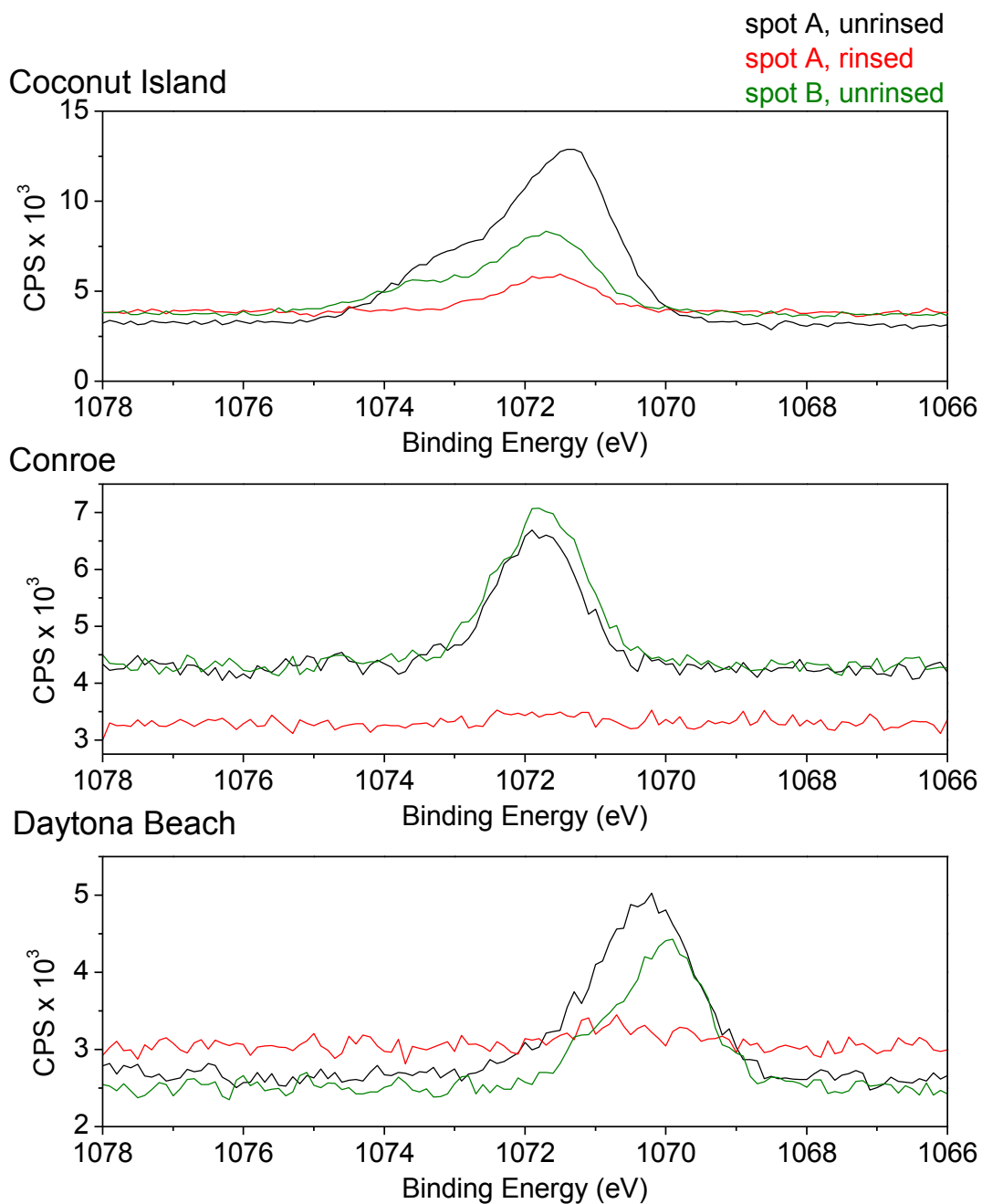


Figure F.16 XPS Na 1s spectra for the samples exposed at Coconut Island, HI (top), Conroe, TX (middle), and Daytona Beach, FL (bottom). The black, red, and green spectra are on spot A unrinsed (dark area), spot A rinsed, and spot B unrinsed (light area), respectively.

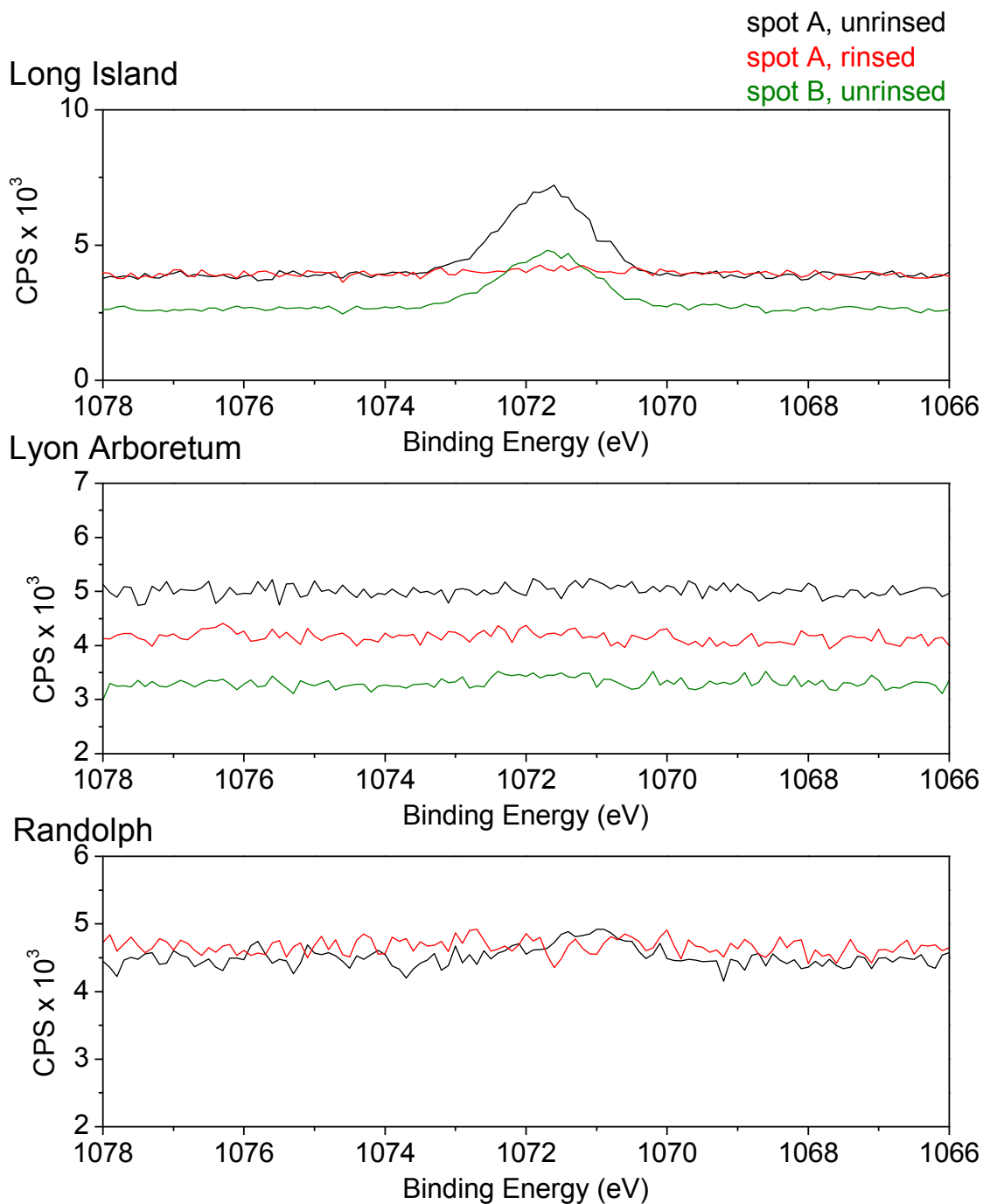


Figure F.17 XPS Na 1s spectra for the samples exposed at Long Island, NY (top), Lyon Arboretum, HI (middle), and Randolph, TX (bottom). The black, red, and green spectra are on spot A unrinsed (dark area), spot A rinsed, and spot B unrinsed (light area), respectively.

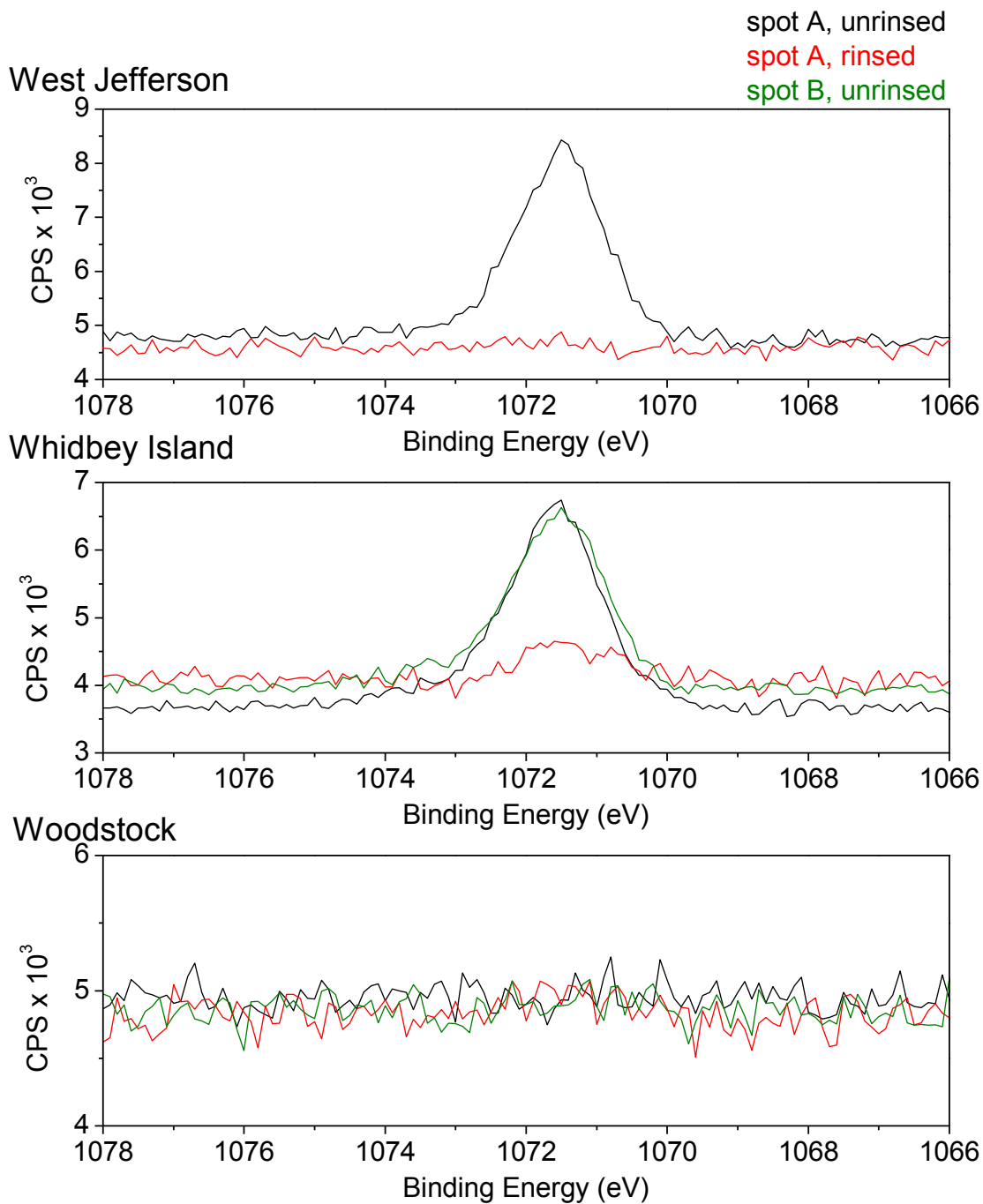


Figure F.18 XPS Na 1s spectra for the samples exposed at West Jefferson, OH (top), Whidbey Island, WA (middle), and Woodstock, ME (bottom). The black, red, and green spectra are on spot A unrinsed (dark area), spot A rinsed, and spot B unrinsed (light area), respectively.

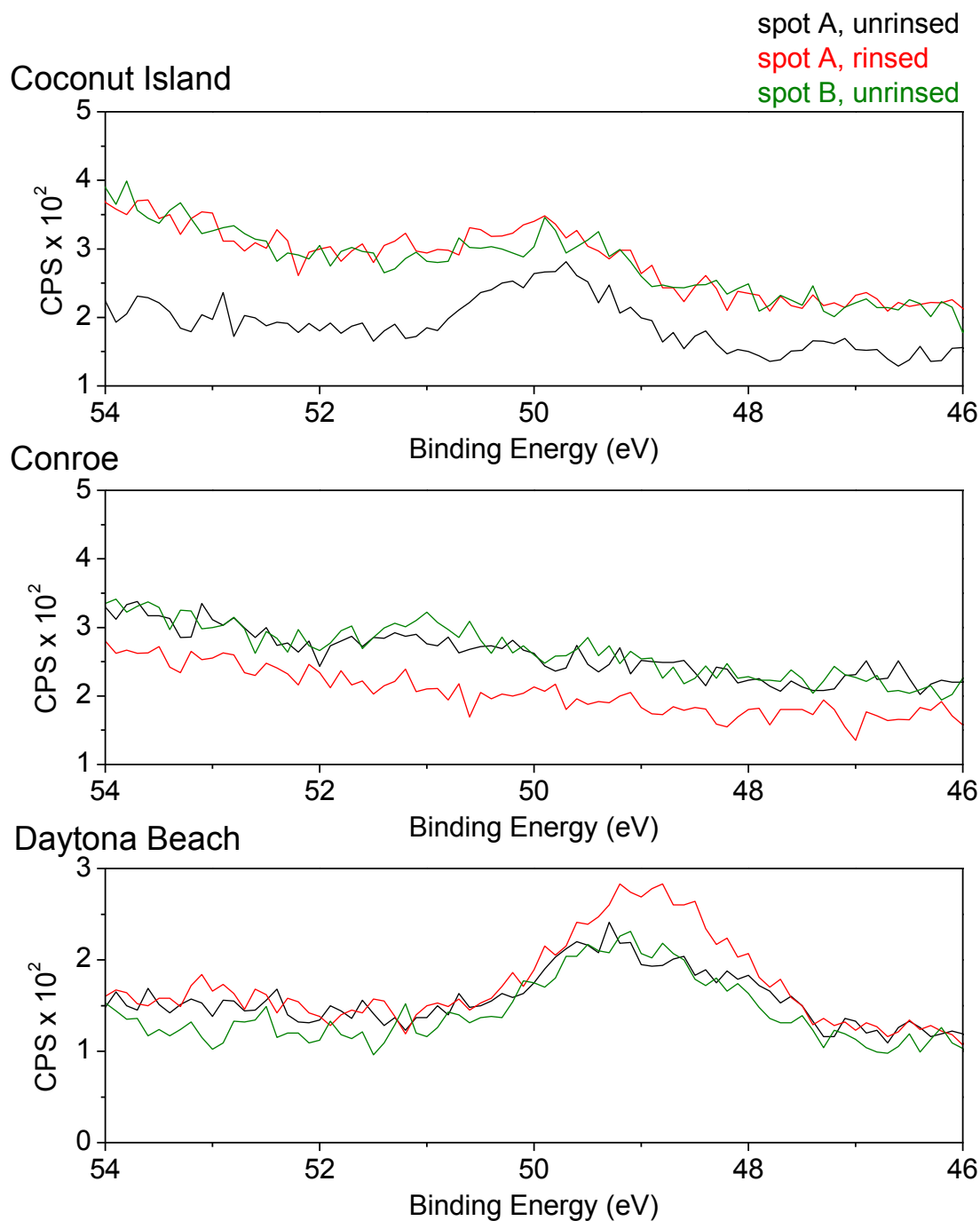


Figure F.19 XPS Mg 2p spectra for the samples exposed at Coconut Island, HI (top), Conroe, TX (middle), and Daytona Beach, FL (bottom). The black, red, and green spectra are on spot A unrinsed (dark area), spot A rinsed, and spot B unrinsed (light area), respectively.

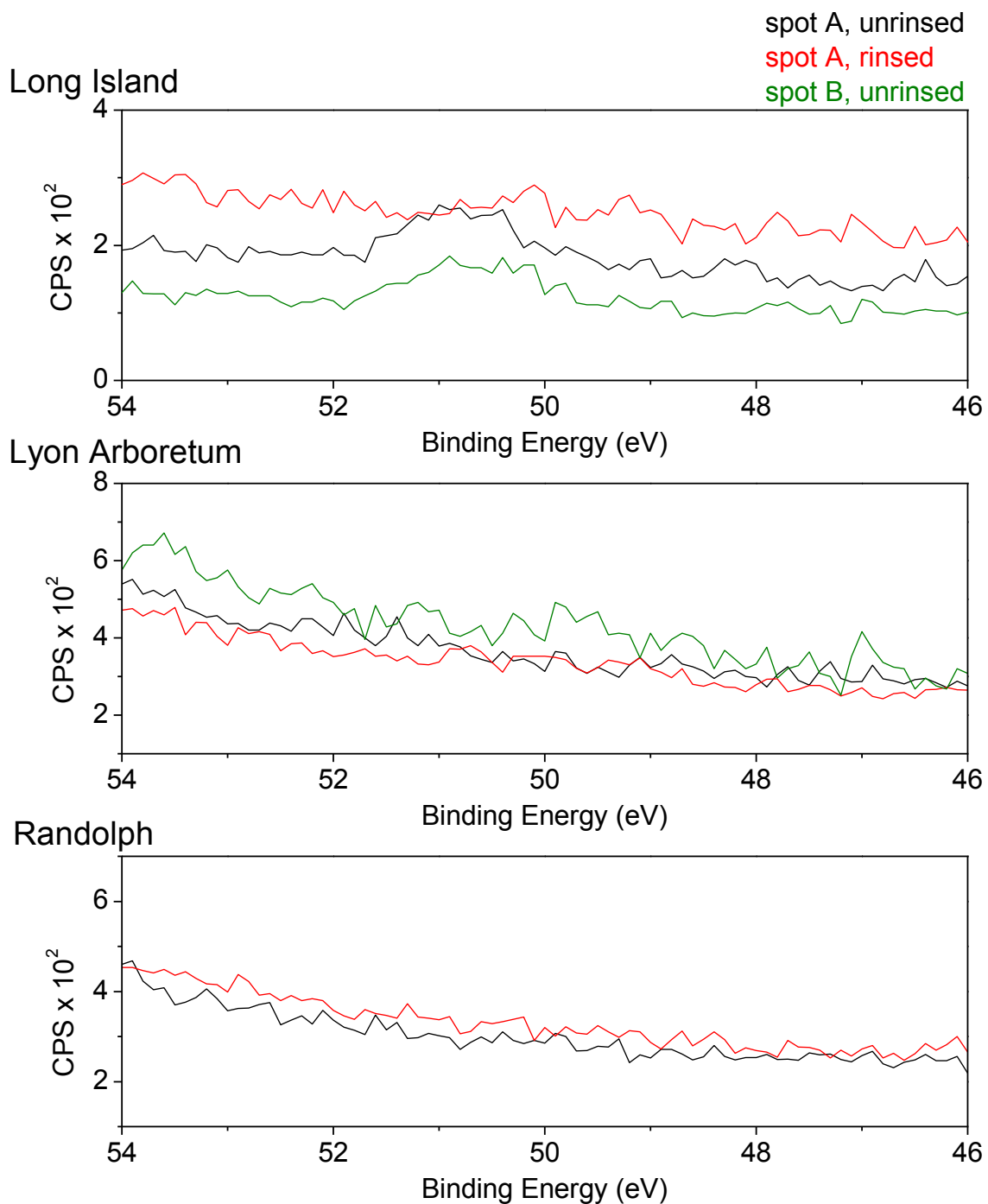


Figure F.20 XPS Mg 2p spectra for the samples exposed at Long Island, NY (top), Lyon Arboretum, HI (middle), and Randolph, TX (bottom). The black, red, and green spectra are on spot A unrinsed (dark area), spot A rinsed, and spot B unrinsed (light area), respectively.

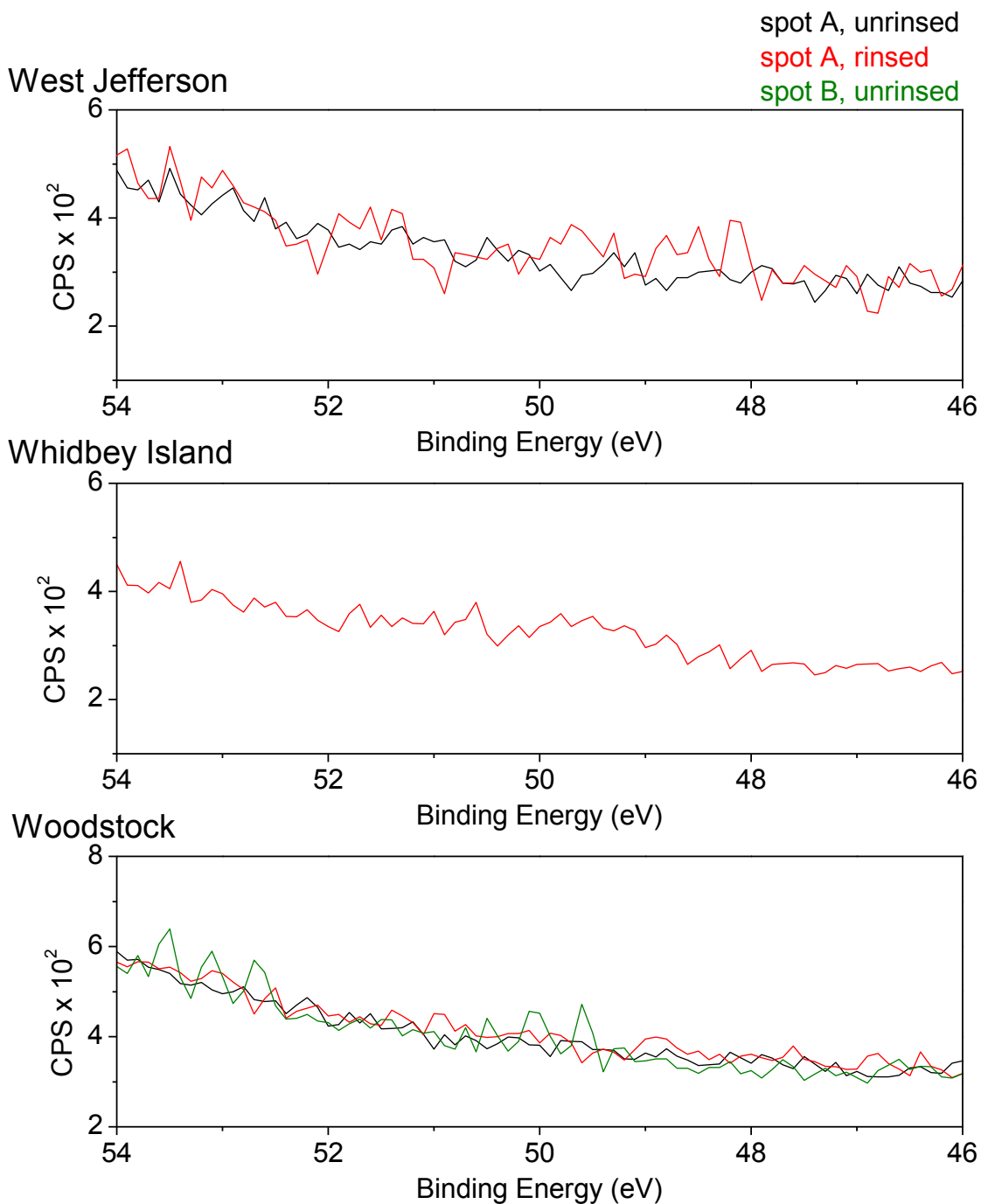


Figure F.21 XPS Mg 2p spectra for the samples exposed at West Jefferson, OH (top), Whidbey Island, WA (middle), and Woodstock, ME (bottom). The black, red, and green spectra are on spot A unrinsed (dark area), spot A rinsed, and spot B unrinsed (light area), respectively.

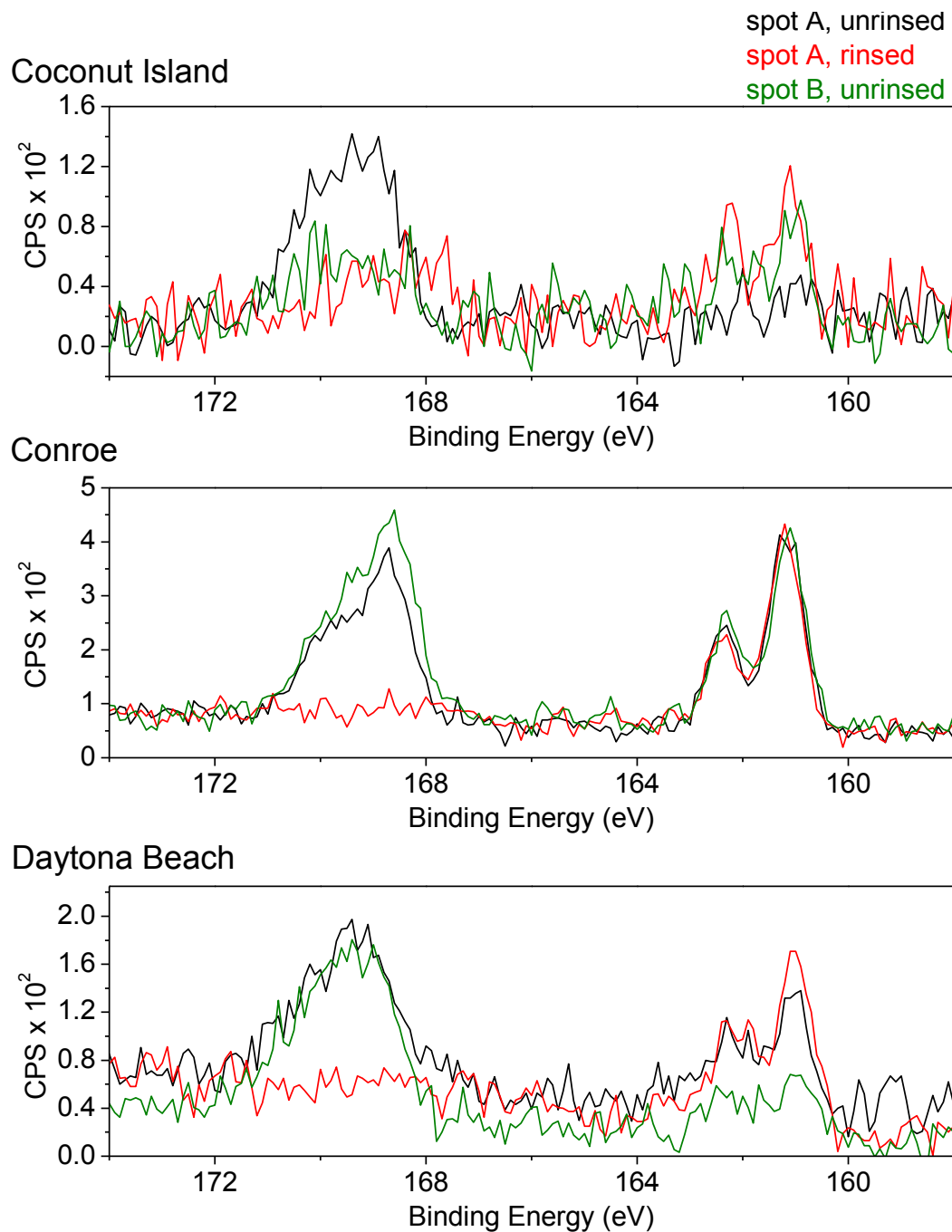


Figure F.22 XPS S 2p spectra for the samples exposed at Coconut Island, HI (top), Conroe, TX (middle), and Daytona Beach, FL (bottom). The black, red, and green spectra are on spot A unrinsed (dark area), spot A rinsed, and spot B unrinsed (light area), respectively.

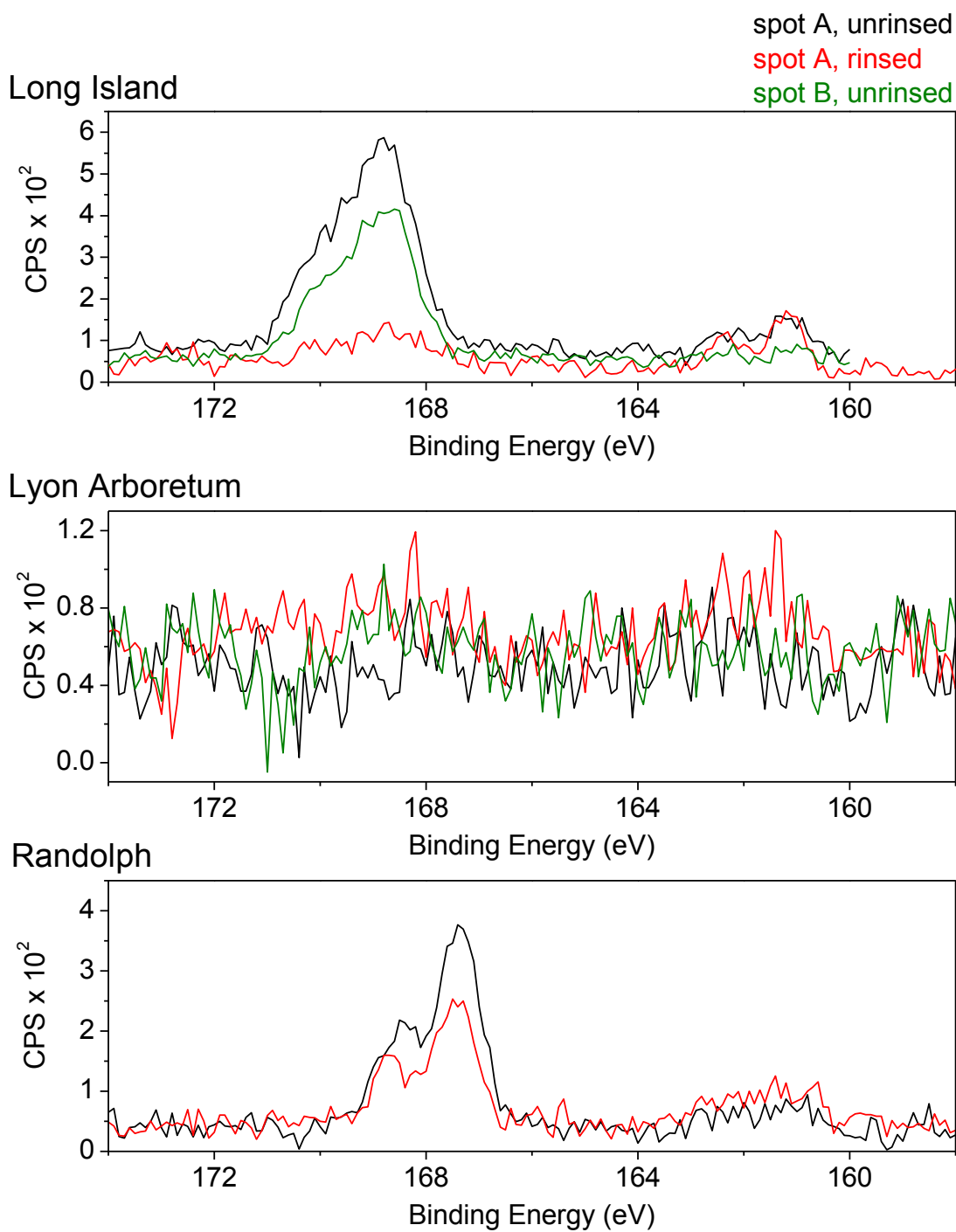


Figure F.23 XPS S 2p spectra for the samples exposed at Long Island, NY (top), Lyon Arboretum, HI (middle), and Randolph, TX (bottom). The black, red, and green spectra are on spot A unrinsed (dark area), spot A rinsed, and spot B unrinsed (light area), respectively.

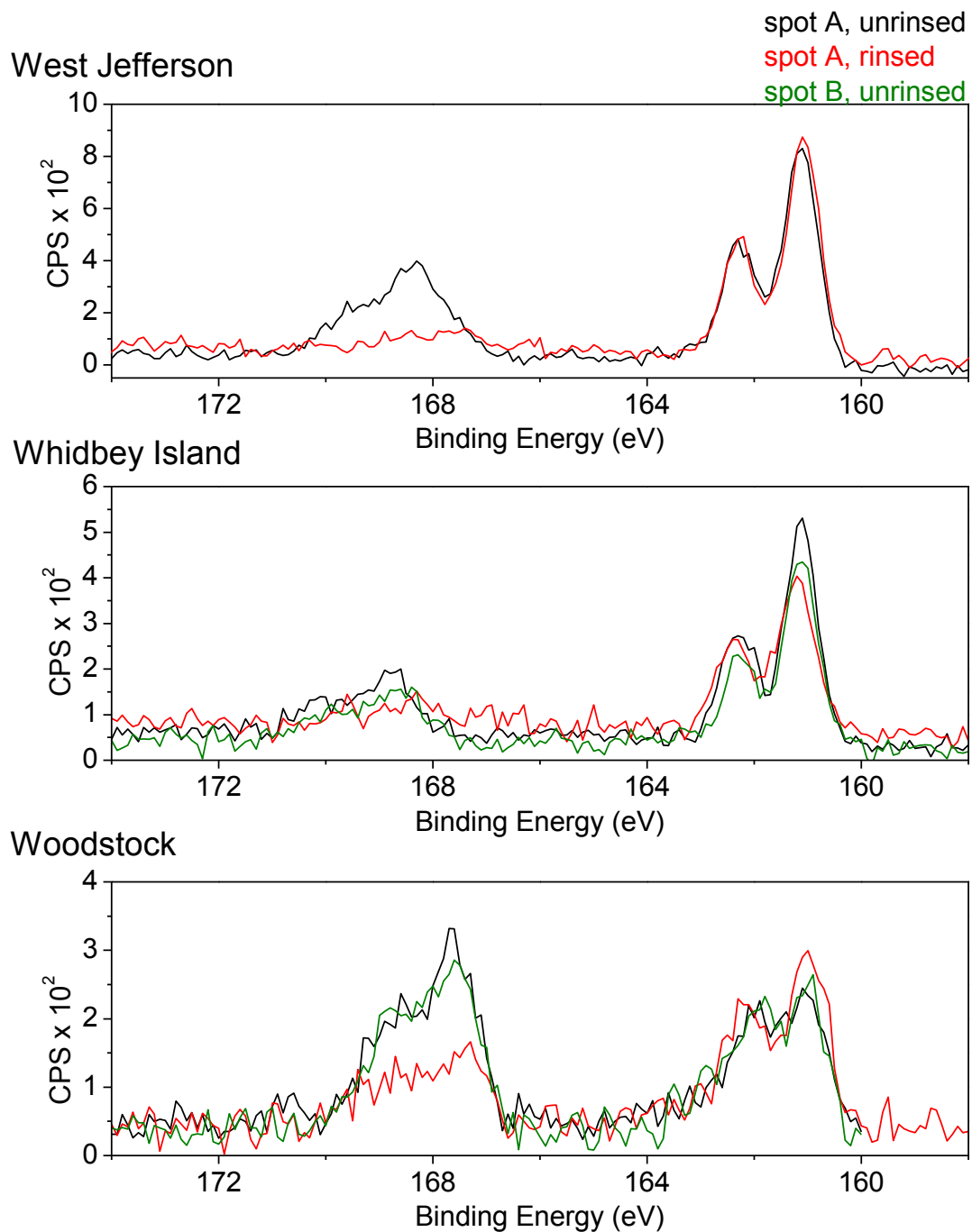


Figure F.24 XPS S 2p spectra for the samples exposed at West Jefferson, OH (top), Whidbey Island, WA (middle), and Woodstock, ME (bottom). The black, red, and green spectra are on spot A unrinsed (dark area), spot A rinsed, and spot B unrinsed (light area), respectively.

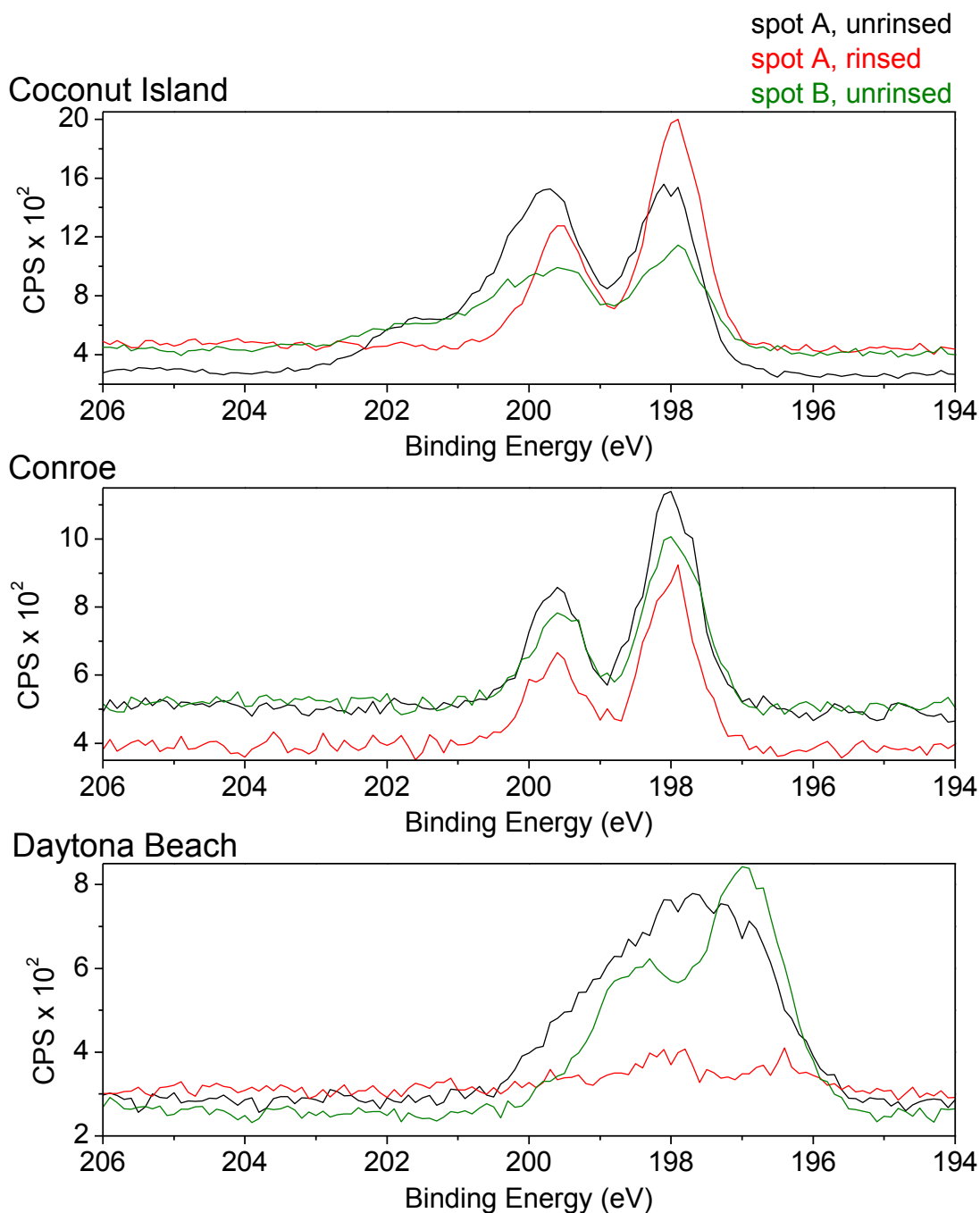


Figure F.25 XPS Cl 2p spectra for the samples exposed at Coconut Island, HI (top), Conroe, TX (middle), and Daytona Beach, FL (bottom). The black, red, and green spectra are on spot A unrinsed (dark area), spot A rinsed, and spot B unrinsed (light area), respectively.

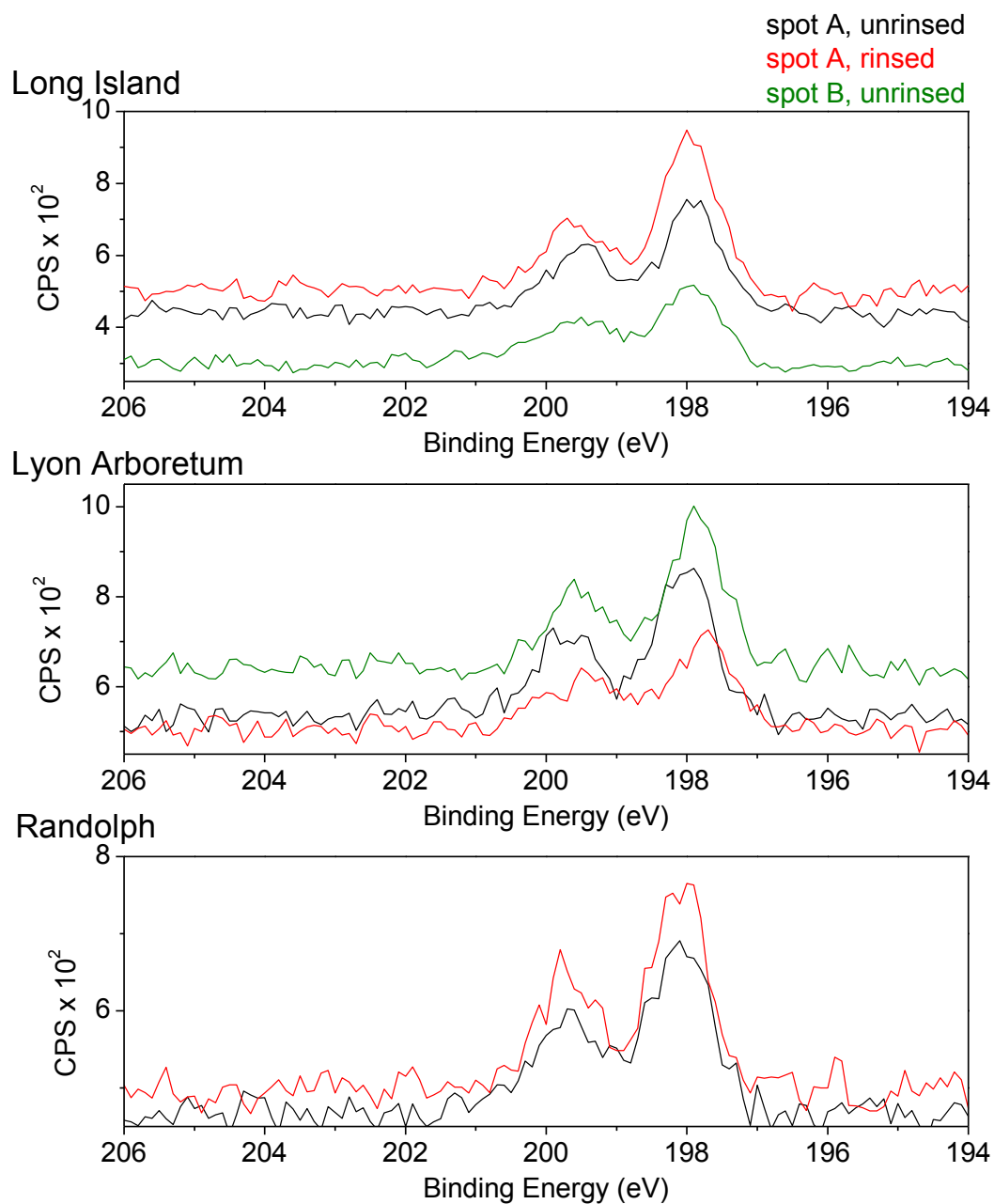


Figure F.26 XPS Cl 2p spectra for the samples exposed at Long Island, NY (top), Lyon Arboretum, HI (middle), and Randolph, TX (bottom). The black, red, and green spectra are on spot A unrinsed (dark area), spot A rinsed, and spot B unrinsed (light area), respectively.

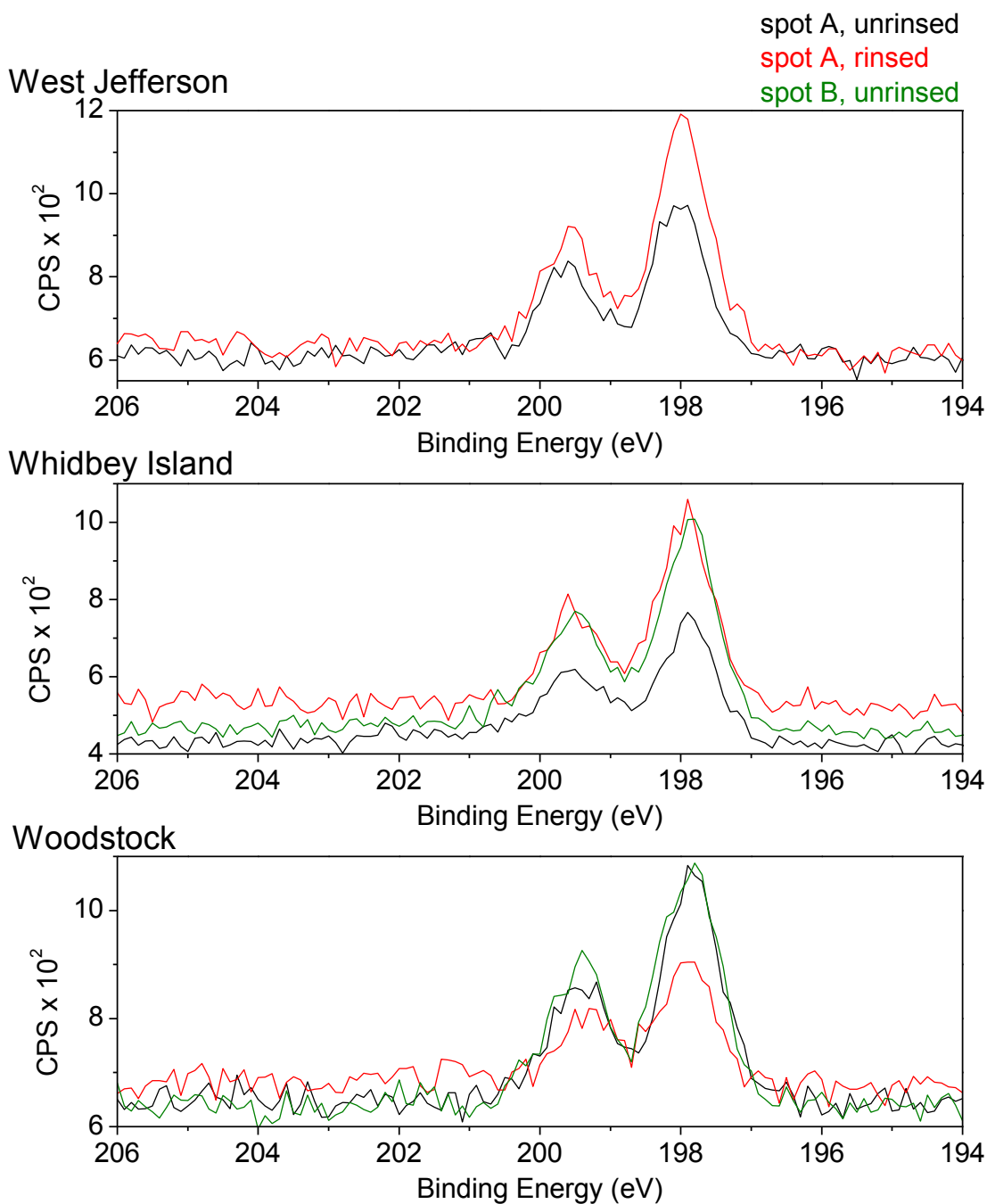


Figure F.27 XPS Cl 2p spectra for the samples exposed at West Jefferson, OH (top), Whidbey Island, WA (middle), and Woodstock, ME (bottom). The black, red, and green spectra are on spot A unrinsed (dark area), spot A rinsed, and spot B unrinsed (light area), respectively.

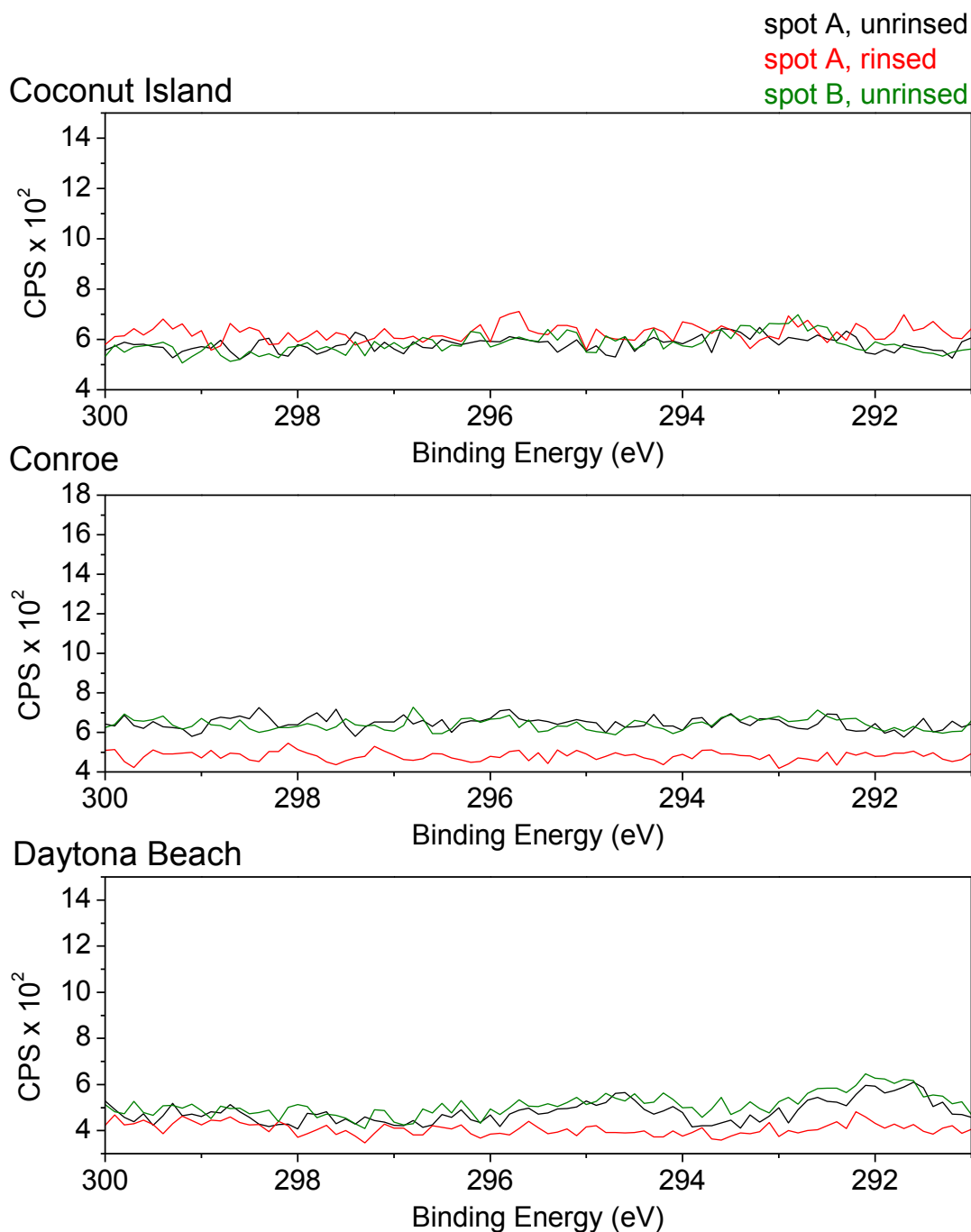


Figure F.28 XPS K 2p spectra for the samples exposed at Coconut Island, HI (top), Conroe, TX (middle), and Daytona Beach, FL (bottom). The black, red, and green spectra are on spot A unrinsed (dark area), spot A rinsed, and spot B unrinsed (light area), respectively.

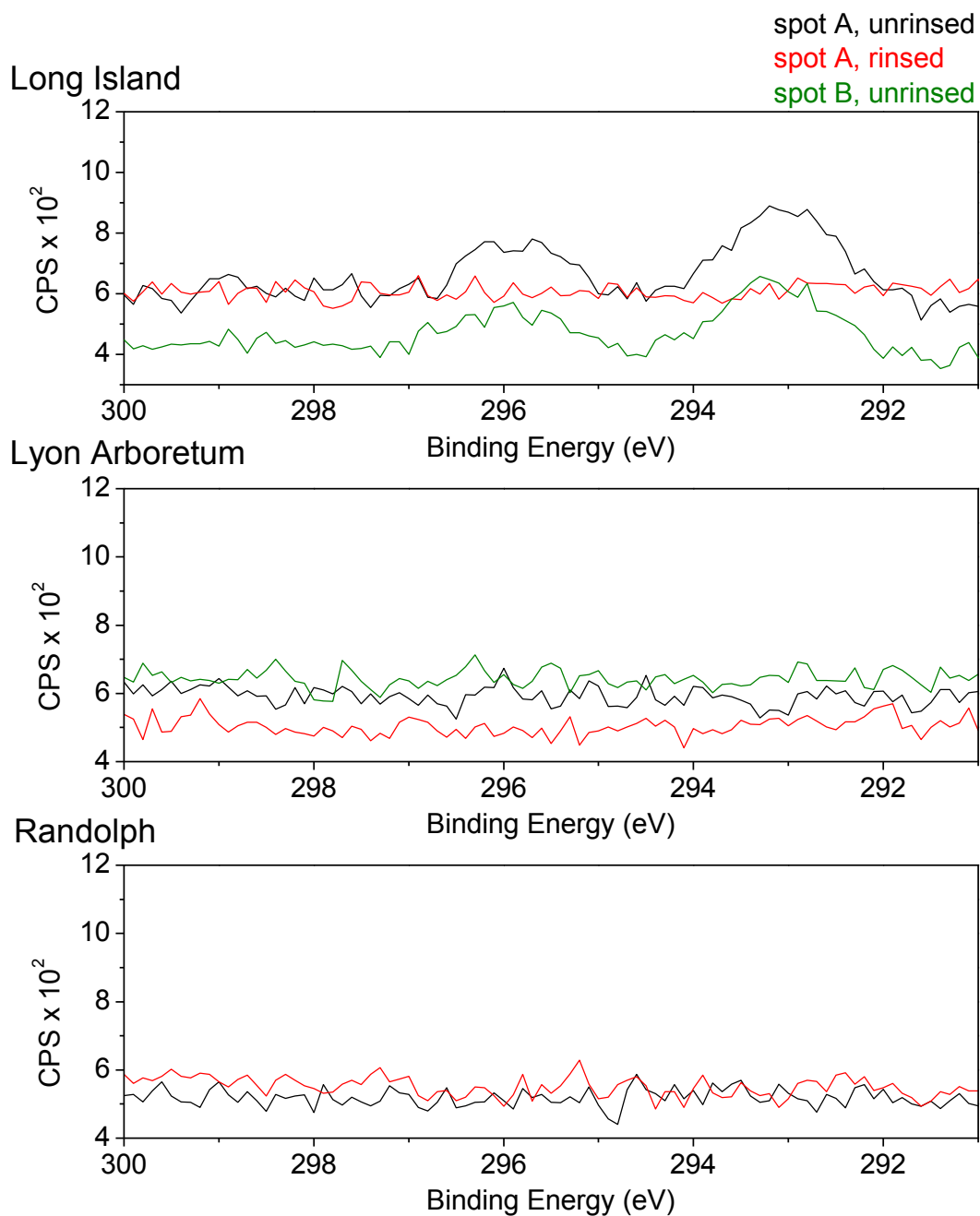


Figure F.29 XPS K 2p spectra for the samples exposed at Long Island, NY (top), Lyon Arboretum, HI (middle), and Randolph, TX (bottom). The black, red, and green spectra are on spot A unrinsed (dark area), spot A rinsed, and spot B unrinsed (light area), respectively.

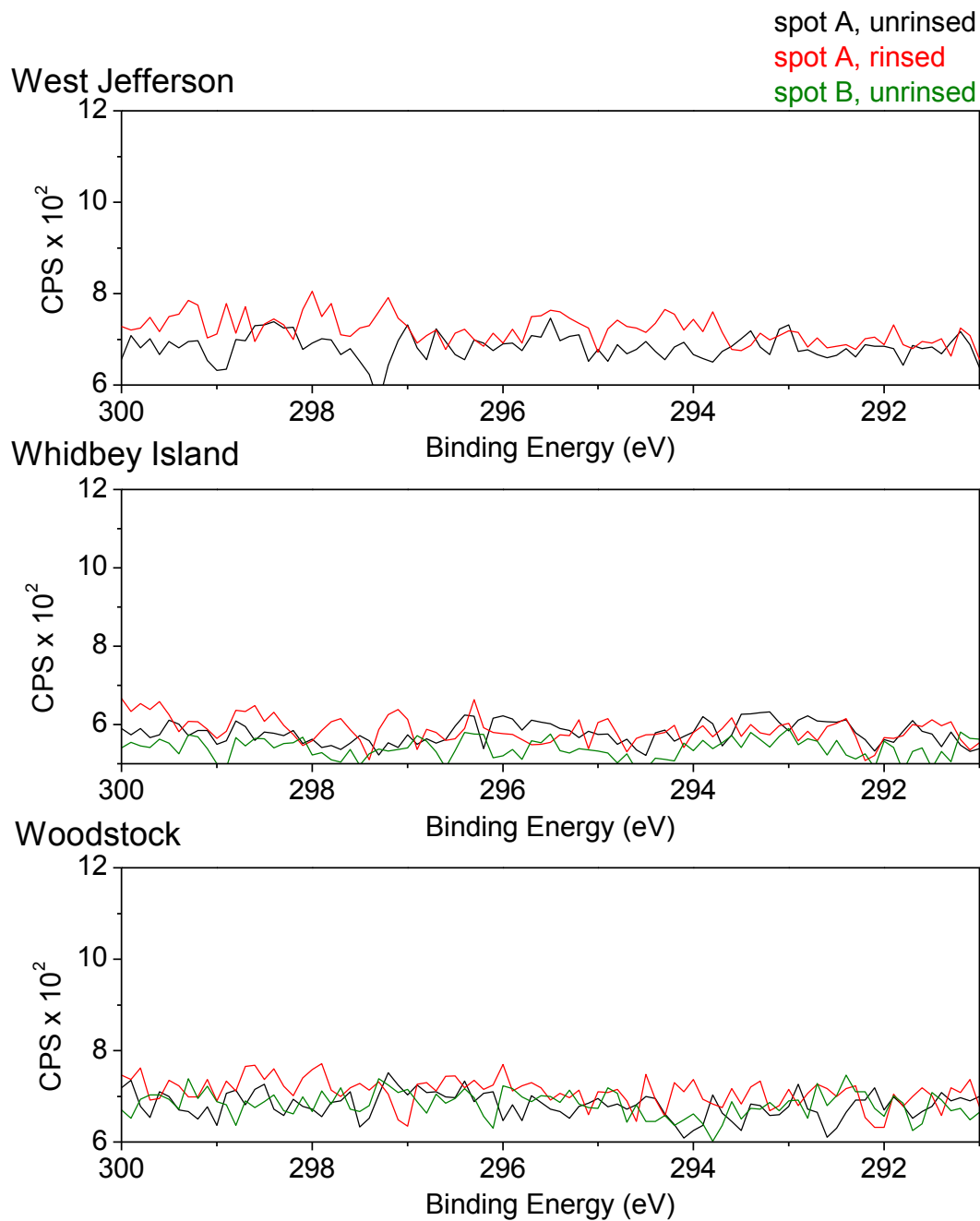


Figure F.30 XPS K 2p spectra for the samples exposed at West Jefferson, OH (top), Whidbey Island, WA (middle), and Woodstock, ME (bottom). The black, red, and green spectra are on spot A unrinsed (dark area), spot A rinsed, and spot B unrinsed (light area), respectively.

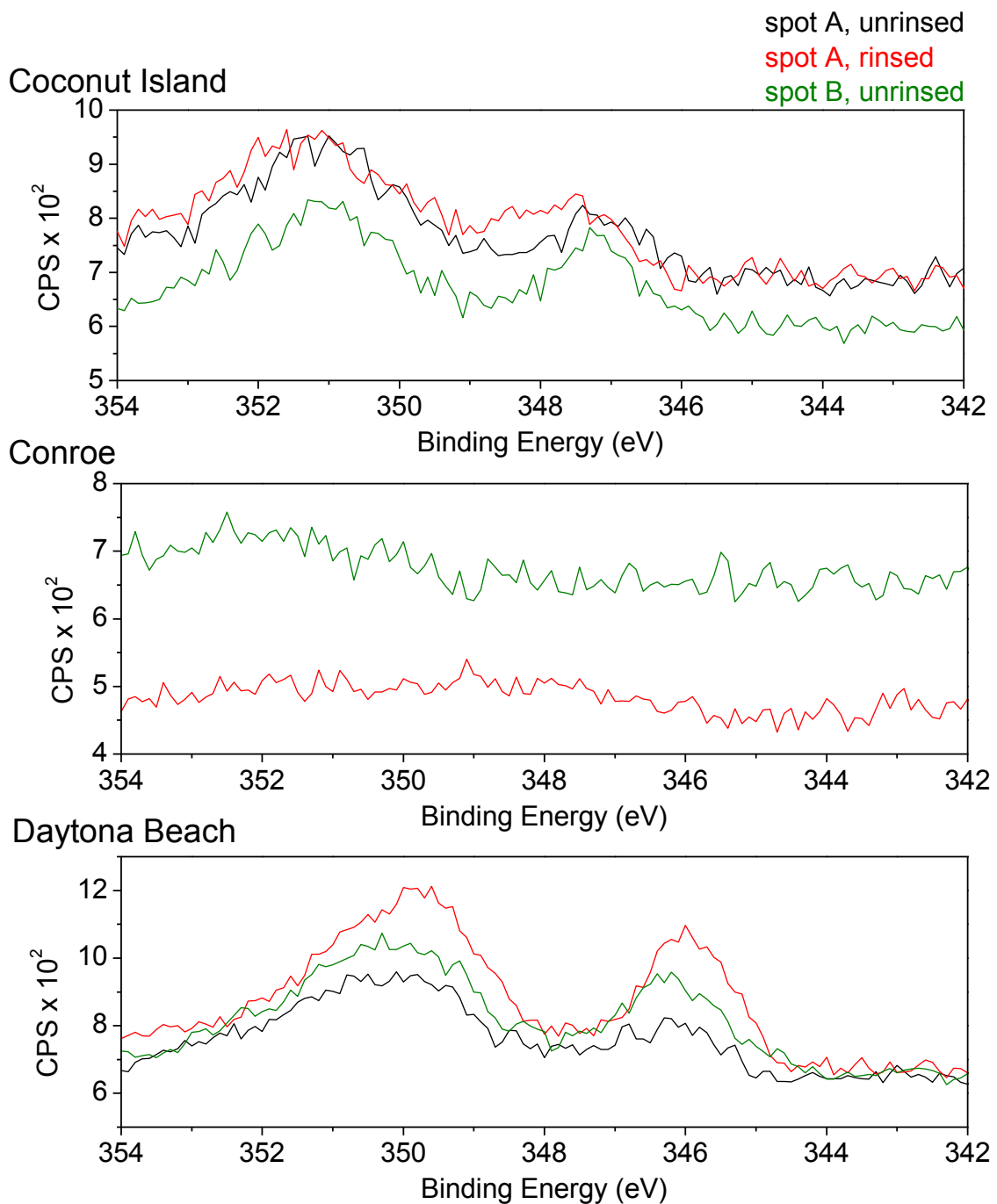


Figure F.31 XPS Ca 2p spectra for the samples exposed at Coconut Island, HI (top), Conroe, TX (middle), and Daytona Beach, FL (bottom). The black, red, and green spectra are on spot A unrinsed (dark area), spot A rinsed, and spot B unrinsed (light area), respectively.

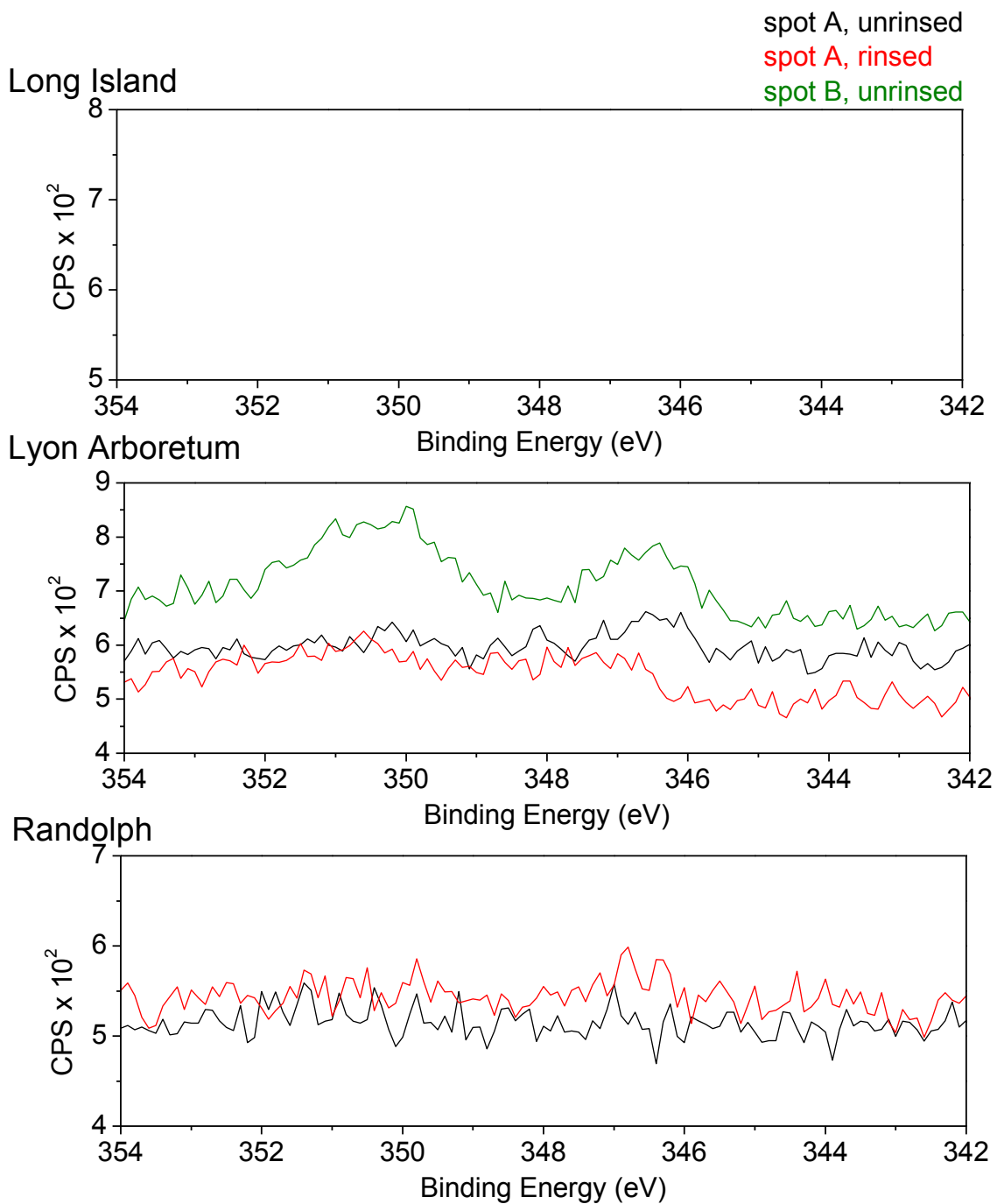


Figure F.32 XPS Ca 2p spectra for the samples exposed at Long Island, NY (top), Lyon Arboretum, HI (middle), and Randolph, TX (bottom). The black, red, and green spectra are on spot A unrinsed (dark area), spot A rinsed, and spot B unrinsed (light area), respectively.

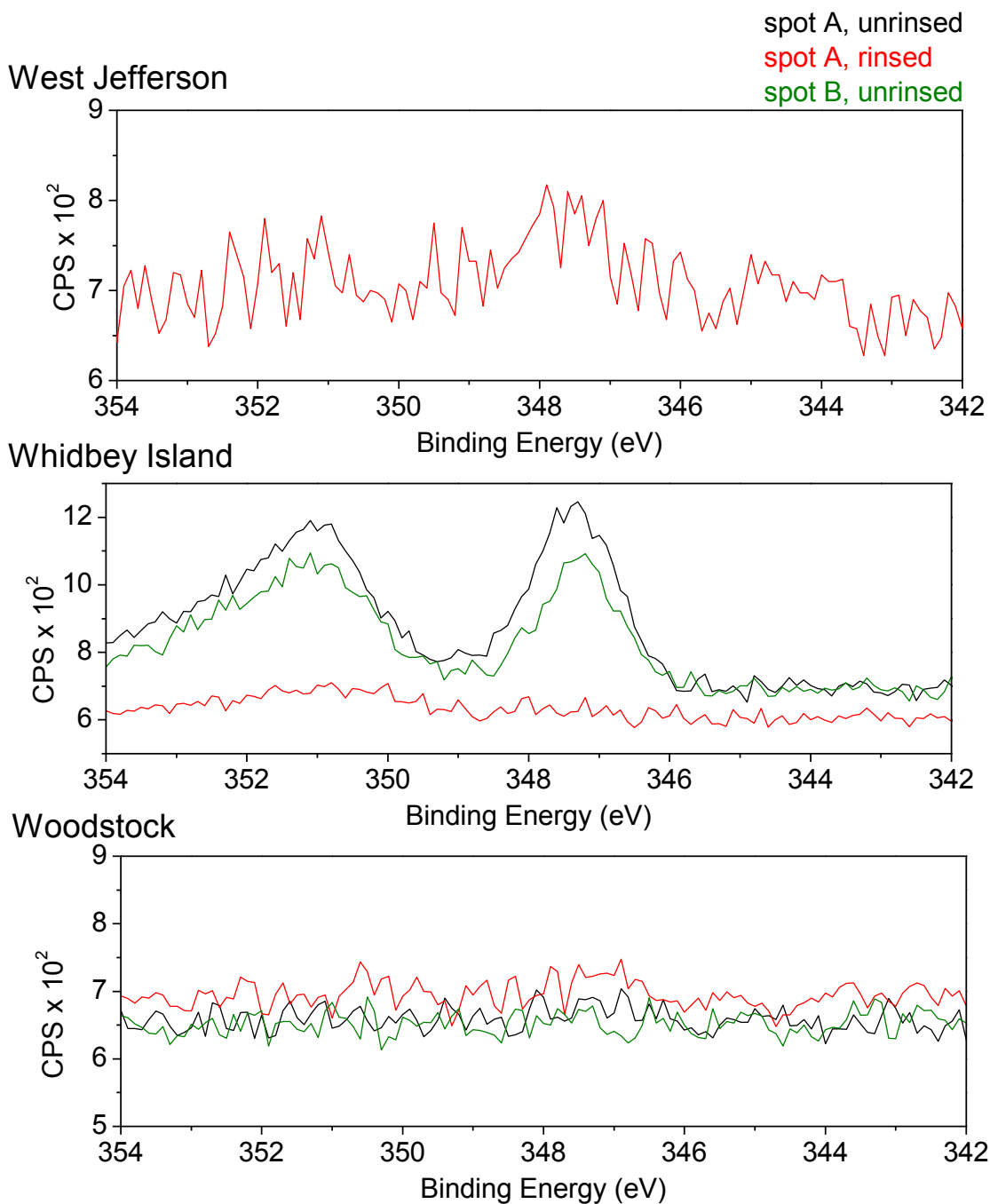


Figure F.33 XPS Ca 2p spectra for the samples exposed at West Jefferson, OH (top), Whidbey Island, WA (middle), and Woodstock, ME (bottom). The black, red, and green spectra are on spot A unrinsed (dark area), spot A rinsed, and spot B unrinsed (light area), respectively.

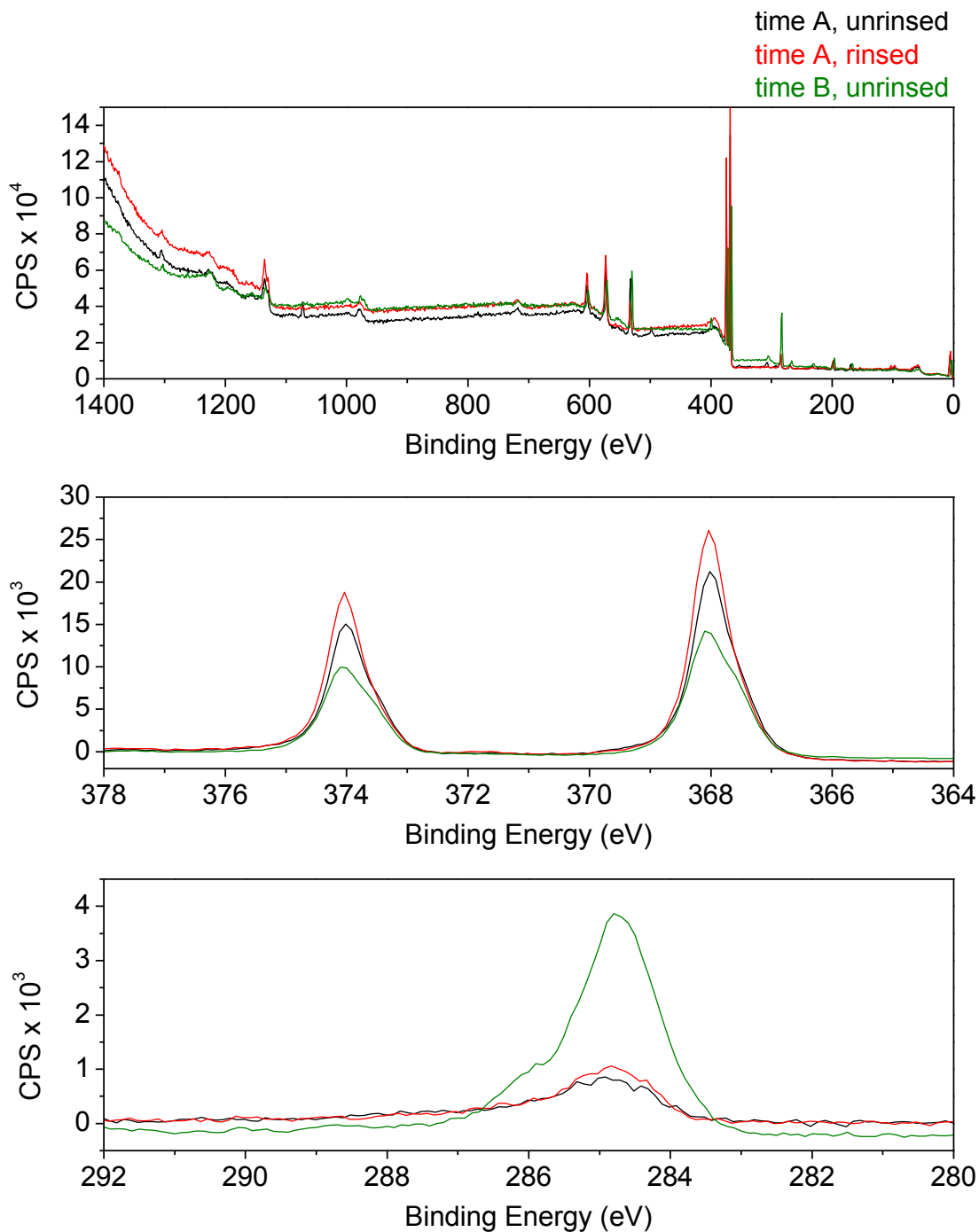


Figure F.34 XPS spectra for the sample exposed at McMurdo, Antarctica; survey (top), Ag 3d (middle), C 1s (bottom). The black, red, and green spectra are on time A unrinsed (upon initial receipt), time A rinsed, and time B unrinsed (2 years after receipt), respectively.

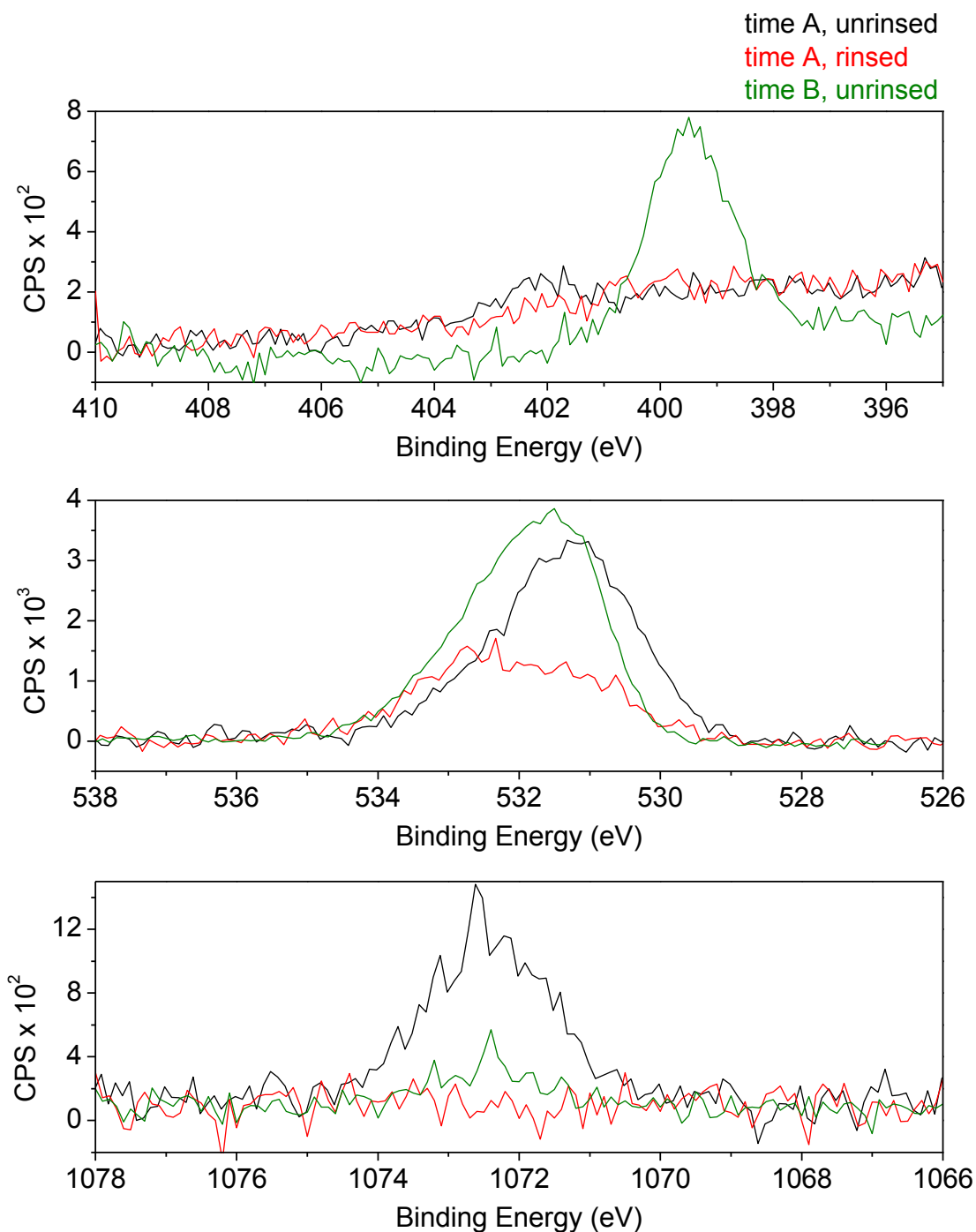


Figure F.35 XPS spectra for the sample exposed at McMurdo, Antarctica; N 1s (top), O 1s (middle), Na 1s (bottom). The black, red, and green spectra are on time A unrinsed (upon initial receipt), time A rinsed, and time B unrinsed (2 years after receipt), respectively.

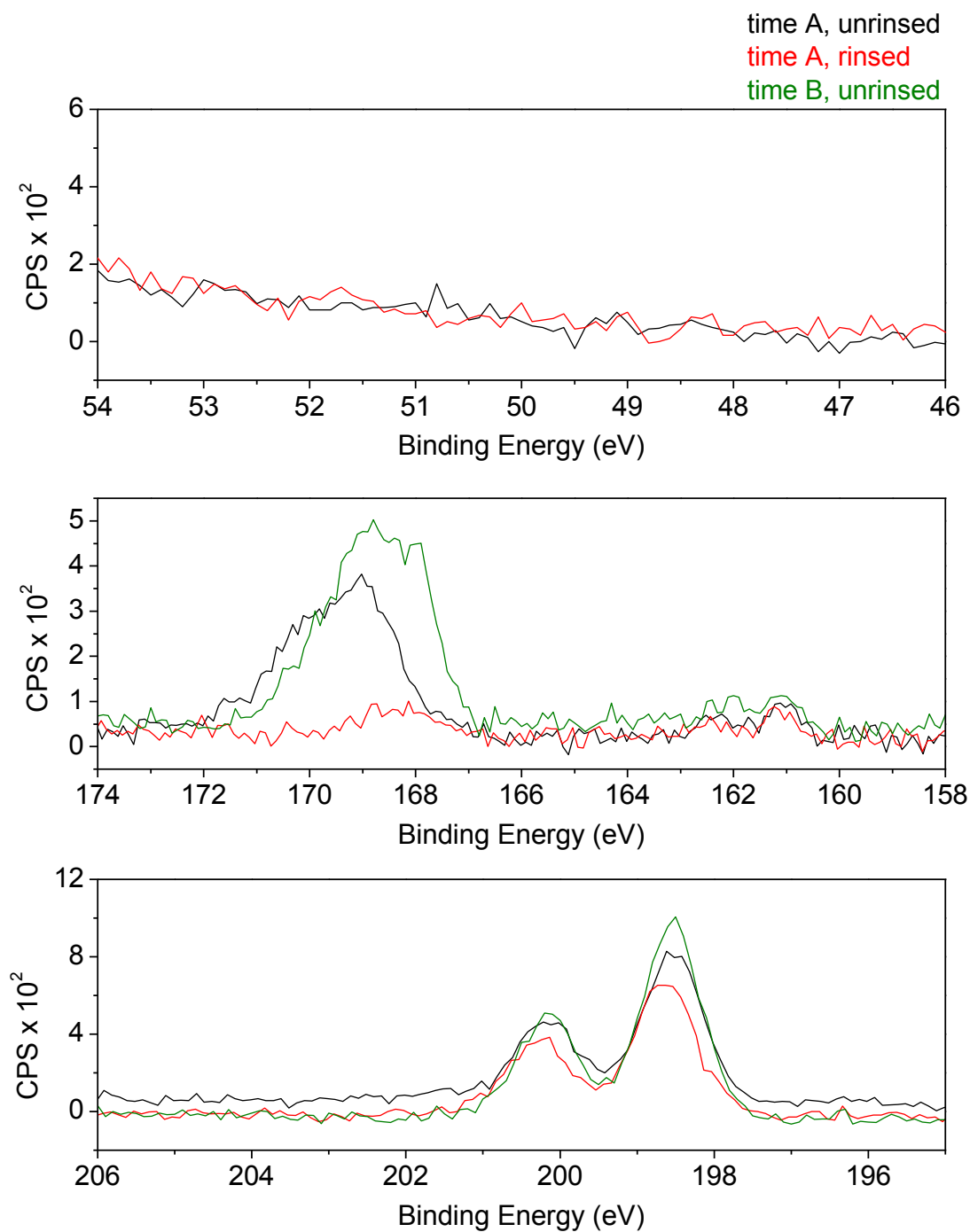


Figure F.36 XPS spectra for the sample exposed at McMurdo, Antarctica; Mg 2p (top), S 2p (middle), Cl 2p (bottom). The black, red, and green spectra are on time A unrinsed (upon initial receipt), time A rinsed, and time B unrinsed (2 years after receipt), respectively.

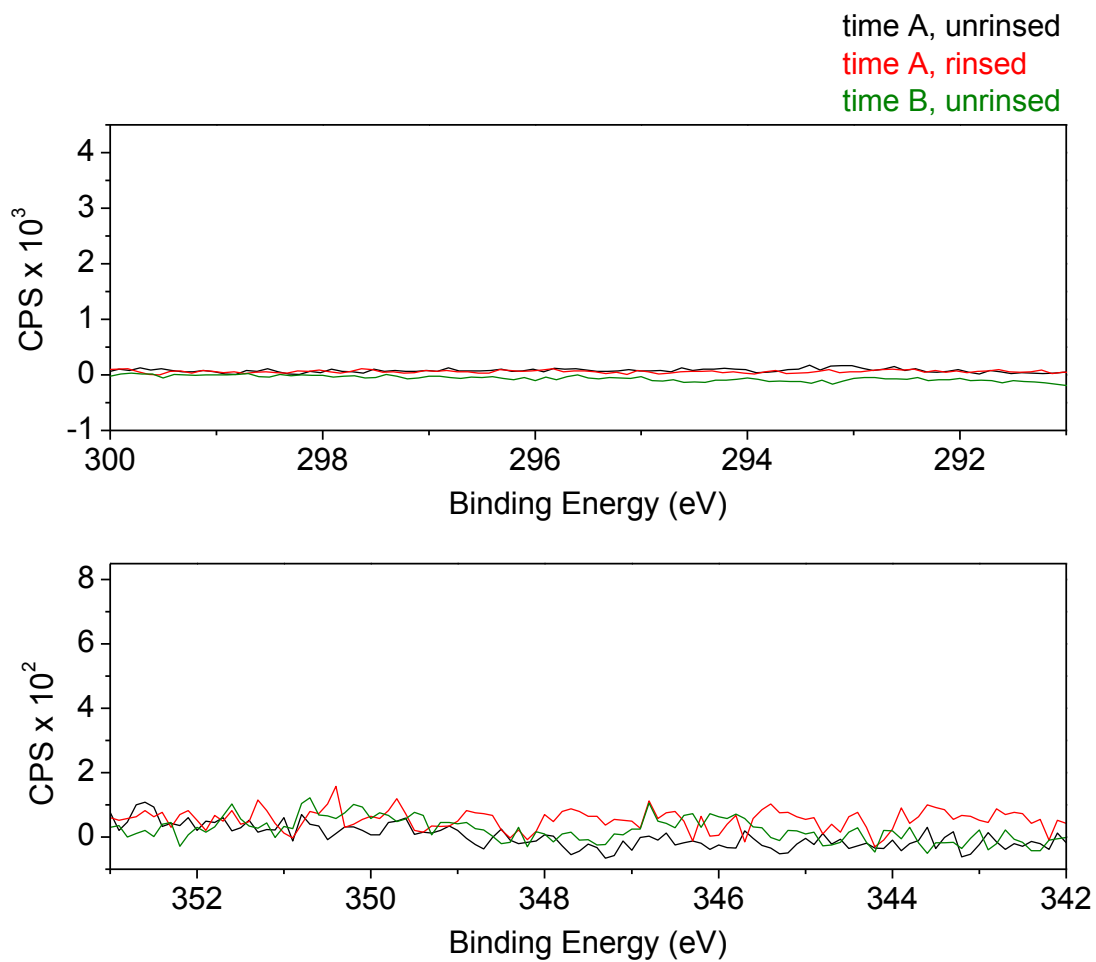


Figure F.37 XPS spectra for the sample exposed at McMurdo, Antarctica; K 2p (top) and Ca 2p (bottom). The black, red, and green spectra are on time A unrinsed (upon initial receipt), time A rinsed, and time B unrinsed (2 years after receipt), respectively.

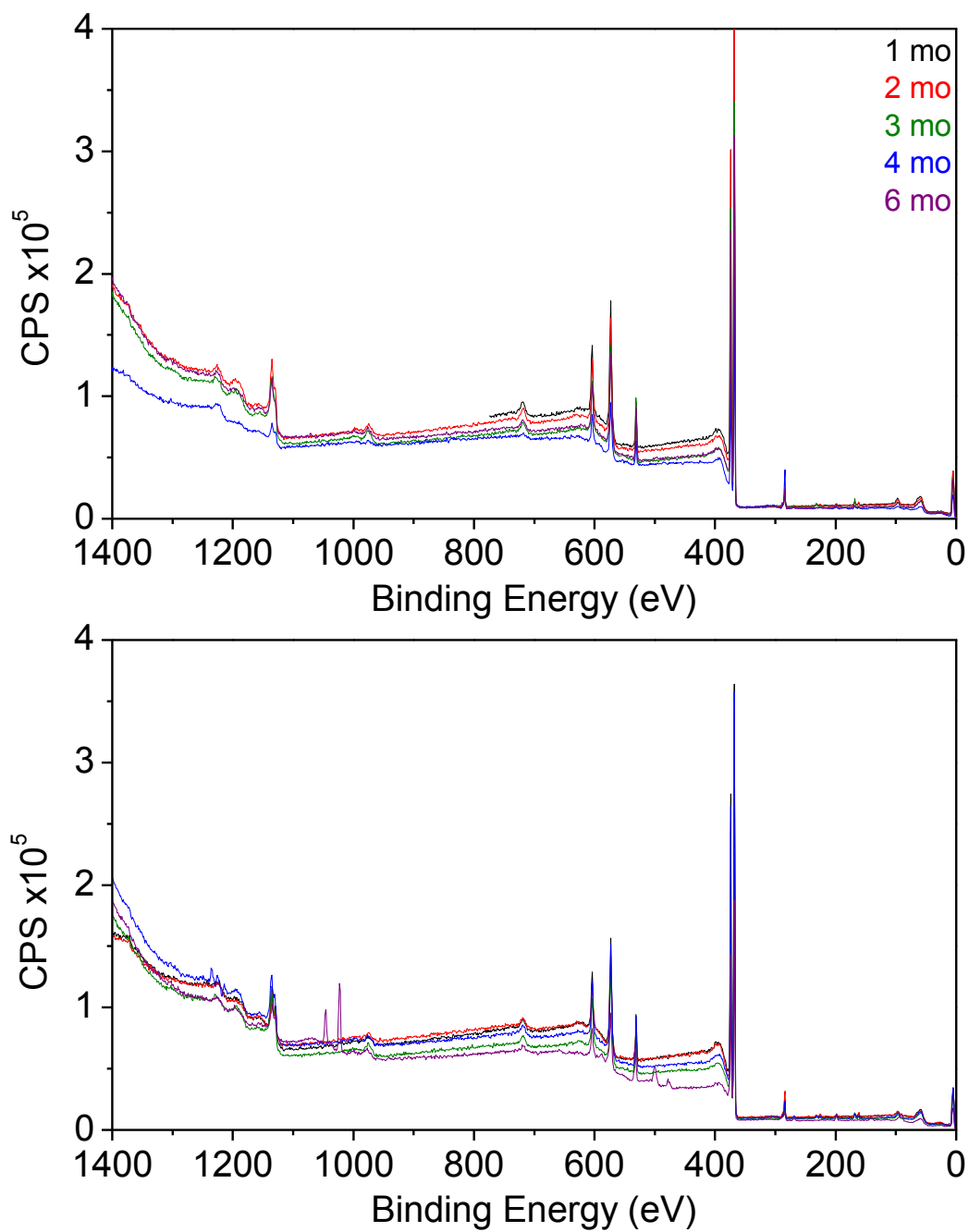


Figure F.38 XPS survey scans of the silver samples exposed at Thompson Farm, NH; sheltered (top) and unsheltered (bottom). Black, red, green, blue, and purple spectra correspond to 1, 2, 3, 4, and 6 month exposures, respectively.

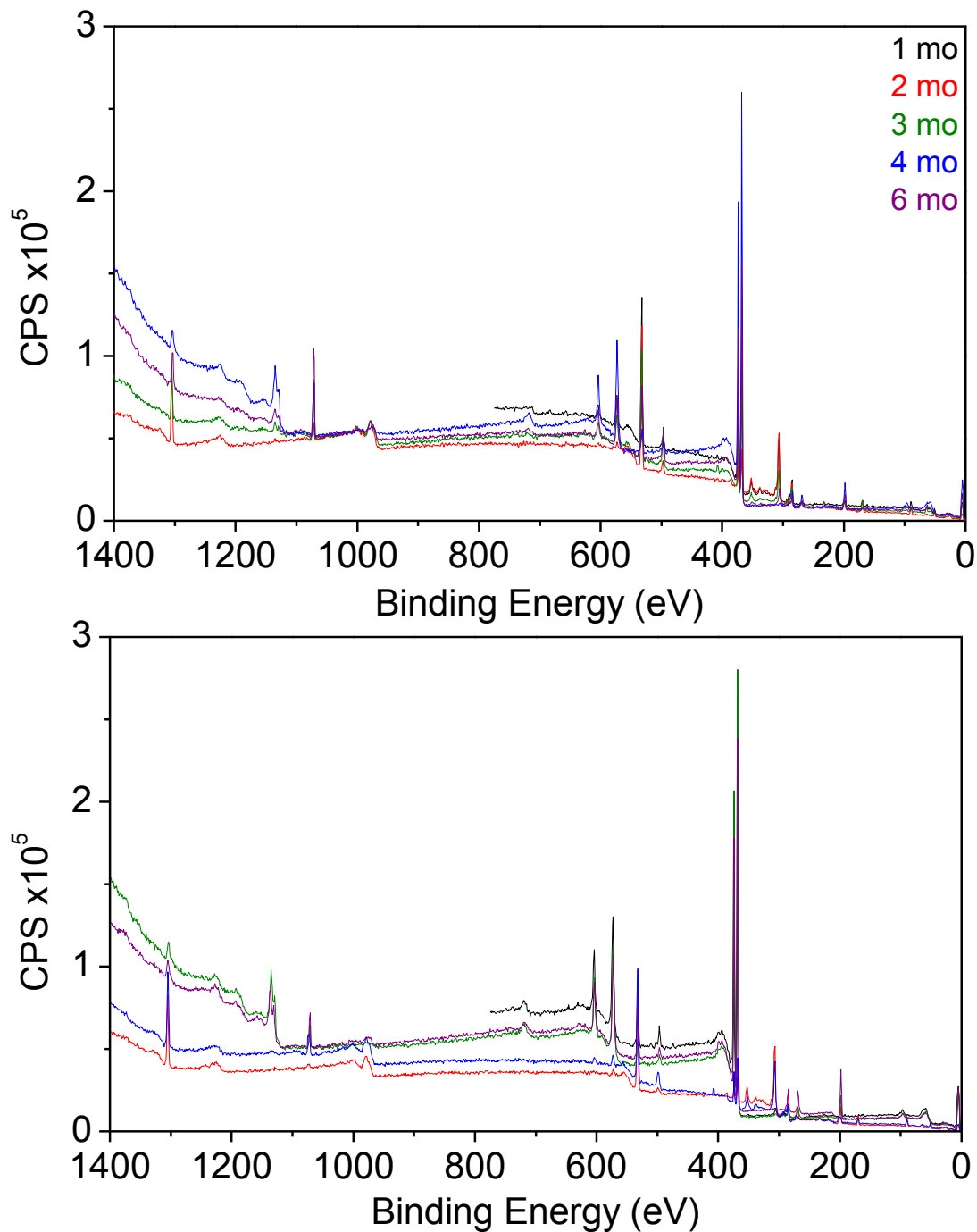


Figure F.39 XPS survey scans of the silver samples exposed at Appledore Island, ME; sheltered (top) and unsheltered (bottom). Black, red, green, blue, and purple spectra correspond to 1, 2, 3, 4, and 6 month exposures, respectively.

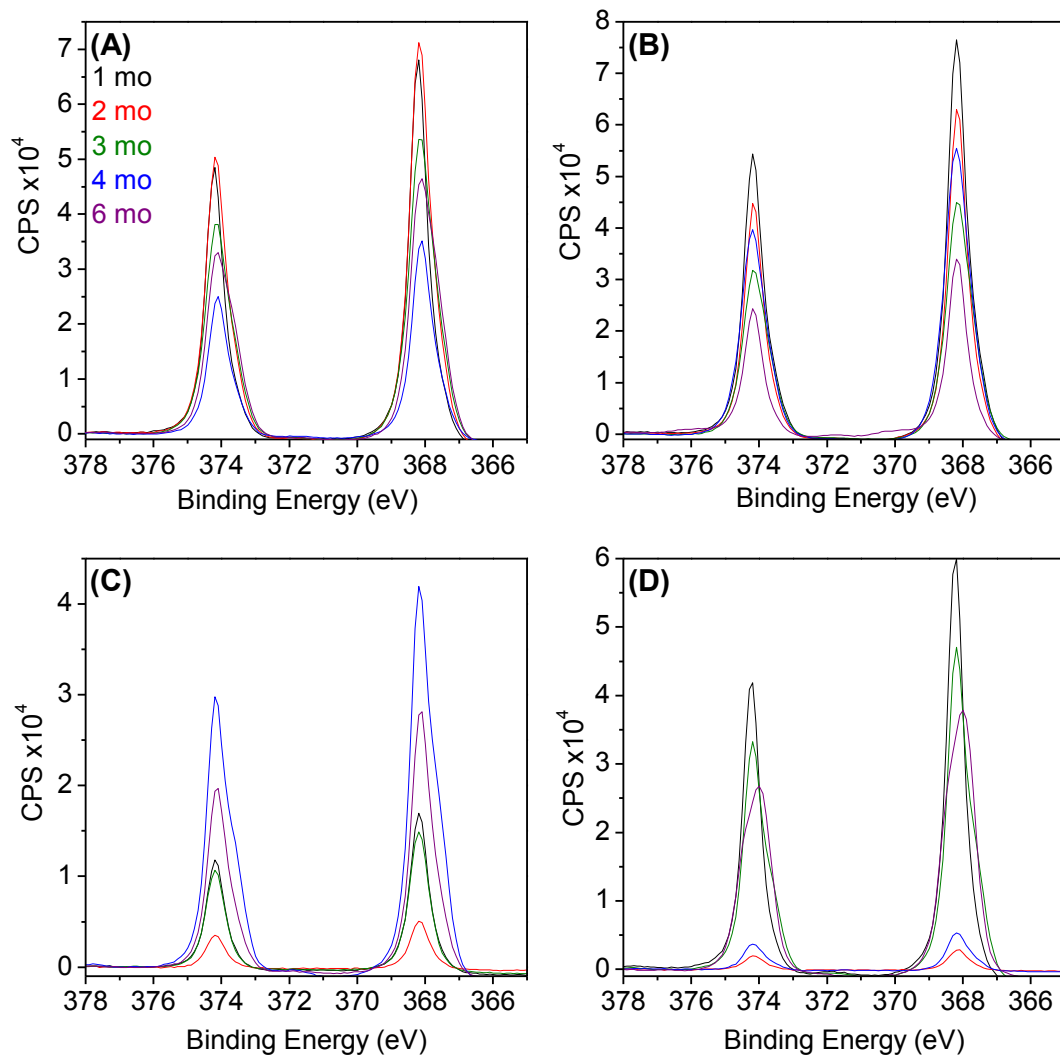


Figure F.40 XPS Ag 3d region scans of all samples exposed at Thompson Farm, NH (A) sheltered (B), unsheltered and Appledore Island, ME (C) sheltered, (D) unsheltered. Black, red, green, blue, and purple spectra correspond to 1, 2, 3, 4, and 6 month exposures, respectively.

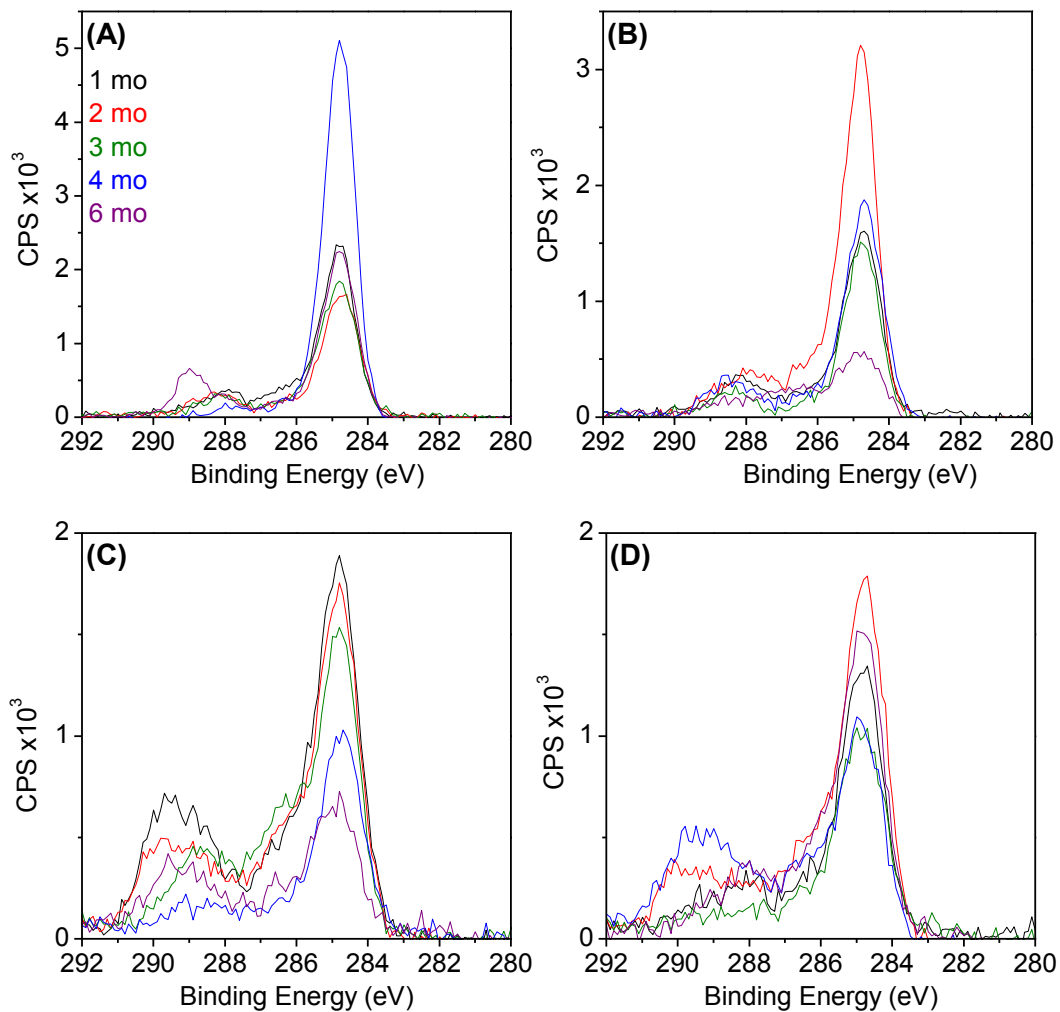


Figure F.41 XPS C 1s region scans of all samples exposed at Thompson Farm, NH (A) sheltered (B), unsheltered and Appledore Island, ME (C) sheltered, (D) unsheltered. Black, red, green, blue, and purple spectra correspond to 1, 2, 3, 4, and 6 month exposures, respectively.

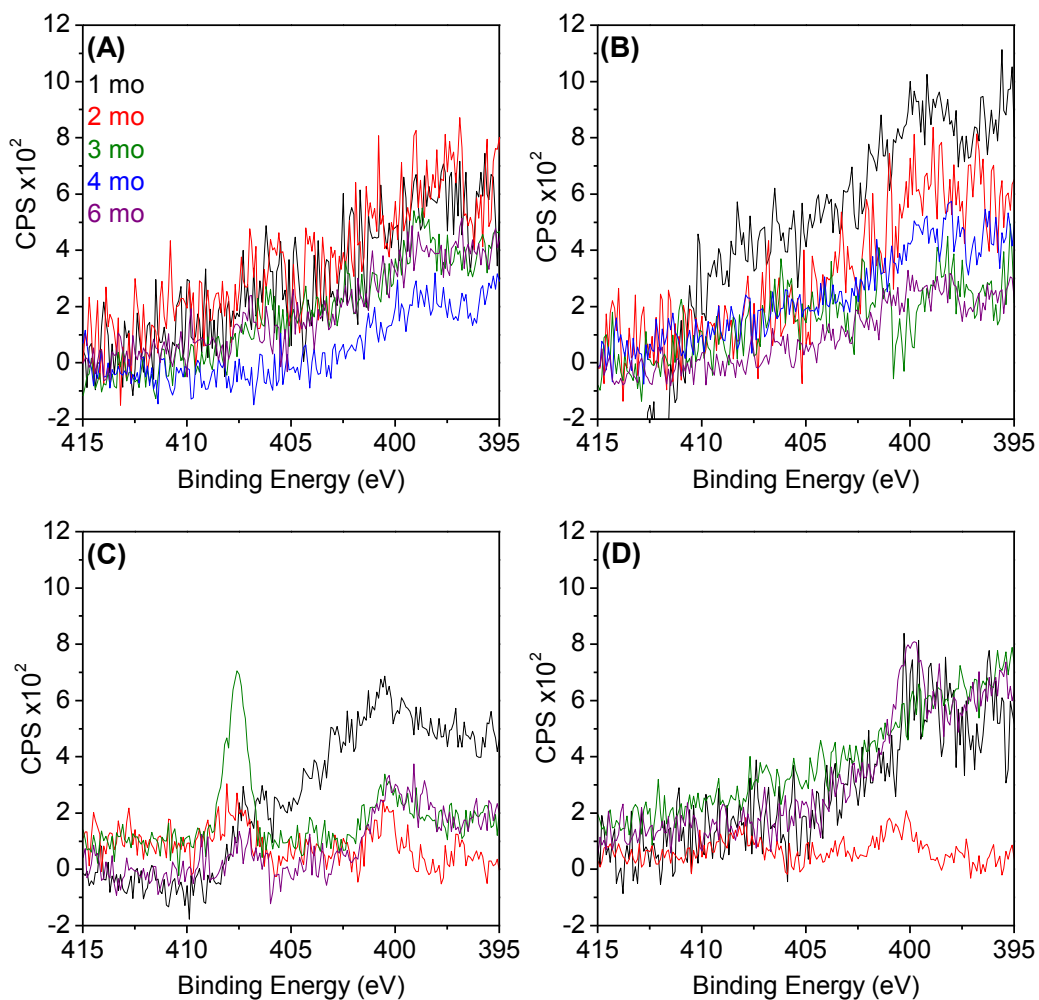


Figure F.42 XPS N 1s region scans of all samples exposed at Thompson Farm, NH (A) sheltered (B) unsheltered and Appledore Island, ME (C) sheltered, (D) unsheltered. Black, red, green, blue, and purple spectra correspond to 1, 2, 3, 4, and 6 month exposures, respectively.

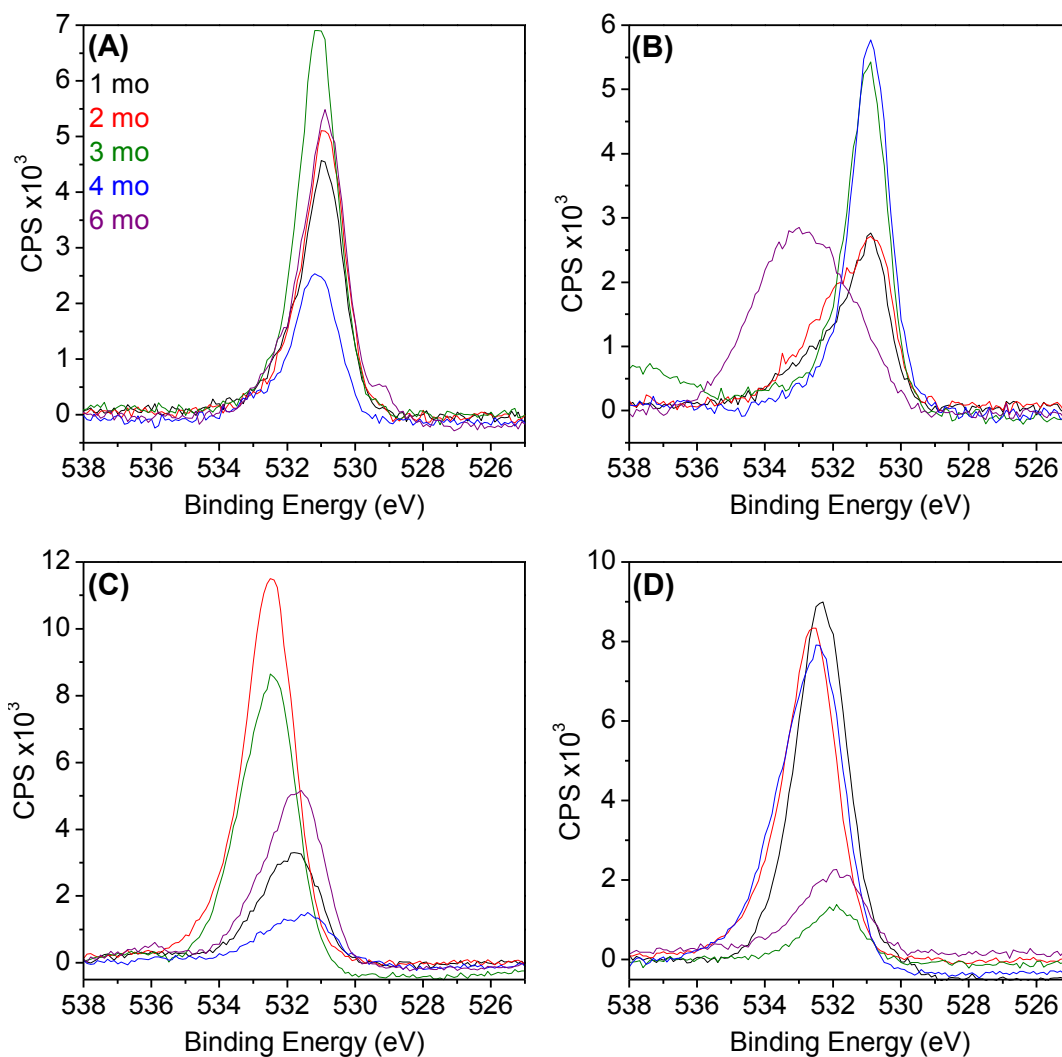


Figure F.43 XPS O 1s region scans of all samples exposed at Thompson Farm, NH (A) sheltered (B), unsheltered and Appledore Island, ME (C) sheltered, (D) unsheltered. Black, red, green, blue, and purple spectra correspond to 1, 2, 3, 4, and 6 month exposures, respectively.

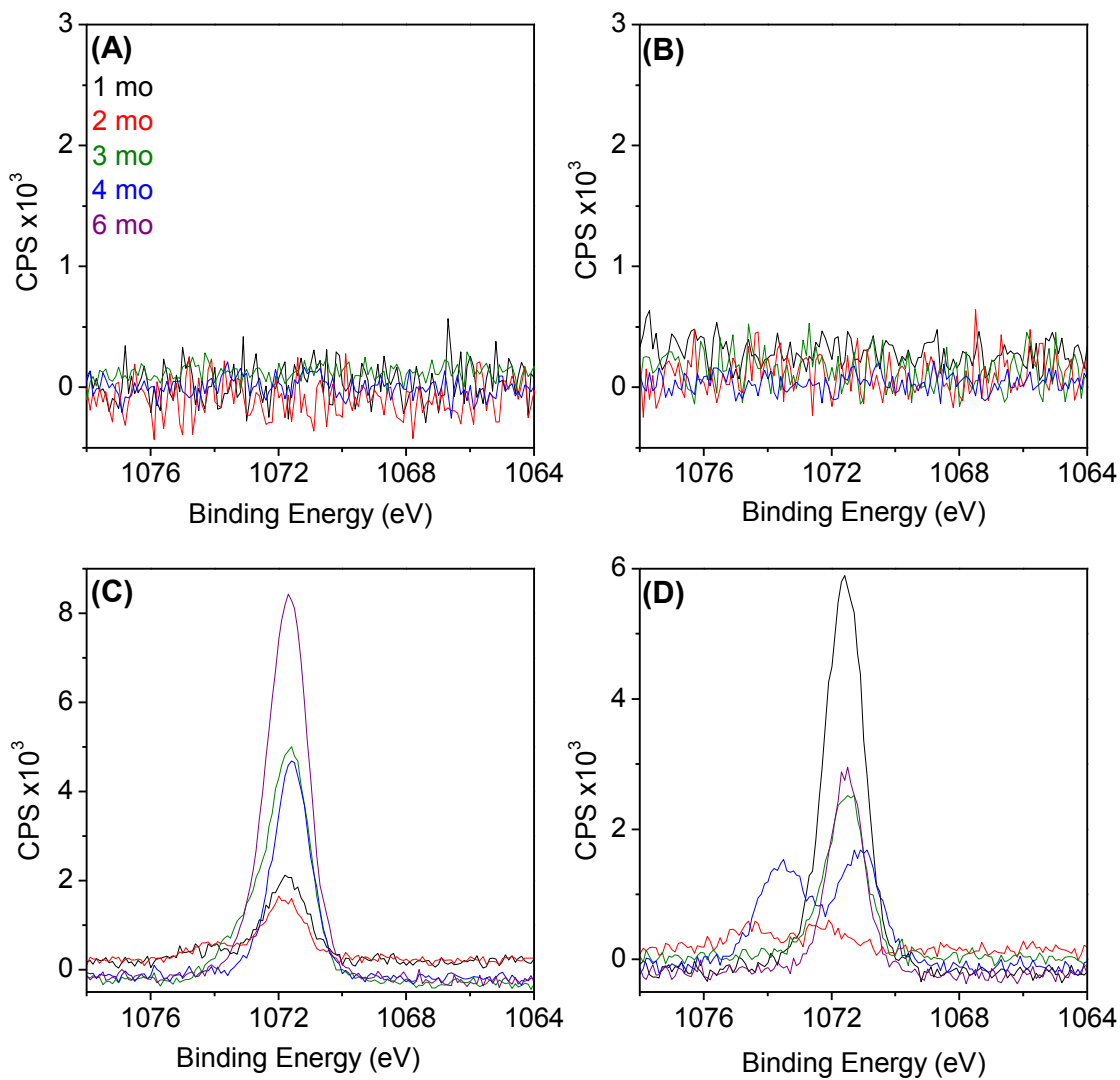


Figure F.44 XPS Na 1s region scans of all samples exposed at Thompson Farm, NH (A) sheltered (B), unsheltered and Appledore Island, ME (C) sheltered, (D) unsheltered. Black, red, green, blue, and purple spectra correspond to 1, 2, 3, 4, and 6 month exposures, respectively.

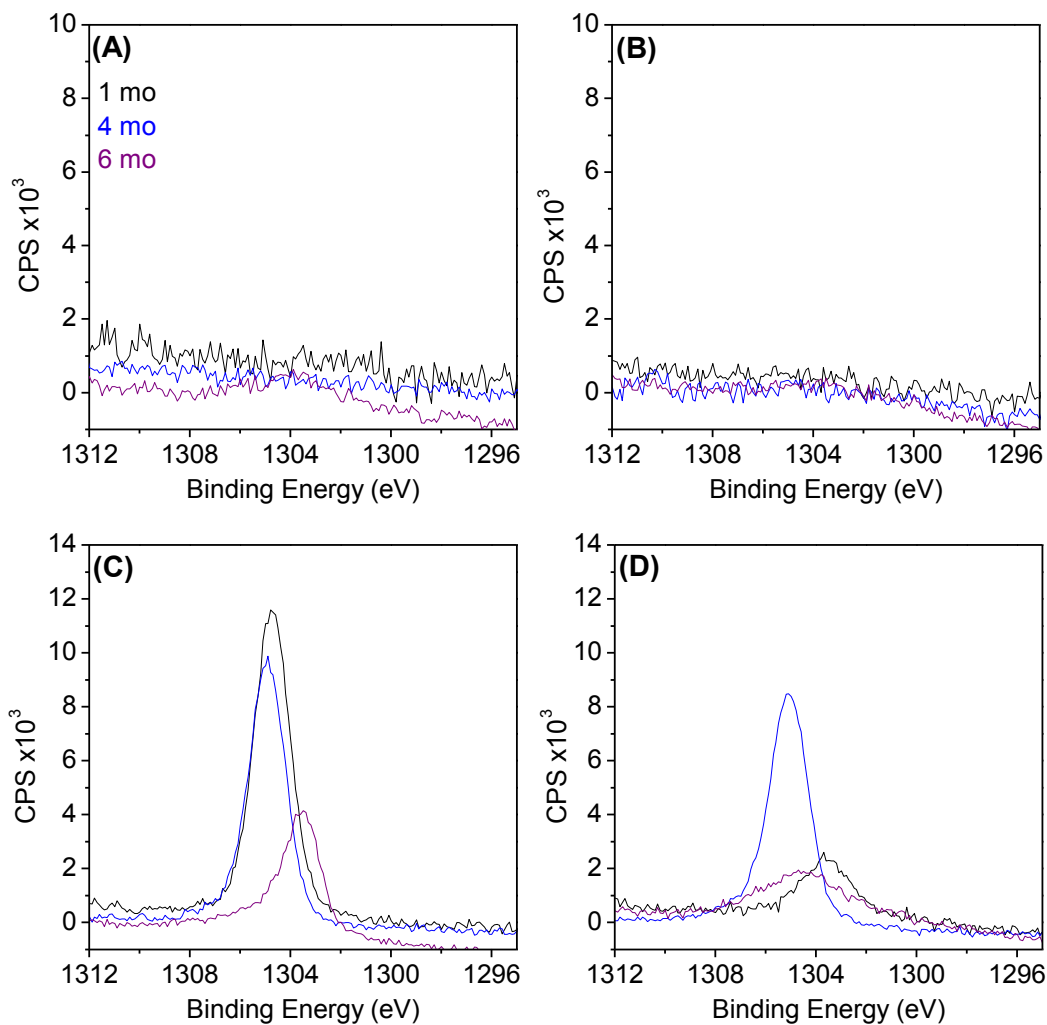


Figure F.45 XPS Mg 1s region scans of all samples exposed at Thompson Farm, NH (A) sheltered (B), unsheltered and Appledore Island, ME (C) sheltered, (D) unsheltered. Black, blue, and purple spectra correspond to 1, 4, and 6 month exposures, respectively.

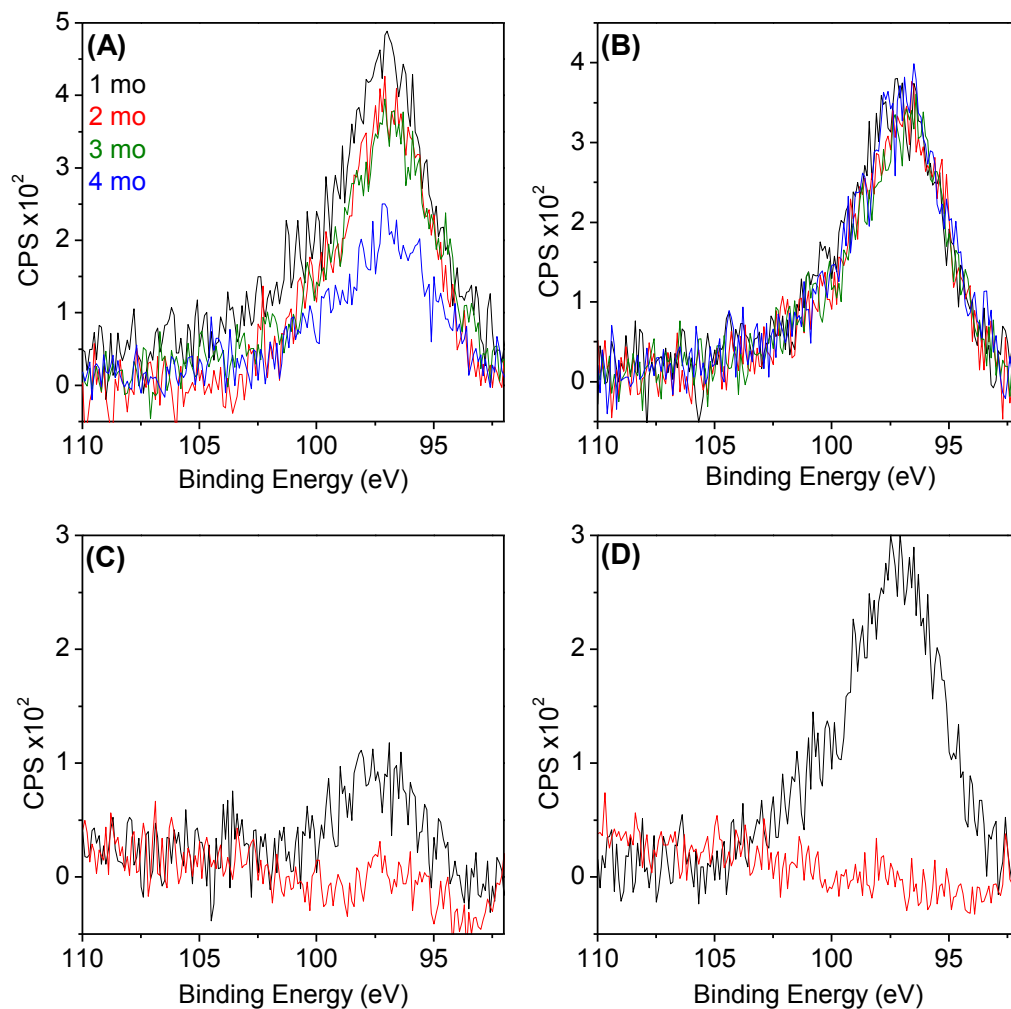


Figure F.46 XPS SI 2p region scans of all samples exposed at Thompson Farm, NH (A) sheltered (B), unsheltered and Appledore Island, ME (C) sheltered, (D) unsheltered. Black, red, green, and blue spectra correspond to 1, 2, 3, and 4 month exposures, respectively.

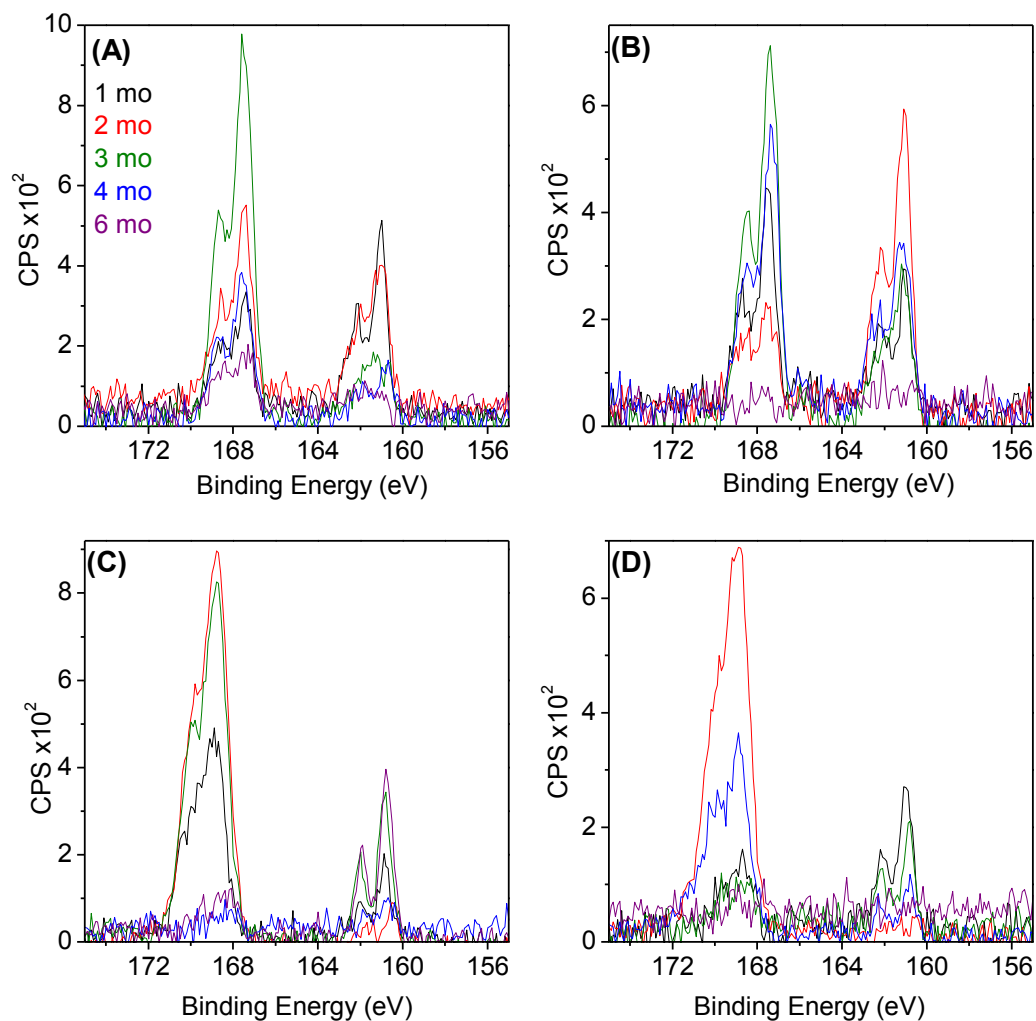


Figure F.47 XPS S 2p region scans of all samples exposed at Thompson Farm, NH (A) sheltered (B), unsheltered and Appledore Island, ME (C) sheltered, (D) unsheltered. Black, red, green, blue, and purple spectra correspond to 1, 2, 3, 4, and 6 month exposures, respectively.

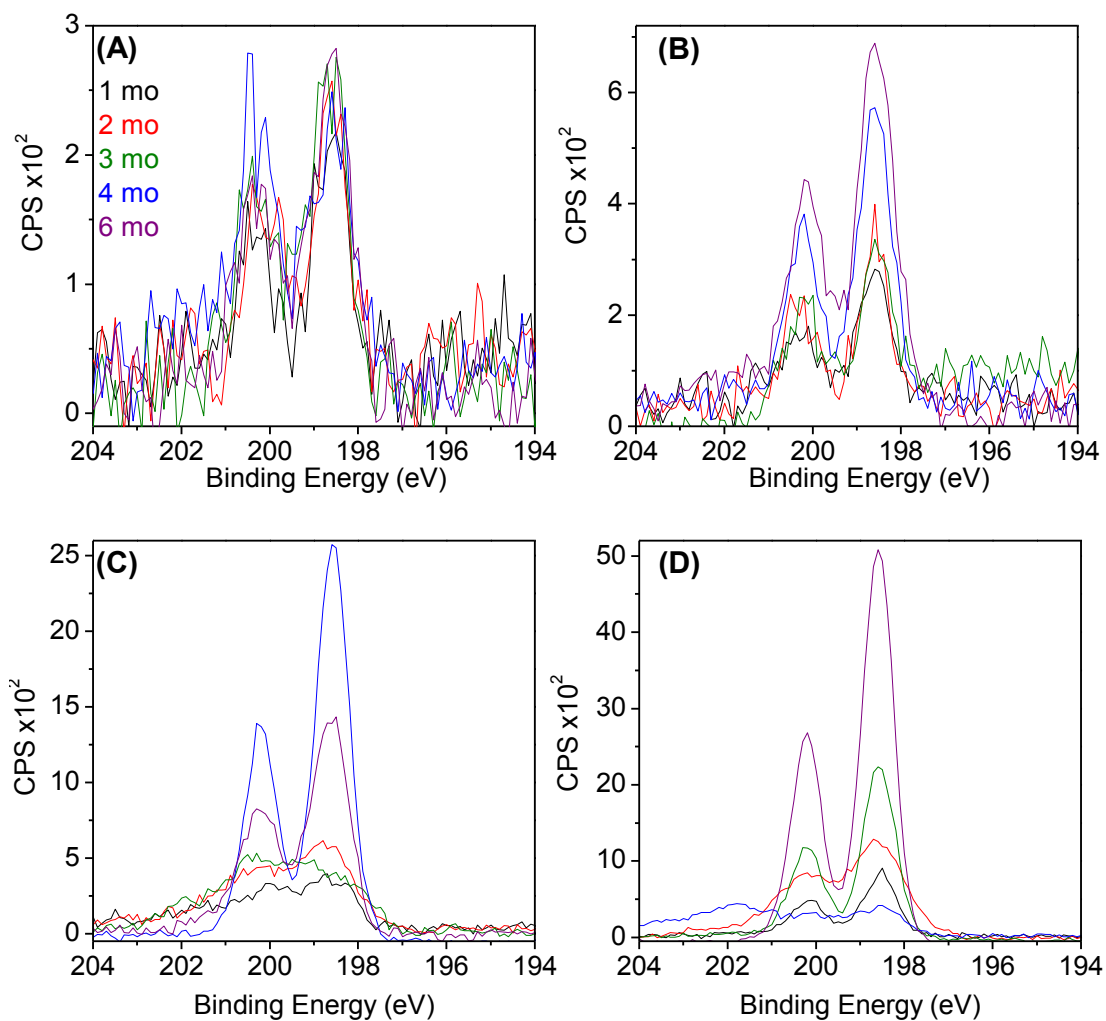


Figure F.48 XPS Cl 2p region scans of all samples exposed at Thompson Farm, NH (A) sheltered (B), unsheltered and Appledore Island, ME (C) sheltered, (D) unsheltered. Black, red, green, blue, and purple spectra correspond to 1, 2, 3, 4, and 6 month exposures, respectively.

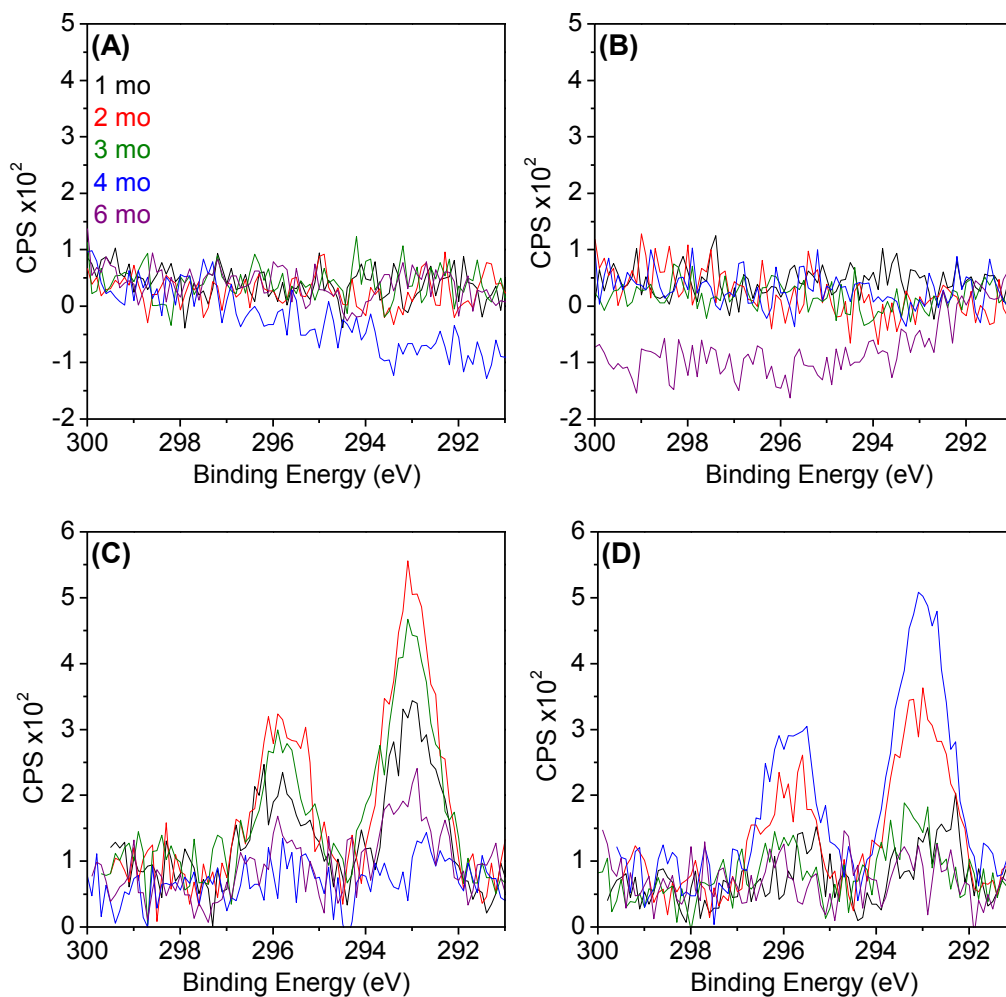


Figure F.49 XPS K 2p region scans of all samples exposed at Thompson Farm, NH (A) sheltered (B), unsheltered and Appledore Island, ME (C) sheltered, (D) unsheltered. Black, red, green, blue, and purple spectra correspond to 1, 2, 3, 4, and 6 month exposures, respectively.

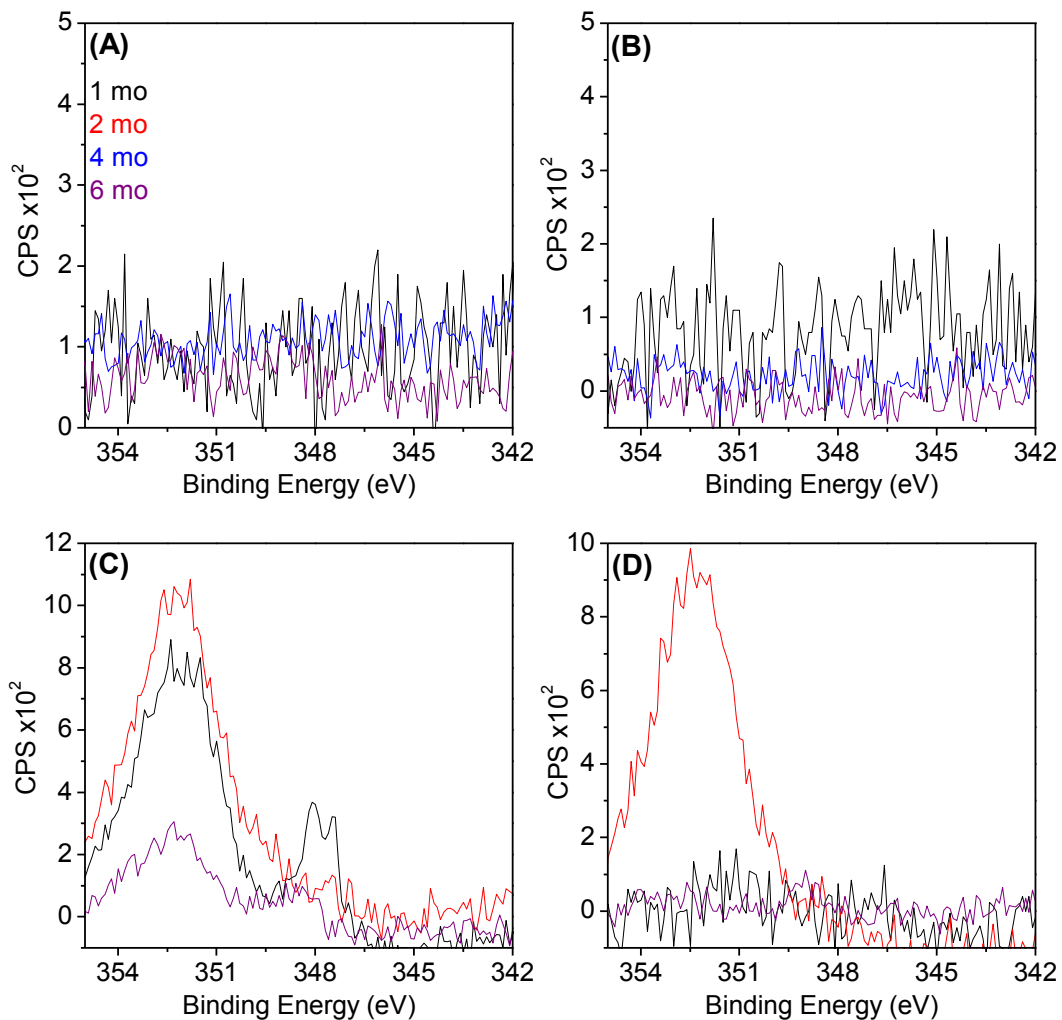


Figure F.50 XPS Ca 2p region scans of all samples exposed at Thompson Farm, NH (A) sheltered (B), unsheltered and Appledore Island, ME (C) sheltered, (D) unsheltered. Black, red, green, blue, and purple spectra correspond to 1, 2, 3, 4, and 6 month exposures, respectively.

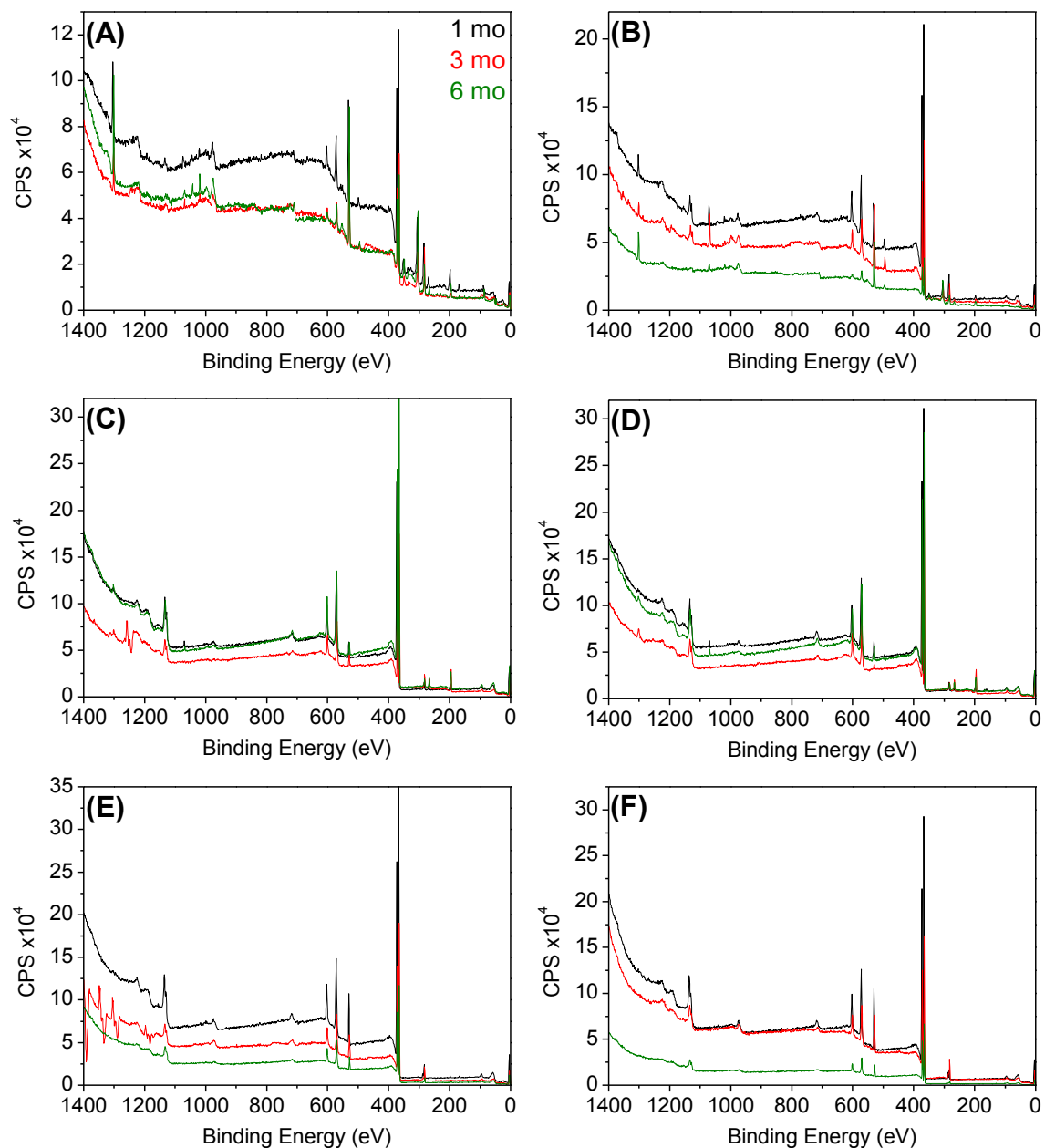


Figure F.51 XPS survey scans of all samples exposed in Hawaii; Kaneohe MAB (A) sheltered (B), unsheltered, Kilauea volcano (C) sheltered, (D) unsheltered, and Mauna Loa observatory (E) sheltered, (F) unsheltered. Black, red, and green spectra correspond to 1, 3, and 6 month exposures, respectively.

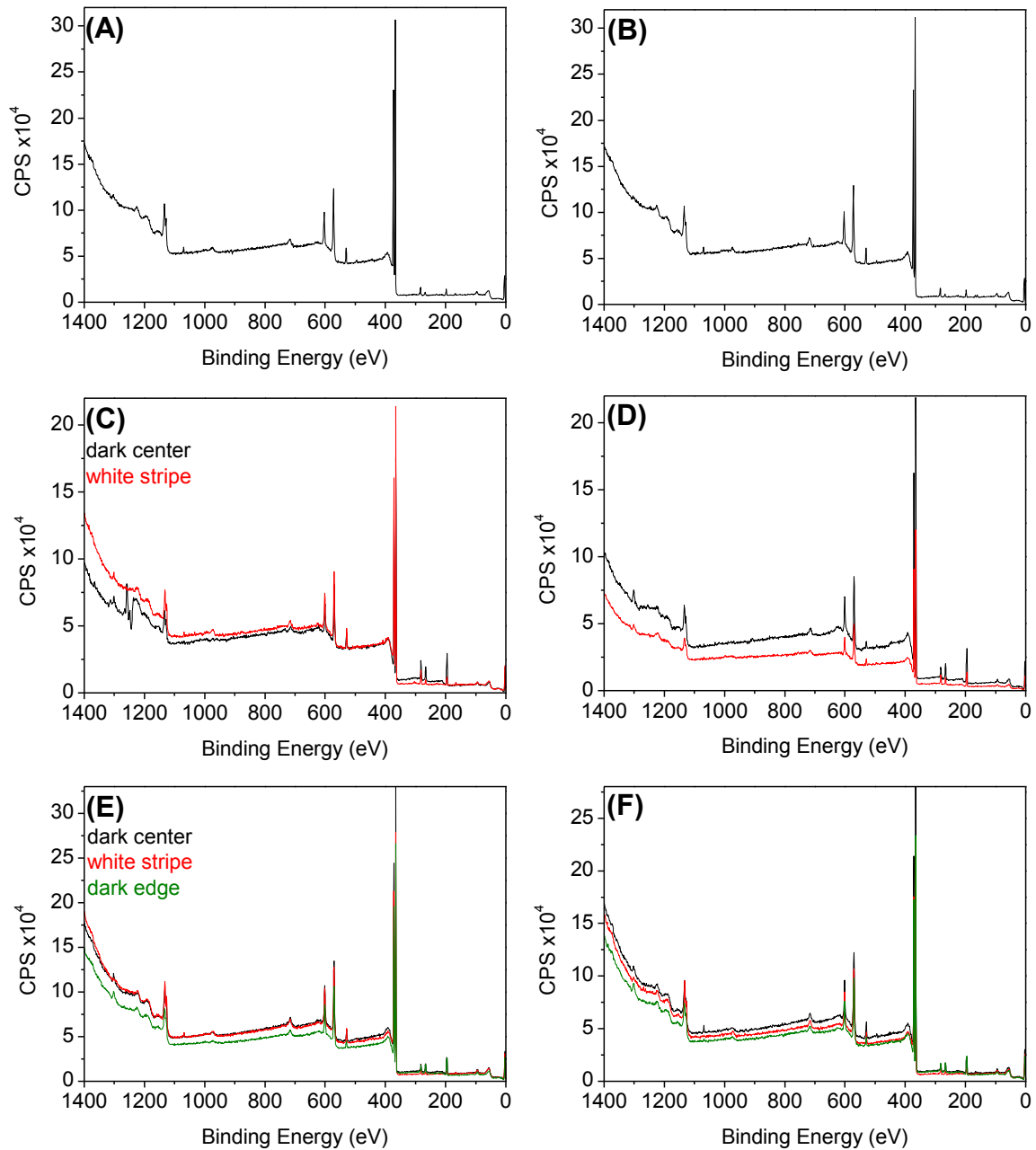


Figure F.52 XPS survey scans of all samples exposed at Kilauea volcano in Hawaii. 1 month (A) sheltered and (B) unsheltered, 3 month (C) sheltered and (D) unsheltered, 6 month (E) sheltered and (F) unsheltered. Black, red, and green spectra correspond to dark center, white stripe, and dark edge, respectively.

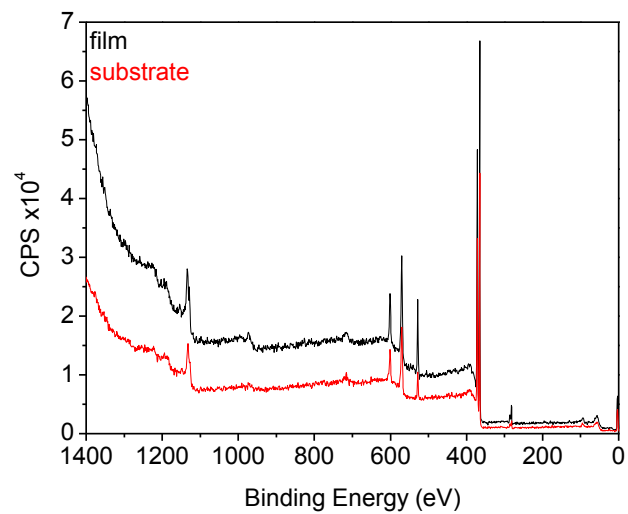


Figure F.53 XPS survey scans of 6 month unsheltered samples exposed at Mauna Loa in Hawaii. Black and red spectra correspond to the dark film and light substrate, respectively.

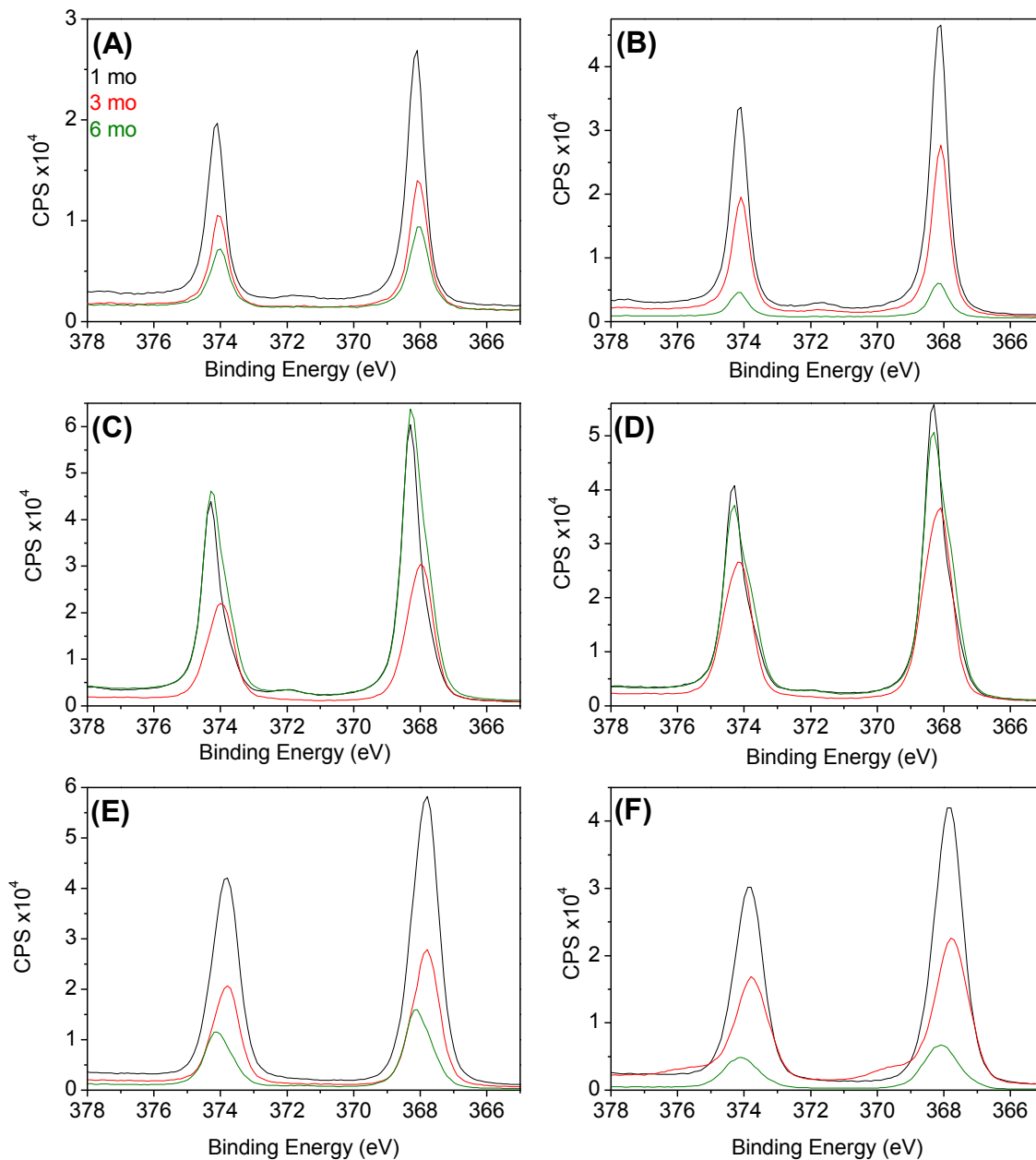


Figure F.54 XPS Ag 3d scans of all samples exposed in Hawaii; Kaneohe MAB (A) sheltered (B), unsheltered, Kilauea volcano (C) sheltered, (D) unsheltered, and Mauna Loa observatory (E) sheltered, (F) unsheltered. Black, red, and green spectra correspond to 1, 3, and 6 month exposures, respectively.

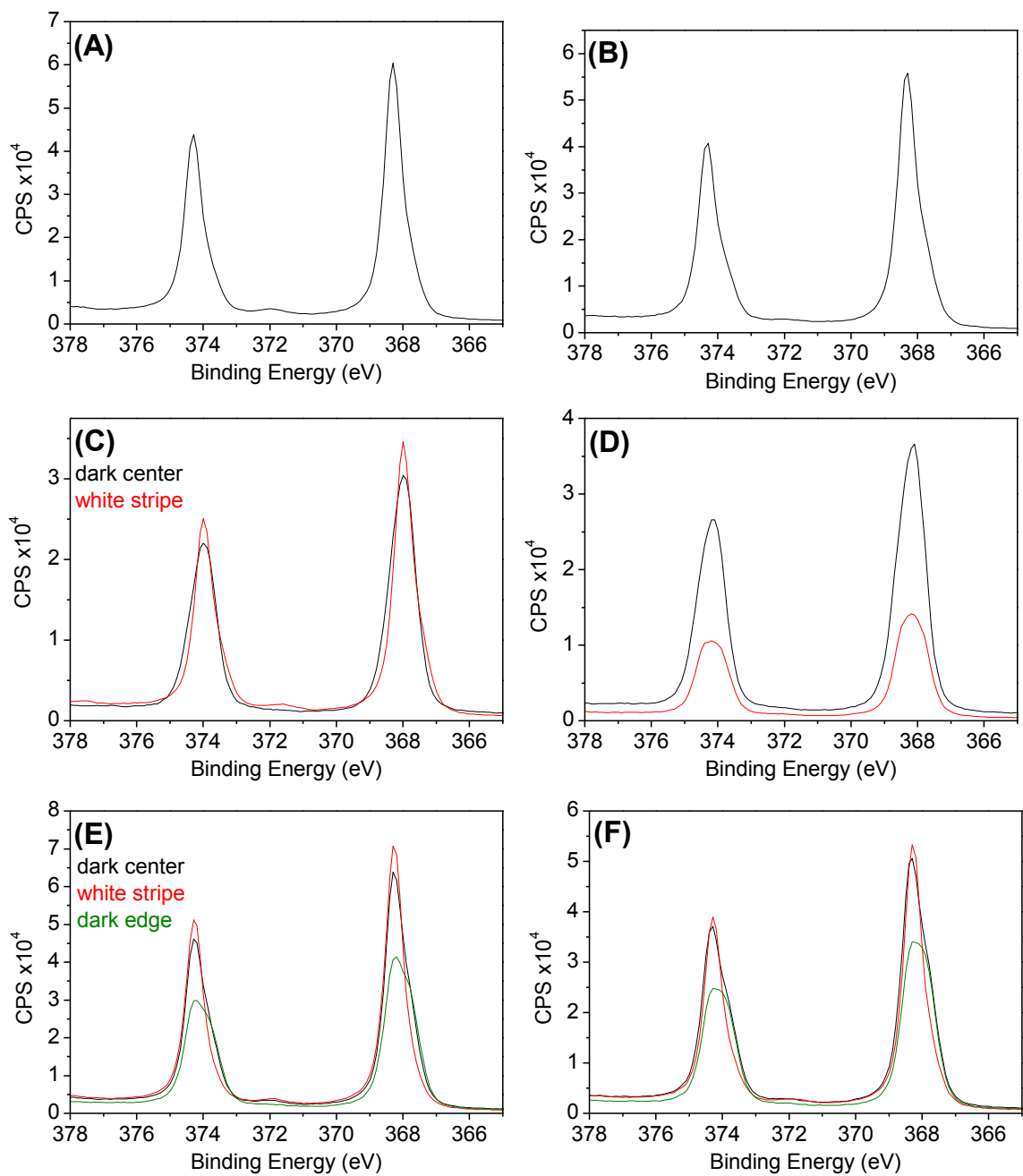


Figure F.55 XPS Ag 3d scans of all samples exposed at Kilauea volcano in Hawaii. 1 month (A) sheltered and (B) unsheltered, 3 month (C) sheltered and (D) unsheltered, 6 month (E) sheltered and (F) unsheltered. Black, red, and green spectra correspond to dark center, white stripe, and dark edge, respectively.

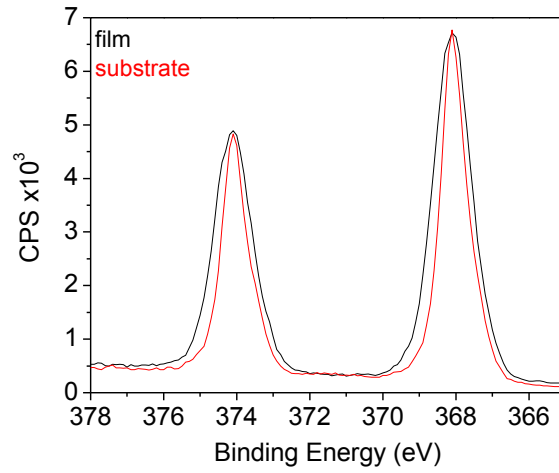


Figure F.56 XPS Ag 3d scans of 6 month unsheltered samples exposed at Mauna Loa in Hawaii. Black and red spectra correspond to the dark film and light substrate, respectively.

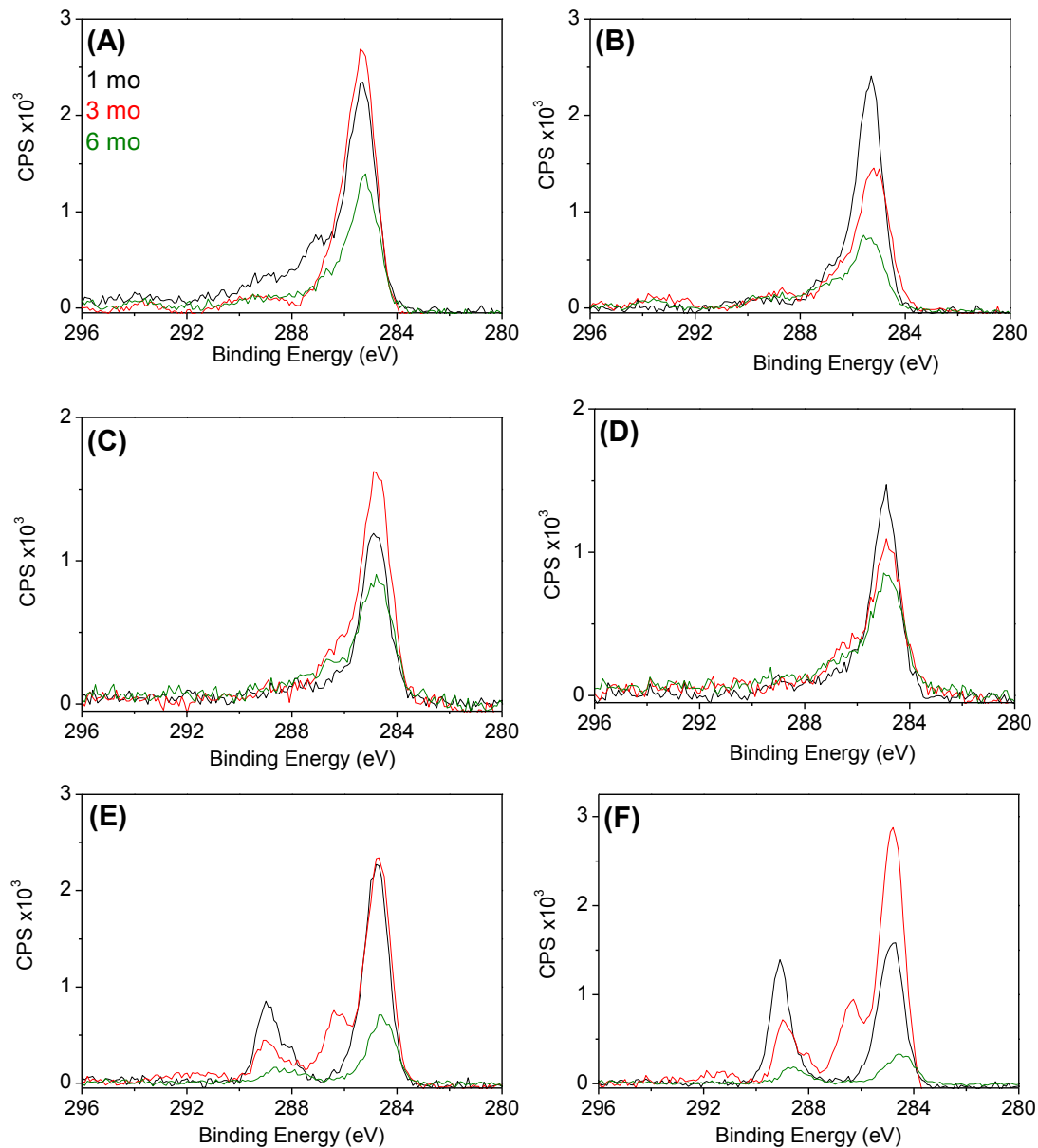


Figure F.57 XPS C 1s scans of all samples exposed in Hawaii; Kaneohe MAB (A) sheltered (B), unsheltered, Kilauea volcano (C) sheltered, (D) unsheltered, and Mauna Loa observatory (E) sheltered, (F) unsheltered. Black, red, and green spectra correspond to 1, 3, and 6 month exposures, respectively.

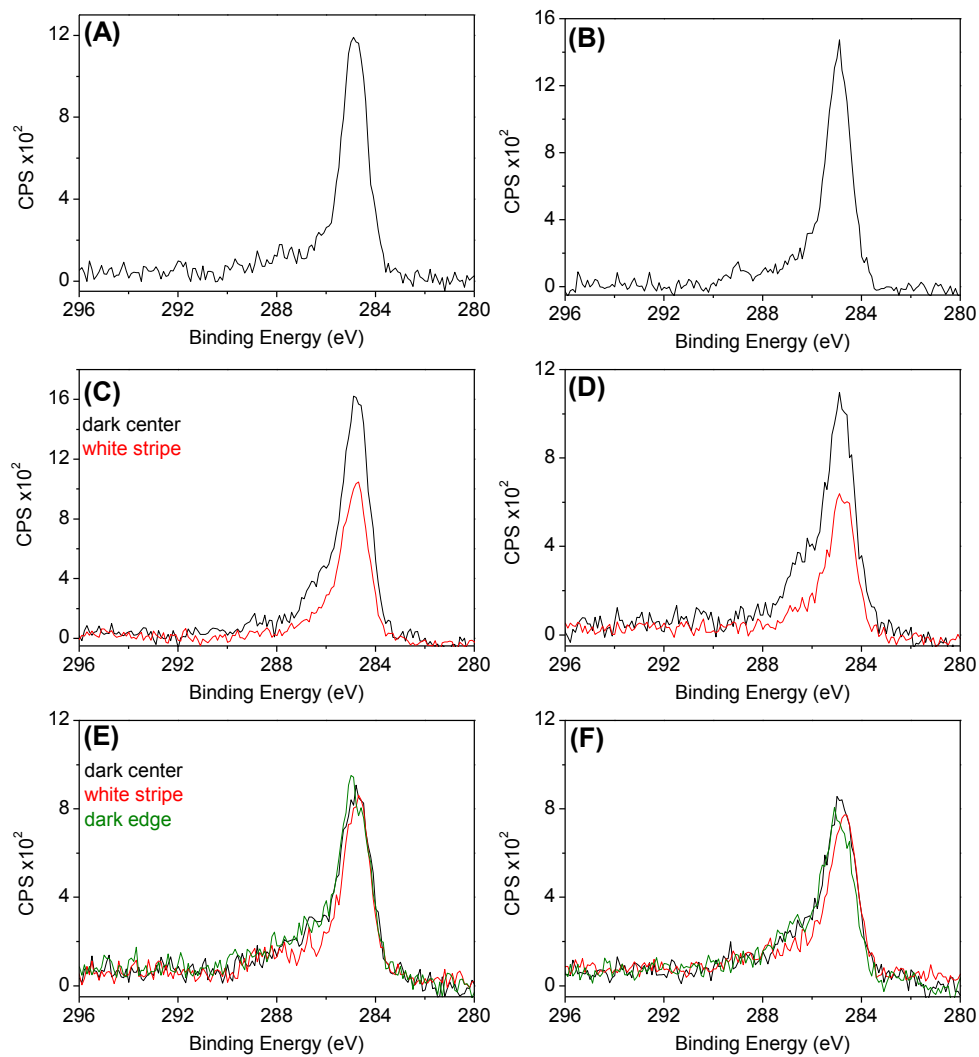


Figure F.58 XPS C 1s scans of all samples exposed at Kilauea volcano in Hawaii. 1 month (A) sheltered and (B) unsheltered, 3 month (C) sheltered and (D) unsheltered, 6 month (E) sheltered and (F) unsheltered. Black, red, and green spectra correspond to dark center, white stripe, and dark edge, respectively.

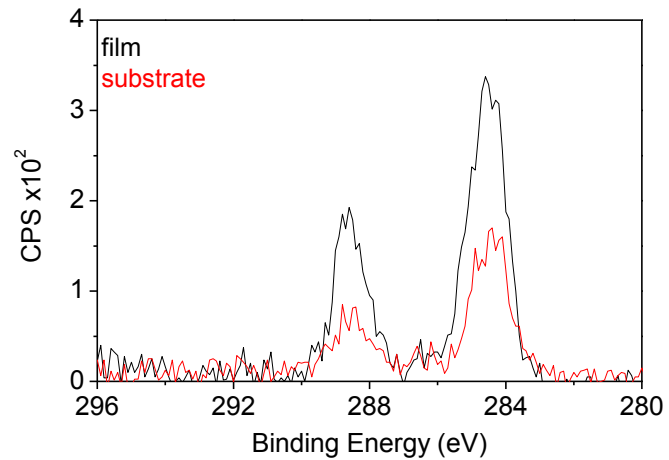


Figure F.59 XPS C 1s scans of 6 month unsheltered samples exposed at Mauna Loa in Hawaii. Black and red spectra correspond to the dark film and light substrate, respectively.

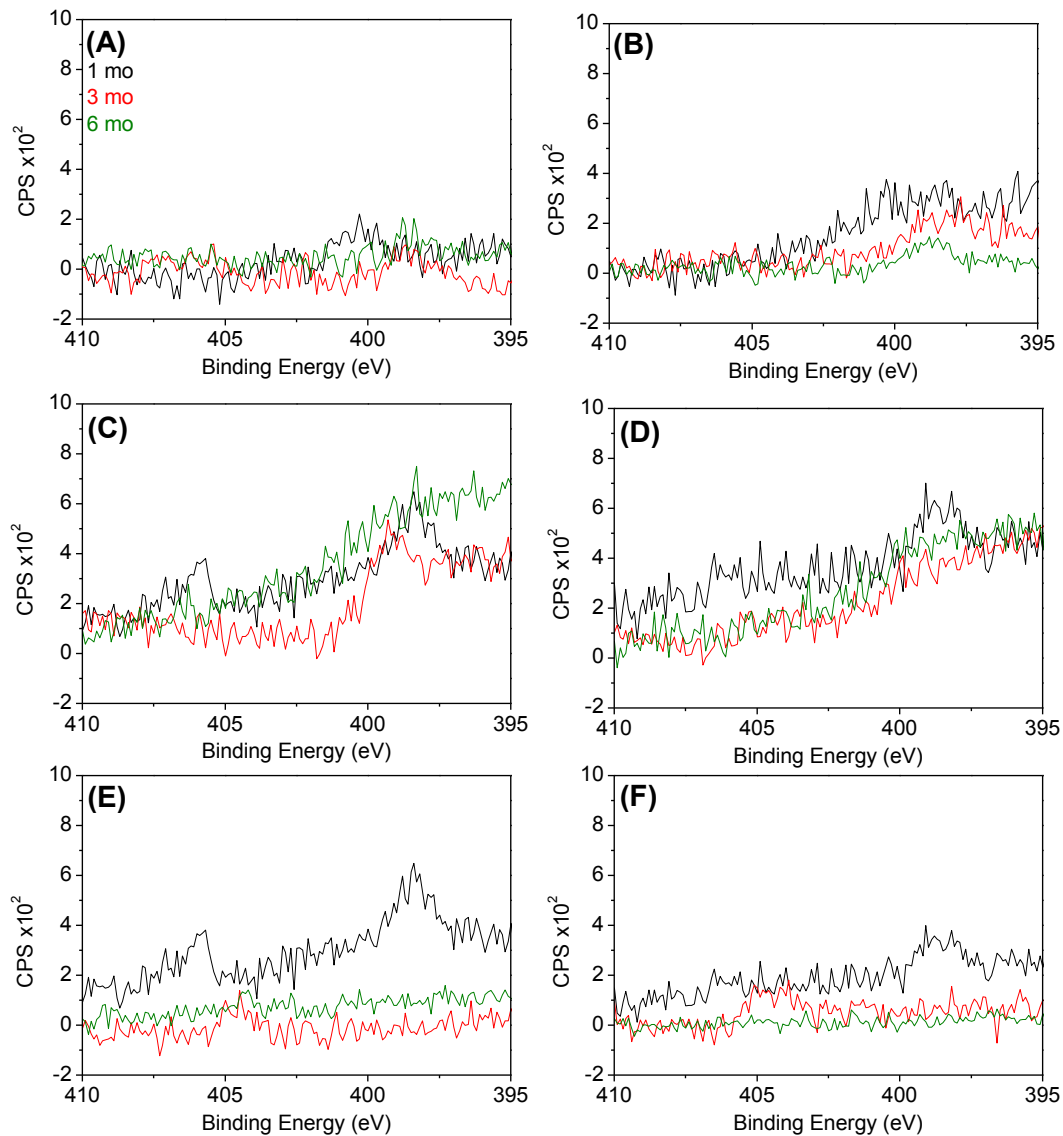


Figure F.60 XPS N 1s scans of all samples exposed in Hawaii; Kaneohe MAB (A) sheltered (B) unsheltered, Kilauea volcano (C) sheltered, (D) unsheltered, and Mauna Loa observatory (E) sheltered, (F) unsheltered. Black, red, and green spectra correspond to 1, 3, and 6 month exposures, respectively.

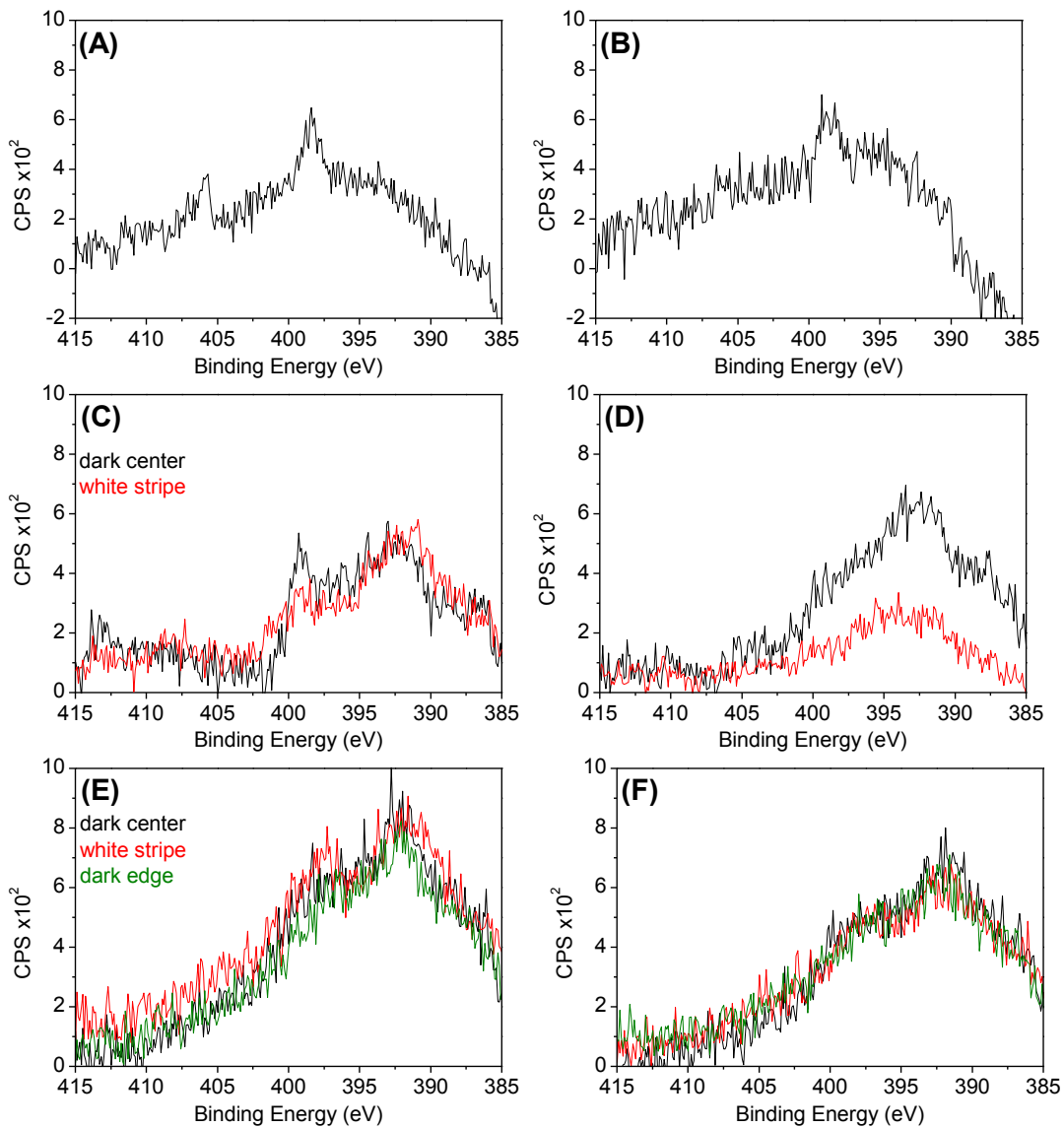


Figure F.61 XPS N 1s scans of all samples exposed at Kilauea volcano in Hawaii. 1 month (A) sheltered and (B) unsheltered, 3 month (C) sheltered and (D) unsheltered, 6 month (E) sheltered and (F) unsheltered. Black, red, and green spectra correspond to dark center, white stripe, and dark edge, respectively.

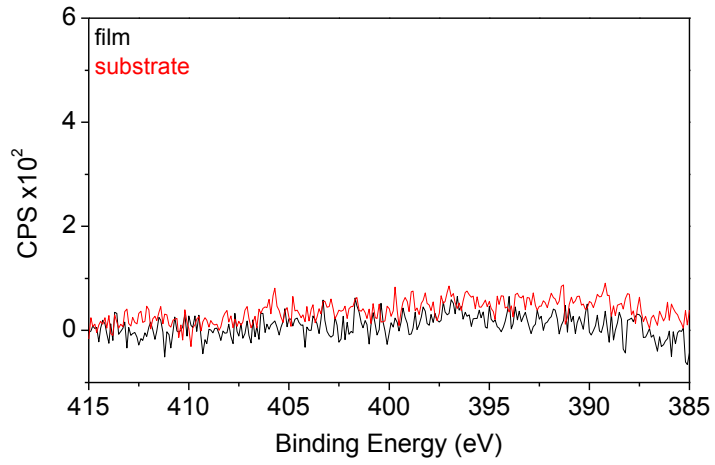


Figure F.62 XPS N 1s scans of 6 month unsheltered samples exposed at Mauna Loa in Hawaii. Black and red spectra correspond to the dark film and light substrate, respectively.

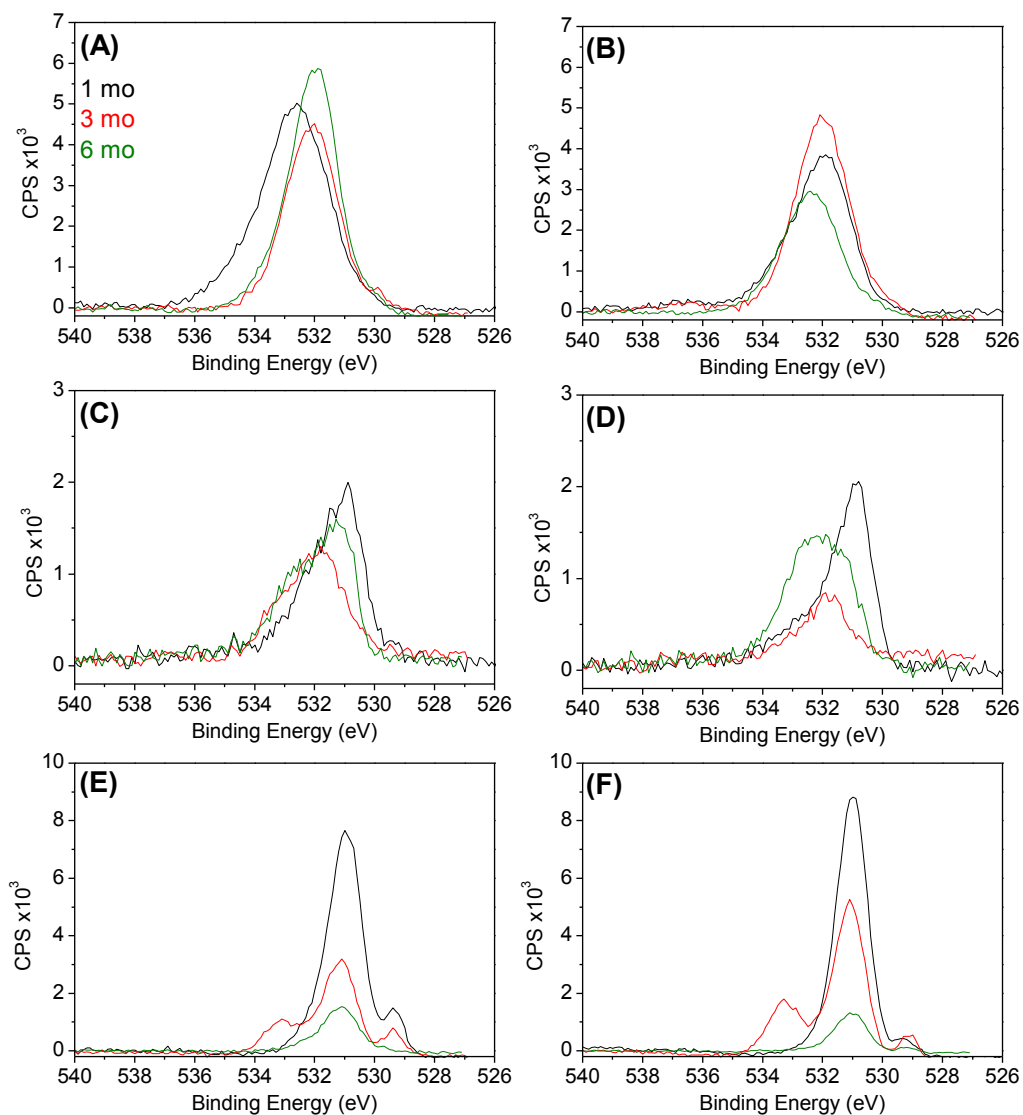


Figure F.63 XPS O 1s scans of all samples exposed in Hawaii; Kaneohe MAB (A) sheltered (B), unsheltered, Kilauea volcano (C) sheltered, (D) unsheltered, and Mauna Loa observatory (E) sheltered, (F) unsheltered. Black, red, and green spectra correspond to 1, 3, and 6 month exposures, respectively.

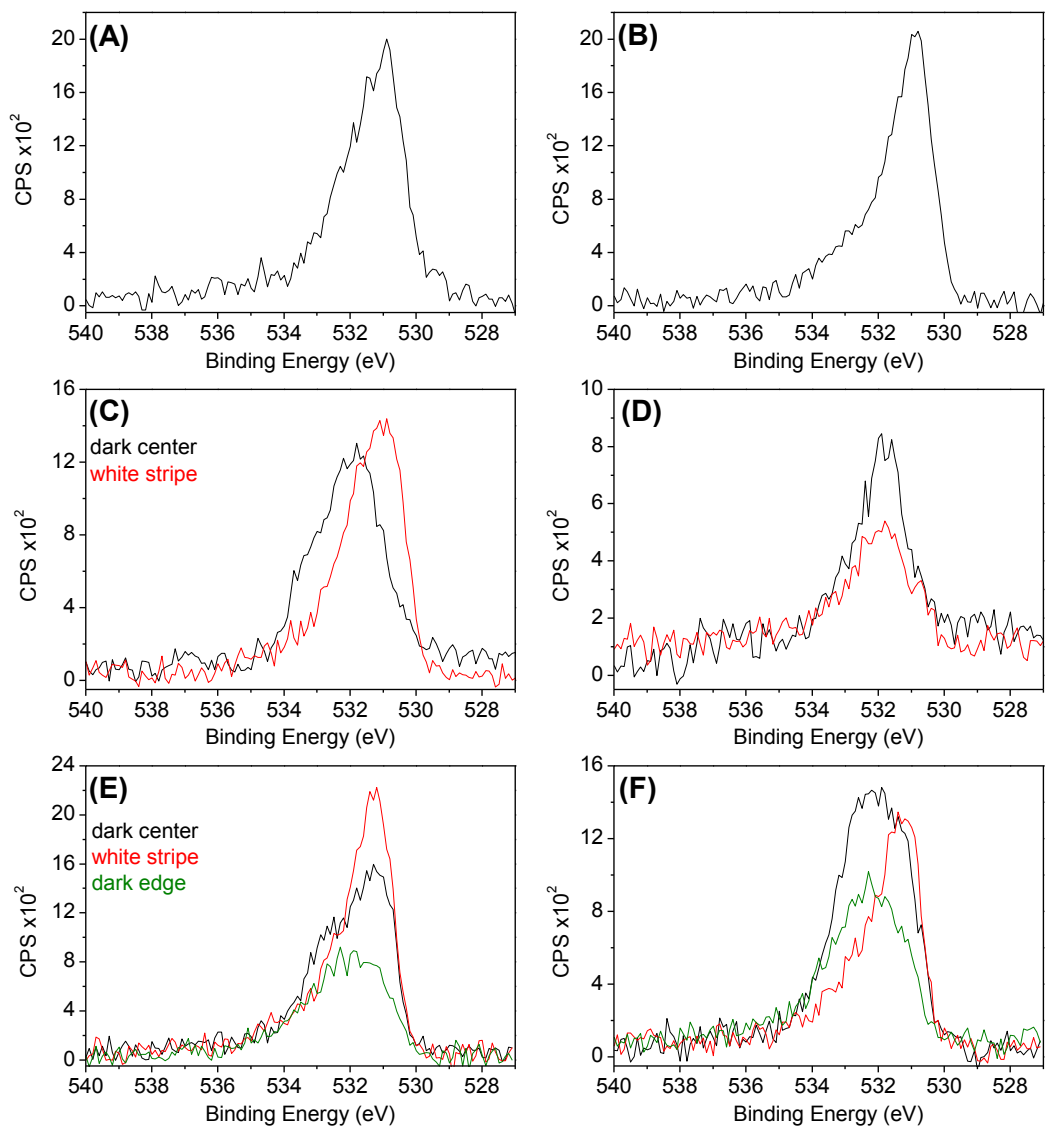


Figure F.64 XPS O 1s scans of all samples exposed at Kilauea volcano in Hawaii. 1 month (A) sheltered and (B) unsheltered, 3 month (C) sheltered and (D) unsheltered, 6 month (E) sheltered and (F) unsheltered. Black, red, and green spectra correspond to dark center, white stripe, and dark edge, respectively.

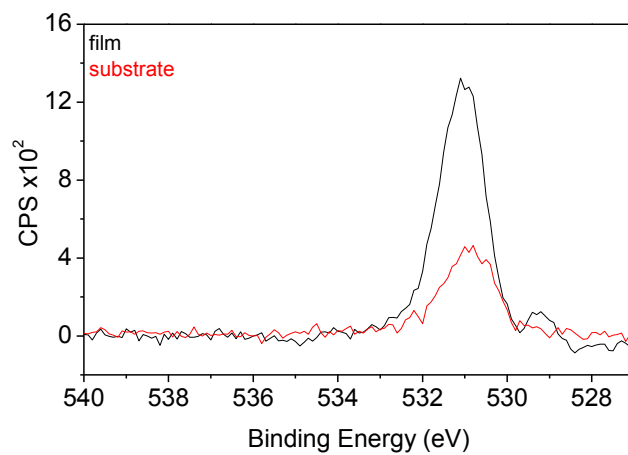


Figure F.65 XPS O 1s scans of 6 month unsheltered samples exposed at Mauna Loa in Hawaii. Black and red spectra correspond to the dark film and light substrate, respectively.

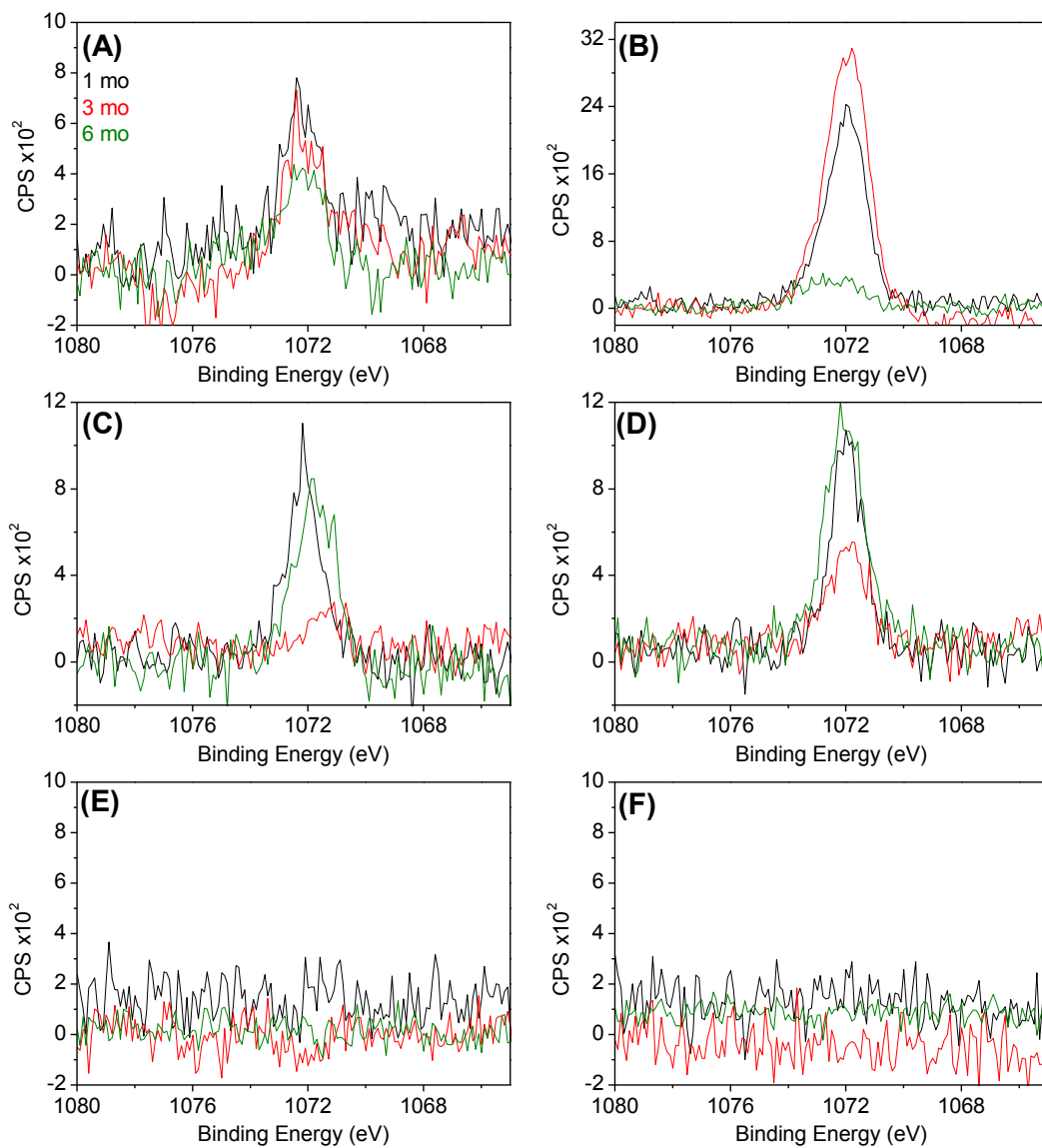


Figure F.66 XPS Na 1s scans of all samples exposed in Hawaii; Kaneohe MAB (A) sheltered (B), unsheltered, Kilauea volcano (C) sheltered, (D) unsheltered, and Mauna Loa observatory (E) sheltered, (F) unsheltered. Black, red, and green spectra correspond to 1, 3, and 6 month exposures, respectively.

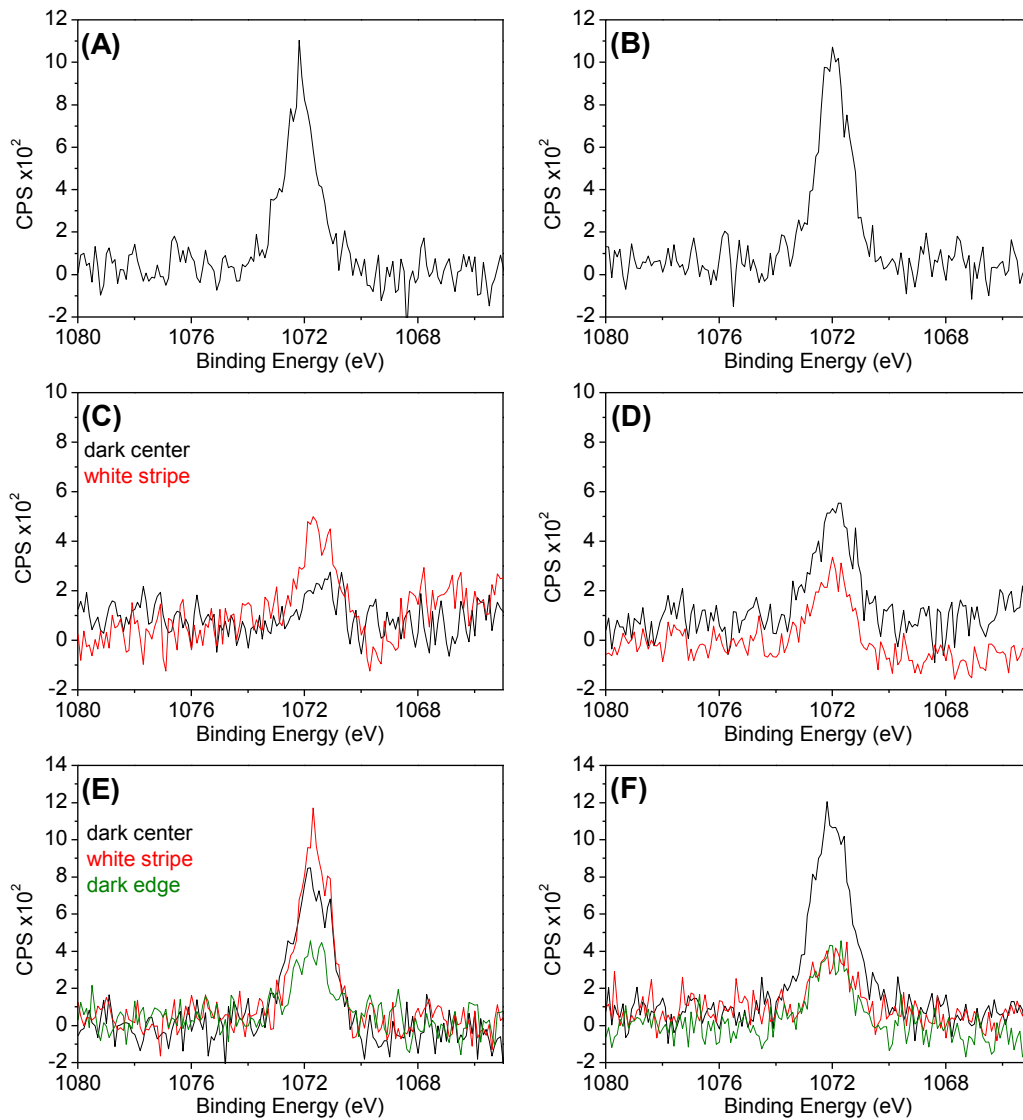


Figure F.67 XPS Na 1s scans of all samples exposed at Kilauea volcano in Hawaii. 1 month (A) sheltered and (B) unsheltered, 3 month (C) sheltered and (D) unsheltered, 6 month (E) sheltered and (F) unsheltered. Black, red, and green spectra correspond to dark center, white stripe, and dark edge, respectively.

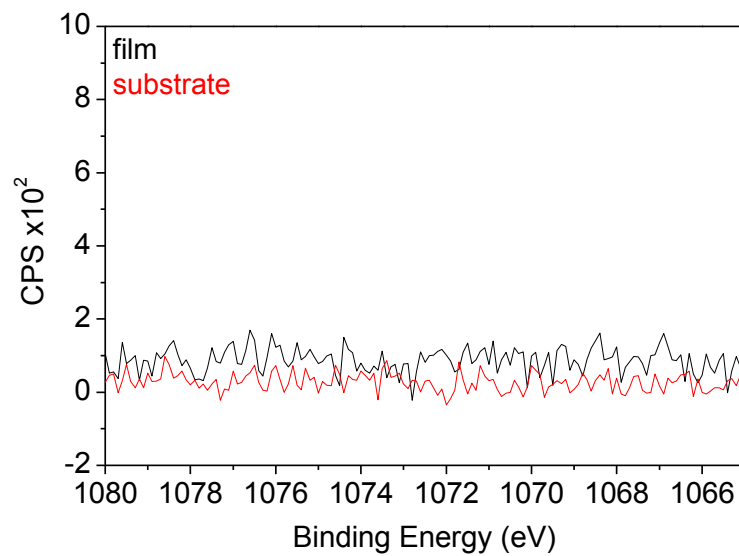


Figure F.68 XPS Na 1s scans of 6 month unsheltered samples exposed at Mauna Loa in Hawaii. Black and red spectra correspond to the dark film and light substrate, respectively.

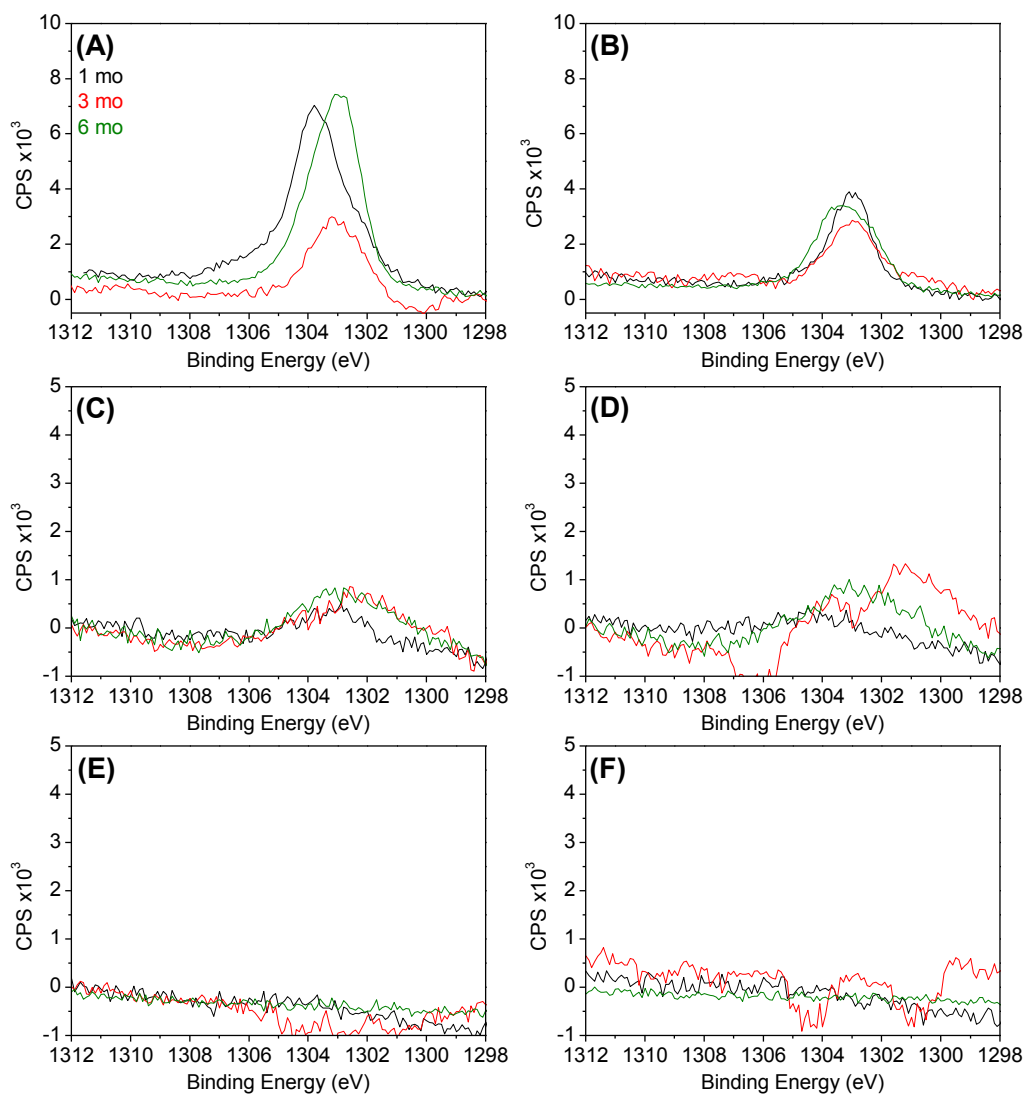


Figure F.69 XPS Mg 1s scans of all samples exposed in Hawaii; Kaneohe MAB (A) sheltered (B), unsheltered, Kilauea volcano (C) sheltered, (D) unsheltered, and Mauna Loa observatory (E) sheltered, (F) unsheltered. Black, red, and green spectra correspond to 1, 3, and 6 month exposures, respectively.

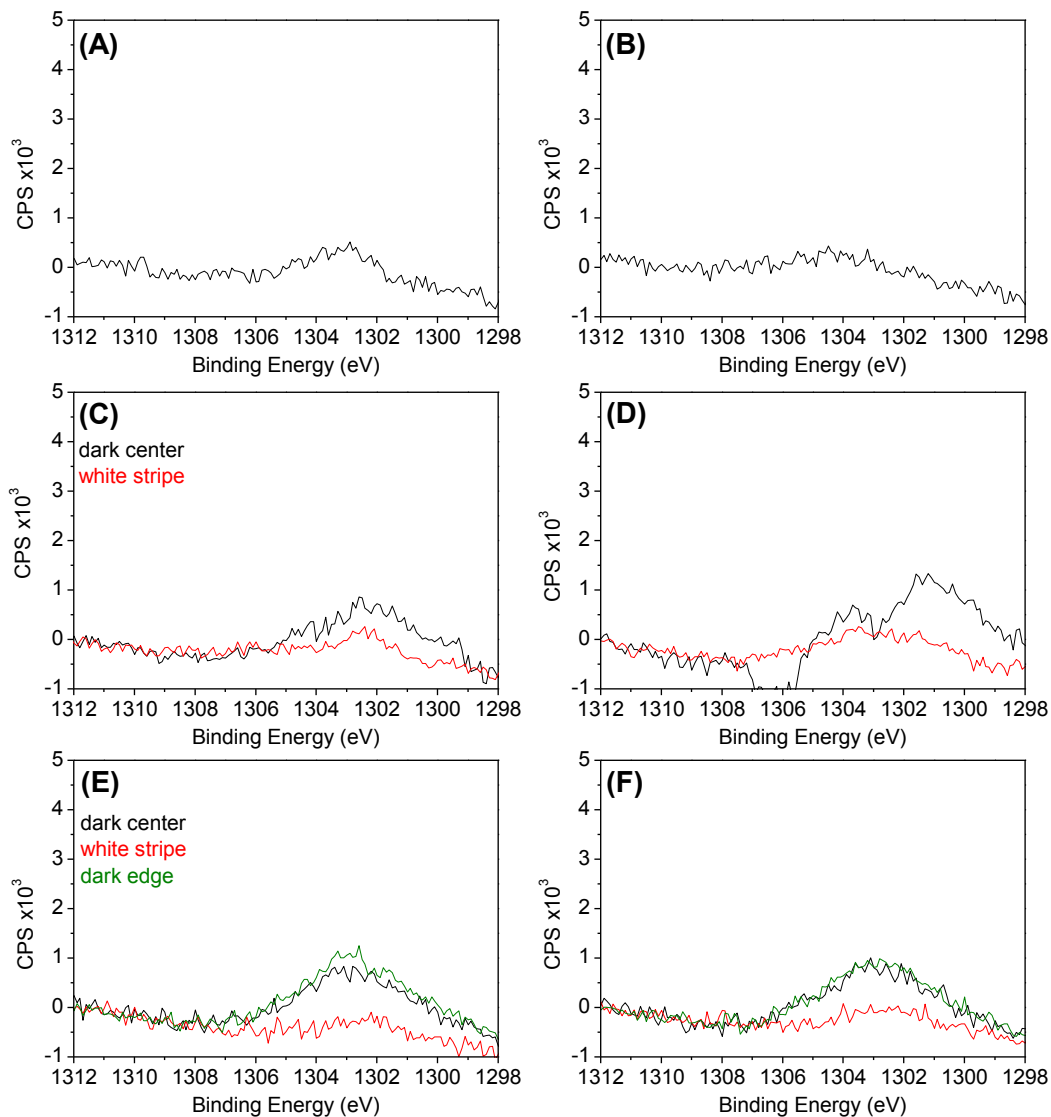


Figure F.70 XPS Mg 1s scans of all samples exposed at Kilauea volcano in Hawaii. 1 month (A) sheltered and (B) unsheltered, 3 month (C) sheltered and (D) unsheltered, 6 month (E) sheltered and (F) unsheltered. Black, red, and green spectra correspond to dark center, white stripe, and dark edge, respectively.

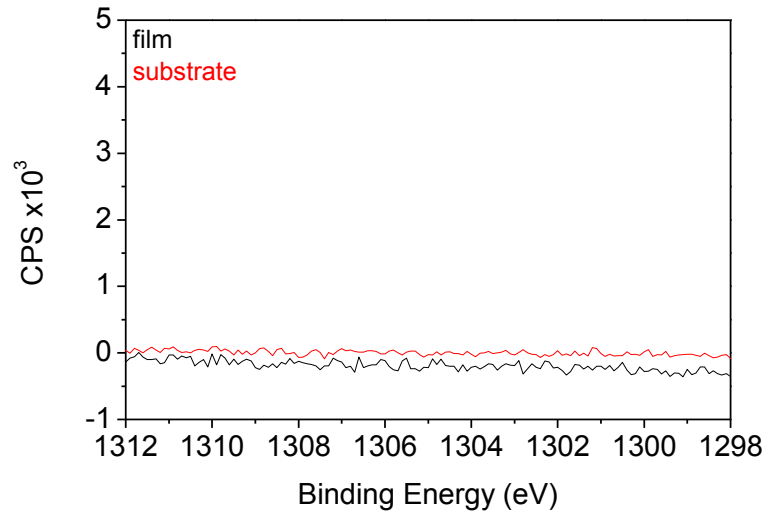


Figure F.71 XPS Mg 1s scans of 6 month unsheltered samples exposed at Mauna Loa in Hawaii. Black and red spectra correspond to the dark film and light substrate, respectively.

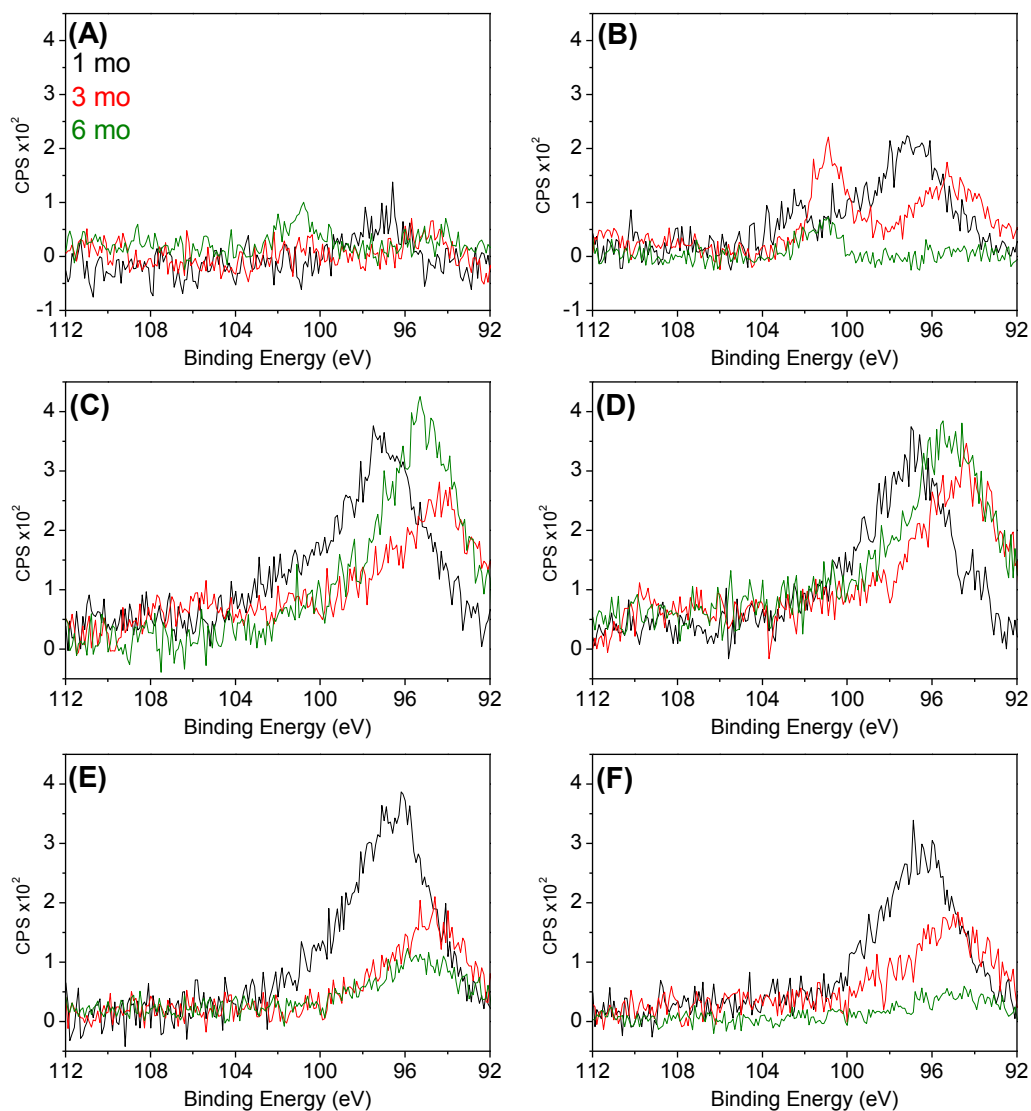


Figure F.72 XPS Si 2p scans of all samples exposed in Hawaii; Kaneohe MAB (A) sheltered (B), unsheltered, Kilauea volcano (C) sheltered, (D) unsheltered, and Mauna Loa observatory (E) sheltered, (F) unsheltered. Black, red, and green spectra correspond to 1, 3, and 6 month exposures, respectively.

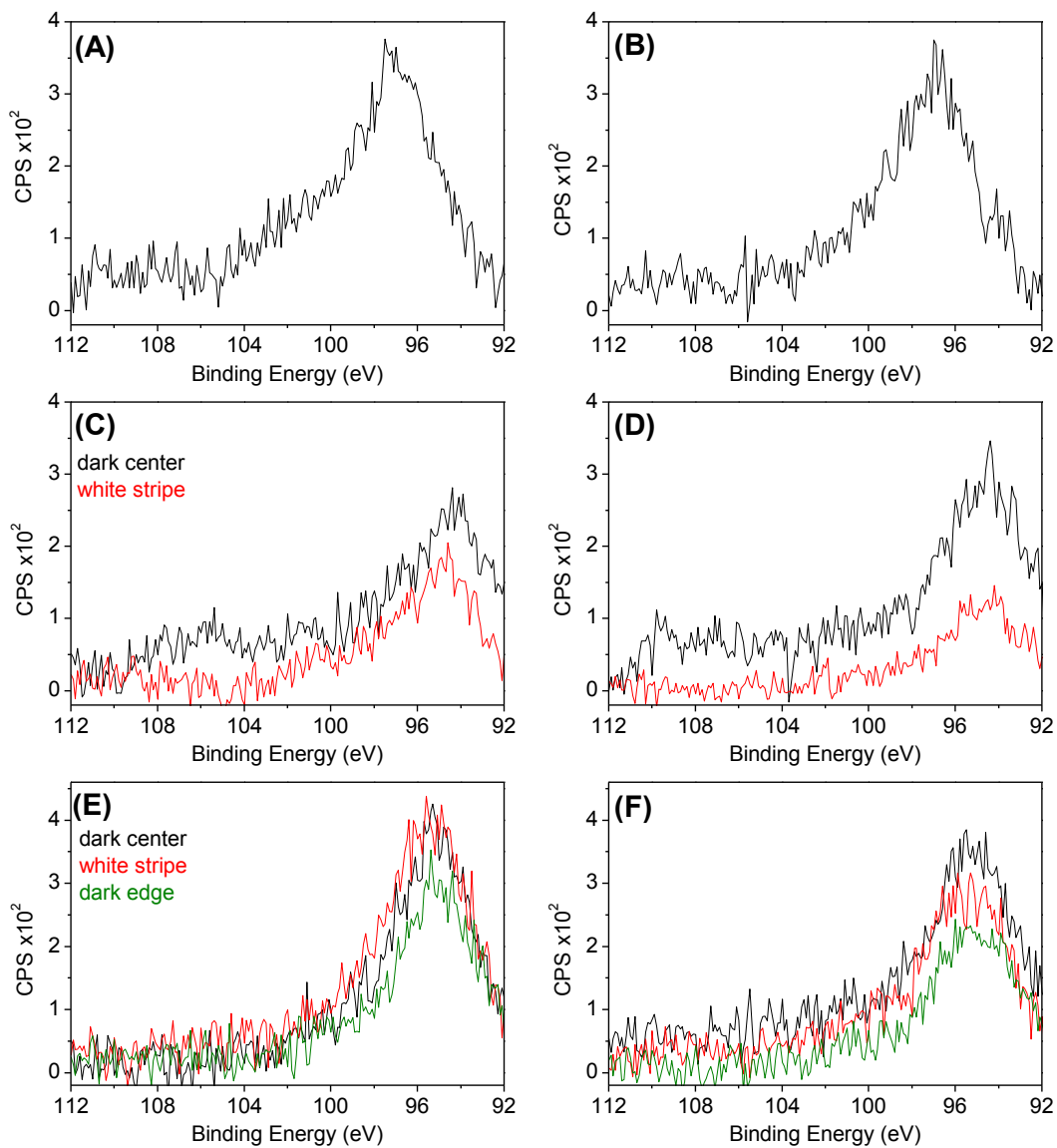


Figure F.73 XPS Si 2p scans of all samples exposed at Kilauea volcano in Hawaii. 1 month (A) sheltered and (B) unsheltered, 3 month (C) sheltered and (D) unsheltered, 6 month (E) sheltered and (F) unsheltered. Black, red, and green spectra correspond to dark center, white stripe, and dark edge, respectively.

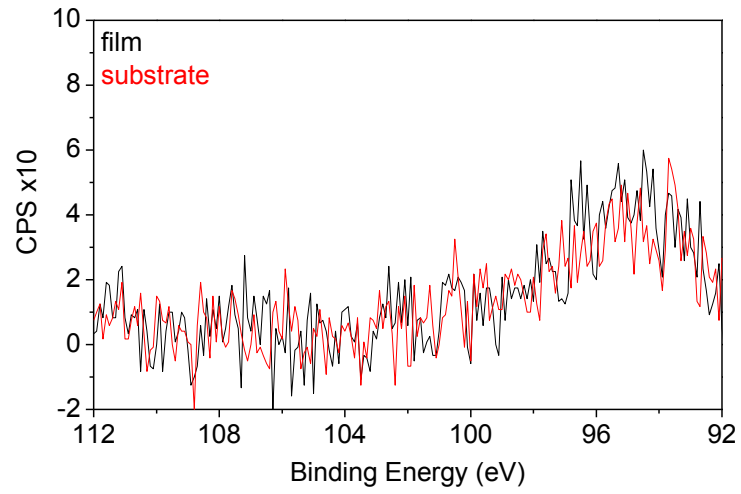


Figure F.74 XPS Si 2p scans of 6 month unsheltered samples exposed at Mauna Loa in Hawaii. Black and red spectra correspond to the dark film and light substrate, respectively.

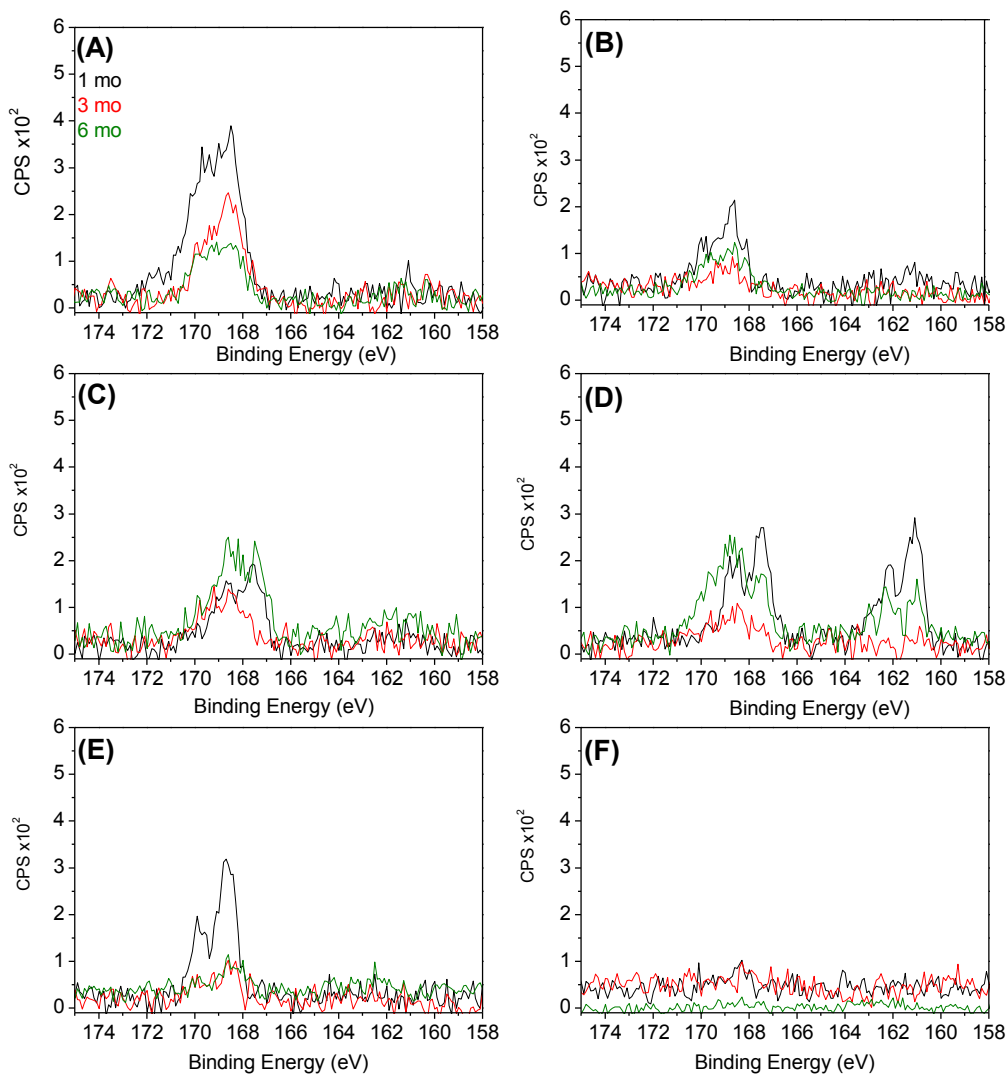


Figure F.75 XPS S 2p scans of all samples exposed in Hawaii; Kaneohe MAB (A) sheltered (B) unsheltered, Kilauea volcano (C) sheltered, (D) unsheltered, and Mauna Loa observatory (E) sheltered, (F) unsheltered. Black, red, and green spectra correspond to 1, 3, and 6 month exposures, respectively.

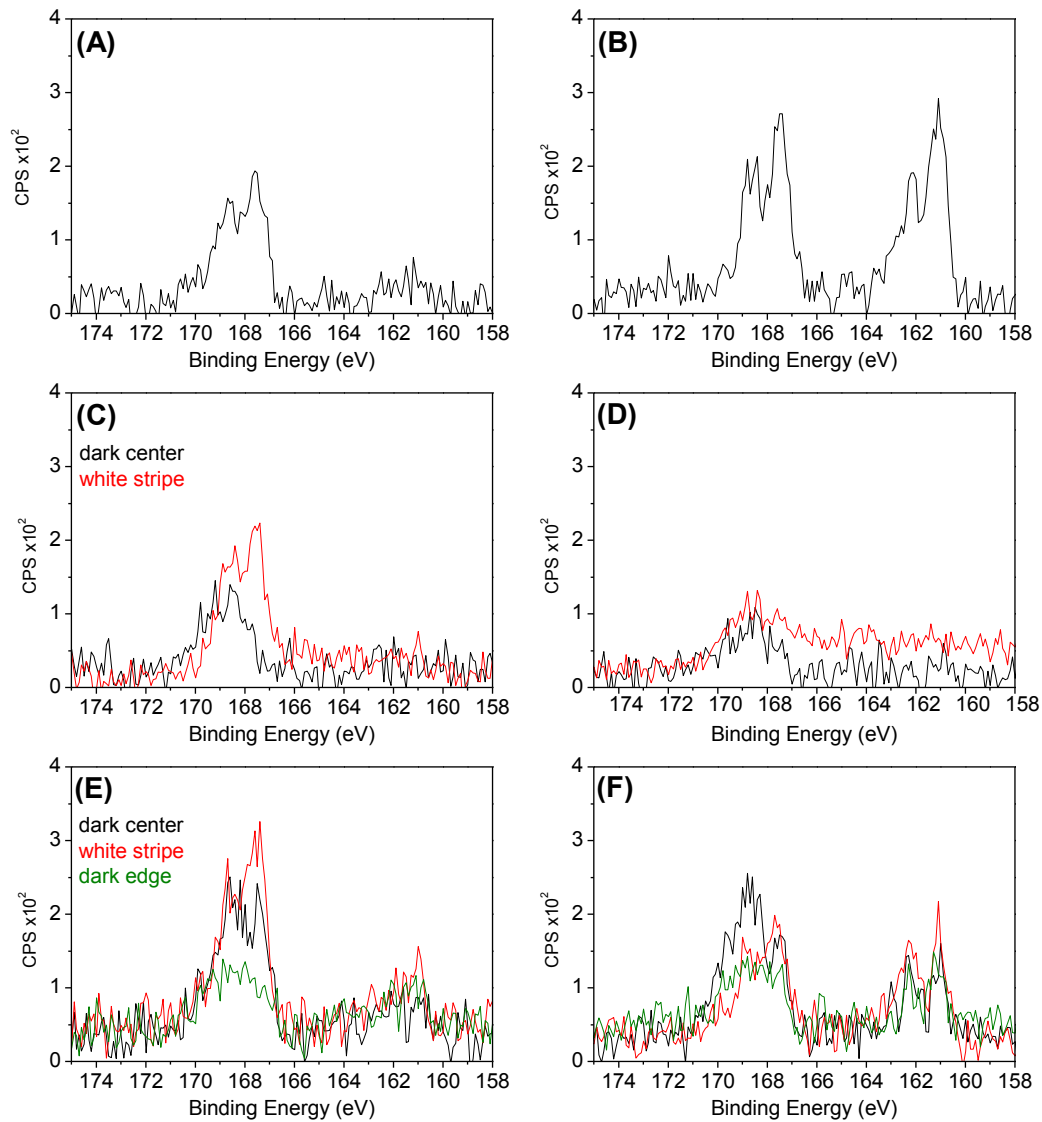


Figure F.76 XPS S 2p scans of all samples exposed at Kilauea volcano in Hawaii. 1 month (A) sheltered and (B) unsheltered, 3 month (C) sheltered and (D) unsheltered, 6 month (E) sheltered and (F) unsheltered. Black, red, and green spectra correspond to dark center, white stripe, and dark edge, respectively.

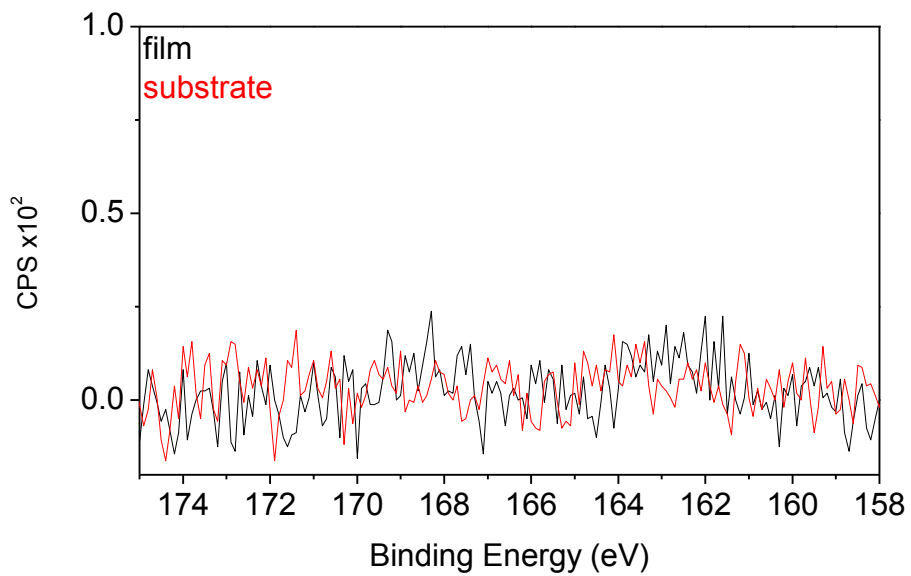


Figure F.77 XPS S 2p scans of 6 month unsheltered samples exposed at Mauna Loa in Hawaii. Black and red spectra correspond to the dark film and light substrate, respectively.

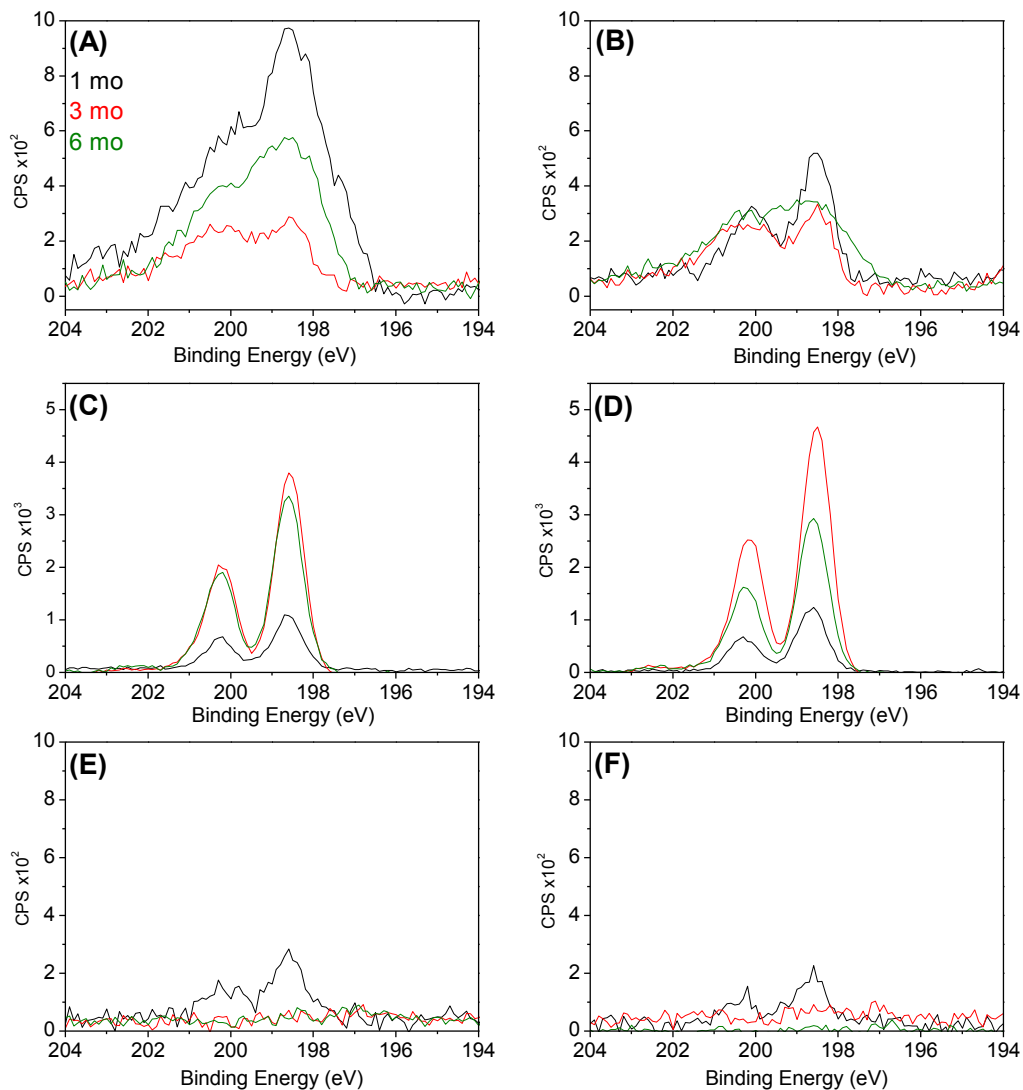


Figure F.78 XPS Cl 2p scans of all samples exposed in Hawaii; Kaneohe MAB (A) sheltered (B), unsheltered, Kilauea volcano (C) sheltered, (D) unsheltered, and Mauna Loa observatory (E) sheltered, (F) unsheltered. Black, red, and green spectra correspond to 1, 3, and 6 month exposures, respectively.

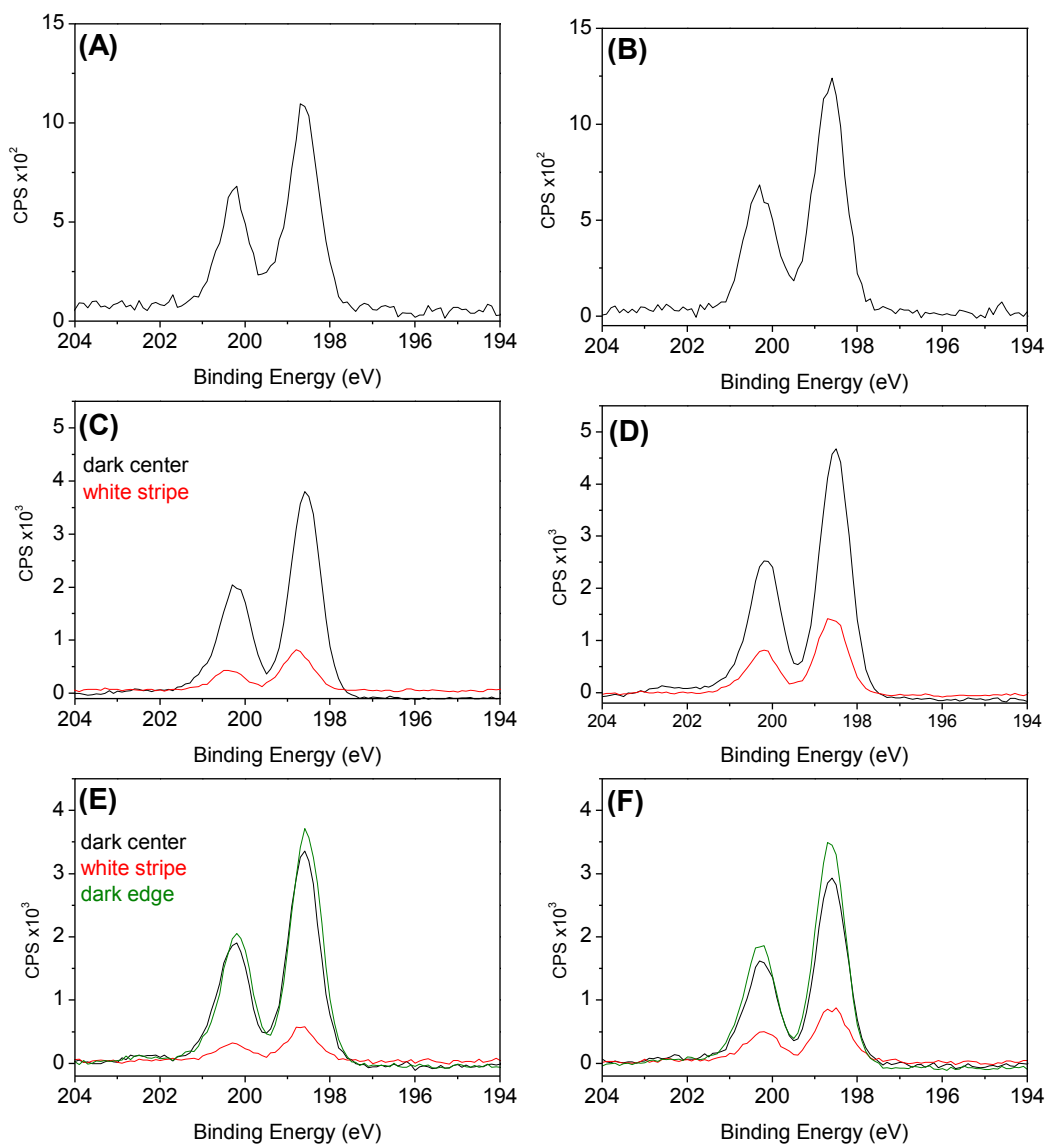


Figure F.79 XPS Cl 2p scans of all samples exposed at Kilauea volcano in Hawaii. 1 month (A) sheltered and (B) unsheltered, 3 month (C) sheltered and (D) unsheltered, 6 month (E) sheltered and (F) unsheltered. Black, red, and green spectra correspond to dark center, white stripe, and dark edge, respectively.

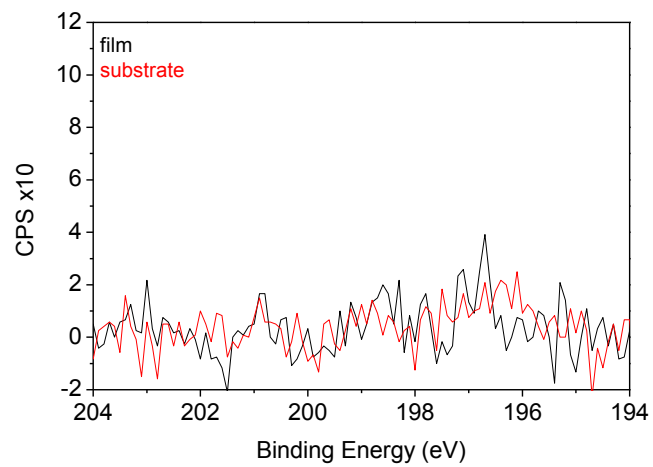


Figure F.80 XPS Cl 2p scans of 6 month unsheltered samples exposed at Mauna Loa in Hawaii. Black and red spectra correspond to the dark film and light substrate, respectively.

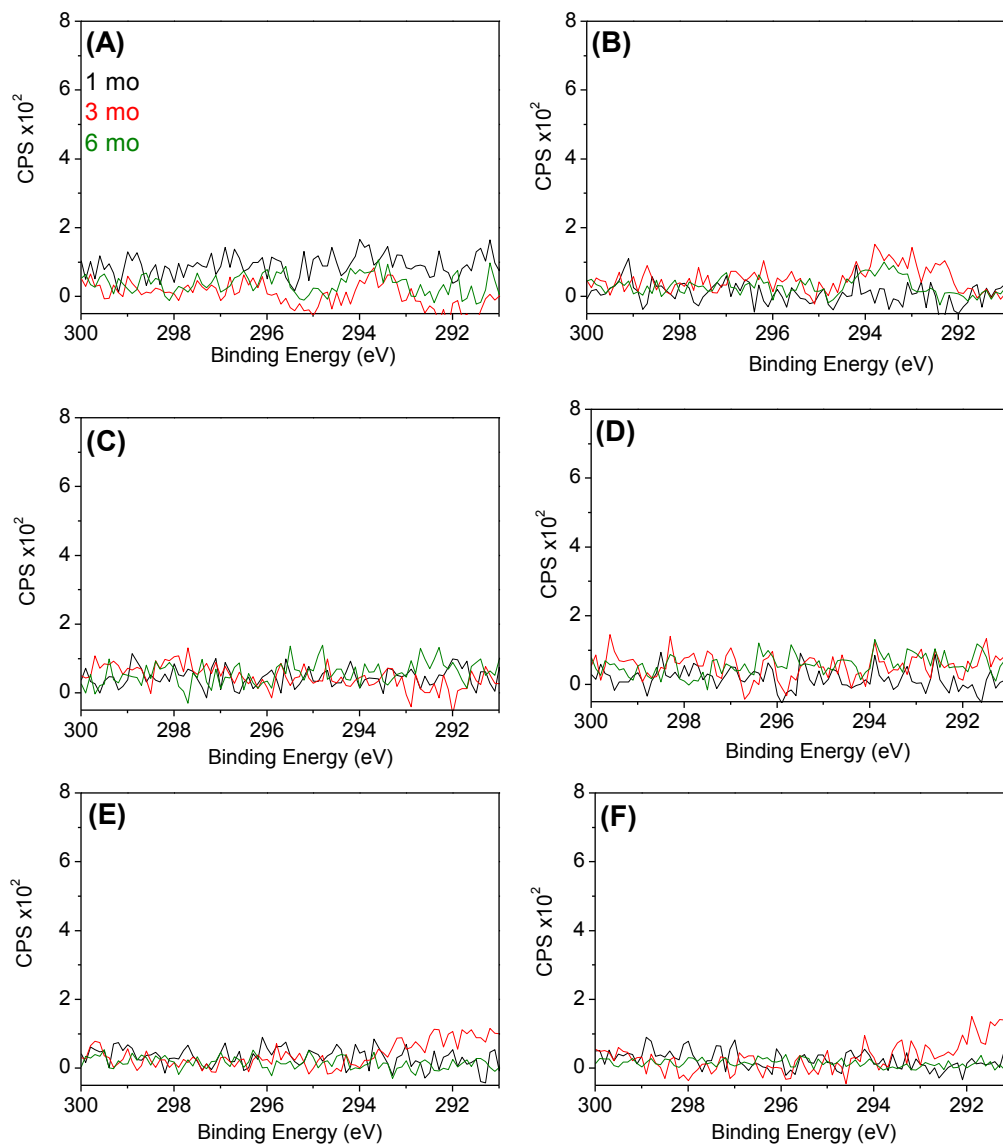


Figure F.81 XPS K 2p scans of all samples exposed in Hawaii; Kaneohe MAB (A) sheltered (B), unsheltered, Kilauea volcano (C) sheltered, (D) unsheltered, and Mauna Loa observatory (E) sheltered, (F) unsheltered. Black, red, and green spectra correspond to 1, 3, and 6 month exposures, respectively.

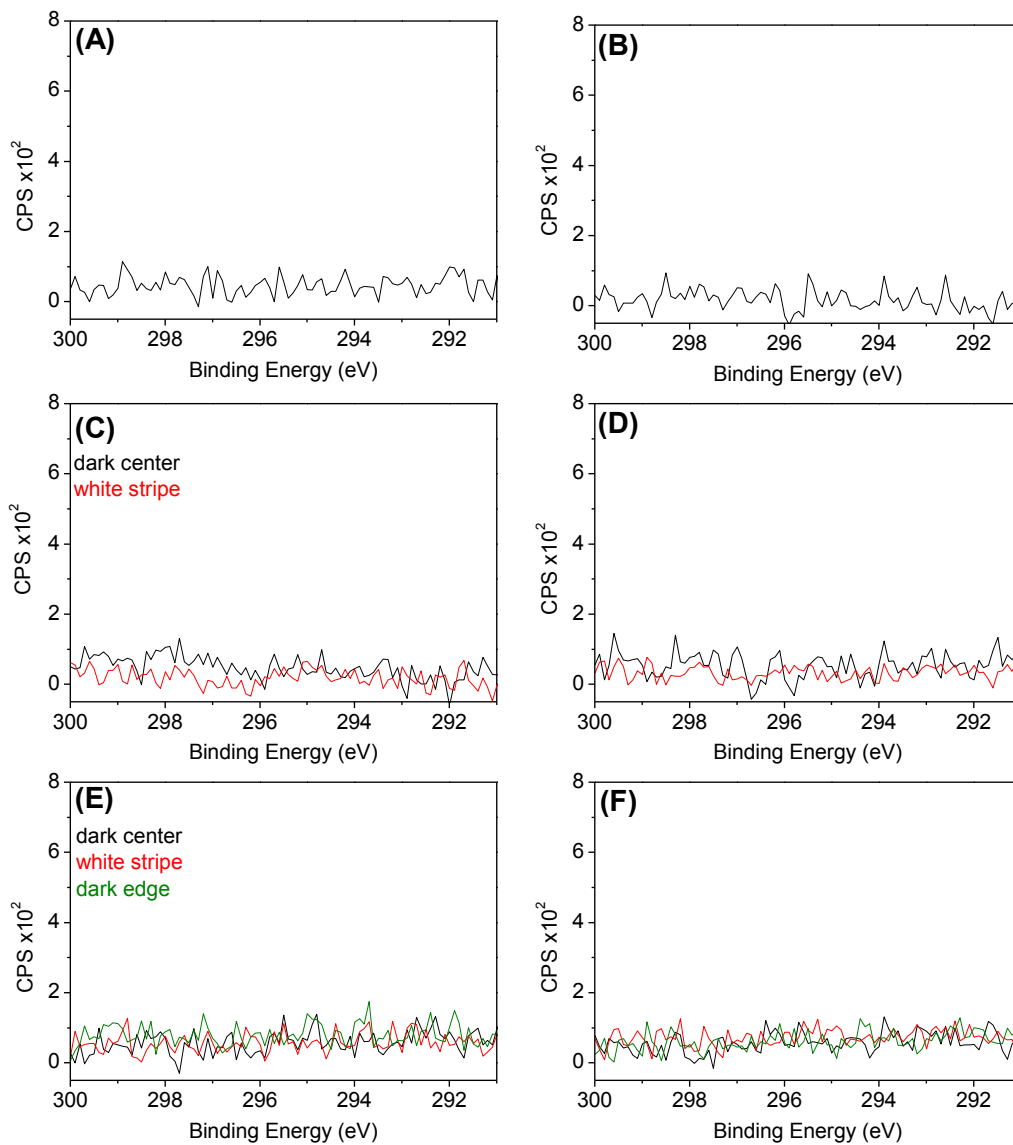


Figure F.82 XPS K 2p scans of all samples exposed at Kilauea volcano in Hawaii. 1 month (A) sheltered and (B) unsheltered, 3 month (C) sheltered and (D) unsheltered, 6 month (E) sheltered and (F) unsheltered. Black, red, and green spectra correspond to dark center, white stripe, and dark edge, respectively.

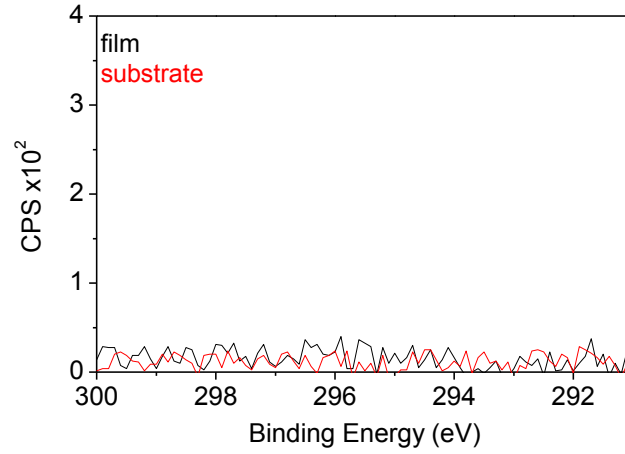


Figure F.83 XPS K 2p scans of 6 month unsheltered samples exposed at Mauna Loa in Hawaii. Black and red spectra correspond to the dark film and light substrate, respectively.

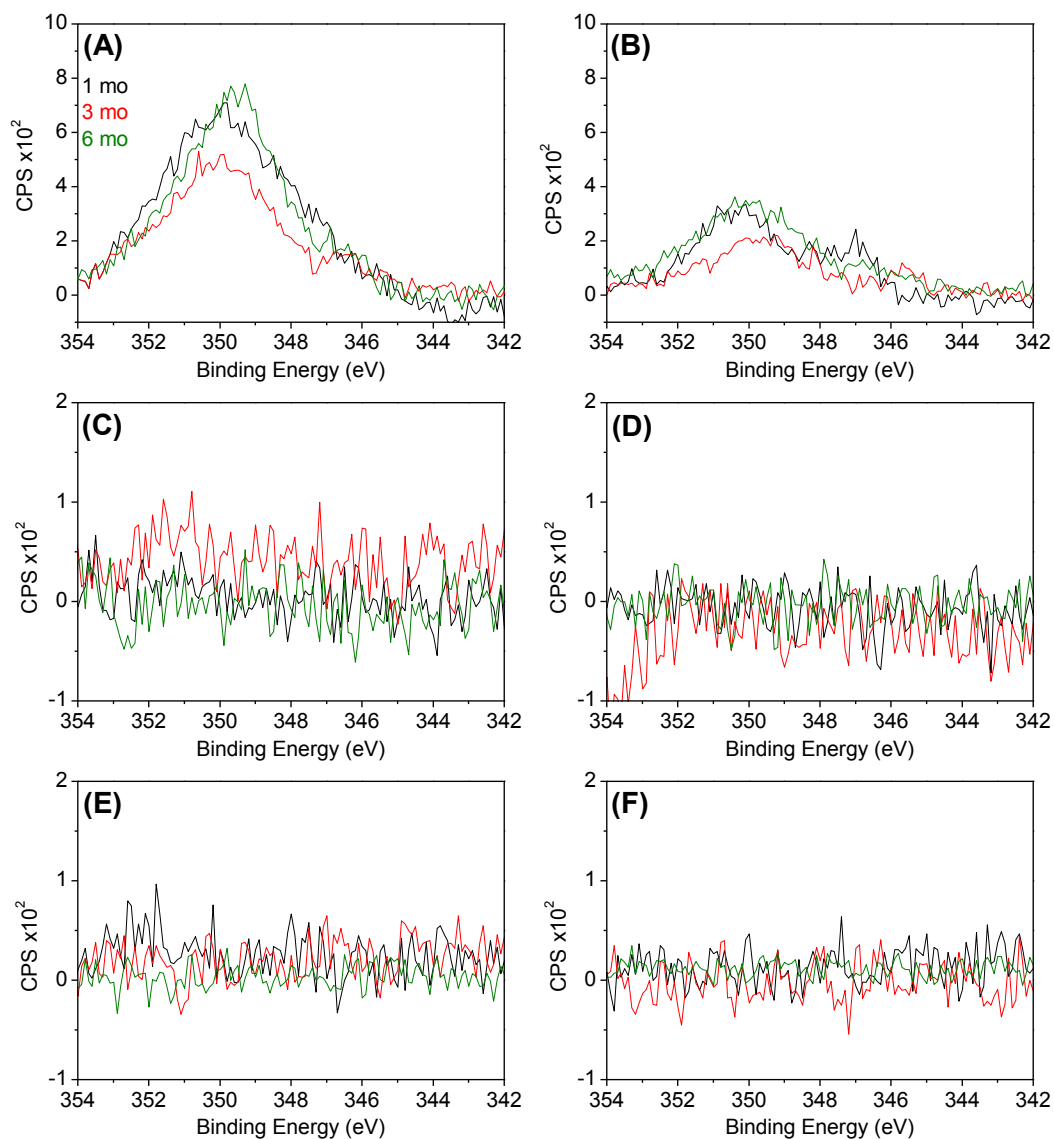


Figure F.84 XPS Ca 2p scans of all samples exposed in Hawaii; Kaneohe MAB (A) sheltered (B) unsheltered, Kilauea volcano (C) sheltered, (D) unsheltered, and Mauna Loa observatory (E) sheltered, (F) unsheltered. Black, red, and green spectra correspond to 1, 3, and 6 month exposures, respectively.

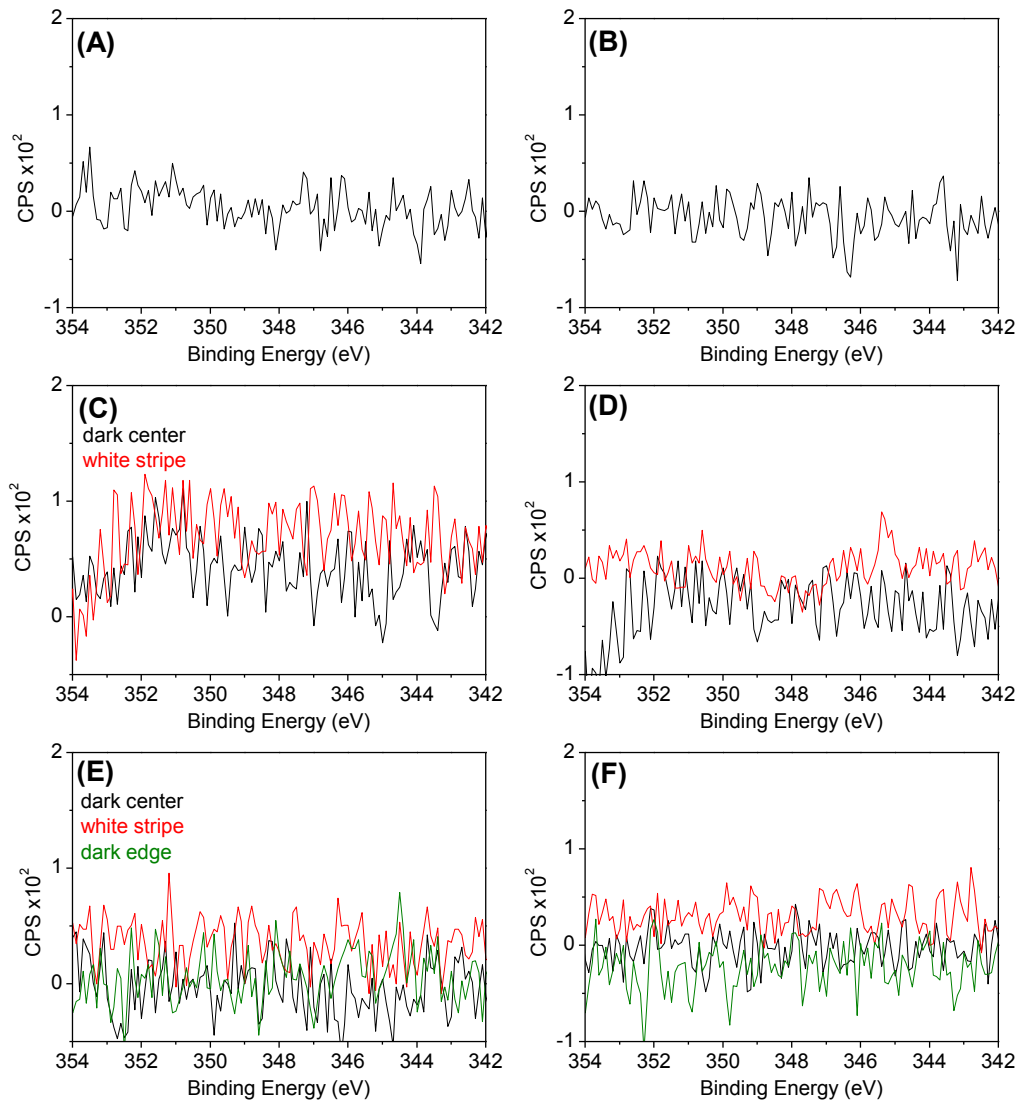


Figure F.85 XPS Ca 2p scans of all samples exposed at Kilauea volcano in Hawaii. 1 month (A) sheltered and (B) unsheltered, 3 month (C) sheltered and (D) unsheltered, 6 month (E) sheltered and (F) unsheltered. Black, red, and green spectra correspond to dark center, white stripe, and dark edge, respectively.

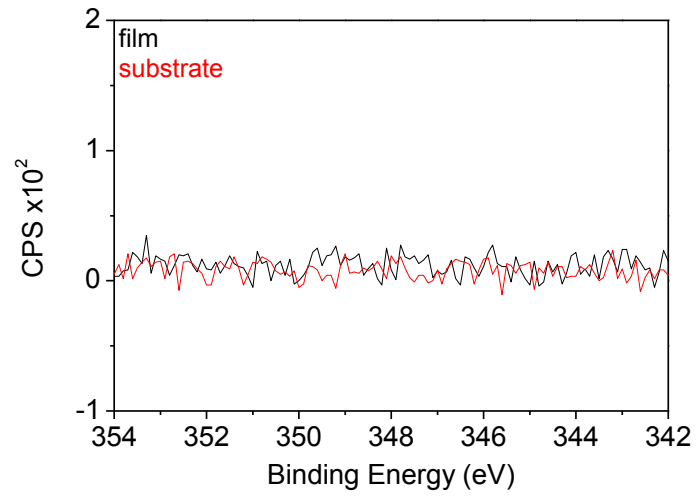


Figure F.86 XPS Ca 2p scans of 6 month unsheltered samples exposed at Mauna Loa in Hawaii. Black and red spectra correspond to the dark film and light substrate, respectively.

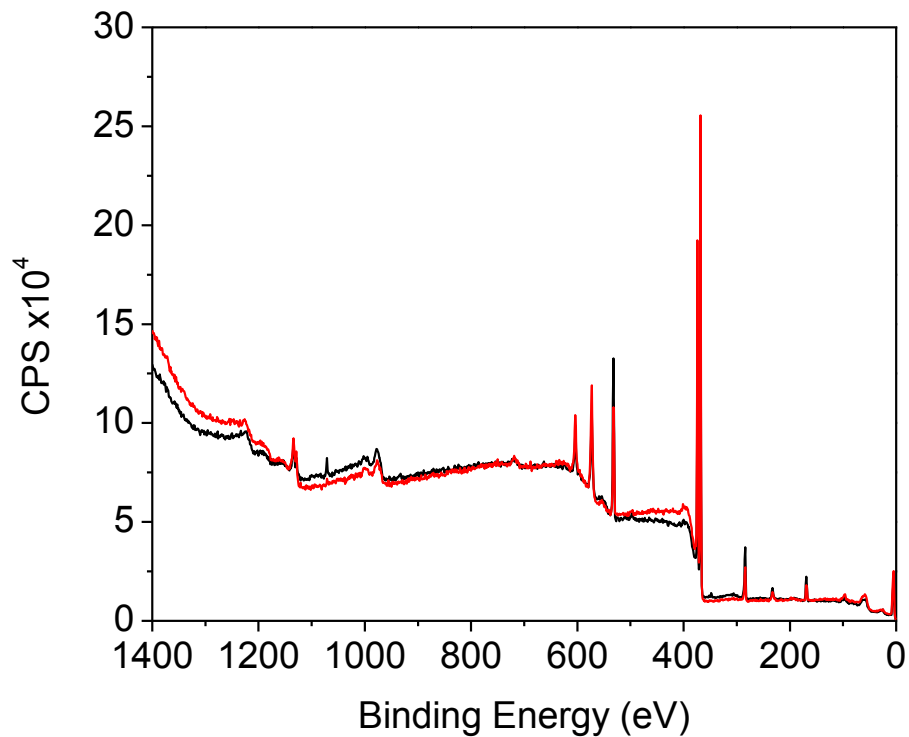


Figure F. 87 XPS survey scans of lab generated samples. The black trace was polarized in H_2SO_4 at $0.7 V_{\text{MSE}}$, the red trace was galvanostatically oxidized in H_2SO_4 at 0.025 mA/cm^2 .

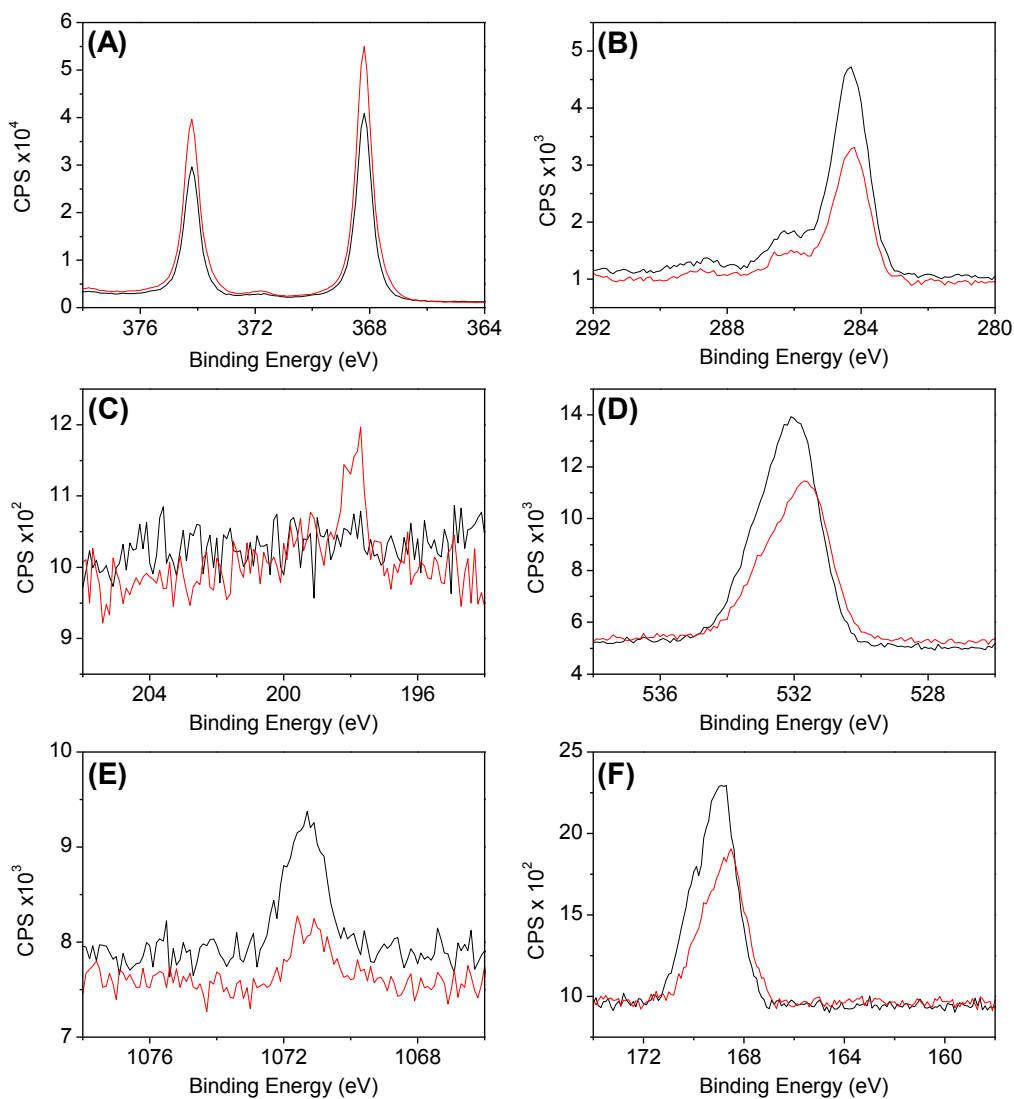


Figure F.88 XPS scans of lab generated samples. (A) Ag 3d, (B) C 1s, (C) Cl 2p, (D) O 1s, (E) Na 1s, (F) S 2p. The black trace was polarized in H₂SO₄ at 0.7 V_{MSE}, the red trace was galvanostatically oxidized in H₂SO₄ at 0.025 mA/cm².

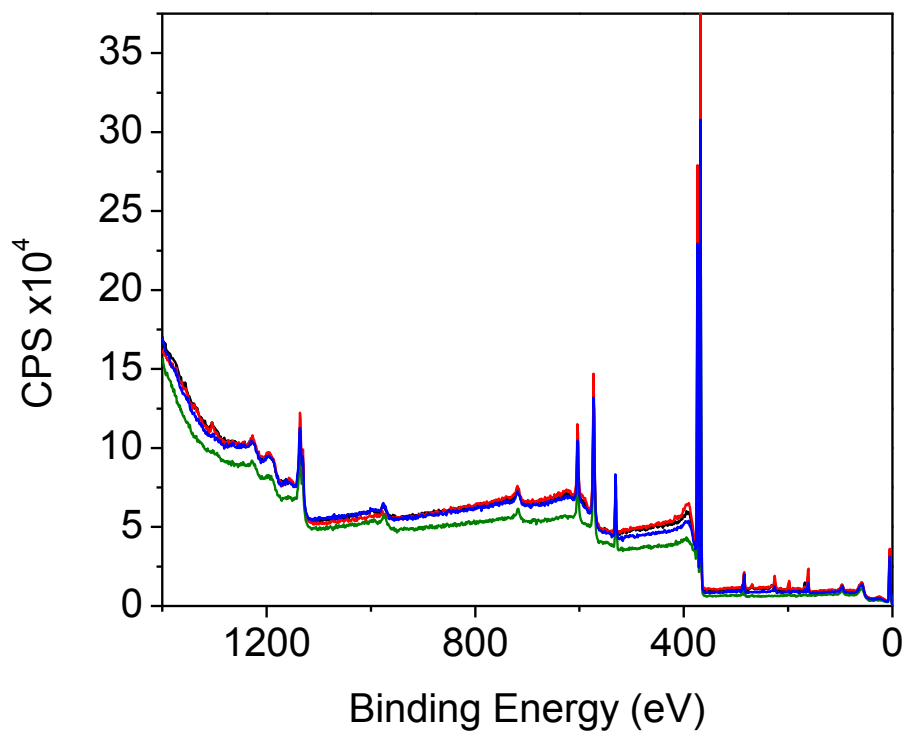


Figure F.89 XPS survey scans of lab created samples. The black trace had Ag₂S deposited for 1 sec, exposed in 0% RH, with 0.63 ppm O₃, for 38 hr; the red trace had Ag₂S deposited for 1 sec, exposed in 90% RH, with 0.63 ppm O₃, for 22 hr; the green trace had Ag₂S deposited for 15 sec, exposed in 90% RH, with 5.5 ppm O₃, for 68 hr; the blue trace had no Ag₂S, exposed in 90% RH, with 5.5 ppm O₃, for 68 hr.

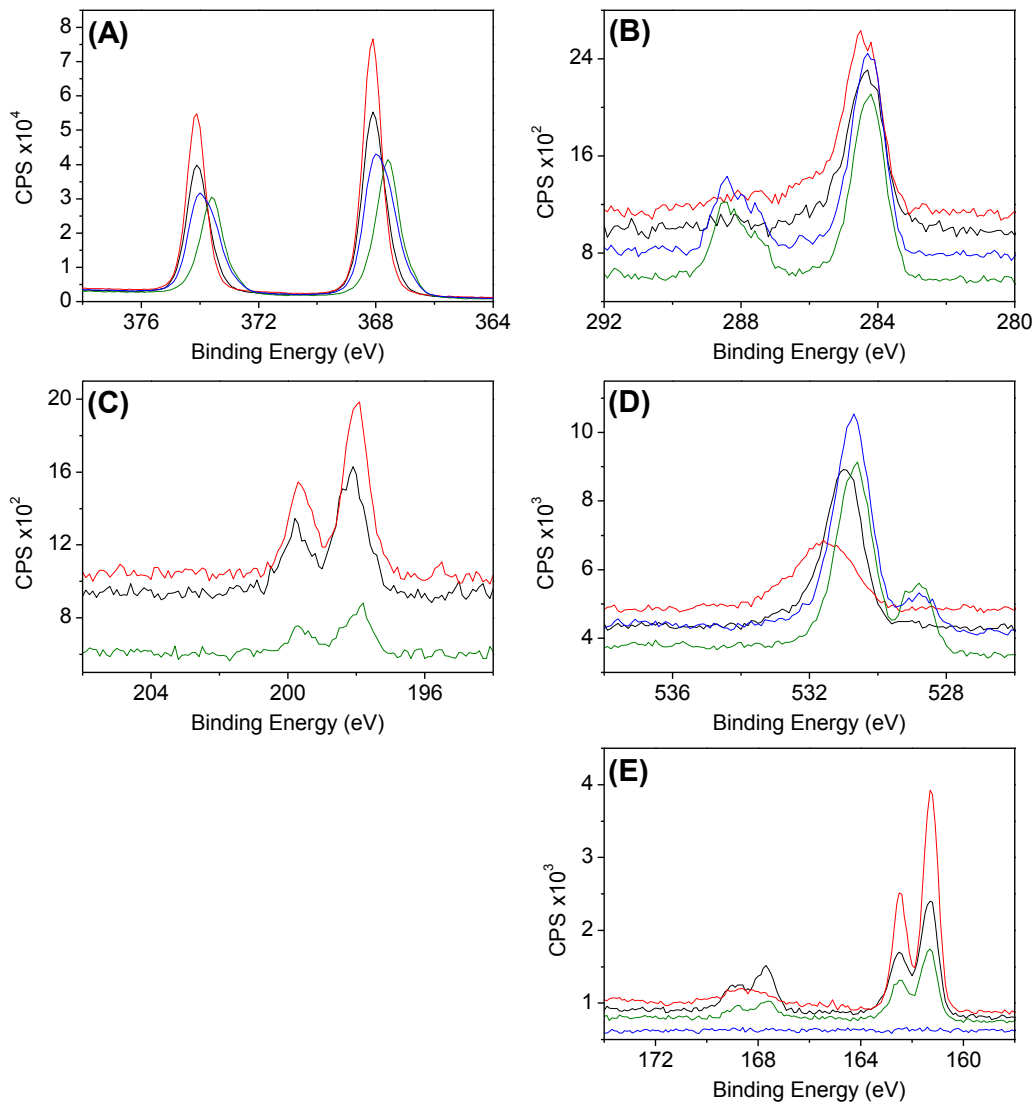


Figure F.90 XPS scans of lab generated samples. (A) Ag 3d, (B) C 1s, (C) Cl 2p, (D) O 1s, (E) S 2p. The black trace had Ag₂S deposited for 1 sec, exposed in 0% RH, with 0.63 ppm O₃, for 38 hr; the red trace had Ag₂S deposited for 1 sec, exposed in 90% RH, with 0.63 ppm O₃, for 22 hr; the green trace had Ag₂S deposited for 15 sec, exposed in 90% RH, with 5.5 ppm O₃, for 68 hr; the blue trace had no Ag₂S, exposed in 90% RH, with 5.5 ppm O₃, for 68 hr.

Appendix G: AIRMAP Data

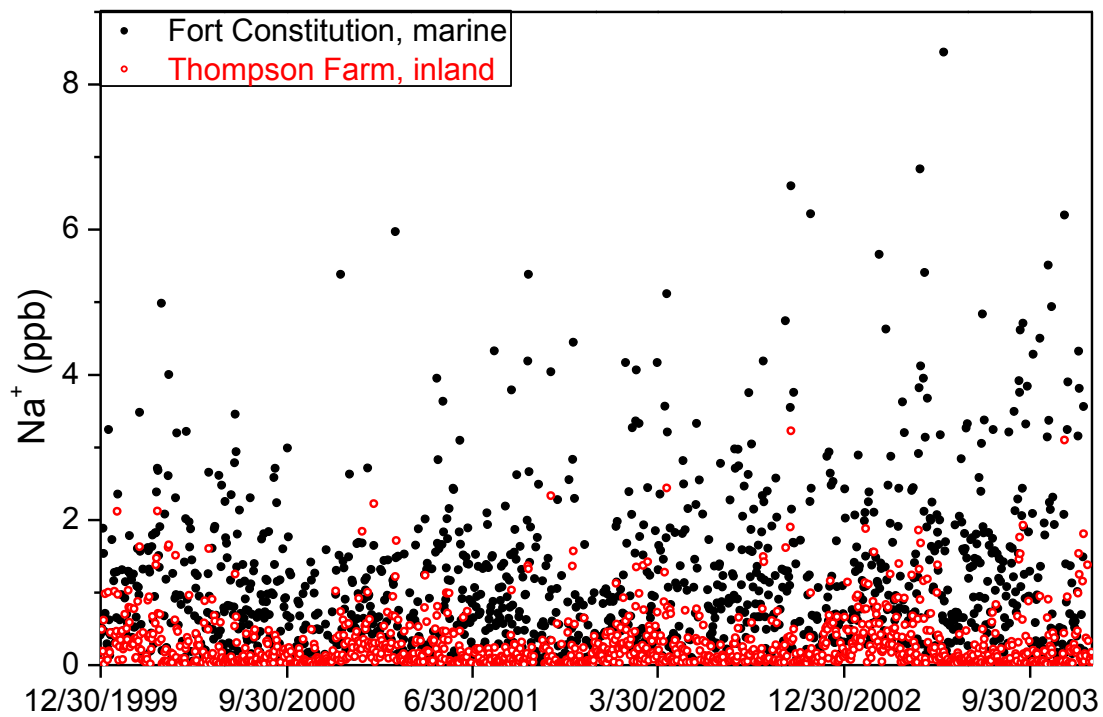


Figure G.1 AIRMAP Na^+ data from Fort Constitution & Thompson Farm.^{170,174} The solid black circles are data from Fort Constitution and the open red circles are the data from Thompson Farm. Samples were taken every 24 hours.

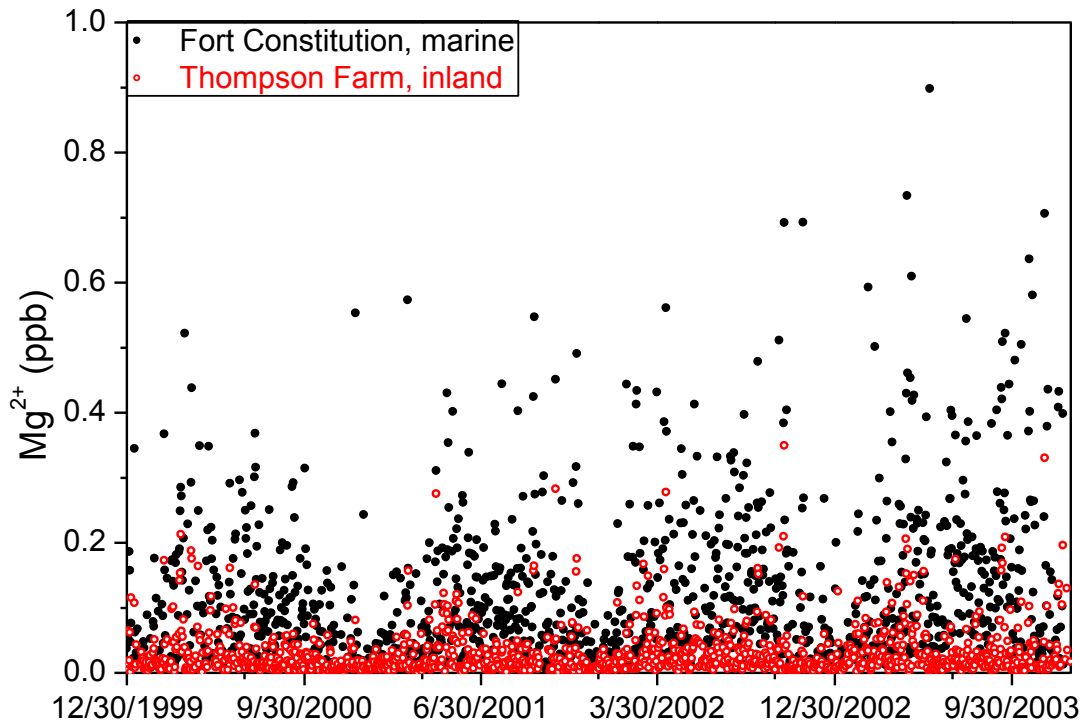


Figure G.2 AIRMAP Mg^{2+} data from Fort Constitution & Thompson Farm.^{170,174} The solid black circles are data from Fort Constitution and the open red circles are the data from Thompson Farm. Samples were taken every 24 hours.

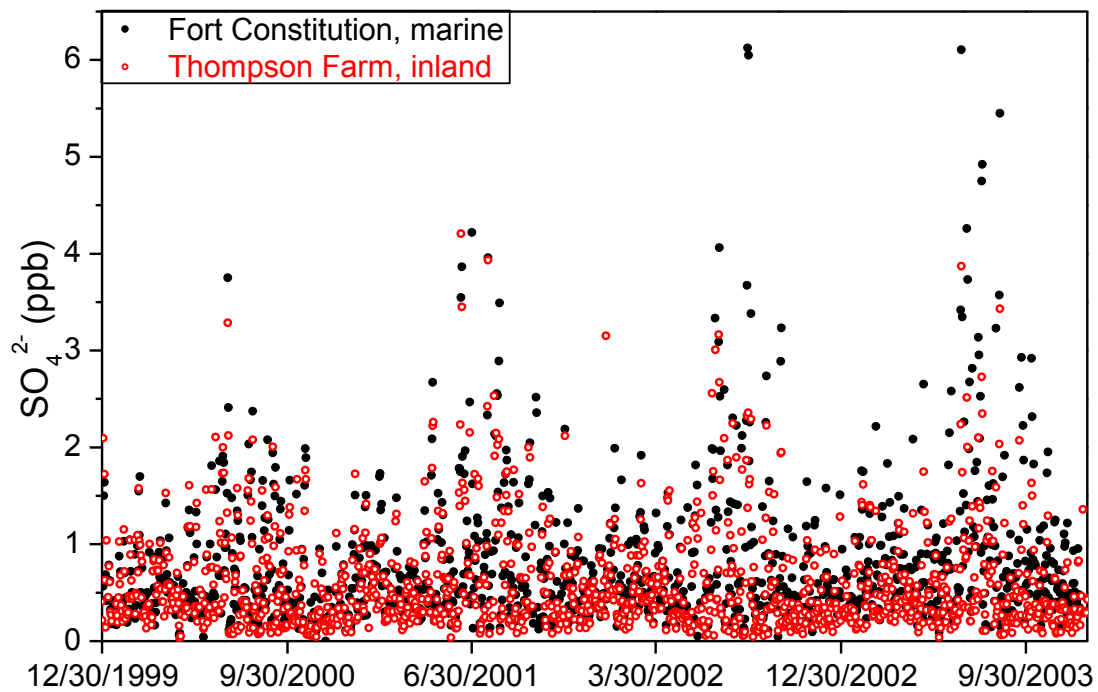


Figure G.3 AIRMAP SO_4^{2-} data from Fort Constitution & Thompson Farm.^{170,174} The solid black circles are data from Fort Constitution and the open red circles are the data from Thompson Farm. Samples were taken every 24 hours.

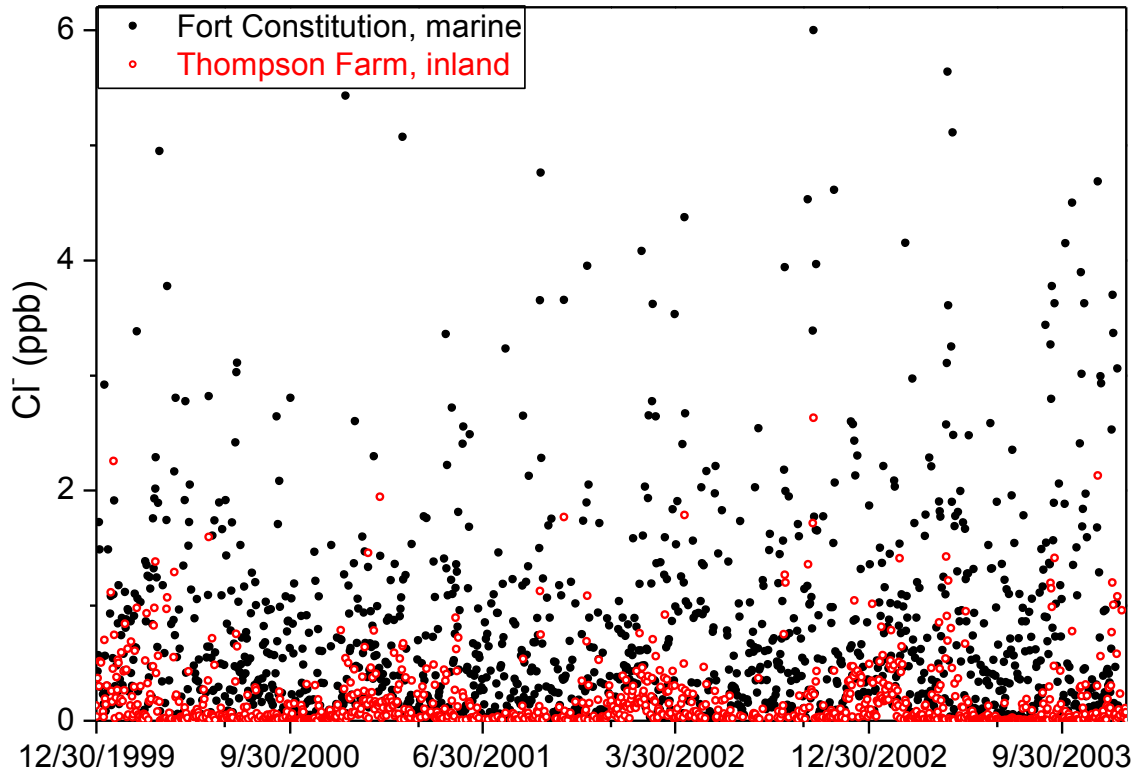


Figure G.4 AIRMAP Cl⁻ data from Fort Constitution & Thompson Farm.^{170,174} The solid black circles are data from Fort Constitution and the open red circles are the data from Thompson Farm. Samples were taken every 24 hours. One data point from FC at 8.8 ppb is not shown.

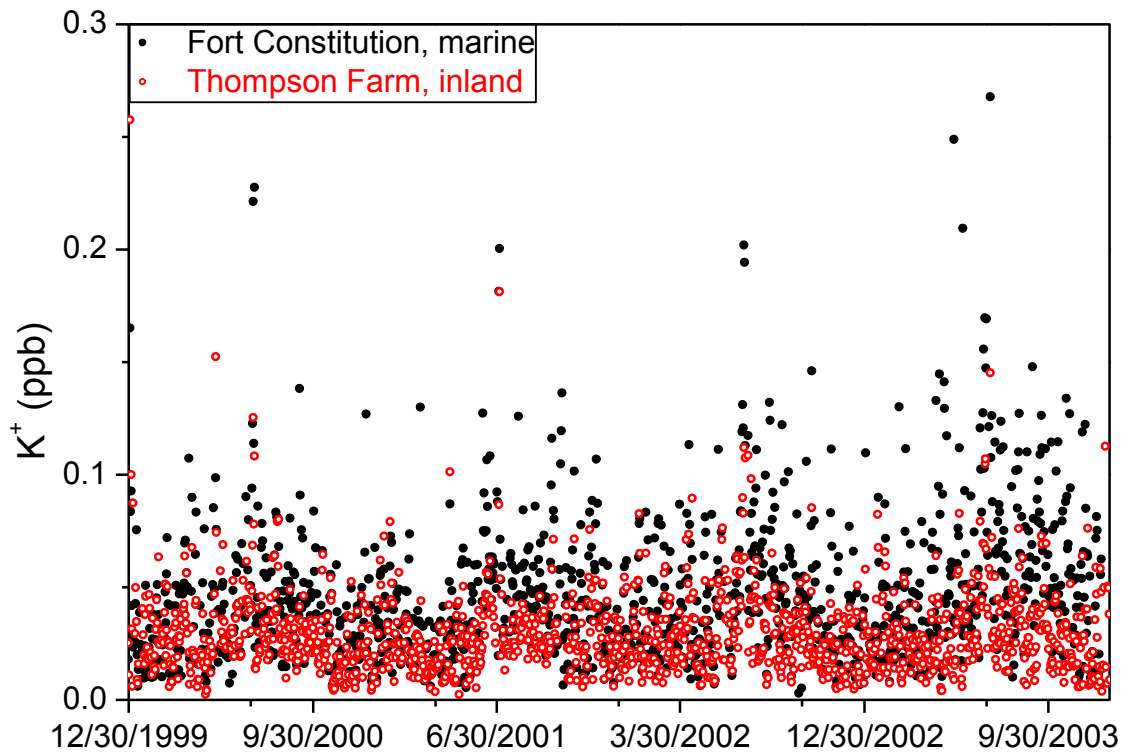


Figure G.5 AIRMAP K^+ data from Fort Constitution & Thompson Farm.^{170,174} The solid black circles are data from Fort Constitution and the open red circles are the data from Thompson Farm. Samples were taken every 24 hours.

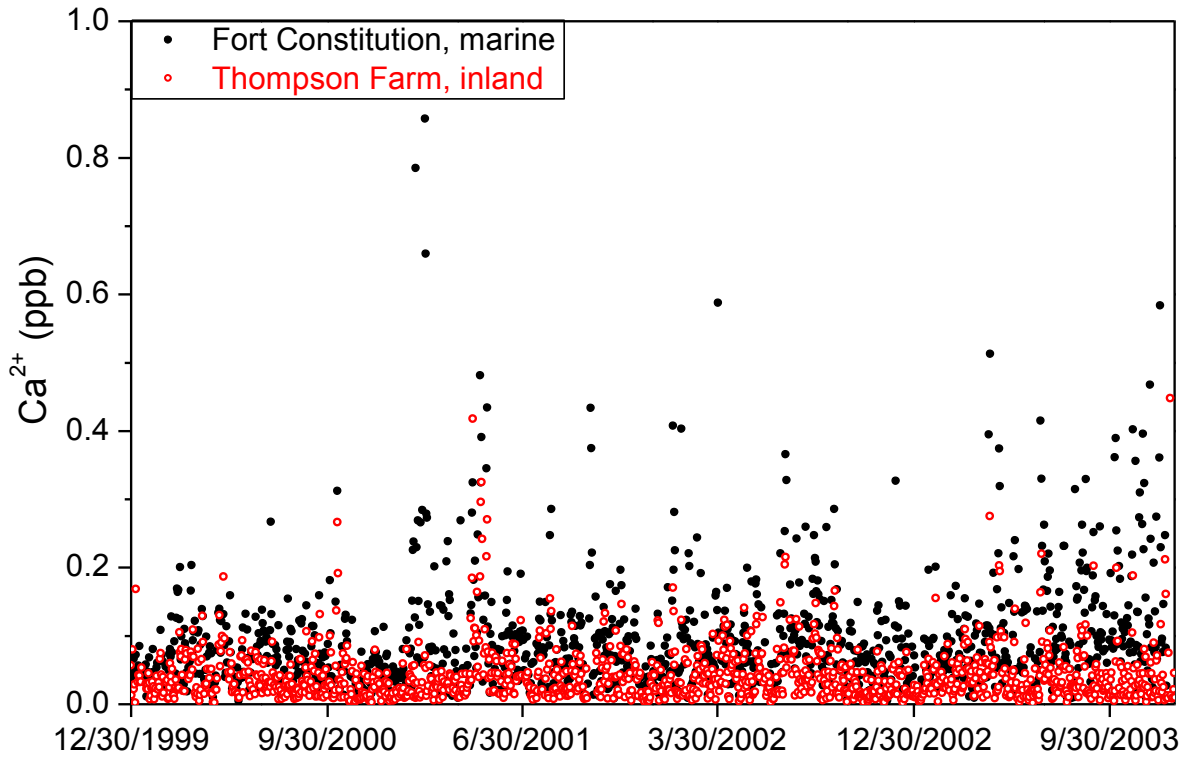


Figure G.6 AIRMAP Ca^{2+} data from Fort Constitution & Thompson Farm.^{170,174} The solid black circles are data from Fort Constitution and the open red circles are the data from Thompson Farm. Samples were taken every 24 hours.